Glycogen metabolism and its regulatory network in *Synechocystis* sp. PCC6803

Dissertation

der Mathematisch-Naturwissenschaftlichen Fakultät
der Eberhard Karls Universität Tübingen
zur Erlangung des Grades eines
Doktors der Naturwissenschaften
(Dr. rer. nat.)

vorgelegt von

Niels Neumann

aus Rastatt

Tübingen

2022

Gedruckt mit Genehmigung der Mathematisch-Naturwissenschaftlichen Fakultät der Eberhard Karls Universität Tübingen.

Tag der mündlichen Qualifikation: 23.03.2023

Dekan:	Prof. Dr. Thilo Stehle
1. Berichterstatter:	Prof. Dr. Karl Forchhammer
2. Berichterstatter:	Prof. Dr. Hannes Link

Erklärung

Ich erkläre hiermit, dass ich die zur Promotion eingereichte Arbeit selbständig verfasst, nur die angegebenen Quellen und Hilfsmittel benutzt und Stellen, die wörtlich oder inhaltlich nach den Werken anderer Autoren entnommen sind, als solche gekennzeichnet habe. Eine detaillierte Abgrenzung meiner eigenen Leistungen von den Beiträgen meiner Kooperationspartner habe ich in „Declaration of author contribution“ vorgenommen.

Tübingen, den _____

Niels Neumann

TABLE OF CONTENTS

TABLE OF CONTENTS

ABBREVIATIONS

2-OG	2-oxoglutarate
aa	amino acid
ABC	ATP-binding cassette
ADP	adenosine diphosphate
ATP	alternative respiratory terminal oxidase
CBB	Calvin-Benson-Bassham cycle
CCM	carbon concentrating mechanism
Ci	inorganic carbon
Cph1	cyanobacterial phytochrome 1
Cyt	cytochrome
ED	Entner-Doudoroff
EMP	Embden-Meyerhof-Parnas
Fd	ferredoxin
FNR	ferredoxin NADP+ reductase
Frc-1,6-BP	fructose-1,6-Bisphosphate
Frc-6P	fructose-6-phosphate
G6PDH	glucose-6-phosphate dehydrogenase
GDH	glutamate-dehydrogenase
Glc-1P	glucose-1-phosphate
Glc-1,6-BP	glucose-1,6-bisphosphate
Glc-6P	glucose-6-phosphate
GlgA	glycogen synthase
GlgB	glycogen branching enzyme
GlgC	glucose-1-phosphate-adenylyltransferase
GlgP	glycogen phosphorylase
GlgX	glycogen debranching enzyme
Gln	glutamine
Glu	glutamate
GOGAT	glutamate-2-oxoglutarate-aminotransferase
GS	glutamine synthetase
GSH	glutathione
GSSG	glutathione disulfide
GS	glutamine synthetase
GSH	glutathione
K_{cat}	turnover number
K_M	Michaelis Menten-constant
NADP+/ NADPH	nicotinamide adenine dinucleotide phosphate
NAD+/ NADH	nicotinamide adenine dinucleotide
NDH	NAD(P)H dehydrogenase
PC	plastocyanin
PEPC	Phosphoenolpyruvate carboxylase
Pfk	phosphofructokinase
Pgm,	phosphoglucomutase
Pi	inorganic phosphate
PPI	pyrophosphate
PQ	plastoquinone
PS	photosystem
ROS	reactive oxygen species
RTO	respiratory terminal oxidase
SDH	succinate dehydrogenase
TCA	tricarboxylic acid
TrX	thioredoxin
V_{max}	maximum velocity
WT	Wild type

I. ZUSAMMENFASSUNG

Glykogen ist ein stark verzweigtes Glukosepolymer und der wichtigste Kohlenstoffspeicher in den meisten freilebenden Bakterien. In Cyanobakterien ist der Glykogen-Stoffwechsel eng an eine photosynthetische Lebensweise gekoppelt, bei der Glykogen während photoautotrophen Wachstums aufgebaut und während heterotropher Phasen abgebaut wird. Neben dem Tag/Nacht Wachstum spielt Glykogen auch eine entscheidende Rolle während Nährstoffmangelsituationen, von welchen Stickstoffmangel bei nicht-diazotrophen Cyanobakterien am häufigsten auftritt. Unter Stickstoffmangel geht das einzellige Cyanobakterium *Synechocystis* sp. PCC6803 in einen dormanten Zustand, genannt „Chlorose" über, der es ermöglicht lange Mangelperioden zu überleben und bei Wiederverfügbarkeit gebundener Stickstoffquellen wieder zu erwachen. Diese metabolischen Anpassungen hängen stark von der schnellen Synthese bzw. dem schnellen Abbau von Glykogen ab, welche präzise reguliert werden müssen. Wie bei vielen andere Cyanobakterien kodiert das Genom von *Synechocystis* für zwei Isoformen der meisten Glykogen assoziierten Enzyme. Trotz der wichtigen Rolle des Glykogenstoffwechsels in Cyanobakterien ist die Rolle und Regulation vieler dieser Enzyme nur unzureichend bekannt. In dieser Studie wurden die Regulierung des Glykogenstoffwechsels und die damit verbundenen Enzyme im Detail untersucht.

Glykogenabbau erfolgt durch das Zusammenspiel von Glykogenphosphorylasen (GlgP) und Glykogen-Debranching-Enzymen (GlgX). Diese Studie hat gezeigt, dass GlgP1 einen C-terminalen Redox-Schalter besitzt und durch Oxidation aktiviert wird. GlgP1 Aktivität steht dabei im Zusammenhang mit Stresssituationen, die zur Bildung reaktiver Sauerstoffspezies führen. In dieser Studie wurde auch zum ersten Mal gezeigt, dass GlgX1 das essenzielle Enzym für den Glykogenabbau während des Erwachsens aus der Chlorose ist, wohingegen die Rolle von GlgX2 weiterhin unklar bleibt.

Die Phosphoglucomutase (PGM) Reaktion stellt einen zentralen Schritt im Kohlenstoffmetabolismus dar, der sowohl für die Glykogensynthese als auch für den Glykogenabbau essenziell ist. Die PGM-Reaktion wird durch Glc-1,6-BP aktiviert, dessen Herkunft in Prokaryoten bisher unbekannt war. Diese Arbeit identifizierte das PGM-Homolog Slr1334 als die erste Glc-1,6-BP Synthase. Es wurde gezeigt, dass Slr1334-Homologe in Prokaryoten weit verbreitet sind und dass ein Slr1334-Homolog in *Bacteriodes salyersiae* die gleiche Reaktion katalysiert. Glc-1,6-BP stellt einen bisher nicht berücksichtigten Regulator im bakteriellen Kohlenstoffmetabolismus dar, von dem angenommen wird, dass er neben PGM auch andere Schlüsselenzyme regulieren kann.

Von Eukaryoten ist bekannt, dass Glykogen auf unterschiedliche Weise modifiziert werden kann. Die Entwicklung einer nativen Aufreinigungsmethode und anschließende Analyse des Glykogens aus *Synechocystis* zeigte eine mögliche Modifikation durch Phosphorylierung. Darüber hinaus wurde ein erster Einblick in das Glykogenproteom gegeben. Zusammengenommen geben diese Ergebnisse neue Einblicke in die bisher unterschätzte Komplexität von Glykogen.

II. SUMMARY

Glycogen is a multibranched glucose polymer and the major carbon storage compound in most free-living bacteria. In cyanobacteria glycogen metabolism is tightly coupled to a photosynthetic lifestyle where it is built up during photoautotrophic growth and degraded during heterotrophic phases. Next to being essential for diurnal growth, glycogen is also crucial during nutrient starvation, where the deprivation of nitrogen is the most common form for non-diazotrophic cyanobacteria. When encountering nitrogen starvation, the unicellular cyanobacterium *Synechocystis* sp. PCC6803 enters a dormant like state, called chlorosis, enabling it to outlive long starvation periods from which it can resuscitate upon re-availability of combined nitrogen sources. These metabolic adaptations are dependent on the rapid synthesis or breakdown of glycogen and must be precisely regulated. Like many other cyanobacteria, the genome of S*ynechocystis* encodes for two isoforms for most of the enzymes involved in glycogen turnover. Despite the great significance that glycogen metabolism has in cyanobacteria, the role and regulation of many of these enzymes is only poorly understood. In this study the regulation of glycogen metabolism and its associated enzymes were investigated in detail.

Glycogen degradation is performed by the coordinated action of glycogen phosphorylases (GlgP) and glycogen debranching enzymes (GlgX). This study revealed that GlgP1 is under the control of a C-terminal redox switch and activated upon oxidation. This connects GlgP1 activity to stress conditions that lead to the formation of reactive oxygen species. Furthermore, this study showed for the first time that GlgX1 is the essential glycogen debranching enzyme during resuscitation from nitrogen starvation while the role of GlgX2 remains elusive.

A central step in carbon metabolism is the interconversion of glucose phosphate by the phosphoglucomutase (PGM) reaction which is essential for glycogen synthesis and degradation alike. The PGM reaction is dependent on the availability of the central activator Glc-1,6-BP whose origin in prokaryotes was so far unknown. This work identified the PGM homologue Slr1334 as the first Glc-1,6-BP synthase. It was shown that Slr1334 homologues are widespread among prokaryotes and that a Slr1334 homologue from *Bacteriodes salyersiae* catalyzes the same reaction. Glc-1,6-BP represents a so far unconsidered regulator in bacterial carbon metabolism, which is suggested to regulate several key enzymes besides PGM.

It is known from eukaryotes that the glycogen granule can undergo different modifications. By implementing a native purification method, analysis of glycogen from *Synechocystis* revealed a potential modification by phosphorylation. Furthermore, a first insight into the glycogen proteome was given. Together these results provide new insights in the underestimated complexity of glycogen.

III. Publications

1. Accepted Publications

Publication 1: Research article

Watzer B., Spät P., **Neumann N.**, Koch M., Sobotka R., Macek B., Hennrich O., Forchhammer K.
The Signal Transduction Protein P_{II} Controls Ammonium, Nitrate and Urea Uptake in Cyanobacteria.
Front Microbiol. 2019 10:1428.

Publication 2: Review

Neumann N., Doello S., Forchhammer K.
Recovery of Unicellular Cyanobacteria from Nitrogen Chlorosis: A Model for Resuscitation of Dormant Bacteria.
Microb Physiol. 2021;31(2):78-87.

Publication 3: Research article

Selim KA., Haffner M., Burkhardt M., Mantovani O., **Neumann N.**, Albrecht R., Seifert R., Krüger L., Stülke J., Hartmann MD., Hagemann M., Forchhammer K.
Diurnal metabolic control in cyanobacteria requires perception of second messenger signaling molecule c-di-AMP by the carbon control protein SbtB.
Science Advances 2021 • Vol 7, Issue 50

Publication 4: Research article

Doello, S.; **Neumann, N.**; Forchhammer, K.
Regulatory phosphorylation event of Phosphoglucomutase 1 tunes its activity to regulate glycogen metabolism.
FEBS Journal • Vol 289, No. 19

Publication 5: Research article

Neumann N., Friz S., Forchhammer K.
Glucose-1,6-bisphosphate, a key metabolic regulator, is synthesized by a distinct family of α-phosphohexomutases widely distributed in prokaryotes

mBio • Vol. 13, No. 4

2. Submitted manuscripts

Publication 6: Research article

Neumann N., Lee K., Forchhammer K.

On the role of glycogen degrading enzymes in *Synechocystis* PCC6803

doi: https://doi.org/10.1101/2022.11.21.517384

3. Declaration of author contribution

Publication 1: *„The Signal Transduction Protein P_{II} Controls Ammonium, Nitrate and Urea Uptake in Cyanobacteria"* I conducted the Bacterial-Two-Hybrid experiments and wrote the corresponding part in the methods, and results section.

Publication 2: "*Diurnal metabolic control in cyanobacteria requires perception of second messenger signaling molecule c-di-AMP by the carbon control protein SbtB"*
I designed and conducted the Bacterial-Two-Hybrid experiments and wrote the corresponding parts in the methods and results section. Furthermore, I designed and created the Δ*glgb* knockout mutant

Publication 3: "*Regulatory phosphorylation event of Phosphoglucomutase 1 tunes its activity to regulate glycogen metabolism*"
I provided genetical analysis and designed and created constructs for Sll726 overexpression. Furthermore, I provided knowledge in conducting the PGM enzymatic assays.

Publication 4: "*Recovery of Unicellular Cyanobacteria from Nitrogen Chlorosis: A Model for Resuscitation of Dormant Bacteria*"
I edited the manuscript text and prepared Figure 1 and Figure 2 under the supervision of Prof. Karl Forchhammer.

Publication 5: *"Glucose-1,6-bisphosphate, a key metabolic regulator, is synthesized by a distinct family of α-phosphohexomutases widely distributed in prokaryotes"*
I designed and conducted all the experiments in this study except for the LC-MS measurement. I created all the figures and wrote the manuscript text under the supervision of Prof. Karl Forchhammer and with support from Dr. Libera LoPresti.

Publication 6: "*On the role of glycogen degrading enzymes in Synechocystis sp. PCC6803"*
I designed and conducted all the experiments except for the growth curves. I wrote the text and prepared all the figures under the supervision of Prof. Karl Forchhammer.

IV. INTRODUCTION

1. Cyanobacteria

Cyanobacteria are a phylum of Gram-negative prokaryotes, belonging to the domain of bacteria and date back at least 2.7 billion years, making them one of the most ancient organisms on Earth. They are characterized by being the only prokaryotes able to perform oxygenic photosynthesis. With this ability cyanobacteria initiated one of the biggest environmental changes in Earth's history: The conversion from a reducing to an oxidizing atmosphere, called the great oxidation event. While this event caused a mass extinction, it also laid the foundation for oxygen dependent higher forms of life [6, 7]. Cyanobacteria are able to adapt to a wide range of environmental conditions which allowed them to colonize numerous habitats [8]. Even today, they are central to the Earth's ecosystem: As primary producers they are responsible for about one third of the global CO_2 fixation. In addition, some species are also able to fix atmospheric nitrogen [9]. Based on their morphology cyanobacteria can be classified in five different sections: Section I comprises unicellular cyanobacteria that reproduce by binary fission or budding. Section II also contains unicellular strains but with the ability to form baeocytes and to reproduce by multiple fission. Section III comprises filamentous cyanobacteria but without the formation of any specialized cells. Section IV consists of filamentous cyanobacteria that can form specialized cells within their filaments. Among those are cells for nitrogen fixation (heterocysts), spore-like cells (akinetes) and motile filaments (hormogonia). Section V like Section IV does contain filamentous cyanobacteria with specialized cells but with the ability to divide into more than one plane [10].

2. The cyanobacterial model organisms *Synechocystis* sp. PCC 6803

Synechocystis sp. PCC 6803 (hereafter referred to as *Synechocystis*) is a cyanobacterial strain belonging to Section I. It was first isolated in 1968 from a freshwater lake in Berkeley and has since then become a cyanobacterial model organism [11]. It was the first photoautotrophic organism with a fully sequenced genome. This, together with its ability for the uptake of exogenous DNA lead to the development of genetic tools allowing for genetic modification [12]. Compared to many other cyanobacteria who are obligated photoautotrophs, *Synechocystis* shows a metabolic versatility by being capable of utilizing external carbon sources for mixotrophic and light-activated heterotrophic growth [13]. *Synechocystis* is a non-diazotrophic cyanobacterium, meaning it is unable fix molecular nitrogen out of the atmosphere and is dependent on the supply of combined nitrogen sources. Since combined nitrogen sources are one of the most limiting factors in aquatic ecosystems *Synechocystis* has evolved a metabolic adaptation to outlive periods of nitrogen deficiency by entering a dormant like state [14].While under stress conditions the strain is also known to produce different types of storage polymers including glycogen, polyhydroxybutyrate,

cyanophycin and polyphosphate which as a photoautotrophic growing organism makes it interesting for environmentally friendly biotechnological applications [15-17]. All these characteristics make *Synechocystis* a great model organism to study photosynthesis, stress response, metabolic dormancy and biotechnological utilization among others.

3. Energy metabolism of *Synechocystis* sp. PCC 6803

3.1 Oxygenic photosynthesis

Oxygenic photosynthesis uses light-driven electron transport pathways to gain chemical energy and reduction equivalents. Coupled to that is a light independent reaction in which those energy rich products are used to fix CO_2 into sugars [18] (**see chapter carbon fixation**).

Two pathways can be distinguished for the light dependent reaction:

1. Linear electron flow (LEF), where electrons are transported through photosystem II (PSII) and photosystem I (PSI) to a terminal acceptor leading to the formation of ATP and NADPH.

2. Cyclic electron flow (CEF), revolving only around PSI leading to the solely formation of ATP.

The ratio of electrons used in LEF or recycled via CEF allows for the adjustment of the ATP/NADPH ratio to meet different metabolic demands, adapting to changing environmental conditions and balancing the redox state in the electron transport chain.

3.1.1 Linear electron flow (LEF)

LEF, also known as non-cyclic photophosphorylation, is a two-stage process starting at PSII. PSII is a pigment-protein multimeric complex build of a light harvesting complex, a reaction center and a water splitting/oxygen evolving complex. The light harvesting complex is composed of phycobilisomes which capture the incoming light. They are large structures composed of the chromophore containing proteins phycocyanin, phycoerythrin, phycoerythrocyanin and allophycocyanin. In *Synechocystis* the phycobilisomes consist of a core of allophycocyanin trimers emanating peripheral rods of hemi-discoidal phycocyanin subunits [19, 20]. The core delivers the light energy towards the reaction center of PSII of which the chlorophyll a P_{680} is the primary donor. The absorption of the photon leads to an excitement of P_{680} which donates an electron to reduce an oxidized plastoquinone acceptor to plastoquinol, resulting in the formation of a positively charged P_{680}^+ [21]. P_{680}^+ acts as a strong oxidizing agent and draws electrons from the manganese cluster of the oxygen evolving complex which in turn regains its lost electrons from water, splitting it into protons and O_2. This results in a net yield of 4 protons and molecular O_2 for every 4 e- taken up by P_{680}^+ [22]. The high impermeability of the thylakoid membrane for protons leads to the formation of a proton gradient within the thylokid lumen. The reduced plastoquinone is either re-oxidized by the *b_6f* complex through the Q cycle, which comprises a series of redox reactions, or by reacting with oxygen leading to the formation of reactive oxygen species (ROS) [23]. During these reactions

four protons are emitted into the thylakoid lumen, further building the proton gradient, while two electrons are transferred to the water-soluble electron carriers plastocyanin (PC) and cytochrome c_6 [24]. In *Synechocystis* and most other cyanobacteria plastocyanin is the main electron carrier and cyt c_6 is only relevant at low copper concentrations. In the second stage of LEF light absorbance at PSI excites its P_{700} reaction center, leading to an electron transfer to the terminal electron acceptor ferredoxin. The oxidized P_{700} is rapidly reduced by plastocyanin or cyt c_6. The reduced ferredoxin can be used for electron transfer to the ferredoxin-$NADP^+$ reductase (FNR) yielding the NADPH necessary for CO_2 fixation. Alternatively, reduced ferredoxin also serves as an electron donor for several other anabolic processes, e.g. nitrogen assimilation [25]. The proton gradient built up during the various reactions and the resulting proton motive force is utilized by the ATP synthase, to convert ADP to ATP [25].

3.1.2 Cyclic electron flow (CEF)

CEF revolves solely around PSI and allows the building of a proton gradient for ATP generation without the coupled generation of NADPH. In CEF the energized electrons yielded from PSI are transferred back to the membrane to follow a cyclic pathway. This is done via the NADPH dehydrogenase I (NDHI) complex which receives electrons from reduced ferredoxin which is either obtained by receiving electrons from PSI or the reverse reaction of FNR. NDH-I transfers the electrons to PQ followed to transfer to b_6f and back to PSI closing the cycle and creating a proton motif force in the process used for ATP synthesis [25, 26].

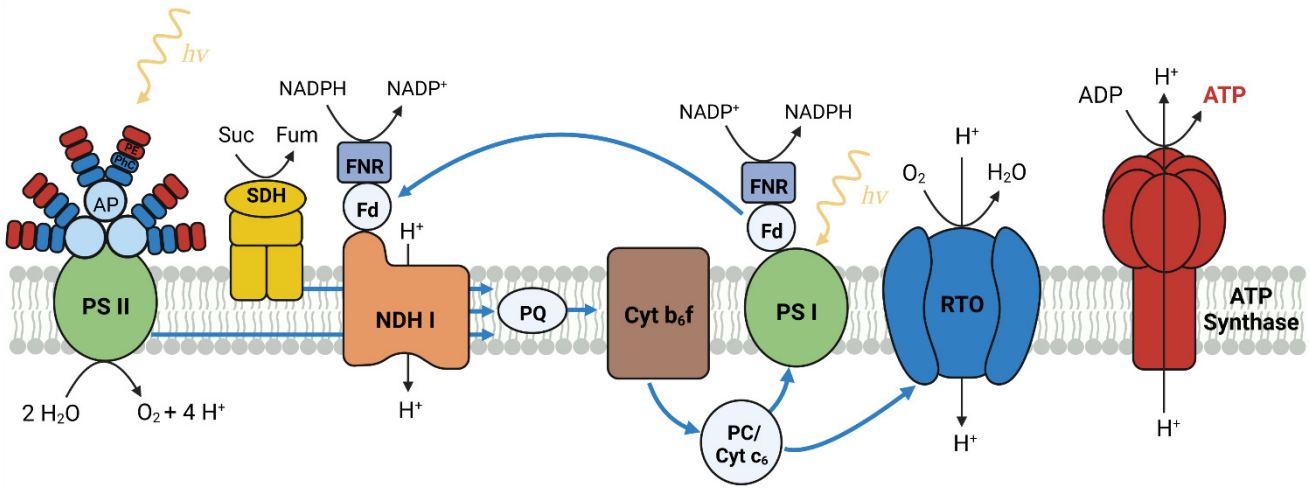

Figure 1: Schematic overview of cyanobacterial electron transport chain during photosynthesis and respiration on the thylakoid membrane. Modified from [5].

Blue arrows indicate the electron transport. PSI/PSII: Photosystem I/II; NDH I: NADPH dehydrogenase I; SDH: Succinate dehydrogenase; Fd: Ferredoxin; FNR: Ferredoxin-NADP(+) reductase; PQ: Plastoquinone; PC: Plastocyanine; RTO: respiratory terminal oxidase; AP: Allophycocyanin; PhC: Phycocyanine; PE: Phycoeryhtrin

3.2. Respiration

Respiration, also known as oxidative phosphorylation, can be considered the reversed process of oxygenic photosynthesis: The energy rich end products of photosynthesis and O_2 are used to produce energy, CO_2 and water. Like in oxygenic photosynthesis respiration creates an electrochemical gradient caused by electron transport resulting in the synthesis of ATP. Most of the respiratory activity in cyanobacteria is carried out on the thylakoid membranes. The used electron acceptors for respiration are the same as for the photosynthetic electron transport chain, making cyanobacteria the only organisms to combine both pathways in one compartment [27, 28]. The initial respiratory electron transport starts at NDH-1 and the succinate dehydrogenase (SDH) which gain electrons from ferredoxin and succinate respectively and transfer them to the plastoquinone pool. Subsequently, electron transport continues via cyt b_6f to the soluble plastocyanin and cyt *c6*, building a proton gradient in the process. In a final step those electrons are donated to the respiratory terminal oxidases (RTO), where molecular oxygen as terminal electron acceptor is reduced to water and protons are translocated across the membrane [25, 29]. In *Synechocysti*s the main type of RTO is the cytochrome c oxidase (COX), which accepts electrons from cyt b_6f. The other RTOs, a *bd* quinol oxidase (Cyd) and the alternative terminal oxidase (ARTO) receive electrons directly from plastoquinol [30]. Like in photosynthesis the ATP synthase uses the proton motive force to generate ATP. While sharing many components and similar in their process, oxygenic photosynthesis and respiration at the thylakoid membranes usually run separately in time. The temporal separation of these two processes is known as the Kok effect [31].

In addition to the thylakoid membrane, where the main bioenergetic processes occur, the plasma membrane also harbors a more rudimentary respiratory chain. in *Synechocysti*s this includes SDH and a type II NAD(P)H dehydrogenase (NDH-2) which accepts electrons from NAD(P)H. Electrons are transferred from NDH-2 via plastoquinone to the alternative respiratory oxidase (ARTO). Under normal growth, respiration on the plasma membrane plays only a minor role in energy transduction but is associated with motility, nutrient uptake and efflux pump activity [32]. A special role of the plasma membrane comes into play in situations where proton translocation is unfavorable e.g., during resuscitation from chlorosis. Here a sodium motif force can be used for the generation of ATP instead [5].

4. Carbon metabolism

As photoautotrophic organisms, cyanobacteria alternate their carbon metabolism between an autotrophic and a heterotrophic mode:

Inorganic carbon is fixed during the day where energy and reduction equivalents from LEF are used in the light independent reaction. The excess of carbon is stored as carbon polymers which are degraded for respiration during dark phases [33].

4.1 Carbon fixation

Like other phototrophic organisms, cyanobacteria mainly fix carbon through the Calvin-Benson-Bassham cycle (CBB). Here the ribulose 1,5-bisphosphate carboxylase/oxygenase (RuBisCO) uses CO_2 and ribulose-1,5-bisphosphate to generate two molecules of 3-phosphoglycerate (3-PG). The obtained 3-PG can either be used for different biosynthetic reactions or to regenerate rublose-1,5-bisphosphate [9]. Although showing a higher affinity for CO_2 RuBisCO can also incorporate O_2 instead, producing one molecule of 3-phosphoglycerate alongside 2-phosphoglycolate. 2-phosphoglycolate cannot be further used in the CBB and must be converted in an energy demanding process to avoid a toxic accumulation in a process known as photorespiration [34]. To reduce the incorporation of O_2 into RuBisCO cyanobacteria developed a carbon concentrating mechanism (CCM) which strongly increases CO_2 concentration around RuBisCO. Five different carbon uptake systems contribute to Ci uptake and its accumulation by CCM in the cytoplasm: NDH-1_3 and NDH-1_4 transport CO_2 and are located in the thylakoid membrane. BCT1, SbtA and BicA transport HCO_3^- and are located in the plasma membrane. After entering the cytoplasm, Ci is further transported to the carboxysomes. These polyhedral organelles provide a microcompartment and inherit RuBisCO together with a carbonic anhydrase which converts HCO_3^- to CO_2. Due to the impermeability of the carboxysome protein shell for CO_2 it cannot exit, resulting in a high CO_2 concentration around RuBisCO.

Due to the exposure to alternating day night regimes cyanobacterial carbon metabolism has to permanently switch between autotrophic CO_2 fixation and heterotrophic respiration. Therefore, Ci uptake is tightly regulated and limited to photosynthetic activity. The switch between these two modes is operated by a sophisticated network including a circadian clock machinery, the sensing of redox state and C/N ratio and others. Recently this regulatory network has been expanded by showing that phytochromes sensing red and far-red light play in important role in regulation of carbon uptake by SbtB [35].

An additional way for CO_2 fixation in cyanobacteria is the phosphoenolpyruvate carboxylase (PEPC). This enzyme catalyzes the addition of bicarbonate to phosphoenolpyruvate to form oxaloacetate. The PEPC reaction is responsible for up to 20% of total carbon fixation and is essential for providing TCA-cycle intermediates [36].

4.2 Carbon storage

4.2.1 Glycogen and its turnover[1]

Glycogen is the major carbon storage compound in animals, fungi and most free-living bacteria. It's a glucose polymer linked at position α-1,4 with branches at position α-1,6. In bacteria, particularly in free living strains, glycogen is usually built up under conditions of carbon surplus and degraded when energy or carbon supplies are limited [37-39]. In cyanobacteria glycogen

[1]Parts of this section are quotes from: Neumann N., Lee K., Forchhammer K. "On the role and regulation of glycogen catabolic isoenzymes in *Synechocystis* sp. PCC6803" bioRxiv 2022.11.21.517384; doi: https://doi.org/10.1101/2022.11.21.517384

plays a key role in carbon metabolism and is tightly coupled to a photoautotrophic lifestyle where excess fixed CO_2 is stored as glycogen during the day which thereon gets catabolized during the night when metabolism switches to a heterotrophic mode. This essential role is further underlined by the fact that glycogen metabolic enzymes are conserved in all known cyanobacteria [40].

Glycogen synthesis starts by the formation of ADP-glucose carried out by the glucose-1P adenylyltransferase (GlgC), utilizing ATP and glucose-1P and releasing ADP and pyrophosphate. Glycogen synthase (GlgA) transfers ADP-glucose to the non-reducing end of a glucan chain by creating a α-(1-4)-glycosidic linkage. Unlike in eukaryotes, de-novo synthesis of glycogen in bacteria does not involve a central protein like glycogenin. How the initial formation of the linear glucan chain is initiated is so far unclear, but it has been suggested that GlgA itself can initiate *de-novo* synthesis by catalyzing its own glycosylation. The linear glucan chains reach a typical length of 10 to 14 glucose residues. They are interlinked via α-(1-6)-linkages by the activity of the glycogen branching enzyme (GlgB). This enzyme hydrolyzes a α-(1-4)-linkage and attaches a segment to an existing chain, via an α-(1-6) linkage. This process forms a highly branched structure and facilitates a spherical growth that can reach about 10^7 - 10^8 Da in size [41]. The final conformation of the granule is mainly defined by the branching and debranching activity catalyzing the addition and removal of α-(1-6) ramifications, respectively. The maximum size of a granule is defined by activity of the synthesizing, branching and degrading enzymes and cannot exceed a certain size. It has recently been shown that like in eukaryotes these β-particles can agglomerate to a larger complex of α-particles [42]. The formation of greater agglomeration influences total storage capacity as well as degradation speed. Data from eukaryotic glycogen indicate that the granule can undergo several modifications in the form of protein attachment or phosphorylation [43]. However, if this is the case for bacterial glycogen is currently unknown.

Glycogen breakdown requires the coordinated action of glycogen phosphorylase (GlgP) and glycogen debranching enzyme (GlgX). GlgP releases glucose-1P by transferring orthophosphate to the non-reducing end of a α-(1-4) glucan chain. This processive reaction continues until the last four glucose residues left on a branch are reached. In prokaryotes, those remaining glucose units are then specifically hydrolyzed by a “direct” debranching enzyme, releasing maltotetraose which can be metabolized by maltodextrin phosphorylase (MalP) and by a-1,4-glucanotransferase (MalQ) reactions [3, 44-46]. The GlgP reaction is considered the rate limiting step in glycogen catabolism [47]. The released Glc-1P is then turned to Glc-6P by phosphoglucomutase (PGM) and can fuel different metabolic pathways including the EMP, ED and the OPP pathway. Like many other cyanobacteria, the genome of the unicellular model organism *Synechocystis* sp. PCC6803 encodes for several isoenzymes involved in glycogen catabolism including the glycogen phosphorylases *sll1356* (*glgP1*) and *slr1367* (*glgp2*) and the glycogen debranching enzymes *slr0237* (*glgX1*) and *slr1857* (*glgX2*). It has been shown for some cases that these different isoenzymes have distinctive roles und only some of them work under specific conditions [48-51].

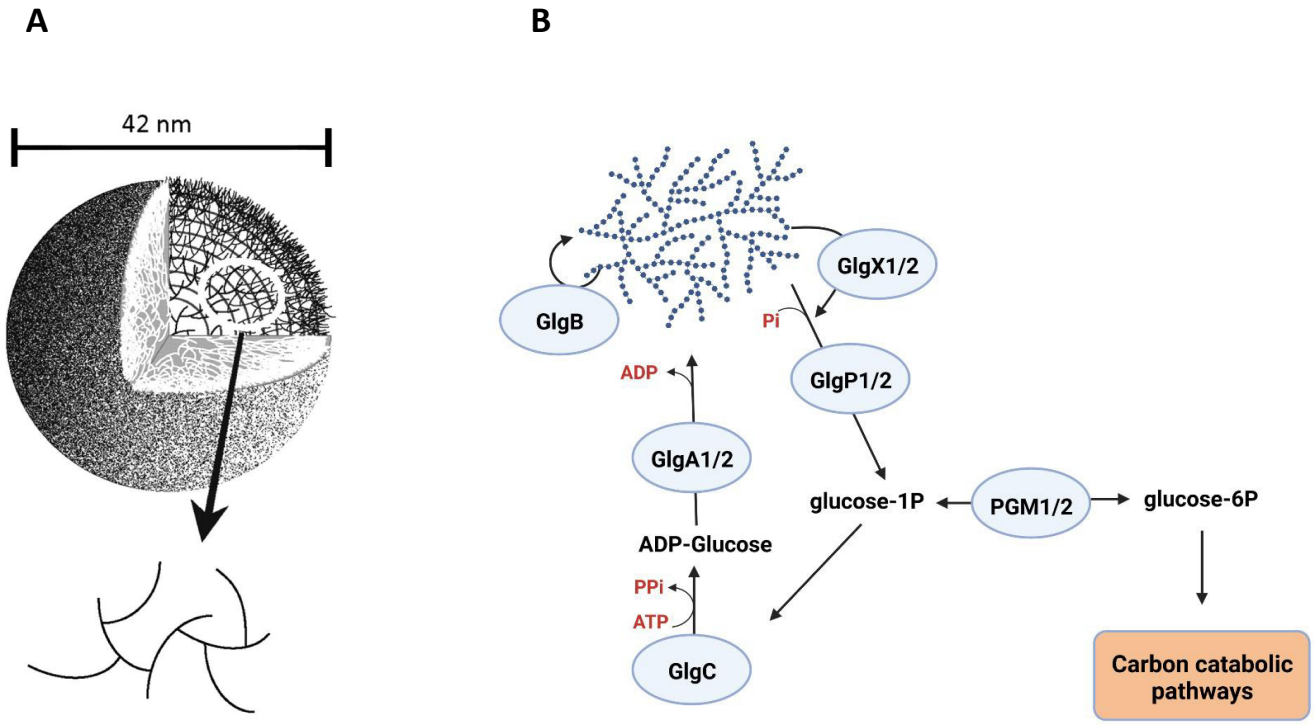

Figure 2: (A): Depiction of glycogen granule adapted from [3]Ball et al. 2011. (B): Enzymes involved in glycogen turnover.

4.2.2 The PGM reaction[1]

One of the key reactions where the fate of a glucose molecule is decided is the reaction of phosphoglucomutase (PGM). This enzyme catalyzes the interconversion of glucose-1P and glucose-6P, thus playing a crucial role in glycogen turnover, glycolysis and gluconeogenesis. PGM belongs to the large superfamily of α-D-phosphohexomutases (αPHM), which is ubiquitous and found in all domains of life. All known members of this superfamily are similar in structure and general reaction mechanism but prefer different phosphosugar substrates [52]. In *Synechocystis* the known members of PHMs are Sll0726, carrying out the main PGM activity, Slr1334 an enzyme with low PGM activity of unknown function and a phosphoglucosamine mutase GlmM (sll1758) [49]. The reactions of all PHM members have in common that they require a bound metal ion (usually Mg_2^+) and a phosphorylated seryl residue in the active site which is highly conserved among all members of the superfamily. The interconversion of Glc-1P to Glc-6P by PGM is mediated by a transfer of the phosphate group from the active site serine to the 1' or 6' position of the substrate respectively. This leads to the formation of a transient Glc-1,6-BP intermediate. This intermediate undergoes a reorientation inside the enzyme and transfers the phosphate of its 6' or 1' position back to the active site

[1]Parts of this section are quotes from Neumann N., Friz S., Forchhammer K. Glucose-1,6-bisphosphate, a key metabolic regulator, is synthesized by a distinct family of α-phosphohexomutases widely distributed in prokaryotes *mBio* • Vol. 13, No. 4

serine, re-phosphorylating it in the process and releaseing Glc-6P or Glc-1P, respectively. Glc-1,6-BP itself acts as an essential activator of PGM by providing the initial phosphorylation of the active site. Due to the loss of the phosphorylation after several reaction cycles a constant Glc-1,6-BP level is required to keep PGM in an active state [53, 54]. Despite its essential role in regulating PGM activity no enzyme producing free Glc-1,6-BP has been identified so far. Once glucose-6P has been formed by the PGM reaction it can enter different catabolic pathways.

4.3 Carbon pathways

In *Synechocysti*s there are three central routes that carbon can take: The Embden–Meyerhof–Parnas (EMP) pathway, the pentose phosphate (PP) pathway, and the Entner-Doudoroff (ED) pathway. While all those pathways provide energy and reduction equivalents in catabolic direction they differ strongly in their ATP/NAD(P)H ratios, their protein demand, and the biosynthetic precursors they provide. EMP is the pathway with the highest output of ATP and reducing equivalents (NADH) but has a comparatively high enzyme demand. The central enzyme in this pathway is the phosphofructokinase (Pfk) converting fructose-6P to fructose-1,6-BP. The PP pathway can be divided in an irreversible oxidative part (OPP) and a reversible non-oxidative part (NOPP). The OPP pathway is driven by the enzymes glucose-6P dehydrogenase (G6PDH) followed by the 6-phosphogluconate dehydrogenase (GDH) reaction catalyzing the conversion of 6P-gluconate to ribulose-5P. Both reactions provide reducing equivalents in the form of NADPH. This pathway is most important during heterotrophic growth [55]. In addition to reduction equivalents, ribulose-5P can be either used the regain ribulose-1,5-BP for RuBisCO or enter the NOPP for the formation of biosynthetic precursors for nucleic acids and others. In the NOPP, the C4, C5, C6 and C7 sugars can be reversibly transformed into each other. No ATP or reduction equivalents are gained or consumed during these processes. These reactions are catalyzed by several enzymes: Ribulosephosphat-3-Epimerase (RPE) and Ribose-5-phosphat-Isomerase (RPI) transform ribulose-5P to xylulose-5P and ribose-5P respectively. This is followed by the reactions of a transketolase (Tkt) and a transaldolase (Tal) transferring two and three carbon units respectively. By involving enzymes from the lower glycolysis, this pathway is responsible for the regeneration of Ribulose-1,5-BP from glycerate-3P during carbon fixation (see chapter 4.1). The ED pathway was only recently discovered. It uses the unique enzymes 6-phosphogluconate dehydratase aldolase (Edd) and KDPG aldolase (Eda) to form glyceraldehyde-3P and pyruvate out of gluconate-6P. The pathway has been shown to be important during mixotrophic growth e.g. in the transition from dark to light [55]. The fine-tuned regulation of those pathways is crucial to ensure optimal use of cellular resources under different conditions.

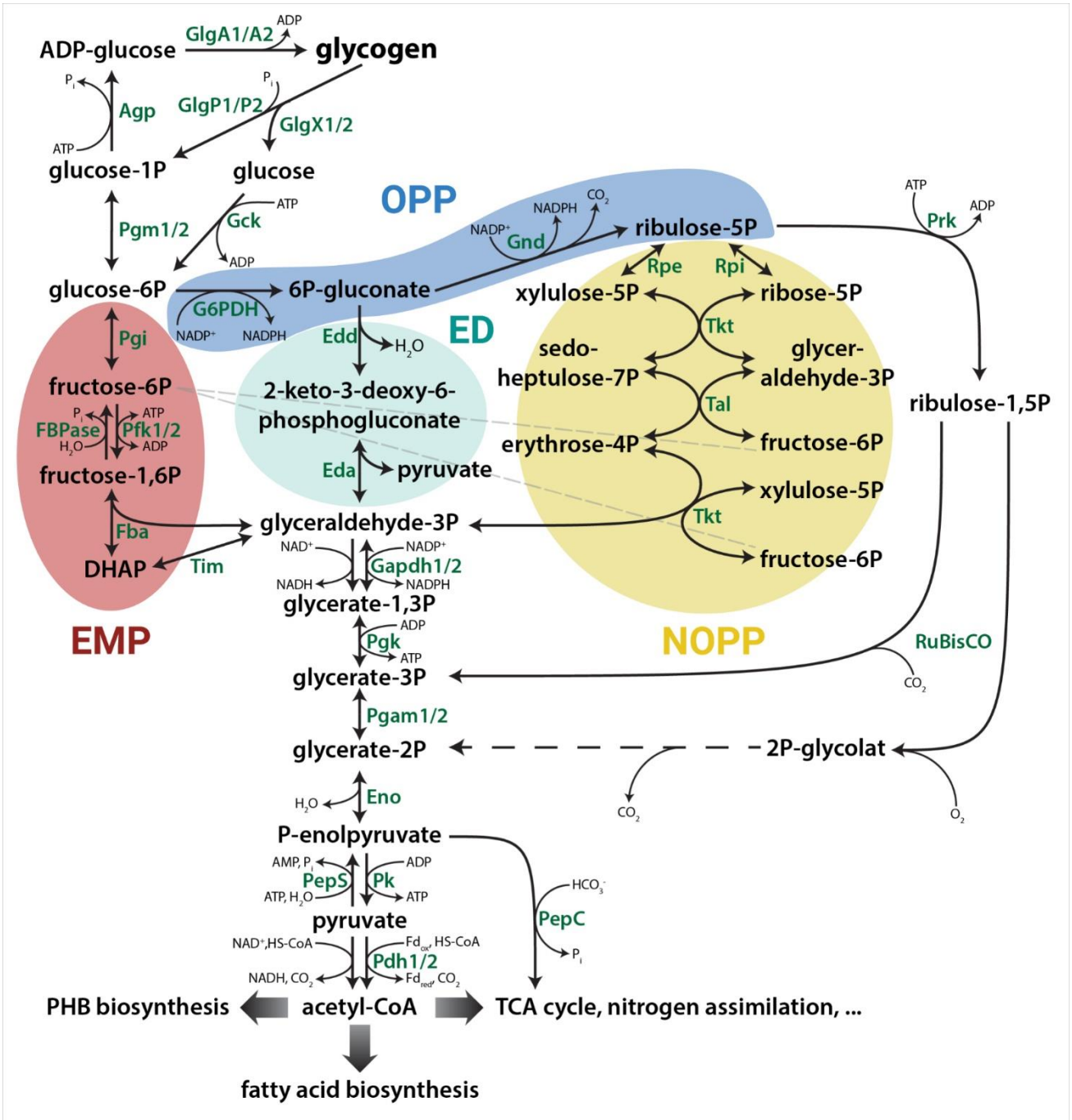

Figure 3: Central carbon pathways *in Synechocystis* adapted from Koch et al 2019 [1]:
EMP: Embden-Meyerhof-Parnas (red); OPP: Oxidative Pentose-Phosphate (blue); NOPP: Nonoxidative Pentose-Phosphate (yellow); ED: Entner-Doudoroff (green)

5. Nitrogen metabolism

5.1 Nitrogen assimilation

Nitrogen is an essential macronutrient for all living organisms and its availability is often a limiting factor for bacterial growth [56]. Whereas diazotrophic cyanobacteria are able to fix atmospheric nitrogen by the nitrogenase reaction, non-diazotrophic cyanobacteria like *Synechocystis* are fully dependent on the availability of combined nitrogen sources like ammonia, nitrate or urea. The uptake of those compounds is achieved by different transporter systems. Ammonia is taken up by diffusion via the ammonia permease Amt1 [57]. Nitrate and urea require an active uptake by the ABC-transporters NrtABCD and UrtABCDE respectively [58, 59]. For incorporation in nitrogen metabolism all nitrogen sources have to be reduced to ammonia, making it the preferred nitrogen source. Nitrate on the other hand is the most common and abundant source of nitrogen in cyanobacterial ecosystems. After entering the cell, nitrate gets reduced to nitrite by nitrate reductase followed by the reduction to ammonium by nitrite reductase. Both of these enzymes use reduced ferredoxin as an electron donor, suggesting a close connection between nitrogen assimilation and photosynthetic activity [60]. Urea is hydrolyzed by urease to two units of ammonia and CO_2. Ammonia gets assimilated by the sequential reaction of the glutamine synthetase (GS) and the glutamate-2-oxoglutarate-aminotransferase (GOGAT) in the so-called GS-GOGAT cycle: The GS uses ammonia, glutamate and ATP to form glutamine. The GOGAT reaction uses 2-OG as a carbon backbone together with glutamine gained from the GS reaction to form two units of glutamate. Depending on the GOGAT enzyme the reaction requires either NADPH or reduced ferredoxin as electron donor [61]. The glutamate can then either be used for GS reaction or for the synthesis of other nitrogen containing compounds. An alternative way for nitrogen assimilation is the reaction by the glutamate dehydrogenase (GDH). GDH can form glutamate by directly utilizing ammonia and 2-OG in an NADPH dependent reaction. However, GDH only shows low affinity for ammonia which is why this reaction is considered to only play a minor role in nitrogen assimilation compared to the GS/GOGAT cycle. **Figure 4** gives an overview on nitrogen transport and assimilation**.**

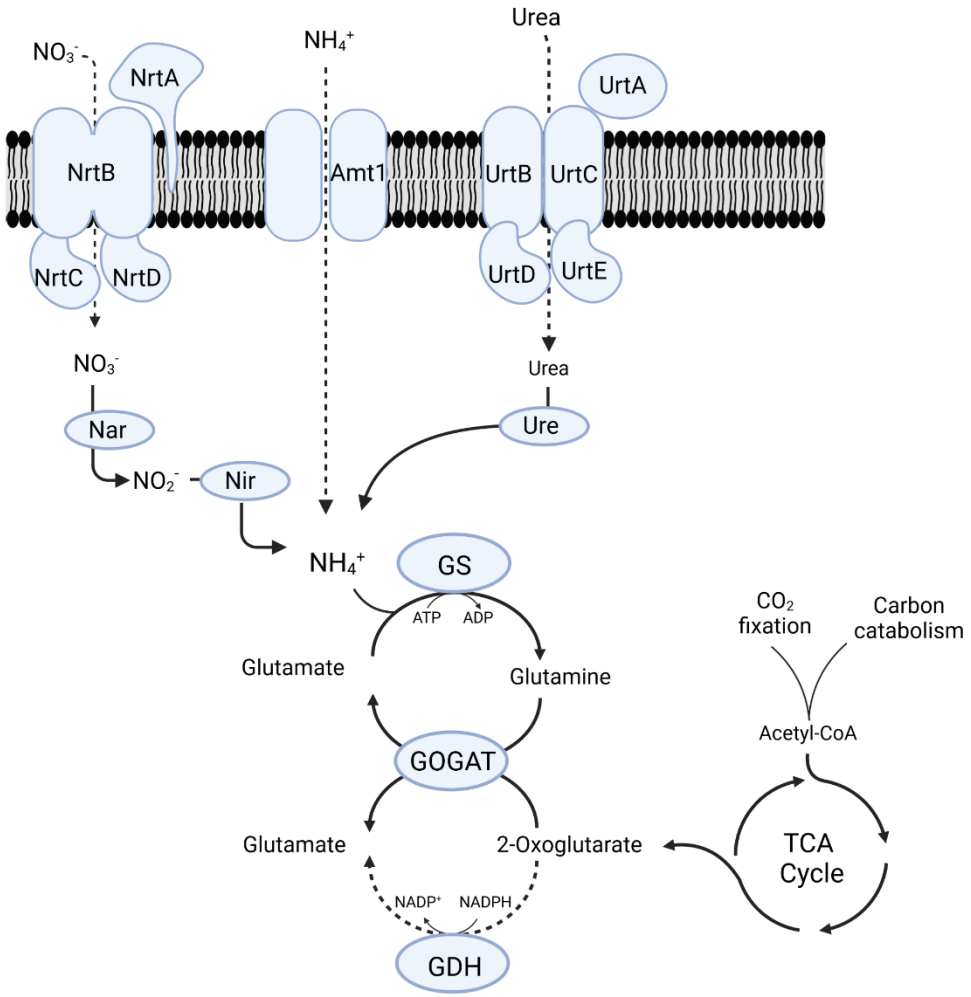

Figure 4: Schematic overview of nitrogen uptake and assimilation in *Synechocystis.*
Amt1: Ammonia permease; NrtABCDE: Nitrate transporter; UrtABCDE: Urea transporter; Nar: nitrate reductase; Nir: nitrite reductase; Ure: urease; GS: glutamine synthetase; GOGAT: glutamine-2-oxoglutarate-aminotransferase; GDH: glutamate dehydrogenase; TCA: tricarboxylic acid cycle; CoA: Coenzym A

5.2 Regulation of nitrogen metabolism

As described in the previous section, the assimilation of ammonia requires the availability of a carbon skeleton in the form of 2-OG. Because 2-OG itself is an intermediate of the TCA cycle it represents a junction for the intracellular carbon and nitrogen cycle. The ratio between carbon and nitrogen must be closely regulated to ensure optimal growth. The three main regulators of nitrogen metabolism are the signal transduction protein P_{II}, the transcription regulator NtcA and the NtcA activator PipX. P_{II} belongs to one of the largest and most ancient families of signaling proteins that is widespread in all domains of life. They are homotrimeric proteins characterized by a large surface exposed T-loop that serves as an interaction module for a large variety of interaction partners. P_{II} can be considered as a control center for the intracellular carbon and nitrogen ratio and associated anabolic processes. P_{II} can sense the energy status of the cell by competitively binding ATP or ADP [62]. The consecutive binding of 2-OG together with ATP

allows P_{II} to also sense the carbon/nitrogen ratio of the cell, where high amounts of 2-OG are associated with a high C/N ratio [63]. In addition to binding different metabolites, P_{II} also undergoes a second level of regulation by posttranslational modification. In case of cyanobacterial P_{II} this is achieved by a phosphorylation of the T-loop in dependence of the nitrogen status [64]. Together, all these signals determine the conformation of the surface exposed T-loop which determines the binding of various interaction partners. One of these partners is PipX. When 2-OG levels are low PipX is bound to P_{II}. If 2-OG levels rise, indicating low nitrogen levels, PipX is released and binds its target NtcA. NtcA regulates the expression of genes involved in nitrogen uptake and assimilation and adaptation to nitrogen starvation. When PipX is bound the affinity of NtcA for its target promoters is strongly enhanced. The binding of PipX to NtcA is additionally enhanced by 2-OG interaction with NtcA. Without PipX, NtcA only has a low affinity for its target promoters [65].

5.3 Adaptation to nitrogen limitation

The lack of combined nitrogen sources is one of the most common environmental stress conditions in aquatic and terrestrial ecosystems and therefore frequently faced by cyanobacteria. [56] Adaptation to nitrogen starvation in non-diazotrophic cyanobacteria is characterized by initiation of a developmental program, where cells enter a state of metabolic dormancy, enabling them to outlive long periods of nitrogen deprivation [5]. A lack of nitrogen leads to a high carbon to nitrogen ratio represented by an immediate rise in 2-OG levels, followed by the activation of NtcA as described above. One of the targets of NtcA are the group of *nbl* (“non-bleaching”) genes. Among those genes *nblA*, encodes a Clp protease associated adaptor protein (NblA). The expression of NblA itself is regulated by a very complex network that also includes the other *nbl* genes. In addition, *nbla* is regulated by the Hik33/RpaB two component system. Due to the lack of the precursors provided by nitrogen assimilation, the anabolic reactions for amino acid and nucleic acid synthesis come to halt, leading to uncontrolled accumulation of ATP and reducing equivalents in the cytoplasm. To prevent damage by overreduction of the photosynthetic electron carriers, cells adjust their photosynthetic apparatus through degradation of the phycobilisomes which is mediated by NblA. This adjustment is also found as a response to a limitation of other nutrients but is particularly rapid under nitrogen starvation [14, 66]. The degradation of the phycobilisomes and their associated pigments leads to a change in color from blue-green to yellow-orange. The name chlorosis is derived from this bleaching process. Another immediate response to a C/N imbalance is the high accumulation of glycogen. In fact, all of the carbon fixed by photosynthesis is channeled towards glycogen synthesis [15]. The starting point for fixed CO_2 in primary metabolism is 3-phosphoglycerate (3-PG) in the lower glycolysis. From here 3-PG can either go down the glycolytic route or it can go up the gluconeogenetic route towards glycogen synthesis. A key control point for the fate of 3-PG is the reaction of the 2,3-phosphoglycerate–independent phosphoglycerate mutase (Pgam) which converts 3-PG into 2-PG. To ensure that newly fixed carbon is not deviated towards lower glycolysis the Pgam enzyme is blocked by PirC, a recently discovered competitive inhibitor. Under balanced C/N ratios PirC is bound to P_{II}. When 2-OG levels elevate, PirC is released from P_{II} and binds to

Pgam, blocking its activity [67]. The accumulation of glycogen is essential for a successful chlorosis. Mutants defective in glycogen synthesis show metabolic deficiencies and are impaired in phycobilisome degradation, showing a non-bleaching phenotype. They lose viability within a couple of days [15]. All the events described above can be attributed to the first phase chlorosis which all happen in the first 24 hours. The following second phase is characterized by a gradual decline in metabolic activity due to a drastic intracellular re-organization mainly driven by proteolysis. This involves degradation of thylakoid membranes to a level where only a residual low level of photosynthetic activity remains [68]. After 8 – 14 days the terminal phase 3 and the actual dormant state is. During this state the low-level photosynthesis enables long term survivability [69].

When combined nitrogen sources are available again, chlorotic cells can rapidly recover and restore vegetative cell cycle. This process of resuscitation involves a genetically determined program [2]. The first phase of recovery is determined by an upregulation of genes for ATP synthesis, nitrogen assimilation and translation machinery. This is fueled by a rapid degradation of the previously accumulated glycogen, providing the building blocks by shuffling glucose through the OPP pathway and the energy via respiration [70]. Since the cells are not able to synthesize fresh enzymes at the start of resuscitation, the basis for glycogen degradation was already laid when cells entered chlorosis: Here the glycogen catabolic genes were induced alongside its synthesis but kept inactive to avoid a premature degradation [71, 72]. The start of resuscitation initiates the glycogen degradation by a yet unknown signaling. After 24 hours the cells visibly regreen and restart their photosynthetic activity while still respiring, resulting in a mixotrophic phase. Respiration is continuously decreasing and pure photoautotrophic growth together with cell division continues after 48 hours completing the resuscitation process [2].

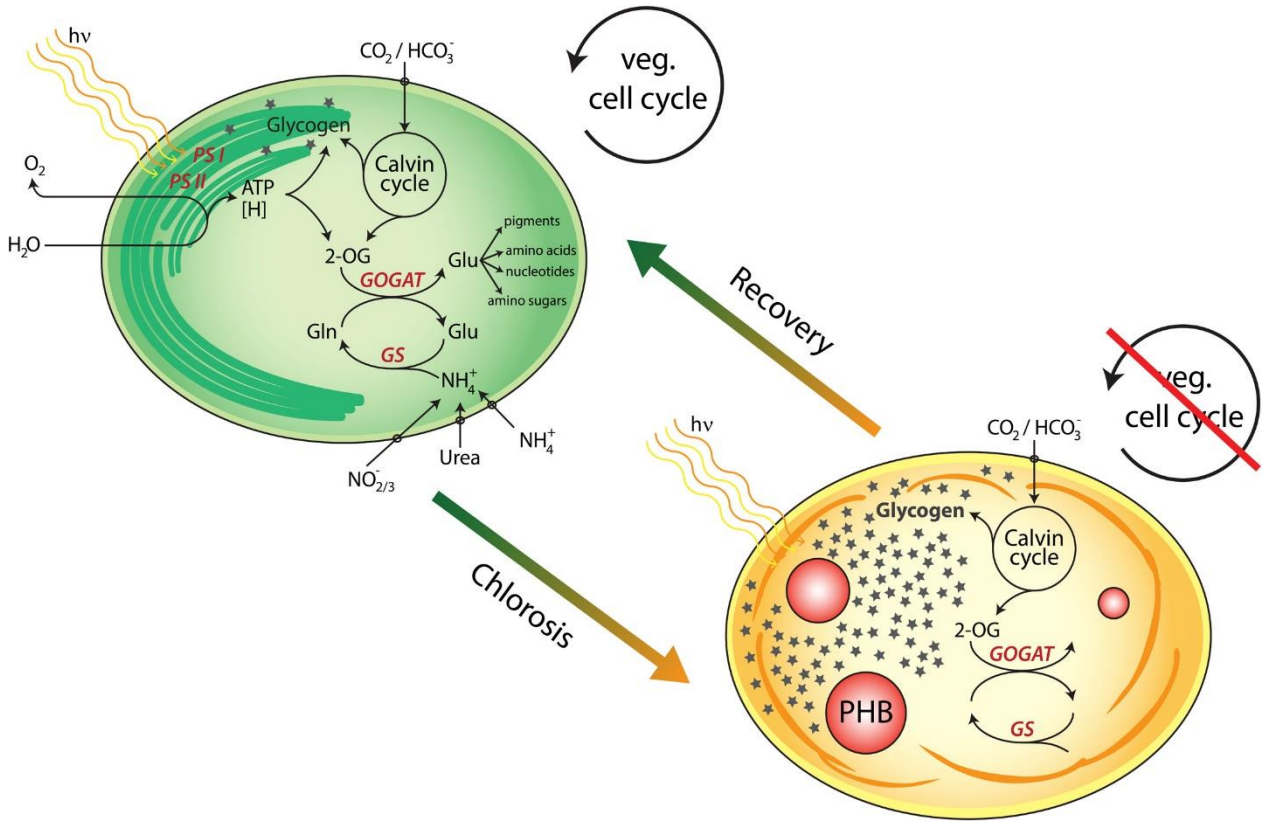

Figure 5: Scheme of *Synechocystis* cells undergoing chlorosis and resuscitation. Adapted from [2].

6. Research questions

Glycogen metabolism plays an essential role in *Synechocystis* for diurnal growth and adaptation to nutrient starvation. The initiation of glycogen synthesis and degradation at the right timepoints is crucial for survivability and indicates a sophisticated regulatory network. For most of the glycogen associated enzymes two isoenzymes are encoded by the genome of *Synechocystis*. While some of these isoforms have been investigated, the role and regulation for the majority of these enzymes has so far only been suggested. In this study the regulation of glycogen metabolism and its associated enzymes were investigated in detail by the following research questions:

1. Glycogen catabolism must be tightly regulated to prevent premature degradation of glycogen. Glycogen phosphorylase (GlgP) catalyzes the first step in glycogen breakdown and the two isoenzymes in *Synechocystis* were shown to be active in different situations. From this we assume that those enzymes are directly regulated in different ways which was investigated in this study.

2. Glycogen debranching enzymes (GlgX) are essential for an efficient degradation of glycogen. The role of the two GlgX isoenzymes and their contribution to glycogen degradation has so far not been investigated.

3. The phosphoglucomutase (PGM) reaction is a central step in glycogen turnover and carbon metabolism in general. Despite this essential role, PGM regulation remained under-investigated. This study aimed on investigating a potential regulation of the two PGM isoenzymes.

4. In eukaryotes it was shown that glycogen can undergo various modifications. Glycogen produced by the two different glycogen synthases (GlgA) in *Synechocystis* has been shown to have different properties. This study addressed if glycogen modifications are also present in prokaryotes and if they affect the properties of the glycogen.

V. RESULTS

The main results of the following publications are summarized in this chapter. This chapter also contains non-published results summarized in a separate section.

Publication 1: Research article

Watzer B., Spät P., **Neumann N.**, Koch M., Sobotka R., Macek B., Hennrich O., Forchhammer K.
The Signal Transduction Protein P_{II} Controls Ammonium, Nitrate and Urea Uptake in Cyanobacteria.
Front Microbiol. 2019 10:1428.

Publication 3: Research article

Selim KA., Haffner M., Burkhardt M., Mantovani O., **Neumann N.**, Albrecht R., Seifert R., Krüger L., Stülke J., Hartmann MD., Hagemann M., Forchhammer K.
Diurnal metabolic control in cyanobacteria requires perception of second messenger signaling molecule c-di-AMP by the carbon control protein SbtB.
Science Advances 2021 • Vol 7, Issue 50

Publication 4: Research article

Doello, S.; **Neumann, N.**; Forchhammer, K.
Regulatory phosphorylation event of Phosphoglucomutase 1 tunes its activity to regulate glycogen metabolism.
FEBS Journal (ahead of print)

Publication 5: Research article

Neumann N., Friz S., Forchhammer K.
Glucose-1,6-bisphosphate, a key metabolic regulator, is synthesized by a distinct family of α-phosphohexomutases widely distributed in prokaryotes

mBio (ahead of print)

Publication 6: Research article

Neumann N., Lee K., Forchhammer K.
On the role of glycogen degrading enzymes in *Synechocystis* PCC6803

1. PII controls nitrogen transporters (Publication 1)

Combined nitrogen is taken up via different types of transporters and permeases for ammonia, nitrate and urea. A P_{II} pull-down analysis indicated a direct interaction of P_{II} with those transporters and permeases. To further analyze this possible interaction a bacterial two hybrid (B2H) assay was used to test interaction with the ABC-type transporters for nitrate (NrtABCD), urea (UrtABCDE) as well as for the ammonia permease Amt1. For the nitrate and urea transporters only the cytoplasmatic localized ATP binding subunits NrtC, NrtD and UrtD, UrtE were tested respectively. As a positive control the known P_{II} interactor PipX was used. The B2H results revealed an interaction of P_{II} with Amt1, NrtC and NrtD of the nitrate transporter, and UrtE of the urea transporter, while no interaction could be detected for UrtD. Thereby, all the interactions were dependent on the orientation of the tagged adenylate cyclase subunit, indicating a specific interaction. In addition to wildtype P_{II}, three different variants of P_{II} have been tested for binding to the transporter subunits: The phosphomimetic variant P_{II}(S49D), the $_{II}$(I86N) variant, showing a change in T-loop conformation and the P_{II}(R9L) variant which shows impaired binding of 2-OG. Interaction with Amt1 was not detectable for the I86N and R9L variants while for S49D a weak interaction was detected. NrtC and NrtD interactions were not detectable for the R9L variant while a weak interaction could be detected for the I86N and S49D variants. The interaction of UrtE was detectable for all tested P_{II} variants, indicating a different, T-loop independent mode of interaction (**Publication 1, Figure 5**).

2. GlgP1 is activated by oxidation (Publication 6)

Degradation of glycogen is essential for survival during dark phases and for resuscitation from chlorosis. The first step in glycogen breakdown is carried out by the glycogen phosphorylase (GlgP). It is crucial that a premature degradation of glycogen is prevented and gets initiated at the right timepoint. An obvious control point is the direct regulation of the GlgP activity. The genome of *Synechocystis* encodes for two isoenzymes of glycogen phsophorylases: *glgp1* (*sll1356*) and *glgp2 (slr1367)*. While it was shown that GlgP2 is essential for glycogen degradation during the night and during resuscitation from chlorosis, GlgP1 is not able to degrade glycogen under these conditions. It was shown that GlgP1 is important under high temperatures but its overall role in the organism is far less understood [48]. The diverging role of those enzymes implies a different mode of regulation.

To get deeper insights into the role and regulation of the two GlgP isoenzymes, both enzymes were overexpressed in *E. coli* and purified. The enzymatic activity has been determined *in vitro* in an enzymatic assay that couples the GlgP1 reaction to the PGM and the G6PDH reaction. As a substrate, glycogen derived from oyster was used. It turned out that both enzymes are active *in vitro* while GlgP1 showed an overall higher catalytic efficiency than GlgP2. Based on hints on a possible redox control of glycogen associated enzymes we tested how the two GlgP enzymes behaved under reducing conditions by adding different reducing agents [73, 74]. Remarkably, GlgP1 activity strongly declined in the presence of reducing agents and stopped following standard Michaelis-Menten kinetics but showed a sigmoidal kinetic profile instead.

GlgP2 activity on the other hand was unaffected. Among the tested reducing agents, DTT and thioredoxin A (TrXA) had the strongest effect on GlgP1 activity **(Publication 6, Figure 1, and Figure 2)**. The activity of the reduced GlgP1 could be restored by treatment with oxidizing agents. This worked best by treatment with H_2O_2 as well as with oxidized glutathione (GSSG) **(Publication 6 Figure 3)**. This results strongly implied that GlgP1 must feature a redox switch that is strongly regulating its enzymatic activity. To figure out where this redox switch is located, we investigated the amino acid sequence as well as the predicted structure of GlgP1 from AlphaFold and discovered a C-terminal domain with two cysteines at position 837 and 842 that were predicted to form a disulfide bond. This motif was not present in GlgP2 **(Publication 6, Figure 4)**. To investigate if this residue is responsible for the redox regulation of GlgP1 a variant of GlgP1 was created where the cysteine at position 837 was replaced by a serine (C837S variant). Enzymatic assays with this variant revealed that activity was strongly reduced and on the level of a fully reduced GlgP1 WT variant. Furthermore, this variant was insensitive to treatment by H_2O_2 or DTT **(Publication 6, Figure 4 and Figure S1)**. This clearly shows that GlgP1 is activated by oxidation and inactive in its reduced state and likely links GlgP1 activity to situations where cells face high rates of ROS production e.g., during light or heat stress.

3. GlgX1 is the main glycogen debranching enzyme (Publication 6)

GlgP activity alone is assumed to be able to degrade around one third of a glycogen granule [75]. Further breakdown requires the cleaving of α-1,6-residues and therefore the activity of a glycogen debranching enzyme (GlgX). GlgX cuts off those branching points and enables GlgP to continue its degradation. Therefore, GlgX is essential for a full and efficient degradation of the glycogen granule. Analogous to GlgP, the genome of *Synechocystis* also encodes for two GlgX isoenzymes, *glgx1* and *glgx2*. The role and the contribution to glycogen degradation of these enzymes in *Synechocystis* has so far not been investigated.

Knockout mutants of *glgx1* and *glgx2* have been created to investigate the role of glycogen debranching enzymes under different growth conditions. Drop plate assays at growth under constant light and growth at diurnal rhythm showed no phenotype for any of the mutants, indicating that neither of the GlgX enzymes is essential for glycogen degradation during the night or that GlgX1 and GlgX2 can compensate for each other in this situation. Drop plate assays during resuscitation from chlorosis revealed a strong impairment for the Δ*glgx1* mutant while a Δ*glgx2* deficient mutant showed no impairment and behaved like the WT. The Δ*glgx1* phenotype got more pronounced if resuscitation was done at day/night rhythm (**Publication 6, Figure 6**). To see if GlgX1 and GlgX2 can enhance GlgP activity both debranching enzymes were overexpressed in *E. coli* followed by purification. The activity was tested by adding the enzymes to the GlgP assay. We found that GlgX1 can enhance the activity of both, GlgP1 and GlgP2 by about 25%. GlgX2 on the other hand did not show any effect on GlgP activity. The results for GlgX1 and GlgX2 indicate that, analogous to GlgP, only one of the isoenzymes is essential during resuscitation. The experiments were all carried out by using glycogen derived

from oyster, which is widely commercially available. To investigate if degradability of glycogen originating from *Synechocystis* differs from oyster glycogen, glycogen was purified from *Synechocystis* cultures that were nitrogen starved for two days. Both glycogen phosphorylases showed a lower activity with *Synechocystis* glycogen compared the oyster glycogen, but the decline in activity was stronger for GlgP2 than for GlgP1. Adding GlgX1 to the assay with *Synechocystis* glycogen showed an enhancement of 80% for GlgP1 and 120% for GlgP2, which was much stronger than for oyster glycogen. Like with oyster glycogen GlgX2 showed no effect on GlgP activity (**Publication 6, Figure 7).** This showed that in case of the *Synechocystis* glycogen, GlgX1 contributes much stronger to overall GlgP activity.

4. Glycogen associated enzymes are linked to carbon uptake and FR signaling **(Publication 3; This part also contains additional data related to the results)**

Transition from day to night in phototrophic organisms leads to various adaptations in the carbon metabolism. This includes uptake of inorganic carbon which is strictly coupled to photosynthetic activity. Cyanobacteria possess a very sophisticated system that includes a circadian clock, sensing of C/N balance, redox sensing and others to adjust their metabolism accordingly. One of the signals used by phototrophic organisms to sense transition from daylight to nighttime is far red light (FR). The signal of far-red light is taken up by phytochromes of which the *Synechocystis* genome encodes for the FR sensing *cph1*. Recently, it has been shown that the diurnal switch for Ci transport activity is also regulated via FR involving the HCO_3^- transporter SbtA and its regulator SbtB [35]. However, a direct link between SbtA/SbtB and Cph1 has not been found yet. Regulation of glycogen metabolism is also associated to carbon uptake and transition from day to night. We showed via a B2H assay that the glycogen branching enzyme (GlgB) interacts with the bicarbonate transport regulator SbtB (**Publication 3, Figure 3**) and that a *sbtb* knockout mutant strongly affects glycogen accumulation. To investigate if glycogen associated enzymes might be related to Cph1 signaling, we performed a B2H assay in which we tested the interaction of Cph1 with the enzymes involved in glycogen turnover. This assay clearly revealed an interaction of C-terminal tagged Cph1 with N-terminal tagged GlgA2, GlgB and GlgP1. A weak interaction could also be detected for GlgA1 while no interaction could be detected for GlgP2, GlgC and PGM (**Figure 6**). GlgX1 and GlgX2 were excluded from the assay because they continuously show unspecific interaction in various assays tested (data not shown). This results clearly indicate an interaction of glycogen associated enzymes with Cph1. Intriguingly, GlgB is an interaction partner of both, SbtB and Cph1. Therefore, GlgB might be linking Cph1 signaling to carbon uptake by SbtB.

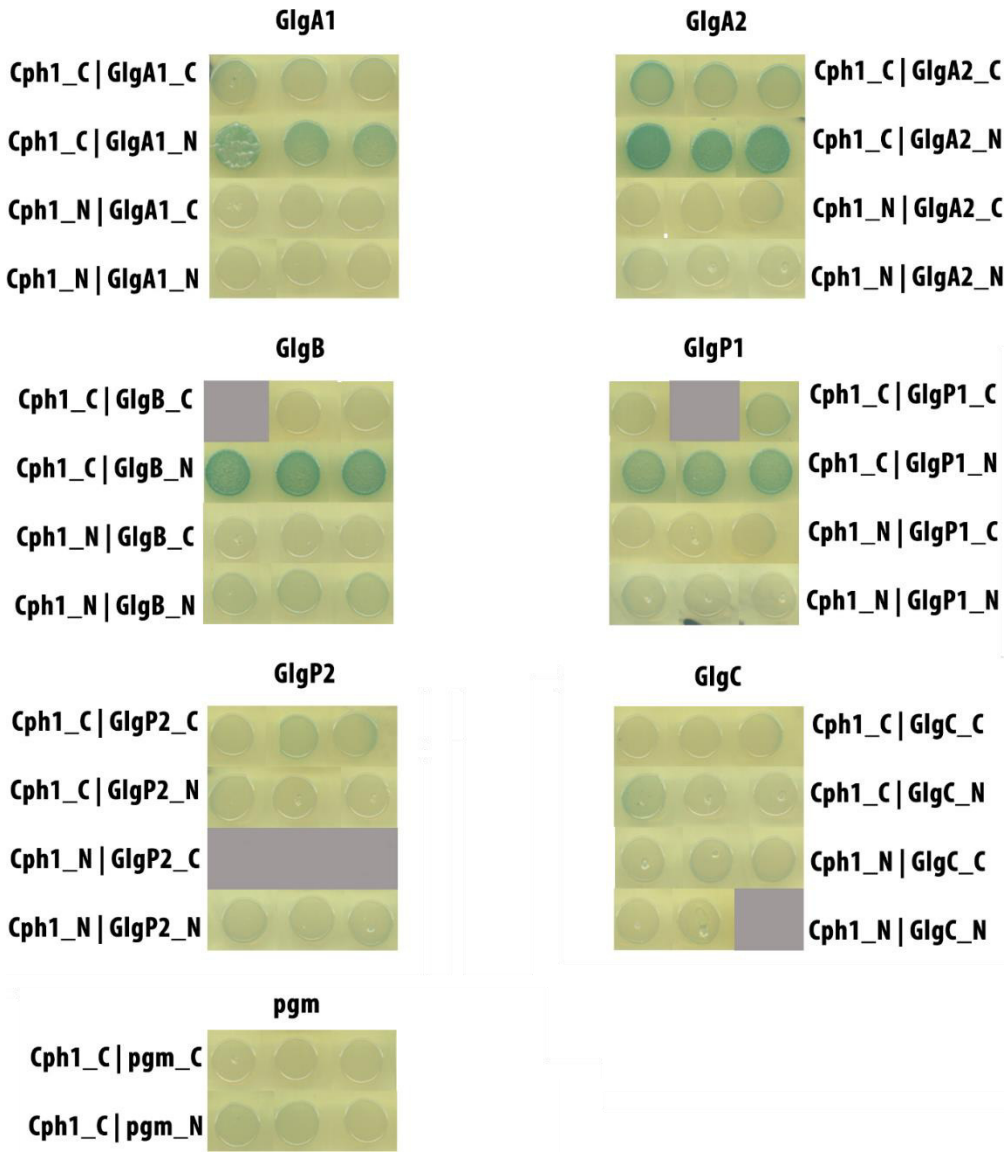

Figure 6: B2H assay of Cph1 tested against glycogen associated enzymes on LB-X-Gal plates. Blue colonies indicate a positive interaction. No colonies were obtained for areas in grey.

5. Slr1334 is the first identified bacterial glucose-1,6-BP synthase
(Publication 5)

One of the essential reactions in carbon metabolism is the interconversion of Glc-1P to Glc-6P and vice versa carried out by phosphoglucomutase (PGM). Of the two annotated PGM enzymes in *Synechocystis,* Sll0726 is responsible for the majority of the PGM activity. The role of Slr1334, on the other hand, remains elusive, but it has been shown that it is an essential enzyme [49]. To gain deeper insights in the diverging roles of the two PGMs we purified both enzymes after overexpression in *E. coli* and determined their enzymatic activity and kinetic parameters. This confirmed the low PGM activity of Slr1334 compared to Sll0726 (**Publication 5, Figure 2**). The PGM reaction is strongly dependent on the activator Glc-1,6-BP, responsible for efficient phosphorylation of the active site serine. When Glc-1,6-BP was added to the assay, both enzymes were strongly enhanced in their catalytic efficiency as expected. This was primarily a result of a strongly reduced K_M. When the enzymatic assay was performed with Frc-1,6-BP as effector instead, the two enzymes behaved fundamentally different: Sll0726 was strongly inhibited due to an increase in K_M. This was not surprising since an inhibitory effect of Frc-1,6-BP on PGM enzymes has been reported before [76, 77]. However, for Slr1334 the K_M was reduced strongly and catalytic efficiency of Slr1334 increased by 50-fold in the presence of Frc-1,6-BP. We considered two ways to explain this phenomenon on Slr1334: First, Frc-1,6-BP might act as an alternative activator for Slr1334 by phosphorylating its active site like Glc-1,6-BP. Second, Slr1334 might utilize Frc-1,6-BP to form a product, probably Glc-1,6-BP, out of Frc-1,6-BP that leads to strong activation. To investigate if such a product is formed Slr1334 was incubated with Frc-1,6-BP alongside other phosphosugars. The supernatant of this reaction was used to see if Sll0726 activity gets enhanced. This revealed that Slr1334 in fact forms a product by using Frc-1,6-BP and either Glc-1P or Glc-6P that activates Sll0726 in the same way as Glc-1,6-BP. We figured out that this product was also formed by incubation with 1-3-BPG instead of Frc-1,6-BP but at a much lower efficiency **(Publication 5, Figure 3)**. A subsequent LC/MS analysis confirmed that the formed product was indeed Glc-1,6-BP (**Publication 5, Figure 4**). This makes Slr1334 the first identified Glc-1,6-BP synthase in bacteria and the first enzyme known to use Frc-1,6-BP for this reaction. In a follow-up experiment we could show that Slr1334 was also catalyzing the reverse reaction by using Glc-1,6-BP and Frc-6P to form Frc-1,6-BP and Glc-1P/6P (**Publication 5, Figure 6**). Due to its essential role in PGM activation and use of glycolysis intermediates, we assume Slr1334 to be a major regulator of central carbon metabolism.

6. Homologues of Slr1334 and Sll0726 are widespread in prokaryotes **(Publication 5 and publication 6)**

Slr1334 is a member of a large subfamily of phosphohexomutases (PHM) that is widespread in prokaryotes. To see if other members of this subfamily might be able to carry out the Glc-1,6-BP synthase reaction as well, we purified the Slr1334 homologue from the human commensal bacterium *Bacteroides salyersiae* to test if it also shows Glc-1,6-BP synthase activity. Indeed, like Slr1334, the *Bacteriodes salyersiae* enzyme showed low PGM activity but was able to carry out the Glc-1,6-BP synthase reaction (**Publication 5, Figure 7**). Based on this result we assume that the Glc-1,6-BP synthesis might be a general feature of this subfamily. The characteristic N-terminal serine which was discovered to strongly control Sll0726 activity is also conserved in certain PHM subfamilies (**Publication 4, Figure 4; Publication 5, Figure 1**). The findings for *Synechocystis* PGMs might therefore be highly relevant for other organisms carrying those PHM subfamilies and expand our knowledge of carbon metabolism and its regulation.

7. Additional research

7.1 GlgP1 and GlgP2 differ in their putative interaction partners

During chlorosis the carbon catabolic enzymes needed at the start of resuscitation must already be present since chlorotic cells are not able to synthesize new proteins up until their protein biosynthetic machinery has been restored. This includes enzymes for glycogen breakdown like GlgP. These enzymes must remain in an inactive state during chlorosis and must immediately become active once the resuscitation program is induced. While the above results revealed a redox regulation of GlgP1, a regulation of the essential GlgP2 has not been found so far. A reasonable assumption is that the signaling for the activation of glycogen breakdown relates to the re-availability of combined nitrogen sources and is transmitted via protein-protein interaction. To test for possible interaction partners for GlgP1 and GlgP2, we bound the purified affinity tagged enzymes to magnetic beads and incubated them with cell extract of cultures that were nitrogen starved for two weeks and where resuscitation was initiated 12 h ago respectively. After several washing steps, the remaining proteins were analyzed via quantitative proteomics. From the proteins identified we calculated the ratio between the GlgP1 and GlgP2 pulldown to see which proteins are specifically enriched and to see how the abundance of these proteins is changing between chlorosis and resuscitation. **Figure 7** shows a scatter plot of the most significantly enriched proteins for GlgP1 and GlgP2 during chlorosis and resuscitation. **Figure 8** shows the proteins with the highest change in abundance between chlorosis and resuscitation.

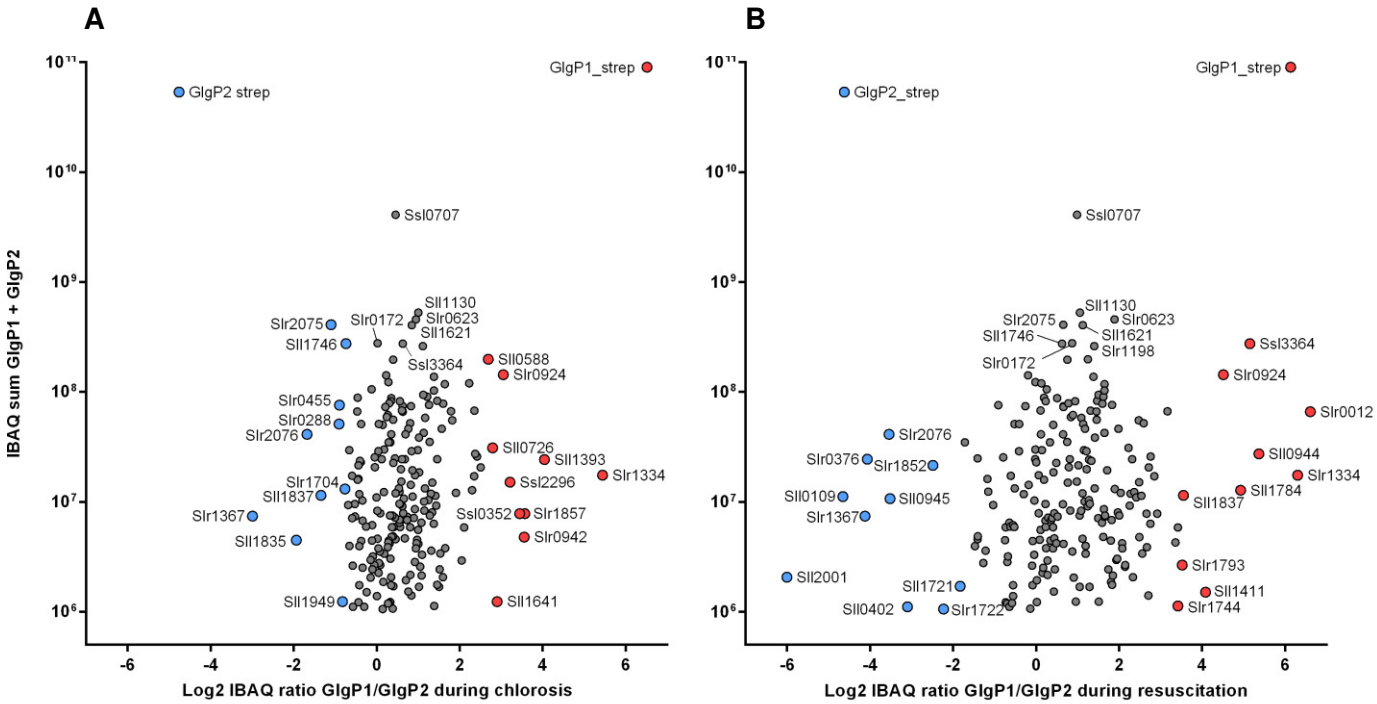

Figure 7: Scatter plot of the ratio of proteins identified in the GlgP1 and GlgP2 pulldown. (A): proteins identified during chlorosis (14d); (B): proteins identified during resuscitation (12h). Red dots indicate proteins with the highest abundance in GlgP1; blue dots represent proteins with highest abundance in GlgP2; gray dots represent other proteins that were not specifically enriched.

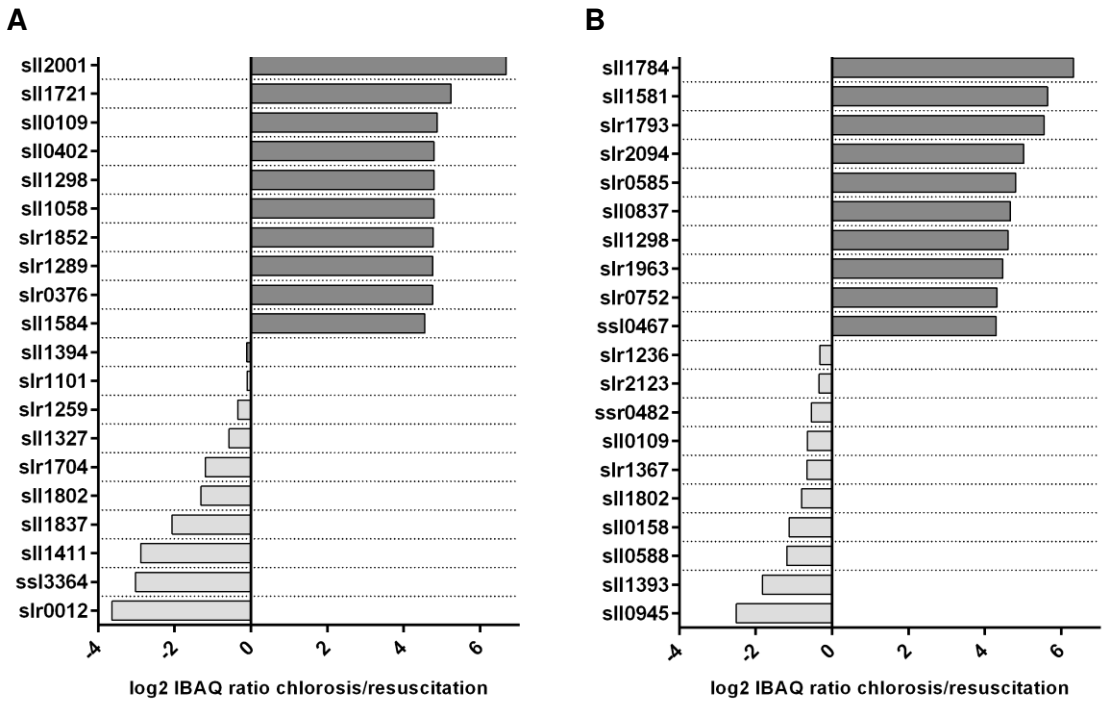

Figure 8: Ratio of protein abundance in chlorosis and resuscitation for GlgP1 (A) and GlgP2 (B). Light grey bars show proteins with biggest decrease in abundance from chlorosis to resuscitation; dark grey bars show proteins with the strongest increase in abundance.

Protein ID	Annotated function	Protein ID	Annotated function
Sll2001	leucine aminopeptidase	Slr0376	hypothetical protein
Sll0109	chorismate mutase	Slr0455	hypothetical protein
Sll0158	1,4-α-glucan branching enzyme (GlgB)	Slr0585	argininosuccinate synthetase
Sll0402	aspartate aminotransferase	Slr0752	enolase
Sll0588	unknown protein	Slr0924	periplasmic protein, function unknown
Sll0726	phosphoglucomutase (PGM)	Slr0942	alcohol dehydrogenase [NADP+]
Sll0837	periplasmic protein, function unknown	Slr1101	hypothetical protein
Sll0944	P_{II} interacting regulator PirC	Slr1236	hypothetical protein
Sll0945	glycogen synthase (GlgA1)	Slr1259	hypothetical protein
Sll1058	dihydrodipicolinate reductase	Slr1289	isocitrate dehydrogenase (NADP+)
Sll1298	putative carboxymethylenebutenolidase	Slr1334	PGM/Glc-1,6-BP Synthase
Sll1327	ATP synthase gamma chain	Slr1367	glycogen phosphorylase (GlgP2)
Sll1393	glycogen (starch) synthase (GlgA2)	Slr1704	hypothetical protein
Sll1394	peptide methionine sulfoxide reductase	Slr1722	inosine-5-monophosphate dehydrogenase
Sll1411	hypothetical protein	Slr1744	N-acetylmuramoyl-L-alanine amidase
Sll1433	hypothetical protein	Slr1793	transaldolase
Sll1581	hypothetical protein	Slr1852	unknown protein
Sll1584	ferredoxin like protein	Slr1857	isoamylase
Sll1641	glutamate decarboxylase	Slr1963	water-soluble carotenoid protein
Sll1721	PDH E1 component, β subunit	Slr2075	10kD chaperonin
Sll1746	50S ribosomal protein L12	Slr2076	60kD chaperonin
Sll1784	unknown protein, preriplasmic	Slr2094	FBP/SBPase
Sll1802	50S ribosomal protein L2	Slr2123	similar to 3-PG dehydrogenase
Sll1835	unknown protein, periplasmic	Ssl0352	hypothetical protein
Sll1837	unknown protein, periplasmic	Ssl0467	unknown protein
Sll1949	unknown protein	Ssl2245	unknown protein
Sll2001	leucine aminopeptidase	Ssl2296	pterin-4a-carbinolamine dehydratase
Slr0012	RuBisCO small subunit	Ssl3364	CP12 polypeptide
Slr0288	glutamate-ammonia ligase (GS)	Ssr0482	30S ribosomal protein S16

Table 1 Legend of the most abundant proteins identified in Figures 6 and 7.

We discovered a strong difference between the proteins bound to GlgP1 and GlgP2 during both resuscitation and chlorosis. For GlgP1 we found a strong enrichment of the glycogen associated proteins Sll1393 (GlgA2) and Slr1857 (GlgX2). Interestingly together with GlgP1 those are the glycogen associated proteins that are considered non-essential during chlorosis and resuscitation. During resuscitation we did not find those proteins to be significantly enriched anymore in GlgP1. The strongest enrichment we found for GlgP1 was the essential Slr1334 (PGM/glucose-1,6-BP synthase) in both chlorosis and resuscitation. In case of GlgP2 we found

the alternative glutamine synthetase GlnN (Sll0288), which was enriched in chlorosis but not in resuscitation. Furthermore, we found the proteins Sll1835 and Sll1837 and the heat shock proteins Slr2075 and Slr2076 strongly enriched in GlgP2 during chlorosis. During resuscitation we identified Sll0945 (GlgA1) to be strongly enriched in the GlgP2 fraction, which is the essential glycogen synthase for chlorosis. Together with GlgA2 (Sll1393) and GlgB (sll0158) those are the enzymes that increase the most in abundance in resuscitation (**Figure 7**). Additionally, we identified several proteins involved in nitrogen and carbon metabolism: Sll0402 is an aspartate aminotransferase using 2-OG and forms glutamate and oxalacetate, which connects this enzyme directly to the C/N ratio. Sll0109, a chorismate mutase, and Sll2001, a leucine aminopeptidase, are both involved in amino acid catabolism. Furthermore, we found the hypothetical protein Slr0376 (Ycf46) involved in CO_2 utilization as one of the strongest enriched proteins in GlgP2 in resuscitation [78]. Since GlgP enzymes are known to be homodimers, we would expect that the enzymes also interact with GlgP1 and GlgP2 in the cell extract. However, this is only the case for GlgP2 where we can detect WT GlgP2 besides the affinity tagged version. In the GlgP1 samples only the affinity tagged GlgP1 was detected.

7.2 Modifications of the glycogen granule

Like for the other glycogen associated enzymes, the *Synechocystis* genome harbors two paralogous genes for glycogen synthesis, *glga1* (*sll0945*) and *glga2* (*slr1393*). Studying Δ*glga1* and Δ*glga2* knockout mutants revealed that both glycogen synthases produce comparable total amounts of glycogen but a Δ*glga1* mutant is non-viable when entering chlorosis [1]. The difference between glycogen produced by GlgA1 and GlgA2 could be caused by different modifications. While several glycogen modifications have been shown in eukaryotes, there are no studies at all in prokaryotes [43]. Since glycogen accumulation happens rapidly in the first two days of chlorosis, we investigated if not only the total amount but also the ratio of glycogen accumulation is comparable in the two Δ*glga* mutants. Therefore, the glycogen content of *Synechocystis* Δ*glga1* and Δ*glga2* mutants was measured during chlorosis over time and compared with glycogen content of the WT. The result confirmed that both glycogen synthases form the same total amounts of glycogen, but also that synthesis happens equally fast and peaks after around 24 hours (**Figure 9**). While it has been shown that the average chain length, an indicator for the branching pattern, of Δ*glga1* and Δ*glga2* glycogen is comparable to glycogen from the WT, we wanted to answer the question of what is causing the different properties of the glycogen produced by the two synthases [79]. Assuming different glycogen modifications would result in a different density of glycogen, we purified glycogen from WT, Δ*glga1* and a Δ*glga2* mutant and applied it on a continuous gradient ranging from 15 to 75% glycerol (w/w) followed by ultracentrifugation until an equilibrium was reached. Thereby, a difference in sedimentation behavior indicates a difference in density.

Two different methods of glycogen purification were established and used:

1. An extraction where disrupted cells are heated and glycogen is precipitated by in a final step by ethanol. This leads to a clean glycogen extraction, but most likely causes denaturation of all attached proteins.

2. A method where glycogen was purified from the cell extract by different centrifugation steps. This method, while less clean, can preserve proteins that might be attached to glycogen.
(See chapter "Material and Methods of the Additional Results for detailed description)

Strikingly, the sedimentation behavior of the different glycogen fractions differed clearly from each other: Δ*glga1* glycogen showed a lower average density with a high heterogeneity and spreaded over a large area of the gradient. In contrast, Δ*glga2* glycogen showed the highest density, sedimenting below the other fractions. The glycogen from WT appeared to be a mix of the Δ*glga1* and Δ*glga2* fractions, sedimenting at a height between glycogen from Δ*glga1* and Δ*glga2*. On a closer look, the WT glycogen showed two distinguishable fractions of glycogen separated by a thin band with seemingly low glycogen content. Interestingly, the glycogen extracted under the two different methods behaved exactly the same in the gradient centrifugation, which led us to the conclusion that the difference in density and sedimentation behavior is not caused by bound proteins but by other modifications such as phosphorylation which was reported for glycogen in eukaryotes.

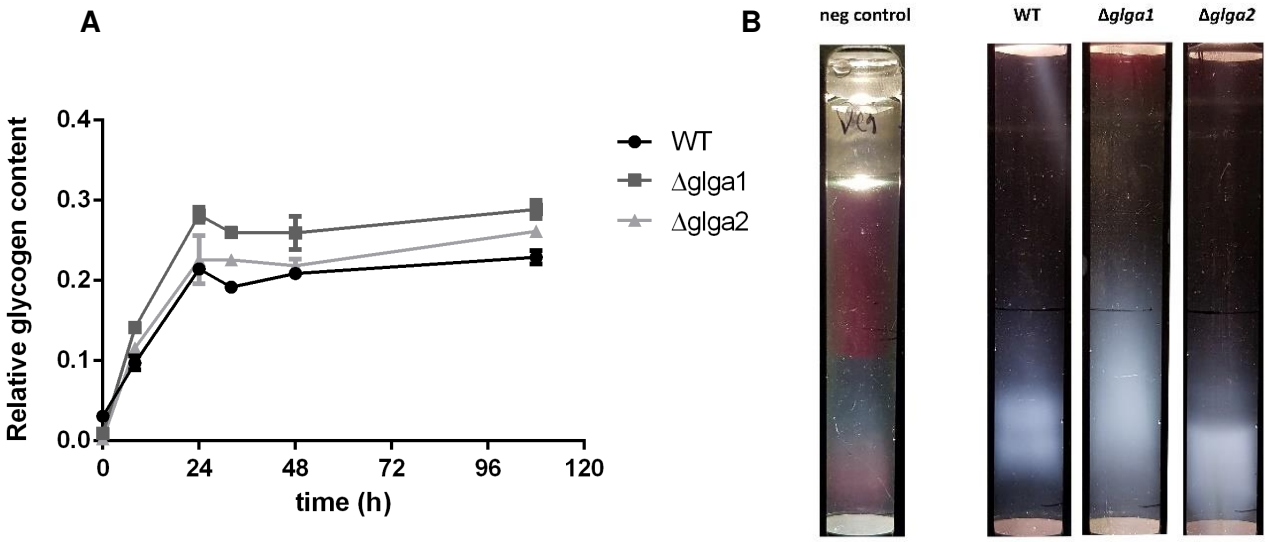

Figure 9: (A): Glycogen content during chlorosis over time for *Synechocystis* WT (black dots), Δ*glga1* mutant (dark grey squares) and Δ*glga2* (light grey triangles). Values are means of triplicates, error bars represent the SD. (B): Purified glycogen on a 15 to 75% glycerol gradient after 12h of ultracentrifugation from WT, *Δglga1* and *Δglga2* chlorotic cells (48h). Glycogen is visible as a white precipitate. As a negative control, extract from vegetatively growing cells under constant light was used.

To investigate if glycogen in *Synechocystis* is in fact modified by phosphorylation, we treated glycogen purified from *Synechocystis* WT and a Δ*glga1* mutant (Δ*glga2* glycogen was not available at this timepoint) with alkaline phosphatase (AP) for 30 minutes, which should cleave of phosphorylation sites and lead to the release of inorganic phosphate (Pi). When using this AP treated glycogen for the GlgP assay, we observed that GlgP activity was negatively correlated with AP treatment. The decline in activity was significantly stronger for GlgP1, which showed around 40% remaining activity for the WT glycogen and 20% remaining activity for the Δ*glga2* glycogen. GlgP2 on the other hand showed about 75% remaining activity for WT glycogen, while glycogen from Δ*glga2* did not show a significantly decline in activity after AP treatment. A phosphate measurement revealed that AP treatment released higher amounts of free phosphate compared to the untreated control. More phosphate was released for Δ*glga2* and the released phosphate correlates with the stronger activity decline in GlgP1. Interestingly, also untreated glycogen gave a phosphate signal. This might be due to contaminations with phosphate from the purification process or due to the very low pH of the phosphate detection assay, which could lead to phosphate release by hydrolysis. These results indicate that *Synechocystis* glycogen is phosphorylated. Removing this phosphorylation is negatively affecting GlgP activity with a stronger effect for GlgP1 than for GlgP2. Thereby, the amount of phosphate incorporated might differ for glycogen produced by different glycogen synthases.

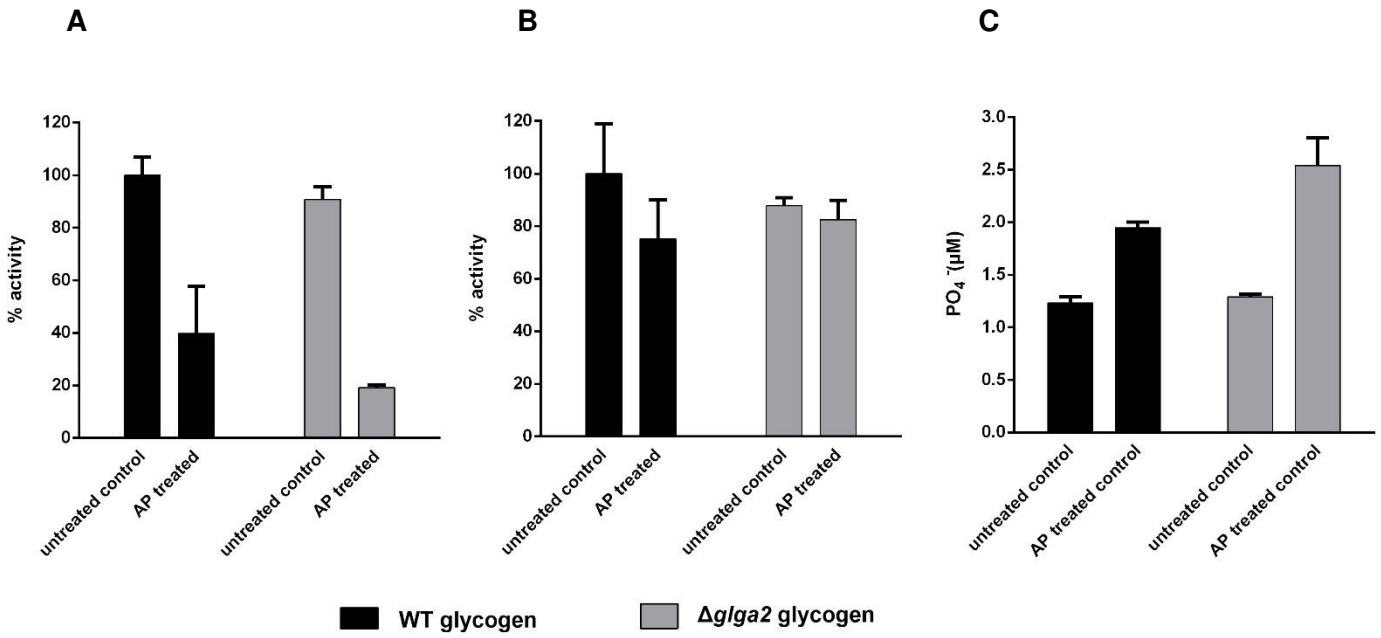

Figure 10: (A) and (B) shows the GlgP activity with glycogen purified from *Synechocystis* WT. (A): GlgP1 activity for glycogen treated with 1U of AP for 30 min compared against an untreated control which was considered 100%. Black bars: WT glycogen; grey bars: Δ*glga2* glycogen. (B): same as (A) but for GlgP2. Values are means of triplicates. Error bars represent the SD.
(C): Shown is the OD_{650} representing the relative phosphate concentration quantified by a malachite green assay. In black WT glycogen; in dark grey *Δ*glga2 glycogen. Values are means of triplicates. Error bars represent the SD.

7.3 A first insight into the glycogen proteome

The regulation of glycogen turnover during chlorosis and resuscitation is still under investigation. Potential regulators that also determine the glycogen properties are proteins which are directly attached to the glycogen granule itself. To gain insights into the glycogen proteome, we purified glycogen from *Synechocytis* WT, with a method that preserves proteins potentially bound to glycogen. After application to a glycerol gradient, the different fractions were carefully collected using a gradient fractionater and prepared for quantitative proteomic analysis. **Table 2** shows the 10 most abundant proteins in the glycogen containing fractions.

Protein ID	Annotated function
Sll0185	hypothetical protein
Sll6055	hypothetical protein
Sll0735	hypothetical protein
Sll1665	unknown protein
Sll1342	NAD(P)-dependent glyceraldehyde-3P
Slr0483	dehydrogenase hypothetical protein
Sll1356	glycogen phosphorylase (GlgP2)
Sll1393	glycogen (starch) synthase (GlgA2)
Sll1621	thioredoxin-dependent peroxiredoxin
Sll1769	hypothetical protein
Sll0982	unknown thylakoid associated protein
Sll1638	unknown protein

Table 2: Most abundant proteins in the glycogen containing fractions

Of those identified proteins Sll0185 and Sll0735 appeared to be promising candidates for further investigation: Sll0185 was the most abundant protein in the glycogen fractions and is strongly regulated by the response regulator Rre37 which is responsible for the upregulation of sugar catabolic genes during nitrogen starvation [71]. Sll0735 is annotated as a potential glucan branching enzyme, making it an obvious candidate for direct glycogen association. To investigate which role those proteins might have in the regulation of glycogen turnover during chlorosis and resuscitation, we created knockout mutants of *sll0185* and *sll0735* and tested the strains for survivability during chlorosis and resuscitation. Additionally, we also measured glycogen accumulation during chlorosis. It turned out that both knockout strains can perform a successful chlorosis and resuscitation without visible impairment. Although we detected a decrease in OD_{750} for the Δ*sll0735* mutant after two weeks of chlorosis, this did not result in a delayed or worse resuscitation when cells were supplied with nitrogen (**Figure 11**). Glycogen accumulation was comparable in all strains until day 7 where Δ*sll0735* started to show a slight decline in glycogen content, which was still detectable at the final measurement after two weeks

(Figure 12). This lower amount of glycogen is in line with the observed drop in OD_{750} but ultimately does not seem to affect survivability during chlorosis and resuscitation in our test scenario. It is possible that the observation period was too short and a longer period of chlorosis would lead to further decline in OD_{750} and glycogen content, which could lead to a manifestation of a phenotype for Δ*sll0735*. However, from these results we conclude that Sll0185 and Sll0735, while potentially associated with glycogen, do not play a crucial role during chlorosis and resuscitation.

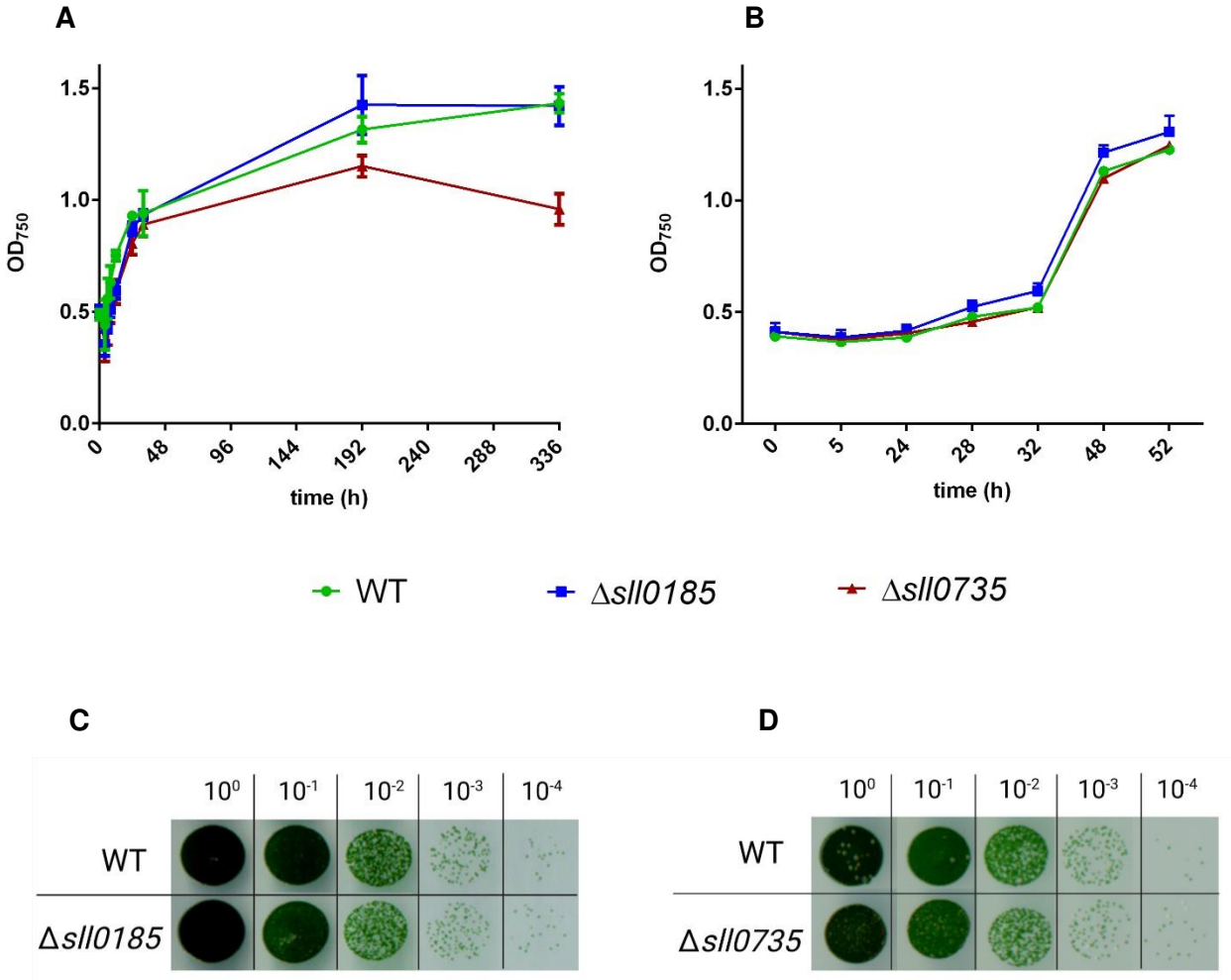

Figure 11 (A) and (B): OD_{750} of *Synechocystis* WT (green dots); Δ*sll0185* (blue squares) and Δ*sll0735* (red triangles) during chlorosis (A) and resuscitation (B). Values are means of triplicates. Error bars represent the SD.
(C) and (D): Drop viability assays of resuscitating cells from Δ*sll0185*; (C) Δ*sll0735* (D).

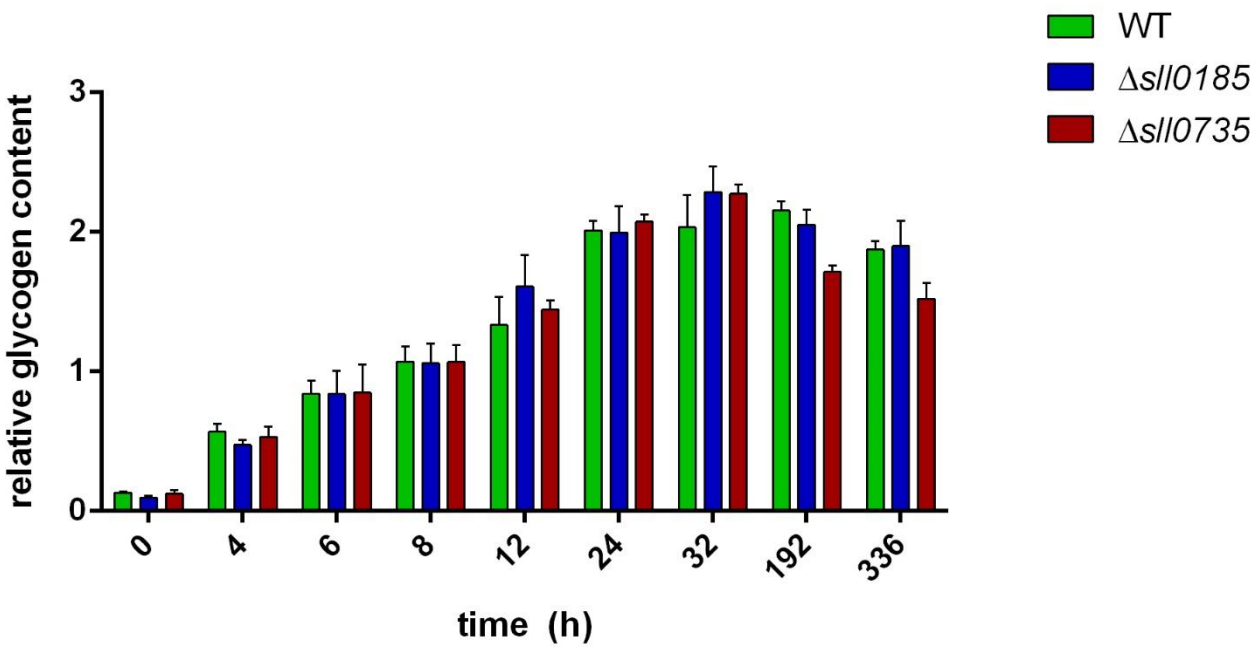

Figure 12 Relative glycogen content during different timepoints of chlorosis of *Synechocystis* WT (green), Δ*sll0185*(blue) and Δ*sll0735* (red). Values are means of triplicates. Error bars represent SD.

8. Material and Methods of the Additional Results

8.1 Cultivation of *Synechocystis*

If not otherwise stated all strains used on this study were grown in BG_{11} supplemented with 5 mM $NaHCO_3$ as described by [10]. Nitrogen starvation was induced by washing two times with $BG_{11\text{-}0}$, which contains all BG_{11} components except for $NaNO_3$ [2, 16]. For resuscitation 17 mM $NaNO_3$ was added to nitrogen starved cells in $BG_{11\text{-}0}$. Cultivation of *Synechocystis* cells was performed at continuous illumination (50 to 60 µmol photons m^{-2} s^{-1}) and continuous shaking (130 to 140 rpm) at 27 °C. For cultivation of mutant strains medium was supplemented with the appropriate concentration of antibiotics.

8.2 Protein purification

Protein purification was performed as described in **publication 6**.

8.3 Glycogen quantification

Glycogen content was quantified as based on [15]: For every sample 2 mL of culture were collected and pelleted by centrifugation. The pellet was washed with MilliQ water, followed by another centrifugation step. Cell lysis was performed by resuspending the pellet in 1 mL of 30% KOH and incubation at 95°C for 2h in a heating block. For glycogen precipitation ice-cold ethanol was added to a final concentration 70% followed by an overnight incubation at -20 °C. After incubation, glycogen was pelleted by centrifugation at 20000 g for 10 min at 4 °C. The supernatant was carefully removed and the pellet was carefully washed with 70% ethanol and 98% absolute ethanol, consecutively. After removing the supernatant, the glycogen pellet was dried and resuspended in 1 mL of sodium acetate (pH 4.5). For glycogen digestion 35 U of amyloglucosidase (10115, Sigma Aldrich) were added and incubated for 2 h at 60°C. For glycogen quantification 200 µl of the samples were mixed with 1 mL of 6% O-toluidine in acetic acid and incubated at 100 °C for 10 min. Absorbance was then detected at 635 nm in a photometer. Glycogen concentration was calculated by using a glucose calibration curve. At least three biological replicates have been measured for every condition.

8.4 Creation of crude cell extracts

For cell disruption the pellet was resuspended in 750 µL lysis buffer (100 mM Tris, 10 mM MgCl, pH 7.6) complemented with lysozyme, “Roche cOmplete protease Inhibitor” and DNAse and incubated on ice for one hour. After incubation cells were transferred in a 1.5 mL screw top vial containing a sufficient amount of glass beads. Lysis was performed five times for 20 s at 6.5 m/s with 5 min intervals in between using the FastPrep®-24 Ribolyser (MP Biomedicals Cell disruption was performed in a FastPrep 245 G homogenizer (MP Biomedicals, Irvine, USA) at 4°C. Avoiding the glass beads the supernatant was transferred into a fresh 1.7 mL centrifugation tube and kept on ice.

8.5 Glycogen purification from *Synechocystis*

Cultivation of *Synechocystis* for glycogen purification

For glycogen extraction 1l of *Synechocystis* cultures were grown in 2l Erlenmeyer flasks. Cultivation, harvesting and cell lysis was performed as described above.

Purification Method A (denaturing)

For glycogen purification under denaturing conditions the cell extract was centrifuged at 20000g for 10 minutes. Avoiding the pellet, the supernatant was transferred into a new 1.7 ml centrifugation tube. and incubated in a heating block at 85°C for 10 minutes, denaturing the majority of the protein. Subsequently, centrifugation at 20000g for 5 minutes was performed. Avoiding the pellet, the supernatant was transferred into a fresh 1.7 mL centrifugation tube. Absolute ethanol was added until a concentration of 80% ethanol was reached. Centrifugation

was performed for 5 minutes at 20000g resulting in a white pellet of glycogen. Supernatant was carefully removed by pipetting and the pellet was washed two times with 70% ethanol. Glycogen pellet can be air dried or by using a vacuum concentrator. Purification from 1l of chlorotic *Synechocystis* cultures should result in roughly 30 mg of glycogen.

Purification Method B (non-denaturing)

All centrifugation steps are performed at 4°C. First the supernatant is centrifuged at 20000g for 10 minutes. Avoiding the soft pellet, the supernatant is carefully transferred into a fresh 1.7 mL centrifugation tube. Another centrifugation step is performed at 25000g for 60 minutes leading to the formation of a yellowish/brownish pellet. The supernatant is carefully extracted and discarded using a pipette. Pellet is resuspended in 1 mL of buffer by vortexing thoroughly. Pellet washed/resuspended in 1 ml Buffer (100mM Tris, 10mM MgCl, pH 7.6). A series of 3 x 5 min centrifugations at 20000g is performed. After each centrifugation the supernatant is transferred into a fresh 1.7 mL centrifugation tube. A final centrifugation step is performed at 25000g for 60 minutes. Supernatant is discarded and the pellet is directly used for further experiments.

8.6 Pull-down assays

MagStrep “type3” XT Beads were aliquoted (150 µl) and washed twice with 1 ml binding buffer (50 mM HEPES, 100 mM KCl, pH 7.5) for equilibration. Then 10 µM of purified GlgP1 and GlgP2 strep tagged protein were added respectively and incubated under agitation on an orbital shaker for 30 minutes at RT. Beads were washed again and cell extracts of chlorotic or resuscitating *Synechocystis* cells were added and incubated for another 30 min on an orbital shaker. The supernatant was removed and crude extract of chlorotic and resuscitating cells was added respectively. Incubation on an orbital shaker for 30 minutes. Supernatant was removed and beads were washed four times with binding buffer.

Elution

Preparation for proteomic analysis

8.7 Bacterial two hybrid assays

B2H assays were performed as described in publication 1

VI. DISCUSSION

1. Slr1334 is the first bacterial Glc-1,6-BP synthase

The interconversion of Glc-1P to Glc-6P and vice versa is one of the key reactions in central carbon metabolism. The reaction is carried out by phosphoglucomutase (PGM), a member of the αPHM superfamily, which is widespread in all domains of life. It is known since a long time that PGM activity is dependent on the activating compound Glc-1,6-BP, which is needed for keeping the active site serine of PGM in a phosphorylated state. Therefore, the levels of Glc-1,6-BP are a strong regulator for PGM activity. Despite PGMs essential role in carbon metabolism no Glc-1,6-BP synthesizing enzyme was identified in prokaryotes so far. In this work the cyanobacterial model organism *Synechocystis* was used to identify Slr1334 as the first bacterial Glc-1,6-BP synthase.

1.1 Glc-1,6-BP and its role in carbon metabolism

The results of this work clearly showed that Slr1334 is a Glc-1,6-BP synthase, utilizing Frc-1,6-BP and Glc-1P or Glc-6P to form Glc-1,6-BP. Being the first identified prokaryotic Glc-1,6-BP synthase, the discovery of this enzyme closes a long-overlooked gap in carbon metabolism. As expected, Glc-1,6-BP is strongly activating Sll0726 which is responsible for the majority of PGM activity in *Synechocystis* [49]. However, while it was shown that a *sll0726* knockout mutant is viable under conditions which don't rely on glycogen turnover, attempts to knockout *slr1334* failed in other studies [49]. This indicates that Glc-1,6-BP might have further targets besides PGM. Those targets likely include the other members of the PHM superfamily, which might get activated by Glc-1,6-BP as well. This is because all members of the αPHMs superfamily work after the same reaction principle, which involves the formation of a bisphosphorylated intermediate. In case of the other phosphohexose converting reactions common in bacteria, carried out by PMM and PGNM, these intermediates would be α-d-mannose-1,6-BP and α-d-glucosamine-1,6-BP. Inferred from the effect of Glc-1,6-BP on PGM, those intermediates would also serve as activating compounds for their corresponding phosphohexomutases. However, these intermediates are not known to be formed as free metabolites by any reaction. Therefore, it was suggested that Glc-1,6-BP could serve as a general activator for those enzymes. This is supported by the fact that all members of the PHM superfamily show at least some residual PGM activity, making it likely that Glc-1,6-BP can enter their active site [80]. In fact, it has been shown that an *E. coli* that PGNM gets activated in the presence of Glc-1,6-BP [81]. This enzyme carries out one of the central reactions in amino-sugar metabolism and is considered essential. In *Synechocystis* PNGM is expressed by *sll1758 (glmM)*. The lack of Glc-1,6-BP would greatly diminish GlmM activity and would be one of the reasons for the failed knockout attempt on *slr1334*. Besides members of the PHM superfamily, other targets of Glc-1,6-BP were identified in the central carbon metabolism in mammals. Here, an inhibitory effect was shown for hexokinases, 6-phosphogluconate dehydrogenase and fructose-1,6-bisphosphatase, while an activating effect was shown for

phosphofructokinase and pyruvate kinase [82]. The fact that all these enzymes are part of central carbon metabolism and highly conserved among most organisms from all domains of life makes it likely that glucose-1,6-BP can also regulate those enzymes in prokaryotes. In addition, it was shown that Glc-1,6-BP is especially elevated in brain tissue, where a low level of Glc-1,6-BP can lead to severe neurological disorders in newborns [83]. Therefore, it is assumed that at least in mammalian brain there are other targets and roles of Glc-1,6-BP that have yet to be discovered. A main difference to the mammalian glucose-1,6-BP synthase is that Slr1334 uses Frc-1,6-BP for Glc-1,6-BP generation. While Glc-1,6-BP is not a free metabolite in any pathway, Frc-1,6-BP is an obligatory metabolite in the EMP and CBB pathways. Frc-1,6-BP itself has been shown to be an activator of pyruvate kinase and inhibitor of PGM and is also a potential regulator of several other enzymes. Frc-1,6-BP levels are determined by the opposing reactions of phosphofructokinase (PFK) and fructose-1,6-bisphosphatase (FBPase) as well as by the activity of Frc-1,6-BP aldolase. Those enzymes are regulated by the energy state: PFK is activated by ADP, AMP and inhibited by ATP and citrate, whereas FBPase is downregulated by AMP [84]. By utilizing Frc-1,6-BP for Glc-1,6-BP synthesis and by also forming Frc-1,6-BP through the reverse reaction it is likely that Slr1334 contributes to balancing the levels of Frc-1,6-BP and Glc-1,6-BP. In addition, the level of Frc-6P, which is one of the most important precursors for amino-sugar formation, is likely affected by Slr1334 as well. In case of Sll0726 it has been shown that Glc-1,6-BP and Frc-1,6-BP are conversely regulating the activity of this enzyme. This dynamic could be conceivable for other interactions as well. **Figure 13** shows an overview of the regulatory network of Slr1334 and Glc-1,6-BP.

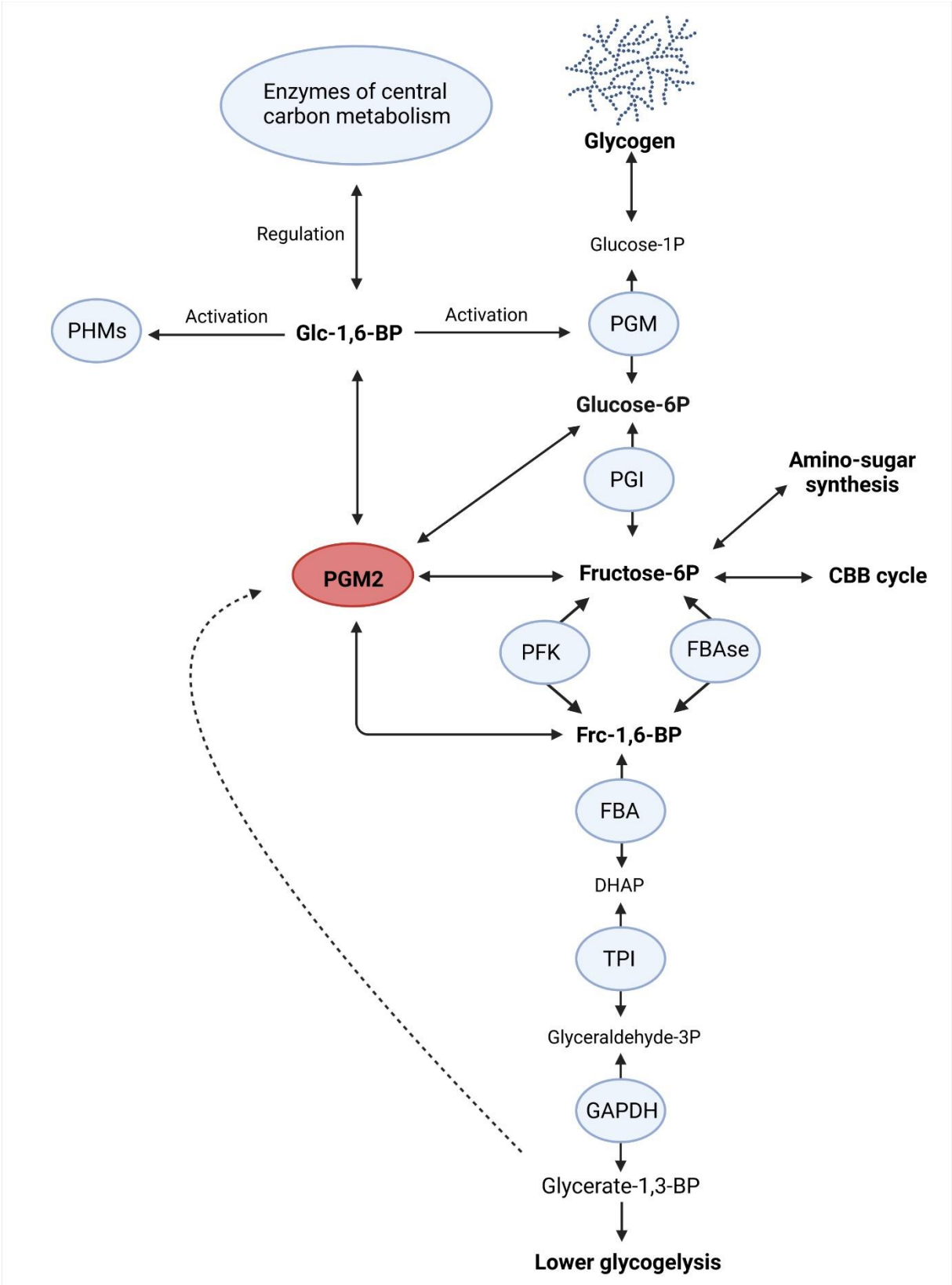

Figure 13 The potential regulatory network of Slr1334 and Glc-1,6-BP

1.2 Subfamilies in other bacteria

The PHM superfamily comprises several different subfamilies. **Table 4** gives an overview of these subfamilies according to the Conserved Domain Database (CDD) [85]. Slr1334 is part of a large subfamily of PHMs that was of so far unknown function. The fact that a Slr1334 homologue of the same group, derived from *Bacteroides salyersiae*, shows the same properties by catalyzing the Glc-1,6-BP synthase reaction and showing low general PGM activity suggests that this might be a general feature of the entire subfamily.

CDD group name	CDD identifier	Proposed main function
PGM1	cd03085	Phosphoglucomutase
PGM2	cd05799	Phosphopentomutase (PGM2)/Glc-1,6-BP synthase (PGM2L1)
PGM3(PAGM)	cd03086	Phosphoacetylglucosamine mutase
PMM/PGM	cd03089	Bi-functional phosphomanno-/phosphoglucomutase
PGM like 1	cd03087	Unknown
PGM like 2	cd05800	Unknown/Glc-1,6-BP synthase
PGM like 3	cd05801	Phosphoglucomutase
PGM like 4	cd05803	Unknown
ManB	cd03088	Phosphomannomutase
GlmM	cd05802	Phosphoglucosamine mutase

Table 4 Subfamilies in the aPHM superfamily with their identifier and proposed main function according to the NCBI conserved domain database (CDD)

Slr1334 homologues are widespread in other prokaryotes but interestingly, they are especially found in deeply branching free-living bacteria which are relatively close to the last common universal ancestor (LUCA). This includes: *Deinococci*, *Aquificae*, *Thermotogae*, *Bacteroidetes* and *Cyanobacteria* among others. In addition, Slr1334 homologues are also found in several archaea. This is in line with phylogenetic analysis of the subfamilies, showing that the subfamily of Slr1334 appears to be the most primordial in the superfamily (**Figure 14**).

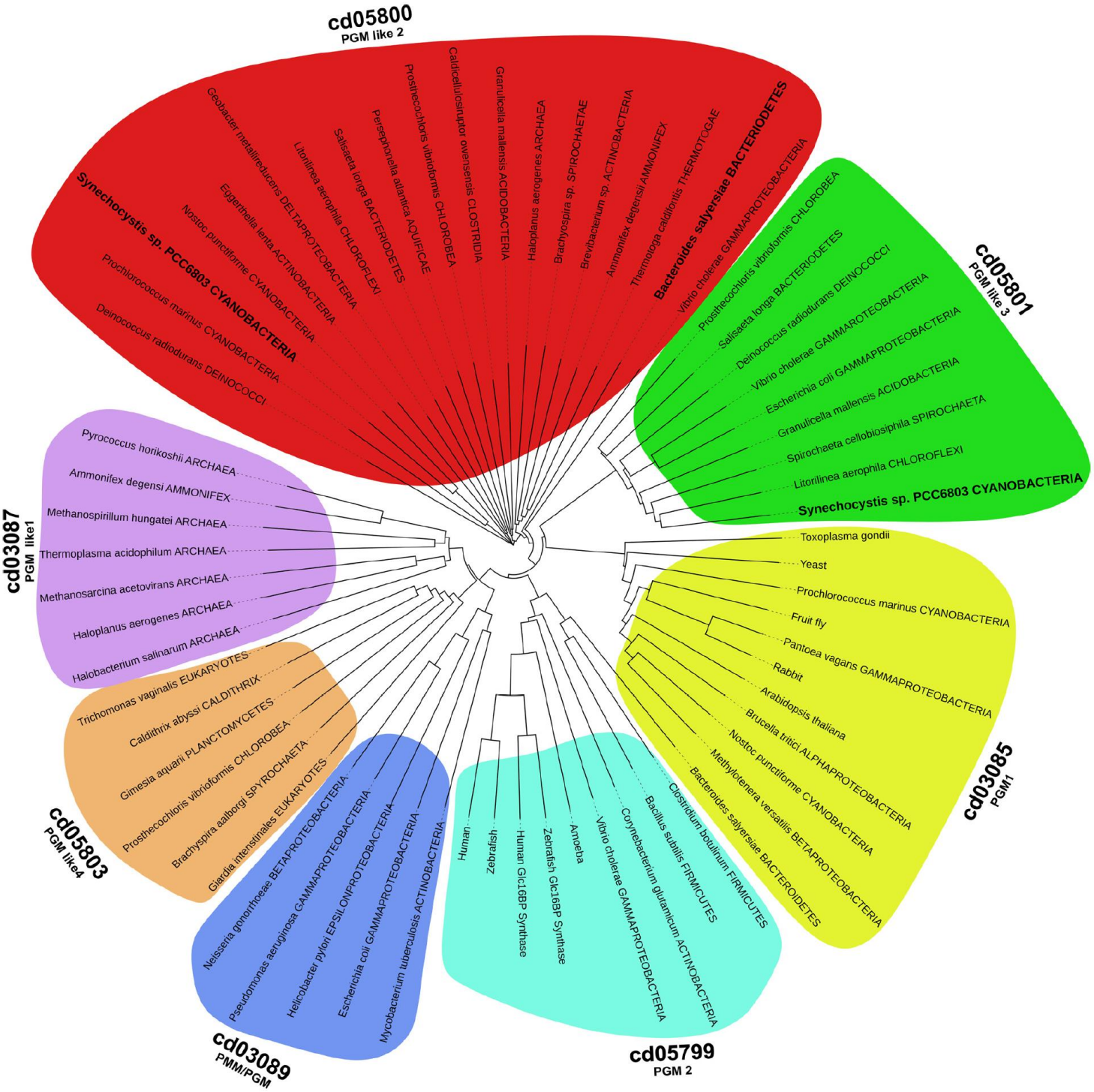

Figure 14: Phylogenetic tree of the aPHM subfamilies that are considered "PGM-like" according to CDD. Adapted from [4]. The tree was built on the taxonomy based on the protein sequences present in the NCBI RefSeq_protein database. The CDD subfamilies cd03086, cd03088, cd05802 and cd05805, which are known to catalyze distinct reactions, were omitted from the analysis. The organisms investigated in this study are highlighted in bold letters.

Looking at the substrates that can potentially be used by Slr1334 it is remarkable that it can carry out a wide variety of reactions compared to other PHMs. Among those reported reactions are the PGM, PMM and Glc-1,6-BP synthase reaction, while for the latter Frc-1,6-BP and 1,3-BPG can be used as substrates [49]. All of these reactions are carried out with a relative low efficiency compared to reactions catalyzed by other PHMs that seem to be more specialized on specific substrates (e.g. Sll0726), making Slr1334 more of a "generalist PHM". It is possible that during evolution the superfamily developed towards more specialized enzymes that can carry out specific reactions with higher efficiency at the cost of losing other functions like for example the Glc-1,6-BP synthesis. This is supported by the observation that Slr1334 can be found as the sole PGM in several organisms, while other, more specialized PGMs are usually accompanied by other subfamily members. For prokaryotes that do not harbor a Slr1334 homologue the question arises how those organisms synthesize Glc-1,6-BP. Since the requirement of Glc-1,6-BP is conserved for all known PGMs, it is likely that there are other ways for Glc-1,6-BP synthesis in these organisms. The most promising candidates for this are other subfamilies of PHM that are so far of unknown function. Further investigation of other PHM subfamily members and potential Glc-1,6-BP synthesizing enzymes might therefore greatly expand the general understanding of carbon metabolism in other bacteria. The fact that also pathogenic prokaryotes carry the Slr1334 homologue, but it is absent in eukaryotes makes it a potential target for the development of new antimicrobial drugs with little collateral damage to the host. PGM has been considered to be a virulence factor especially due to its role in bacterial capsule formation [86, 87]. In addition, Slr1334 homologues might provide a new cheap way to produce Glc-1,6-BP due to the substrates Frc-1,6-BP and Glc-1P/Glc-6P being widely available at relatively low cost.

2. Role and regulation of glycogen associated isoenzymes

Glycogen turnover is essential in *Synechocystis* to overcome situations of nutrient starvation. Regulating glycogen catabolic enzymes to prevent a premature degradation of glycogen on the one hand and initiate degradation when needed on the other hand is essential. The glycogen catabolic enzymes are expressed at the onset of chlorosis but must remain inactive until the resuscitation process is initiated. While it has been shown that the regulation of PGM (Sll0726) plays an essential role in this regard, no regulation for enzymes directly acting on glycogen has been shown so far. Most glycogen associated enzymes are present as a pair of two isoenzymes. It has been shown that at least some of these isoenzymes likely fulfill different roles in the organism. Therefore, also a different mode of regulation is expected.

2.1 Redox regulation of GlgP1

GlgP initiates the first step in glycogen breakdown. Compared to eukaryotes there is only little knowledge about the regulation of glycogen degrading enzymes in bacteria. Of the two glycogen phosphorylases in *Synechocystis* it has been shown that GlgP2 is essential for

recovery from chlorosis as well as for glycogen degradation during dark phases. GlgP1 on the other hand does not contribute to glycogen degradation under those conditions [70]. Although a study has shown that GlgP1 plays an important role during growth at high temperatures, its overall role in the organism is only poorly understood [48]. The fact that GlgP1 is unable to degrade glycogen during resuscitation even though it shows comparable abundance levels than GlgP2, indicates a different mode of regulation [88]. The results of this work clearly showed that GlgP1 activity is strongly regulated by an isoenzyme specific C-terminal redox switch. Thereby, GlgP1 degrades glycogen with high efficiency in its oxidized state and is mostly inactive when in the reduced state. Although a redox regulation of glycogen associated enzymes has been suggested in *Synechocystis*, this is the first time this regulation mechanism has been shown for a glycogen catabolic enzyme in prokaryotes [74, 89]. A redox regulation of glycogen phosphorylase outside of the bacterial domain has been shown for the GlgP in human brain, one of the three GlgP isoenzymes found in humans. This enzyme is enhanced in binding its activator AMP when in the reduced state [90]. However, an effector dependent regulation via AMP is not known in bacteria. Being active in the oxidized state and by showing that reduced GlgP1 can get activated by H_2O_2 and GSSG links GlgP1 activity to situations with increased ROS formation. In all photosynthetic organisms ROS formation is a consequence of photosynthesis and the amount of ROS correlates with photosynthetic activity. GSSG, the oxidized form of GSH is a direct indicator for ROS species since GSH is one of the main compounds to counter ROS induced damage in photosynthetic organisms, including cyanobacteria [91]. The link of GlgP1 to photosynthetic activity is unexpected, since the activity of a carbon catabolic enzymes like GlgP is generally attributed to heterotrophic growth. However, this is in line with the expression levels of *glgP1* where it was shown that, conversely to *glgP2*, *glgp1* is upregulated during light and downregulated during dark periods [33]. In addition, the essential role of GlgP1 during high temperatures could only been shown during illumination [48]. In nature, high light and high temperatures are often correlating with each other. Furthermore, high temperatures are also known to induce ROS formation in bacteria which means both high light and high temperature conditions could potentially activate GlgP1 [92]. An explanation for GlgP activity and thus glycogen degradation during these conditions could be the regeneration of ribulose-1,5-BP. During high temperatures the CO_2/O_2 ratio in water gets smaller, making it more likely for RuBisCO to incorporate oxygen instead of CO_2. In addition, higher temperatures negatively affect the affinity for CO_2 of RuBisCO itself [93, 94]. The formation of 2-phosphoglycolate as a consequence of oxygen incorporation by RuBisCO is not only energy demanding due to the necessary recycling process of 2-phosphoglycolate via photorespiration, but also a C3 body is lost in the process, which is not available for ribulose-1,5-BP regeneration. While the standard pathway for ribulose-1,5-BP regeneration requires a sequence of various reactions in the gluconeogenetic and RPP pathway, ribulose-1,5-BP can also be formed via the OPP pathway. Here, the degradation of glycogen by GlgP1 followed by the reactions of G6PDH and GND would provide a shortcut compared to the mentioned pathways, improving ribulose-1,5-BP regeneration and CO_2 fixation as a consequence. Additionally, this would also provide reducing equivalents in the form of NADPH which are needed for the recovery of GSH. It has been shown that maintaining high levels of GSH are essential for surviving prolonged periods of ROS formation [95]. The C-terminal

domain harboring this redox switch is only present in certain strains of cyanobacteria making it an exclusive feature of this group. Further phylogenetic analysis of *glgp1* mutants during high light and other stress conditions have to be carried out to confirm the hypothesized function of GlgP1.

2.2 The role of the glycogen debranching enzymes

About one third of a glycogen granule is considered to be freely accessible by GlgP degradation [96]. Therefore, a full and efficient breakdown of glycogen requires the additional activity of glycogen debranching enzymes. The role of the two isoenzymes GlgX1 and GlgX2 in *Synechocystis* has so far not been investigated at all. This work showed for the first time the role these enzymes play for glycogen degradation during different conditions. GlgX1 activity is essential for resuscitation from chlorosis and knockout mutants of *glgx1* show a strong impairment. This phenotype becomes more pronounced for longer periods of chlorosis and when resuscitation is done in day/night rhythm. This can be explained by cells experiencing longer phases of heterotrophy when resuscitating from a deeper chlorosis or into the dark phase, making a more profound degradation of the glycogen granule necessary. The knockout of *glgx2* was without any visible phenotype, indicating that *glgx2* does not contribute to glycogen debranching activity under these conditions. Interestingly, none of the *glgx* knockouts showed a phenotype in day/night during vegetative growth. It can be assumed that during diurnal growth a slower rate of glycogen degradation, provided solely by GlgP2, is sufficient, while during resuscitation the demand especially for carbon building blocks is much higher. A prolongation of the dark phase might lead to a more profound glycogen degradation as described above which could reveal an observable phenotype. By determining the enzymatic activity. it turned out that GlgX1 enhances GlgP activity in dependence of the glycogen source while GlgX2 showed no activity at all. For glycogen originating from *Synechocystis* both GlgPs benefit strongly from GlgX activity, but the effect is more pronounced for GlgP2. This suggests that the properties of the glycogen, presumably the branching pattern, determine the effect of GlgX on GlgP activity. The fact that GlgX1 particularly enhances GlgP2 activity and that a knockout of each enzyme shows a similar phenotype during resuscitation from chlorosis indicates that GlgX1 and GlgP2 form a functional pair.
The GlgX isoenzymes join the ranks of glycogen-associated enzymes in which one homolog is essential for chlorosis and recovery, while the other isoenzyme has a yet unknown role in the organism. However, in case of GlgX2 we could not confirm that this enzyme is carrying out its annotated reaction, which is not the case for any of the other glycogen associated isoenzymes. This challenges the classification of GlgX2 as a debranching enzyme. The group of glycogen debranching enzymes is diverse and there are many enzymes that carry a potential hydrolase domain which is a common reaction in carbohydrate metabolism. Therefore, another function might be assigned to GlgX2 which needs to be further investigated.

With the investigation of the two glycogen debranching enzymes, there is now a full overview of all glycogen associated isoenzymes and their roles in certain metabolic situations. For chlorosis and recovery, only one knockout of an isoenzyme is viable in each case. This is also

partly the case for diurnal growth, but the overall picture is less clear at this condition. The role of isozymes whose knockout does not show a phenotype under these conditions remains to be further investigated.

Knockout strain	Autotrophic (constant light)	Day/Night (12h/12h)	Chlorosis	Resuscitation
Δ*glgC* (*slr1176*)	**O**	**X**	**X**	**X**
Δ*glgA1* (*sll0945*)	**O**	**O**	**X**	**X**
Δ*glgA2* (*slr1393*)	**O**	**O**	**O**	**O**
Δ*glgB* (*sll0158*)	**O**	**X**	**X**	**X**
Δ*glgP1* (*sll1356*)	**O**	**O**	**O**	**O**
Δ*glgP2* (*slr1367*)	**O**	**X**	**O**	**X**
Δ*glgX1* (*slr0237*)	**O**	**O**	**O**	**X**
Δ*glgX2* (*slr1857*)	**O**	**O**	**O**	**O**

Table 5: Knockout mutants of the glycogen associated isoenzymes during different conditions: X: non-viable or significantly impaired in growth, O: viable without detectable phenotype.

2.3 Potential regulatory interaction partners for GlgP1 and GlgP2

While it has been shown that GlgP1 is regulated via redox regulation, no regulatory mechanisms for the essential GlgP2 have been found so far and it is still unclear how the signal of nitrogen availability is transferred towards the glycogen degrading enzymes. The pulldown assays performed in this work revealed different potential interaction partners for GlgP1 and GlgP2 during chlorosis and the early phase of resuscitation. GlgP1 seems to be associated with GlgX2 (Slr1857) and GlgA2 (Slr1393). Interestingly, together with GlgP1, these are the enzymes that do not appear to play a significant role during chlorosis and resuscitation (**Table 4**). Intriguingly, GlgX2 follows the same expression pattern as GlgP1 being upregulated during the day and downregulated during dark phases [33]. GlgP2 on the other hand shows strong enrichment of GlgA1 (Sll0945), the essential glycogen synthase for chlorosis. This finding could indicate that certain glycogen associated isoenzymes form a functional cluster, which is responsible for glycogen turnover at different situations. The essential Slr1334 appears to be

especially associated with GlgP1. Based on data from the quantitative proteomics of glycogen, we assume that GlgP1 may be directly bound to the glycogen granule, which does not seem to be the case for GlgP2. Therefore, in the case of the GlgP1 pulldown, glycogen granules might also have been directly fished and thus proteins bound to glycogen might be more enriched in the GlgP1 pulldown. Next to the glycogen associated enzymes we discovered several potential interaction partners that could have a regulatory function. The most interesting candidate might be the glutamine synthetase GlnN (Sll0288), which was strongly enriched during chlorosis for GlgP2. This is intriguing since this enzyme as part of the GS/GOGAT cycle is directly able to sense the availability of combined nitrogen sources as well as the C/N ratio in general. It was shown before that blocking the GS/GOGAT reaction inhibits the initiation of resuscitation and glycogen degradation [5]. During resuscitation the enrichment of GlnN for GlgP2 declines which could be an indication that GlnN releases GlgP2 once combined nitrogen is available again. Another interesting candidate for GlgP2 regulation is Slr0374, which was one of the most enriched enzymes during resuscitation. Further studies need to elucidate if those interaction partners might truly play a regulatory role for GlgP2 and if glycogen associated enzymes form a real functional cluster.

2.4 GlgB might be the missing link in signaling between SbtB and Cph1

Phototrophic lifestyle requires a permanent metabolic switch between autotrophic and heterotrophic growth. During the day, the excess of newly fixed carbon is stored as glycogen, which gets degraded during the night. These processes are regulated by a very sophisticated system that is far from fully understood. Signaling via FR is one way for phototrophic organisms to measure day length and transition from day to night. Carbon fixation and glycogen turnover play a central role in this scenario. One of the central regulators for carbon uptake is the P_{II} like protein SbtB, which negatively regulates the bicarbonate transporter SbtA. It has been shown that SbtB also has a strong influence on glycogen turnover, since a SbtB deficient mutant is strongly impaired in glycogen accumulation. Thereby, SbtB interacts with the essential glycogen branching enzyme GlgB in dependence of cyclic-di-AMP. Recently it has been shown that the SbtA/SbtB interaction is under control of FR sensing and that FR signaling also influences glycogen levels [35]. However, the mechanism underlying the FR light and the Cph1mediated regulation of SbtA activity via SbtB was so far unknown. By investigating if Cph1 itself might interact with glycogen associated enzymes an interaction with GlgA2, GlgB and GlgP1 was found in a B2H assay. The interaction with GlgB is especially intriguing because this enzyme also strongly interacts with SbtB. Therefore, GlgB could provide the missing link in FR signaling mediation towards SbtB and those might form a signaling network

3. The glycogen granule and its modifications

It was shown that the two glycogen synthases both synthesize glycogen in comparable amounts. Still, the two knockout mutants of *glga1* and *glga2* behave fundamentally different: While a *glga2* knockout mutant can undergo chlorosis and resuscitation like the wildtype, a *glga1* knockout mutant loses viability already when entering chlorosis. This raised the question on what distinguishes glycogen produced by the different synthases from another. From eukaryotes it is known that glycogen can undergo modifications in the form of phosphorylation and protein binding [43]. This study aimed at investigating the glycogen granule and its potential modifications in *Synechocystis*.

3.1 Glycogen phosphorylation and glycogen proteome

While it was not possible to detect a difference in the enzymatic activity of GlgA1 and GlgA2, an analysis of glycogen sedimentation behavior led for the first time to a visible difference between glycogen derived from WT, Δ*glga1* and Δ*glga2*. Here, the glycogen derived from the Δ*glga1* mutant shows the biggest difference in sedimentation behavior which is in line with the observed phenotype. Previous studies which analyzed the average chain length showed that glycogen derived from WT and a Δ*glga1* are especially close, which is why a difference in branching was ruled out as a potential cause [79]. A difference in attached protein could also be excluded, since the difference in density could also be detected when a purification method was chosen that should denature all potentially bound proteins. Therefore, it was assumed that a specific phosphorylation pattern, a known modification of glycogen in eukaryotes, might lead to a difference in density. The treatment of glycogen with alkaline phosphatase revealed that phosphate is released from glycogen and that the AP treated glycogen showed a worse degradability by the glycogen phosphorylases. This clearly indicates that glycogen is modified by phosphorylation, which might shape its properties. The phosphorylation state of glycogen has been shown to play an important role in eukaryotes, where an abnormal over-phosphorylation pattern leads to the accumulation of glycogen inclusion bodies. This is associated with severe neurological disorders called Lafora disease. The reason for the abnormally phosphorylated glycogen is a defect in the gene encoding for a phosphatase called “laforin”, which detects and removes phosphate groups from glycogen [97]. A homologue of this enzyme is not known in prokaryotes, but this reaction could in theory be carried out by other phosphatases. Several ways on how glycogen is phosphorylated have been discussed. The most widely accepted way is that GlgA can phosphorylate glycogen at the C2, C3 or C6 positions. This has been shown to happen as a side reaction by eukaryotic glycogen synthase incorporating the beta-phosphate of UDP-glucose [98, 99]. Although this has not been shown in bacteria, it is conceivable that the same can happen for bacterial GlgA with ADP-glucose. Another way how phosphate might be included is the reaction of GlgC, which forms the glycogen precursor ADP-glucose out of glucose-1P and ATP. Since it is now clear that Glc-1,6-BP is present in *Synechocystis* this enzyme might occasionally use Glc-1,6-BP instead of

Glc-1P, which would lead to a phosphorylated sugar incorporated into the glucan chain by GlgA. It is possible that GlgA1 and GlgA2 are differently prone for this side reaction or have different affinities for the additionally phosphorylated ADP-glucose. Interestingly, the Lafora disease is also associated with an ubiquitin ligase that is strongly interacting with laforin and essential for glycogenolysis [100]. In our glycogen quantitative proteomic analysis, we detected the ubiquitin like protein Sll6055 among the most enriched proteins. In eukaryotes it has been described before that ubiquitylation of glycogen associated enzymes is essential for their regulation [43, 101]. Glycogen is most likely associated with several proteins that are directly bound to the granule. While this work could not identify essential regulatory proteins, it gave a first insight in the complexity of the glycogen proteome and established purification methods for glycogen analysis for future studies. While it is still unclear what causes the difference between the GlgA1 and GlgA2 glycogen, this work for the first time investigated potential glycogen modifications in cyanobacteria. Glycogen in *Synechocystis* seems to be indeed phosphorylated and this phosphorylation appears to be influencing its degradability by GlgP. Thereby, the degree of phosphorylation might differ depending on the glycogen synthase that produced the glycogen. The cause and effect of phosphorylation can so far only be speculated and further studies need to be carried out for clarification. A complete degradation of the glycogen granule by amyloglucosidase followed by LC/MS analysis to detect potential glucose phosphates might be a reasonable approach to analyze the degree and the difference in phosphorylation.

4. Final Conclusions

Overall, the results presented in this work significantly expanded our knowledge on cyanobacterial glycogen metabolism and the regulation of the enzymes involved. In terms of function, configuration and its comprehensive regulatory network it was shown that glycogen metabolism comprises a high level of complexity and goes far beyond a simple glucose storage. Deepening the understanding of glycogen metabolism is not only relevant for cyanobacteria, but also of great importance for organisms in all domains of life. **Figure 15** shows a (simplified) potential glycogen interactome, including the findings of this work. Furthermore, this work provides the discovery of the first bacterial Glc-1,6-BP synthase, which closes a long-overlooked gap in bacterial carbon metabolism. Besides the regulatory functions shown in this study, Glc-1,6-BP is suggested to regulate other key enzymes in carbon metabolism. This work laid the foundation for the investigation of further functions of Glc-1,6-BP in bacterial carbon metabolism and for the search for other enzymes that synthesize this compound.

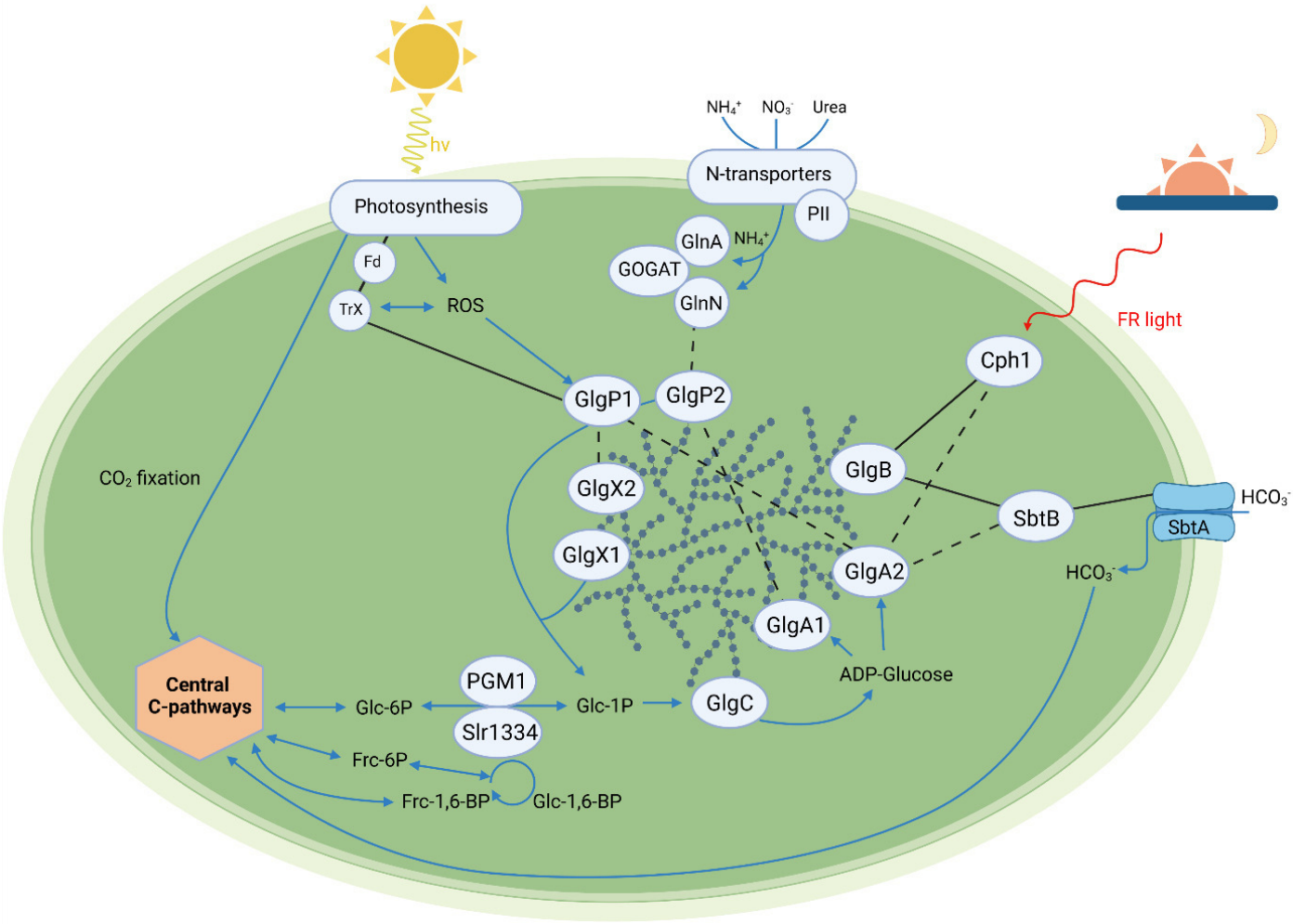

Figure 15: Simplified depiction of a potential glycogen interactome based on results achieved in this work**:** Black lines: confirmed interactions, dashed black lines: indicated interactions; blue arrows: flow of metabolites

VII. REFERENCES

1. Koch, M., et al., *PHB is Produced from Glycogen Turn-over during Nitrogen Starvation in Synechocystis sp. PCC 6803.* Int J Mol Sci, 2019. **20**(8).
2. Klotz, A., et al., *Awakening of a Dormant Cyanobacterium from Nitrogen Chlorosis Reveals a Genetically Determined Program.* Curr Biol, 2016. **26**(21): p. 2862-2872.
3. Ball, S., et al., *The evolution of glycogen and starch metabolism in eukaryotes gives molecular clues to understand the establishment of plastid endosymbiosis.* Journal of Experimental Botany, 2011. **62**(6): p. 1775-1801.
4. Neumann, N., et al., *Glucose-1,6-Bisphosphate, a Key Metabolic Regulator, Is Synthesized by a Distinct Family of α-Phosphohexomutases Widely Distributed in Prokaryotes.* mBio, 2022. **0**(0): p. e01469-22.
5. Doello, S., M. Burkhardt, and K. Forchhammer, *The essential role of sodium bioenergetics and ATP homeostasis in the developmental transitions of a cyanobacterium.* Current Biology, 2021.
6. Schirrmeister, B.E., P. Sanchez-Baracaldo, and D. Wacey, *Cyanobacterial evolution during the Precambrian.* International Journal of Astrobiology, 2016. **15**(3): p. 187-204.
7. Blankenship, R.E., *How Cyanobacteria went green.* Science, 2017. **355**(6332): p. 1372-1373.
8. Houmard, J. *How Do Cyanobacteria Perceive and Adjust to Their Environment?* in *Molecular Ecology of Aquatic Microbes*. 1995. Berlin, Heidelberg: Springer Berlin Heidelberg.
9. Durall, C. and P. Lindblad, *Mechanisms of carbon fixation and engineering for increased carbon fixation in cyanobacteria.* Algal Research, 2015. **11**: p. 263-270.
10. Rippka, R., et al., *Generic Assignments, Strain Histories and Properties of Pure Cultures of Cyanobacteria.* Journal of General Microbiology, 1979. **111**(1): p. 1-61.
11. Zavřel, T., P. Očenášová, and J. Červený, *Phenotypic characterization of Synechocystis sp. PCC 6803 substrains reveals differences in sensitivity to abiotic stress.* PLOS ONE, 2017. **12**(12): p. e0189130.
12. Ikeuchi, M. and S. Tabata, *Synechocystis sp. PCC 6803 — a useful tool in the study of the genetics of cyanobacteria.* Photosynthesis Research, 2001. **70**(1): p. 73-83.
13. Chen, X., et al., *The Entner–Doudoroff pathway is an overlooked glycolytic route in cyanobacteria and plants.* Proceedings of the National Academy of Sciences, 2016. **113**(19): p. 5441-5446.
14. Forchhammer, K. and R. Schwarz, *Nitrogen chlorosis in unicellular cyanobacteria – a developmental program for surviving nitrogen deprivation.* Environmental Microbiology, 2019. **21**(4): p. 1173-1184.
15. Gründel, M., et al., *Impaired glycogen synthesis causes metabolic overflow reactions and affects stress responses in the cyanobacterium Synechocystis sp. PCC 6803.* Microbiology, 2012. **158**(Pt 12): p. 3032-3043.

16. Schlebusch, M. and K. Forchhammer, *Requirement of the Nitrogen Starvation-Induced Protein Sll0783 for Polyhydroxybutyrate Accumulation in Synechocystis sp. Strain PCC 6803.* Applied and Environmental Microbiology, 2010. **76**(18): p. 6101-6107.
17. Watzer, B., et al., *Metabolic pathway engineering using the central signal processor PII.* Microbial Cell Factories, 2015. **14**(1): p. 1-12.
18. Bryant, D.A. and N.-U. Frigaard, *Prokaryotic photosynthesis and phototrophy illuminated.* Trends in Microbiology, 2006. **14**(11): p. 488-496.
19. Pagels, F., et al., *Phycobiliproteins from cyanobacteria: Chemistry and biotechnological applications.* Biotechnology Advances, 2019. **37**(3): p. 422-443.
20. Singh, N.K., et al., *The phycobilisomes: an early requisite for efficient photosynthesis in cyanobacteria.* Excli j, 2015. **14**: p. 268-89.
21. Shevela, D.A.B., Lars Olof%A Govindjee, *Photosynthesis*. Photosynthesis.
22. Shen, J.R., *The Structure of Photosystem II and the Mechanism of Water Oxidation in Photosynthesis.* Annu Rev Plant Biol, 2015. **66**: p. 23-48.
23. Khorobrykh, S. and E. Tyystjärvi, *Plastoquinol generates and scavenges reactive oxygen species in organic solvent: Potential relevance for thylakoids.* Biochimica et Biophysica Acta (BBA) - Bioenergetics, 2018. **1859**(10): p. 1119-1131.
24. Hervás, M., J.A. Navarro, and M.A. De la Rosa, *Electron Transfer between Membrane Complexes and Soluble Proteins in Photosynthesis.* Accounts of Chemical Research, 2003. **36**(10): p. 798-805.
25. Lea-Smith, D.J., et al., *Photosynthetic, respiratory and extracellular electron transport pathways in cyanobacteria.* Biochimica et Biophysica Acta (BBA) - Bioenergetics, 2016. **1857**(3): p. 247-255.
26. Yamori, W., A. Makino, and T. Shikanai, *A physiological role of cyclic electron transport around photosystem I in sustaining photosynthesis under fluctuating light in rice.* Scientific Reports, 2016. **6**(1): p. 20147.
27. Peschek, G.A., *Cytochrome oxidase and the cta operon of cyanobacteria.* Biochimica et Biophysica Acta (BBA) - Bioenergetics, 1996. **1275**(1): p. 27-32.
28. Mullineaux, C.W., *Co-existence of photosynthetic and respiratory activities in cyanobacterial thylakoid membranes.* Biochim Biophys Acta, 2014. **1837**(4): p. 503-11.
29. Westermark, S. and R. Steuer, *Toward Multiscale Models of Cyanobacterial Growth: A Modular Approach.* Frontiers in Bioengineering and Biotechnology, 2016. **4**.
30. Hart, S.E., et al., *Terminal oxidases of cyanobacteria.* Biochemical Society Transactions, 2005. **33**(4): p. 832-835.
31. Kok, B., *On the interrelation of respiration and photosynthesis in green plants.* Biochimica et Biophysica Acta, 1949. **3**: p. 625-631.
32. Huang, F., et al., *Proteomics of Synechocystis sp. Strain PCC 6803: Identification of Plasma Membrane Proteins*.* Molecular & Cellular Proteomics, 2002. **1**(12): p. 956-966.

33. Saha, R., et al., *Diurnal Regulation of Cellular Processes in the Cyanobacterium Synechocystis sp. Strain PCC 6803: Insights from Transcriptomic, Fluxomic, and Physiological Analyses.* mBio, 2016. **7**(3): p. e00464-16.
34. Hagemann, M., et al., *Pathway and importance of photorespiratory 2-phosphoglycolate metabolism in cyanobacteria.* Adv Exp Med Biol, 2010. **675**: p. 91-108.
35. Oren, N., et al., *Red/far-red light signals regulate the activity of the carbon-concentrating mechanism in cyanobacteria.* Science Advances, 2021. **7**(34): p. eabg0435.
36. Scholl, J., et al., *Phosphoenolpyruvate carboxylase from the cyanobacterium Synechocystis sp. PCC 6803 is under global metabolic control by PII signaling.* Molecular Microbiology, 2020. **114**(2): p. 292-307.
37. Henrissat, B., E. Deleury, and P.M. Coutinho, *Glycogen metabolism loss: a common marker of parasitic behaviour in bacteria?* Trends in Genetics, 2002. **18**(9): p. 437-440.
38. Wang, L. and M.J. Wise, *Glycogen with short average chain length enhances bacterial durability.* Naturwissenschaften, 2011. **98**(9): p. 719.
39. Preiss, J., *Bacterial Glycogen Synthesis and its Regulation.* Annual Review of Microbiology, 1984. **38**(1): p. 419-458.
40. Beck, C., et al., *The diversity of cyanobacterial metabolism: genome analysis of multiple phototrophic microorganisms.* BMC Genomics, 2012. **13**(1): p. 56.
41. Wilson, W.A., et al., *Regulation of glycogen metabolism in yeast and bacteria.* FEMS Microbiol Rev, 2010. **34**(6): p. 952-85.
42. Wang, L., et al., *Molecular Structure of Glycogen in Escherichia coli.* Biomacromolecules, 2019. **20**(7): p. 2821-2829.
43. Prats, C., T.E. Graham, and J. Shearer, *The dynamic life of the glycogen granule.* Journal of Biological Chemistry, 2018. **293**(19): p. 7089-7098.
44. Ball, S.G. and M.K. Morell, *From Bacterial Glycogen to Starch: Understanding the Biogenesis of the Plant Starch Granule.* Annual Review of Plant Biology, 2003. **54**(1): p. 207-233.
45. Boos, W. and H. Shuman, *Maltose/maltodextrin system of Escherichia coli: transport, metabolism, and regulation.* Microbiol Mol Biol Rev, 1998. **62**(1): p. 204-29.
46. Lee, B.H., D.K. Oh, and S.H. Yoo, *Characterization of 4-alpha-glucanotransferase from Synechocystis sp. PCC 6803 and its application to various corn starches.* N Biotechnol, 2009. **26**(1-2): p. 29-36.
47. Alonso-Casajús, N., et al., *Glycogen Phosphorylase, the Product of the glgP Gene, Catalyzes Glycogen Breakdown by Removing Glucose Units from the Nonreducing Ends in Escherichia coli.* Journal of Bacteriology, 2006. **188**(14): p. 5266-5272.
48. Fu, J. and X. Xu, *The functional divergence of two glgP homologues in Synechocystis sp. PCC 6803.* FEMS Microbiology Letters, 2006. **260**(2): p. 201-209.

49. Lian Liu, H.H., Hong Gao, and Xudong Xu, *Role of two phosphohexomutase genes in glycogen synthesis in Synechocystis sp. PCC6803.* Chinese Science Bulletin, 2013. **58**(36).
50. Yoo, S.H., et al., *Glycogen synthase isoforms in Synechocystis sp. PCC6803: identification of different roles to produce glycogen by targeted mutagenesis.* PLoS One, 2014. **9**(3): p. e91524.
51. Mills, L.A., A.J. McCormick, and D.J. Lea-Smith, *Current knowledge and recent advances in understanding metabolism of the model cyanobacterium Synechocystis sp. PCC 6803.* Biosci Rep, 2020. **40**(4).
52. Shackelford, G.S., C.A. Regni, and L.J. Beamer, *Evolutionary trace analysis of the α-D-phosphohexomutase superfamily.* Protein Science, 2004. **13**(8): p. 2130-2138.
53. Naught, L.E. and P.A. Tipton, *Formation and Reorientation of Glucose 1,6-Bisphosphate in the PMM/PGM Reaction: Transient-State Kinetic Studies.* Biochemistry, 2005. **44**(18): p. 6831-6836.
54. Ray, W.J., Jr. and G.A. Roscelli, *A KINETIC STUDY OF THE PHOSPHOGLUCOMUTASE PATHWAY.* J Biol Chem, 1964. **239**: p. 1228-36.
55. Makowka, A., et al., *Glycolytic Shunts Replenish the Calvin-Benson-Bassham Cycle as Anaplerotic Reactions in Cyanobacteria.* Mol Plant, 2020. **13**(3): p. 471-482.
56. Vitousek, P.M. and R.W. Howarth, *Nitrogen limitation on land and in the sea: How can it occur?* Biogeochemistry, 1991. **13**(2): p. 87-115.
57. Muro-Pastor, M.I., J.C. Reyes, and F.J. Florencio, *Ammonium assimilation in cyanobacteria.* Photosynth Res, 2005. **83**(2): p. 135-50.
58. Ohashi, Y., et al., *Regulation of nitrate assimilation in cyanobacteria.* J Exp Bot, 2011. **62**(4): p. 1411-24.
59. Valladares, A., et al., *An ABC-type, high-affinity urea permease identified in cyanobacteria.* Mol Microbiol, 2002. **43**(3): p. 703-15.
60. Esteves-Ferreira, A.A., et al., *Nitrogen metabolism in cyanobacteria: metabolic and molecular control, growth consequences and biotechnological applications.* Crit Rev Microbiol, 2018. **44**(5): p. 541-560.
61. Bolay, P., et al., *The Distinctive Regulation of Cyanobacterial Glutamine Synthetase.* Life (Basel), 2018. **8**(4).
62. Zeth, K., O. Fokina, and K. Forchhammer, *Structural basis and target-specific modulation of ADP sensing by the Synechococcus elongatus PII signaling protein.* J Biol Chem, 2014. **289**(13): p. 8960-72.
63. Fokina, O., et al., *Mechanism of 2-oxoglutarate signaling by the Synechococcus elongatus PII signal transduction protein.* Proc Natl Acad Sci U S A, 2010. **107**(46): p. 19760-5.
64. Forchhammer, K. and A. Hedler, *Phosphoprotein PII from cyanobacteria--analysis of functional conservation with the PII signal-transduction protein from Escherichia coli.* Eur J Biochem, 1997. **244**(3): p. 869-75.
65. Zhang, C.-C., et al., *Carbon/Nitrogen Metabolic Balance: Lessons from Cyanobacteria.* Trends in Plant Science, 2018. **23**(12): p. 1116-1130.
66. Selim, K.A., et al., *Molecular and Cellular Mechanisms Underlying the Microbial Survival Strategies: Insights into Temperature and Nitrogen Adaptations*, in *Climate*

Change and the Microbiome: Sustenance of the Ecosphere, D.K. Choudhary, A. Mishra, and A. Varma, Editors. 2021, Springer International Publishing: Cham. p. 717-748.

67. Orthwein, T., et al., *The novel P_{II}-interactor PirC identifies phosphoglycerate mutase as key control point of carbon storage metabolism in cyanobacteria.* Proceedings of the National Academy of Sciences, 2021. **118**(6): p. e2019988118.
68. Görl, M., et al., *Nitrogen-starvation-induced chlorosis in Synechococcus PCC 7942: adaptation to long-term survival.* Microbiology-Uk, 1998. **144**: p. 2449-2458.
69. Sauer, J., et al., *Nitrogen starvation-induced chlorosis in Synechococcus PCC 7942. Low-level photosynthesis as a mechanism of long-term survival.* Plant Physiology, 2001. **126**(1): p. 233-243.
70. Doello, S., et al., *A Specific Glycogen Mobilization Strategy Enables Rapid Awakening of Dormant Cyanobacteria from Chlorosis.* Plant Physiol, 2018. **177**(2): p. 594-603.
71. Azuma, M., et al., *A Response Regulator Rre37 and an RNA Polymerase Sigma Factor SigE Represent Two Parallel Pathways to Activate Sugar Catabolism in a Cyanobacterium Synechocystis sp. PCC 6803.* Plant and Cell Physiology, 2011. **52**(2): p. 404-412.
72. Osanai, T., et al., *Pathway-Level Acceleration of Glycogen Catabolism by a Response Regulator in the Cyanobacterium Synechocystis Species PCC 6803.* Plant Physiology, 2014. **164**(4): p. 1831-1841.
73. Díaz-Troya, S., et al., *Redox Regulation of Glycogen Biosynthesis in the Cyanobacterium Synechocystis sp. PCC 6803: Analysis of the AGP and Glycogen Synthases.* Molecular Plant, 2014. **7**(1): p. 87-100.
74. Lindahl, M. and F.J. Florencio, *Thioredoxin-linked processes in cyanobacteria are as numerous as in chloroplasts, but targets are different.* Proceedings of the National Academy of Sciences, 2003. **100**(26): p. 16107-16112.
75. Meléndez-Hevia, E., T.G. Waddell, and E.D. Shelton, *Optimization of molecular design in the evolution of metabolism: the glycogen molecule.* Biochem J, 1993. **295 (Pt 2)**(Pt 2): p. 477-83.
76. Fazi, A., et al., *Purification and partial characterization of the phosphoglucomutase isozymes from human placenta.* Prep Biochem, 1990. **20**(3-4): p. 219-40.
77. Maino, V.C. and F.E. Young, *Regulation of glucosylation of teichoic acid. II. Partial characterization of phosphoglucomutase in Bacillus subtilis 168.* J Biol Chem, 1974. **249**(16): p. 5176-81.
78. Jiang, H.B., et al., *The hypothetical protein Ycf46 is involved in regulation of CO2 utilization in the cyanobacterium Synechocystis sp. PCC 6803.* Planta, 2015. **241**(1): p. 145-55.
79. Yoo, S.-H., et al., *Glycogen Synthase Isoforms in Synechocystis sp. PCC6803: Identification of Different Roles to Produce Glycogen by Targeted Mutagenesis.* PLOS ONE, 2014. **9**(3): p. e91524.

80. Stiers, K.M., A.G. Muenks, and L.J. Beamer, *Biology, Mechanism, and Structure of Enzymes in the α-d-Phosphohexomutase Superfamily.* Adv Protein Chem Struct Biol, 2017. **109**: p. 265-304.
81. Jolly, L., et al., *Autophosphorylation of Phosphoglucosamine Mutase from Escherichia coli.* Journal of Bacteriology, 2000. **182**(5): p. 1280-1285.
82. Carreras, J., et al., *Bisphosphorylated metabolites of glycerate, glucose, and fructose: Functions, metabolism and molecular pathology.* Clinical Biochemistry, 1986. **19**(6): p. 348-358.
83. Morava, E., et al., *Impaired glucose-1,6-biphosphate production due to bi-allelic PGM2L1 mutations is associated with a neurodevelopmental disorder.* Am J Hum Genet, 2021. **108**(6): p. 1151-1160.
84. Waygood, E.B., J.S. Mort, and B.D. Sanwal, *The control of pyruvate kinase of Escherichia coli. Binding of substrate and allosteric effectors to the enzyme activated by fructose 1,6-bisphosphate.* Biochemistry, 1976. **15**(2): p. 277-282.
85. Lu, S., et al., *CDD/SPARCLE: the conserved domain database in 2020.* Nucleic Acids Res, 2020. **48**(D1): p. D265-d268.
86. Regni, C., P.A. Tipton, and L.J. Beamer, *Crystal structure of PMM/PGM: an enzyme in the biosynthetic pathway of P. aeruginosa virulence factors.* Structure, 2002. **10**(2): p. 269-79.
87. Mehra-Chaudhary, R., et al., *Crystal structure of a bacterial phosphoglucomutase, an enzyme involved in the virulence of multiple human pathogens.* Proteins, 2011. **79**(4): p. 1215-29.
88. Spat, P., et al., *Chlorosis as a developmental program in cyanobacteria: the proteomic fundament for survival and awakening.* Mol Cell Proteomics, 2018.
89. Florencio, F.J., et al., *The diversity and complexity of the cyanobacterial thioredoxin systems.* Photosynthesis Research, 2006. **89**(2): p. 157-171.
90. Mathieu, C., et al., *An Isozyme-specific Redox Switch in Human Brain Glycogen Phosphorylase Modulates Its Allosteric Activation by AMP.* J Biol Chem, 2016. **291**(46): p. 23842-23853.
91. Cameron, J.C. and H.B. Pakrasi, *Essential role of glutathione in acclimation to environmental and redox perturbations in the cyanobacterium Synechocystis sp. PCC 6803.* Plant Physiol, 2010. **154**(4): p. 1672-85.
92. Slimen, I.B., et al., *Reactive oxygen species, heat stress and oxidative-induced mitochondrial damage. A review.* Int J Hyperthermia, 2014. **30**(7): p. 513-23.
93. Salvucci, M.E. and S.J. Crafts-Brandner, *Inhibition of photosynthesis by heat stress: the activation state of Rubisco as a limiting factor in photosynthesis.* Physiol Plant, 2004. **120**(2): p. 179-186.
94. Crafts-Brandner, S.J. and R.D. Law, *Effect of heat stress on the inhibition and recovery of the ribulose-1,5-bisphosphate carboxylase/oxygenase activation state.* Planta, 2000. **212**(1): p. 67-74.
95. Suginaka, K., et al., *Effect of Intracellular Glutathione on Heat-induced Cell Death in the Cyanobacterium, Synechocystis PCC 6803.* Biosci Biotechnol Biochem, 1999. **63**(6): p. 1112-5.

96. Meléndez-Hevia, E., T.G. Waddell, and E.D. Shelton, *Optimization of molecular design in the evolution of metabolism: the glycogen molecule.* The Biochemical journal, 1993. **295 (Pt 2)**(Pt 2): p. 477-483.
97. Verhalen, B., S. Arnold, and B.A. Minassian, *Lafora Disease: A Review of Molecular Mechanisms and Pathology.* Neuropediatrics, 2018. **49**(6): p. 357-362.
98. Contreras, C.J., et al., *Incorporation of phosphate into glycogen by glycogen synthase.* Arch Biochem Biophys, 2016. **597**: p. 21-9.
99. Tagliabracci, V.S., et al., *Phosphate incorporation during glycogen synthesis and Lafora disease.* Cell Metab, 2011. **13**(3): p. 274-82.
100. Donohue, K.J., M.S. Gentry, and R.C. Sun, *The E3 ligase malin plays a pivotal role in promoting nuclear glycogenolysis and histone acetylation.* Ann Transl Med, 2020. **8**(5): p. 254.
101. DePaoli-Roach, A.A., et al., *Genetic depletion of the malin E3 ubiquitin ligase in mice leads to lafora bodies and the accumulation of insoluble laforin.* J Biol Chem, 2010. **285**(33): p. 25372-81.

VIII. APPENDIX

Publication 1: Research article

Watzer B., Spät P., **Neumann N.**, Koch M., Sobotka R., Macek B., Hennrich O., Forchhammer K. The Signal Transduction Protein P_{II} Controls Ammonium, Nitrate and Urea Uptake in Cyanobacteria. *Front Microbiol*. 2019 10:1428.

frontiers in Microbiology

ORIGINAL RESEARCH
published: 25 June 2019
doi: 10.3389/fmicb.2019.01428

The Signal Transduction Protein P_{II} Controls Ammonium, Nitrate and Urea Uptake in Cyanobacteria

Björn Watzer[1†], Philipp Spät[1,2†], Niels Neumann[1], Moritz Koch[1], Roman Sobotka[3], Boris Macek[2], Oliver Hennrich[1] and Karl Forchhammer[1]*

[1] Interfaculty Institute of Microbiology and Infection Medicine Tübingen, Department of Organismic Interactions, University of Tübingen, Tübingen, Germany, [2] Interfaculty Institute for Cell Biology, Department of Quantitative Proteomics, University of Tübingen, Tübingen, Germany, [3] Centre Algatech, Institute of Microbiology, Academy of Sciences of the Czech Republic, Třeboň, Czechia

P_{II} signal transduction proteins are widely spread among all domains of life where they regulate a multitude of carbon and nitrogen metabolism related processes. Non-diazotrophic cyanobacteria can utilize a high variety of organic and inorganic nitrogen sources. In recent years, several physiological studies indicated an involvement of the cyanobacterial P_{II} protein in regulation of ammonium, nitrate/nitrite, and cyanate uptake. However, direct interaction of P_{II} has not been demonstrated so far. In this study, we used biochemical, molecular genetic and physiological approaches to demonstrate that P_{II} regulates all relevant nitrogen uptake systems in *Synechocystis* sp. strain PCC 6803: P_{II} controls ammonium uptake by interacting with the Amt1 ammonium permease, probably similar to the known regulation of *E. coli* ammonium permease AmtB by the P_{II} homolog GlnK. We could further clarify that P_{II} mediates the ammonium- and dark-induced inhibition of nitrate uptake by interacting with the NrtC and NrtD subunits of the nitrate/nitrite transporter NrtABCD. We further identified the ABC-type urea transporter UrtABCDE as novel P_{II} target. P_{II} interacts with the UrtE subunit without involving the standard interaction surface of P_{II} interactions. The deregulation of urea uptake in a P_{II} deletion mutant causes ammonium excretion when urea is provided as nitrogen source. Furthermore, the urea hydrolyzing urease enzyme complex appears to be coupled to urea uptake. Overall, this study underlines the great importance of the P_{II} signal transduction protein in the regulation of nitrogen utilization in cyanobacteria.

Keywords: P_{II} signaling protein, GlnB, cyanobacteria, nitrogen regulation, nitrate uptake, ammonium uptake, urea uptake, ABC transporters

OPEN ACCESS

Edited by:
Jörg Stülke,
University of Göttingen, Germany

Reviewed by:
Wolfgang R. Hess,
University of Freiburg, Germany
Andreas Burkovski,
University of Erlangen-Nuremberg, Germany

***Correspondence:**
Karl Forchhammer
karl.forchhammer@uni-tuebingen.de

† These authors have contributed equally to this work

Specialty section:
This article was submitted to Microbial Physiology and Metabolism, a section of the journal Frontiers in Microbiology

Received: *09 April 2019*
Accepted: *05 June 2019*
Published: *25 June 2019*

Citation:
Watzer B, Spät P, Neumann N, Koch M, Sobotka R, Macek B, Hennrich O and Forchhammer K (2019) The Signal Transduction Protein P_{II} Controls Ammonium, Nitrate and Urea Uptake in Cyanobacteria. Front. Microbiol. 10:1428. doi: 10.3389/fmicb.2019.01428

INTRODUCTION

The emergence of the oxygenic photosynthesis by ancestors of present cyanobacteria (Soo et al., 2017) laid the ground for the evolution of present days life on planet earth. Until today, cyanobacteria occupy a high variety of illuminated habitats, where they represent one of the most abundant primary producers (Whitton, 2012). Accordingly, cyanobacteria are essential contributors to the global carbon cycle. Many cyanobacterial strains have acquired the ability to fix atmospheric nitrogen, making them key players in the global nitrogen turnover

(Herrero and Flores, 2008). Nitrogen represents a necessary macronutrient for all living organisms and therefore constitutes an important growth-limiting factor in most ecosystems (Vitousek and Howarth, 1991). The regulation of nitrogen metabolism in cyanobacteria mainly depends on the fine-tuned network of the signal transduction protein P_{II}, the global nitrogen transcription factor NtcA and the NtcA co-activator PipX (Vegapalas et al., 1992; Espinosa et al., 2006, 2007, 2014; Forchhammer, 2008; Luque and Forchhammer, 2008; Forcada-Nadal et al., 2018).

P_{II} signal-transduction proteins are widespread in all three domains of life, where they represent one of the largest and most ancient families of signaling proteins (Chellamuthu et al., 2013; Forchhammer and Luddecke, 2016). P_{II} proteins are involved in the regulation of various nitrogen- and carbon-anabolic processes (Forchhammer, 2004, 2008). Canonical P_{II} proteins are homo-trimeric with three characteristic loop regions, designated as B-, C-, and T-loops, which compose the effector molecule binding sites (Cheah et al., 1994; Xu et al., 2003; Forchhammer, 2004, 2008; Llacer et al., 2007; Fokina et al., 2010a; Zhao et al., 2010; Zeth et al., 2014). The large surface exposed T-loop is the prevailing protein interaction module of P_{II}. The P_{II} proteins sense the energy status of the cell by the competitive binding of ADP or ATP (Zeth et al., 2014). Binding of ATP and synergistic binding of 2-oxoglutarate (2-OG) allows P_{II} to sense the current carbon/nitrogen status of the cell (Fokina et al., 2010a). 2-OG is an intermediate of the TCA-cycle that provides the carbon skeleton for inorganic nitrogen incorporation by the glutamine synthetase/glutamate synthase (GS/GOGAT) cycle. Due to this, 2-OG links carbon and nitrogen metabolism and acts as an indicator for the intracellular carbon/nitrogen balance (Muro-Pastor et al., 2001; Fokina et al., 2010a). Besides effector molecule binding, post-translational modification of P_{II} represents a second level of regulation (Forchhammer et al., 2004; Merrick, 2014). Depending on nitrogen availability, cyanobacterial P_{II} can be phosphorylated at the apex of the T-loop at position Ser49 (Forchhammer and Tandeau de Marsac, 1995; Forchhammer and Hedler, 1997). In other prokaryotes, like *E. coli*, P_{II} is modified by uridylylation in response to nitrogen availability instead of phosphorylation (Jiang et al., 1998). Binding of effector molecules as well as post-translational modifications lead to various P_{II} conformations. Depending on the conformational state, P_{II} can interact with a variety of interaction partners and thereby regulate the cellular C/N balance (Radchenko and Merrick, 2011; Forchhammer and Luddecke, 2016). In cyanobacteria, P_{II} indirectly regulates the global nitrogen control transcriptional factor NtcA through binding of the NtcA co-activator PipX (Espinosa et al., 2007). In common with other bacteria, the cyanobacterial P_{II} protein can control the acetyl-CoA levels by interacting with the biotin carboxyl carrier protein (BCCP) of acetyl-CoA carboxylase (ACC) (Hauf et al., 2016). Furthermore, P_{II} regulates arginine biosynthesis by interacting with the enzyme *N*-acetylglutamate kinase (NAGK), which catalyzes the rate-limiting step of this pathway (Caldovic and Tuchman, 2003; Heinrich et al., 2004; Llacer et al., 2007; Watzer et al., 2015). If sufficient energy and nitrogen is available, indicated by a high intracellular ATP and low 2-OG level, non-phosphorylated P_{II} interacts with NAGK, enhancing its catalytic efficiency and relieving it from feedback inhibition by arginine (Heinrich et al., 2004; Maheswaran et al., 2004; Llacer et al., 2007). At high intracellular arginine levels, the carbon/nitrogen storage polymer cyanophycin (multi-L-arginyl-poly-L-aspartate) accumulates in *Synechocystis* sp. strain PCC 6803 (hereafter *Synechocystis*) (Maheswaran et al., 2006; Watzer et al., 2015). A P_{II} variant was identified with a single amino acid substitution, Ile86 to Asn86 [thereafter referred as P_{II}(I86N)], which constitutively binds NAGK *in vitro* (Fokina et al., 2010b). Replacing the wild-type P_{II} with a I86N variant in *Synechocystis* generated a mutant strain, which strongly overproduced arginine and cyanophycin (Watzer et al., 2015). On the other hand, the P_{II}(I86N) strain showed a growth defect in ammonium-supplemented medium (Watzer et al., 2015).

Cyanobacteria use nitrogen sources in a hierarchical order, with ammonium being the preferred nitrogen source. As a consequence, when ammonium is provided together with other suitable nitrogen sources, ammonium will be utilized first (Muro-Pastor et al., 2005). In most natural habitats, the ammonium availability is low, so that high affinity ammonium permeases are required for efficient ammonium uptake (Rees et al., 2006). In *Synechocystis,* the Amt1 permease is mainly responsible for ammonium uptake (Montesinos et al., 1998). However, elevated intracellular ammonium concentrations are toxic to the cells (Drath et al., 2008; Dai et al., 2014), and therefore, ammonium transport must be tightly controlled. The ammonium transporter family (Amt) is widespread among all domains of life (Wirén and Merrick, 2004). In *E. coli*, the P_{II} homolog GlnK regulates the ammonium permease AmtB by direct protein–protein interaction. Under ammonium excess conditions, ADP-complexed GlnK blocks an uncontrolled influx of ammonium by inserting the apex of the T-loop into the cytoplasmic exit pores of AmtB (Conroy et al., 2007).

For the assimilation of nitrate, an active nitrate transporter, a nitrate reductase (NR) and a nitrite reductase (NiR) are required (Ohashi et al., 2011). Two types of nitrate transporter systems have been found among cyanobacteria, a high-affinity nitrate/nitrite permease NrtP and the ABC-type transporter NrtABCD (NRT) (Omata et al., 1993; Luque et al., 1994; Sakamoto et al., 1999; Ohashi et al., 2011). NRT is a bispecific nitrate/nitrite transporter showing high affinity for both substrates (Maeda and Omata, 1997). Intracellular nitrate is first reduced to nitrite by NR and subsequently reduced to ammonium by NiR. Subsequently, ammonium is assimilated in the GS/GOGAT cycle (Flores and Herrero, 1994). Both, NR and NiR, use photosystem I reduced ferredoxin as an electron donor, indicating a coupling of photosynthesis and nitrate assimilation (Manzano et al., 1976; Flores and Herrero, 1994). Addition of ammonium to nitrate adapted cells results in an immediate inhibition of nitrate uptake and a repression of proteins involved in nitrate assimilation (NR and NiR). The ammonium-induced inhibition of NRT is regulated by the P_{II} protein and the C-terminal domain of NrtC (Kobayashi et al., 1997; Lee et al., 1998). Phosphomimetic variants of P_{II} and a P_{II} phosphatase (PphA) deletion mutant, in which P_{II} is constitutively phosphorylated, showed

ammonium promoted inhibition of nitrate uptake like the wild-type (Lee et al., 2000; Kloft and Forchhammer, 2005). However, this response was abolished in a P_{II} deficient mutant (Kloft and Forchhammer, 2005).

The ability to utilize urea as nitrogen source is widely distributed among bacteria, fungi and algae (Baker et al., 2009; Solomon et al., 2010; Esteves-Ferreira et al., 2018). In common with other bacteria, the cyanobacteria *Synechocystis* and *Anabaena* sp. PCC 7120 possess a high affinity urea ABC-type transporter, which is capable of urea import at concentrations lower than 1 μM (Valladares et al., 2002). The gene cluster *urtABCDE*, encoding all subunits of this ABC-type urea transporter, is transcriptionally controlled by the global transcription factor NtcA (Valladares et al., 2002).

The present study was inspired by the phenotype of the cyanophycin-accumulating strain variant *Synechocystis* P_{II}(I86N), which was impaired in ammonium utilization. Starting with analyzing a possible regulation of the cyanobacterial Amt1 permease by P_{II}, we found additional evidence for a direct regulation of the nitrate/nitrite transporter NrtABCD and the urea transporter UrtABCDE by the P_{II} signaling protein during this study.

MATERIALS AND METHODS

Cultivation Conditions

Standard cloning procedures were performed in *Escherichia coli* NEB 10-beta (NEB). Strains were grown in LB-medium at 37°C with constant shaking at 300 rpm.

Synechocystis strains were grown photoautotrophically in BG-11 medium supplemented with 5 mM $NaHCO_3$ and nitrate, ammonium, or urea as nitrogen source (Rippka et al., 1979). BG-11 agar plates were produced by adding 1.5% (w/v) Bacto-agar (Difco), 0.3% (w/v) sodium thiosulfate pentahydrate and 10 mM TES-NaOH pH 8 (Roth) to liquid BG-11 medium. Antibiotics were added when required. Cultivation of liquid cultures for physiological experiments occurred in 50, 100, or 500 mL Erlenmeyer flasks, at 28°C and with constant shaking of 120 rpm. Cultures were continuously illuminated with a photon flux rate of 40–50 μE. Growth rates were determined by measuring the optical density at 750 nm (OD_{750}).

For induction of nitrogen starvation conditions, exponentially growing cells (OD_{750} 0.4–0.8) were harvested by centrifugation (3,000 × *g* for 10 min at room temperature), washed and resuspended in BG-11 medium lacking a suitable nitrogen source (BG-11^0).

For spot assays (drop plate method), *Synechocystis* cultures were adjusted to an OD_{750} of 1. A dilution series to the power of 10 was made using BG-11^0. Then, 5 μL of every dilution step (10^0–10^{-4}) were dropped on BG-11 agar plates. Plates were cultivated at 28°C with constant illumination of 40 μmol of photons s^{-1} m^{-2}.

Bacterial Two-Hybrid Assay

Plasmids were constructed by PCR amplification using high-fidelity Q5 polymerase (NEB) and oligonucleotides with overlapping regions. Genomic *Synechocystis* DNA or plasmids served as templates. PCR fragments were inserted in linearized bacterial two-hybrid vectors pUT18 and pKT25 containing the genes for either the T18 or T25 subunit of the adenylate cyclase CyaA (Karimova et al., 2001) by isothermal, single-reaction DNA assembly according to Gibson et al. (2009). Since the multiple cloning site of pKT25 is located downstream of the T25 subunit, allowing only N-terminal localization of the tag, we constructed plasmid pKT25n (**Table 1**; pKT25n_fw and pKT25n_rev) to achieve a C-terminal fusion of the tag to the gene of interest. Therefore, plasmid pKT25 was linearized using PCR and the gene of interest was fused upstream of the T25 subunit. Primers, plasmids, and strains used in this study are listed in **Tables 1–3**, respectively.

Escherichia coli BTH101 cells were co-transformed with plasmid pUT18 and plasmid pKT25 or pKT25n (**Table 2**). Plasmids pKT25 or pKT25n contained the possible P_{II} interaction partner fused N- or C-terminal to the T25 subunit. Plasmid pUT18 contains a gene-fusion of the P_{II}-encoding *gln*B gene or a genetically modified *gln*B gene containing the I86N mutation [Ile (5′ATC) at codon position 86 to Asn (5′AAC)] (Watzer et al., 2015), the R9L mutation [Arg (5′CGC) at codon position 9 to Leu (5′CTG)] (Fokina et al., 2010a) or the S49D mutation [Ser (5′TCG) at codon position 49 to Asp (5′GAT)] (Lee et al., 2000) with the T18 subunit. The *gln*B gene and the modified *gln*B genes were always fused N-terminal with the T18 subunit. Co-transformants were plated on LB-plates (supplemented with 100 μg mL^{-1} ampicillin and 50 μg mL^{-1} kanamycin) and cultivated for 2 days at 30°C.

To reduce the level of heterogeneity, five clones from each plate were picked to inoculate 5 mL LB-medium (containing 100 μg mL^{-1} ampicillin and 50 μg mL^{-1} kanamycin). Cultures were cultivated overnight at 37°C. Overnight cultures were diluted 1:100 in 3 mL of fresh LB-medium (containing 100 μg mL^{-1} ampicillin and 50 μg mL^{-1} kanamycin) and grown to an OD_{600} of 0.7. Three μL of each culture were plated on X-Gal (containing 100 μg mL^{-1} ampicillin, 50 μg mL^{-1} kanamycin, 1 mM IPTG, 40 μg mL^{-1} X-Gal) and MacConkey (containing 100 μg mL^{-1} ampicillin, 50 μg mL^{-1} kanamycin, 1 mM IPTG, 1% maltose) reporter plates. Reporter plates were incubated for 3–4 days at 25°C.

Construction and Cultivation of *Synechocystis* P_{II}-3xFLAG Tag Strains

The previously described pPD-*N*FLAG and pPD-*C*FLAG plasmids were used to construct *Synechocystis* P_{II} (GlnB) fusion proteins with an N- or C-terminal 3xFLAG tag, respectively (Hollingshead et al., 2012; Chidgey et al., 2014). Together with a kanamycin resistance cassette, this construct was inserted in the *Synechocystis* wild-type genome by homologous recombination, replacing the *psbAII* gene (Chidgey et al., 2014). Transformants were selected and segregated by kanamycin resistance. For pull-down experiments, 2 L batch cultures were inoculated at OD_{750} = 0.2 in BG-11 medium and propagated as described above, with magnetic stirring at 120 rpm and bubbling with 2% CO_2 (v/v) supplemented ambient air. Cell harvesting was

TABLE 1 | Oligonucleotides used in this study.

Primer	Sequence (5′–3′ direction)
pKT25n_fw	ACCATGCAGCAATCGCATCAG
pKT25n_rev	CATAGCTGTTTCCTGTGTGAAATTG
glnB_fw	TGTGTGGAATTGTGAGCGGATAACAATTTCACACAGGAAACAGCTATGAAAAAAGTAGAAGCGATTATTC
glnB_rev	CTCGCTGGCGGCTGAATTCGAGCTCGGTACCCGGGGATCAATAGCTTCGGTATCCTTTTC
pipX_fw	TTCACACAGGAAACAGCTATGAGTAACGAAATTTACCTTAAC
pipX_rev	GATGCGATTGCTGCATGGTAAAAGTGTTTTTATGTAACTTTG
pipX_pKT25n_fw	AAGTTACATAAAAACACTTTTACCATGCAGCAATCGCATCAG
pipX_pKT25n_rev	TAAGGTAAATTTCGTTACTCATAGCTGTTTCCTGTGTGAAATTG
amt1_pKT25_fw	CTGGCGCGCACGCGGCGGGCTGCAGGGTCGACTCTAGAGATGTCTAATTCGATATTGTCTAAAC
amt1_pKT25_rev	AAAACGACGGCCGAATTCTTAGTTACTTAGGTACCCGGGGATCTTATTCAGGGACAGTGG
amt1_fw	AACAATTTCACACAGGAAACAGCTATGTCTAATTCGATATTGTCTAAAC
amt1_rev	TGATGCGATTGCTGCATGGTTTCAGGGACAGTGGCACCG
amt1_pKT25n_fw	TCTCCGGTGCCACTGTCCCTGAAACCATGCAGCAATCGCATC
amt1_pKT25n_rev	ACAATATCGAATTAGACATAGCTGTTTCCTGTGTGAAATTGTTATCCGC
nrtC_pKT25_fw	CGCGCACGCGGCGGGCTGCAGGGTCGACTCTAGAGGATCCCCCCTTCATTGAAATTGATCATGTTG
nrtC_pKT25_rev	AGTCACGACGTTGTAAAACGACGGCCGAATTCTTAGTTATTGATTAACTTGATCAATTTGGTCGATGAG
nrtC_fw	AATTTCACACAGGAAACAGCTATGCCCTTCATTGAAATTGATCATG
nrtC_rev	CTGATGCGATTGCTGCATGGTTTGATTAACTTGATCAATTTGG
nrtC_pKT25n_fw	AAATTGATCAAGTTAATCAAACCATGCAGCAATCGCATCAG
nrtC_pKT25n_rev	TCAATTTCAATGAAGGGCATAGCTGTTTCCTGTGTGAAATTG
nrtD_pKT25_fw	CGCACGCGGCGGGCTGCAGGGTCGACTCTAGAGGATCCCCAAACAATGAATGTCAATGACCCTATCC
ntrD_pKT25_rev	CCCAGTCACGACGTTGTAAAACGACGGCCGAATTCTTAGTTAAGACCCTTCCATGGATTCCACTGAGGGGGTAG
nrtD_fw	AATTTCACACAGGAAACAGCTATGCAAACAATGAATGTCAATGACCCTATC
nrtD_rev	CTGATGCGATTGCTGCATGGTAGACCCTTCCATGGATTCCACTGAG
nrtD_pKT25n_fw	TGGAATCCATGGAAGGGTCTACCATGCAGCAATCGCATCAG
nrtD_pKT25n_rev	ATTGACATTCATTGTTTGCATAGCTGTTTCCTGTGTGAAATTG
urtD_pKT25_fw	CGCACGCGGCGGGCTGCAGGGTCGACTCTAGAGGATCCCACCAGCAAAATCTTAGAAATTCAAG
urtD_pKT25_rev	CCCAGTCACGACGTTGTAAAACGACGGCCGAATTCTTAGCTAATCTCCATCCTCATCAAC
urtD_fw	ACACAGGAAACAGCTATGACCAGCAAAATCTTAGAAATTCAAGAC
urtD_rev	GATGCGATTGCTGCATGGTATCTCCATCCTCATCAACACTG
urtD_pKT25n_fw	AGTGTTGATGAGGATGGAGATACCATGCAGCAATCGCATCAG
urtD_pKT25n_rev	TTCTAAGATTTTGCTGGTCATAGCTGTTTCCTGTGTGAAATTG
urtE_fw	GCGCGCACGCGGCGGGCTGCAGGGTCGACTCTAGAGGATGCTATGTTATCCTTTCCCCCATTCTTG
urtE_rev	CCCAGTCACGACGTTGTAAAACGACGGCCGAATTCTTAGTTATACTGCCAAAAATTTTTGGATAAC
urtE_fw	ACAATTTCACACAGGAAACAGCTATGGCTATGTTATCCTTTCCC
urtE_rev	TGATGCGATTGCTGCATGGTTACTGCCAAAAATTTTTGGATAACC
urtE_pKT25n_fw	TATCCAAAAATTTTTGGCAGTAACCATGCAGCAATCGCATCAG
urtE_pKT25n_rev	GGGAAAGGATAACATAGCCATAGCTGTTTCCTGTGTGAAATTG

performed at OD_{750} = 0.6 by mixing the cultures with ice in a 2:1 ratio (w/w) for rapid metabolic inactivation, and centrifugation at 7,477 × *g* for 10 min. Cell pellets were subsequently washed with nitrogen-free BG-11^0 at 4°C and snap frozen in liquid nitrogen. For experimental controls, the wild-type strain was similarly cultivated and subjected to pull-down assays followed by mass spectrometry analyses as described below. Two independent replicates were prepared per condition.

Preparation of Cell Extracts and Anti-FLAG Pull-Down

Frozen cell pellets were washed with 5 mL IP buffer, containing 25 mM MES/NaOH; pH 6.5, 5 mM $CaCl_2$, 10 mM $MgCl_2$, and 20% (v/v) glycerol and subsequently resuspended in 3 mL IP buffer, including protease inhibitors (complete EDTA-free; Roche) for cell lysis. Therefore, an equal volume of glass beads (0.1–0.15 mm diameter) was added and cells were disrupted using a FastPrep-24 Ribolyser (MP Biomedicals) with five cycles of 20 s at 6.5 m s^{-1} and 4°C. After centrifugation for 5 min at 3,314 × *g* and 4°C, the supernatant was transferred and adjusted with IP buffer to a final volume of 6 mL. For membrane protein solubilization, 1.5% (w/v) dodecyl-β-D-maltoside (DDM; Carl Roth) was added and incubated under agitation for 1 h at 4°C, before insoluble cell debris was removed by centrifugation for 20 min at 20,000 × *g* and 4°C. The soluble cell extracts (from 2 L cultures) were subjected to the P_{II}-FLAG pull-down procedure: for this, 400 μL of resuspended anti-FLAG-M2-agarose (Sigma) was added into empty SPE-columns and washed twice with each 1 mL IP buffer, supplemented with 0.04% (w/v) DDM, before

TABLE 2 | Plasmids used in this study.

Plasmid	Tag localization	Description	References
pPD-*N*FLAG	N-terminal	Encoding the N-terminal 3xFLAG tag	Hollingshead et al., 2012
pPD-*C*FLAG	C-terminal	Encoding the C-terminal 3xFLAG tag	Chidgey et al., 2014
pKT25		Encoding T25 fragment of adenylate cyclase CyaA (amino acids 1–224)	Karimova et al., 2001
pKT25n		Derived from pKT25. Upstream of the T25 fragment	This study
pUT18		Encoding T18 fragment of adenylate cyclase CyaA (amino acids 225–399)	Karimova et al., 2001
pUT18 *gln*B	N-terminal	Derived from pUT18. Encoding *gln*B	This study
pUT18 *gln*B (I86N)	N-terminal	Derived from pUT18. Encoding *gln*B containing the I86N mutation	This study
pKT25n *pip*X	C-terminal	Derived from pKT25. Sequence encoding *pip*X. Positive control	This study
pKT25 *pip*X	N-terminal	Derived from pKT25. Sequence encoding *pip*X. Positive control	This study
pKT25n *amt*1	C-terminal	Derived from pKT25. Sequence encoding *amt*1	This study
pKT25 *amt*1	N-terminal	Derived from pKT25. Sequence encoding *amt*1	This study
pKT25n *nrt*C	C-terminal	Derived from pKT25. Sequence encoding *nrt*C	This study
pKT25 *nrt*C	N-terminal	Derived from pKT25. Sequence encoding *nrt*C	This study
pKT25n *nrt*D	C-terminal	Derived from pKT25. Sequence encoding *nrt*D	This study
pKT25 *nrt*D	N-terminal	Derived from pKT25. Sequence encoding *nrt*D	This study
pKT25n *urt*D	C-terminal	Derived from pKT25. Sequence encoding *urt*D	This study
pKT25 *urt*D	N-terminal	Derived from pKT25. Sequence encoding *urt*D	This study
pKT25n *urt*E	C-terminal	Derived from pKT25. Sequence encoding *urt*E	This study
pKT25 *urt*E	N-terminal	Derived from pKT25. Sequence encoding *urt*E	This study

the supernatants were incubated for 5 min and removed by gravity flow. Repeated washing steps with each 5 mL DDM supplemented IP buffer were performed similarly, until the flow through appeared colorless. Elution of coupled proteins from the anti-FLAG resin was performed by incubation in 600 μL DDM supplemented IP buffer containing 0.3 μg/mL 3xFLAG^{TM} peptide (Sigma-Aldrich) for 40 min.

Proteomics Workflow, NanoLC-MS/MS Analysis, and Data Processing

Eluates from the pull-down workflow were subjected to acetone/methanol precipitation and resulting protein pellets were resuspended in denaturation buffer for subsequent tryptic digestion as described elsewhere (Spät et al., 2015). Resulting peptide mixtures were subjected to stage tip purification (Rappsilber et al., 2007). Protein detection by mass spectrometry (MS) was performed as described previously (Spät et al., 2015): in brief, peptide mixtures were loaded onto a 15 cm reversed-phase C_{18} nanoHPLC column on an EASY-LC system (Proxeon Biosystems) and separated in a 90 min segmented linear gradient. Eluted peptides were ionized by the on-line coupled ESI source and injected in a LTQ Orbitrap XL mass spectrometer (Thermo Scientific). MS spectra were acquired in the positive-ion mode. Per scan cycle, one initial full (MS) scan was followed by fragmentation of the 15 most intense multiply charged ions by collision induced dissociation (CID) for MS/MS scans. The scan range was 300–2,000 m/z for precursor ions at resolution 60,000 and sequenced precursors were dynamically excluded for fragmentation for 90 s. The lock mass option was enabled for real time mass recalibration (Olsen et al., 2005). All raw spectra were processed with the MaxQuant software (version 1.5.2.8) (Cox and Mann, 2008) at default settings. Peak lists were searched against a target-decoy database of *Synechocystis* sp. PCC 6803 with 3,671 protein sequences, retrieved from Cyanobase (Nakao et al., 2010) (July 2014), plus the sequence of the N- or C-terminal 3xFLAG tagged P_{II} fusion protein (MDYKDDDDKDYKDDDDKDYKDDDDKAAAKKVEAIIRPF KLDEVKIALVNAGIVGMTVSEVRGFGRQKGQTERYRGSEYT VEFLQKLKIEIVVDEGQVDMVVDKLVSAARTGEIGDGKIFIS PVDSVVRIRTGEKDTEAI or MKKVEAIIRPFKLDEVKIALVN AGIVGMTVSEVRGFGRQKGQTERYRGSEYTVEFLQKLKIEIV VDEGQVDMVVDKLVSAARTGEIGDGKIFISPVDSVVRIRTG EKDTEAIASYKDDDDKDYKDDDDKDYKDDDDK), respectively, as well as 245 common contaminants with the following database search criteria: trypsin was defined as a cleaving enzyme and up to two missed cleavages were allowed; carbamidomethylation of cysteines was defined as a fixed modification

TABLE 3 | Strains used in this study.

Strains	Description	References
E. coli NEB 10-beta	Cloning strain	NEB
E. coli BTH101	Bacterial two-hybrid host strain	Euromedex
Synechocystis sp. PCC 6803	Wild type	Pasteur Culture Collection
Synechocystis sp. P_{II}(I86N)	Genomic P_{II}(I86N) mutant	Watzer et al., 2015
Synechocystis sp. ΔP_{II}	Chromosomal deletion of *glnB*	Hisbergues et al., 1999
Synechocystis sp. ΔP_{II} + P_{II}-Venus	*Synechocystis* sp. ΔP_{II} transformed with pVZ322 encoding a P_{II}-Venus fusion	Hauf et al., 2016

and methionine oxidation and protein N-terminal acetylation as variable modifications. Peptide and protein false discovery rates retrieved from MaxQuant were limited to 1%, each. Raw data acquired by mass spectrometry was deposited at the ProteomeXchange Consortium via the Pride partner repository (Vizcaino et al., 2013) under the identifier PXD013411.

Determination of Nitrate, Nitrite, Ammonium, and Urea in Cell-Free Culture Medium

To determine the nitrate, ammonium, or urea uptake, exponentially growing cells (OD_{750} = 0.4–0.8) were harvested by centrifugation (3,000 × *g* for 10 min at room temperature) and washed twice with BG-11^0 medium lacking combined nitrogen sources. Subsequently, the cultures were adjusted to OD_{750} = 1 with BG-11^0 medium. The assays were started by adding either 200 μM $NaNO_3$, 200 μM NH_4^+ or 150 μM urea, respectively. Cells were cultivated under constant shaking of 120 rpm and illumination of 40–50 μE. 1 mL aliquots of the cell suspensions were taken and subsequently centrifuged (13,000 × *g* for 5 min at room temperature) to remove the cells.

For nitrate quantification, the absorbance at 210 nm was measured in the cell-free medium. Since both nitrate and nitrite absorb at 210 nm, the apparent nitrate values were corrected for the presence of nitrite (Kloft and Forchhammer, 2005). Nitrite concentration of the cell-free medium was determined using the modified Griess reaction according to Fiddler (1977).

The ammonium concentration of cell-free medium was measured by using the Nessler reaction (Vogel et al., 1989). Urea was quantified by using the urea nitrogen (BUN) colorimetric detection kit (Invitrogen).

Microscopy Procedures and Image Evaluation

Fluorescence microscopy was performed using a Leica DM5500B microscope with a 100×/1.3 oil objective. For the detection of Venus fluorescence, an ET500/20× excitation filter and an ET535/30m emission filter were used referred as YFP-channel. To detect cyanobacterial autofluorescence, an excitation filter BP 535/50 and a suppression filter BP 610/75 were used. Image acquisition was done with a Leica DFC360FX black-and-white camera. Captured images were colored with the Leica Application Suite Software (LAS AF) provided by Leica Microsystems. Bright-field images were exposed for 6 ms, Venus fluorescence images for 150 ms and autofluorescence images for 100 ms. Microscope slides covered with dried 2% (w/v) agarose solution were used to immobilize the cells during all microscopical examinations.

Quantitative image evaluation by fluorescence intensity measurements was performed using the open-source software ImageJ (Fiji) (Schindelin et al., 2012). To estimate the fluorescence intensities in different cell compartments, a linear profile of the gray values across the cells through the plasma membrane and cytoplasm was determined. The average gray level of the cytoplasm was subtracted from the maximum gray level of the plasma membrane signal to yield the "Δ fluorescence" value, which indicates the cytoplasmic membrane-localized signal. An example of this profile data quantification is given in **Supplementary Figure 1**.

RESULTS

P_{II} Signaling Mutants Show Increased Sensitivity to Ammonium

P_{II} homologs of the GlnK subfamily from heterotrophic bacteria are known to regulate cellular ammonium influx by direct protein–protein interaction with the ammonium permease AmtB (Huergo et al., 2012). The observation of impaired ammonium utilization in the *Synechocystis* strain, which harbors the P_{II}(I86N) variant, suggested that this P_{II} variant either blocked ammonium uptake or abolished proper ammonium uptake regulation with consequent ammonium sensitivity. The Ile 86 to Asn point mutation in this P_{II} variant causes a specific alteration of the T-loop conformation, which facilitates interaction with NAGK and thus, results in an over-activation of this P_{II} target (Fokina et al., 2010b). Conversely, other P_{II} targets might by negatively affected by the altered T-loop conformation. To gain further insights into the role of P_{II} in ammonium uptake, we tested ammonium utilization of a P_{II} deletion mutant (ΔP_{II}) (Hisbergues et al., 1999) and of the ΔP_{II} strain complemented with P_{II}-Venus (P_{II}-Venus-comp.) (Hauf et al., 2016). The complementation strain was previously generated by introducing a shuttle vector (pVZ322), encoding a P_{II}-Venus fusion under control of the native *gln*B promoter into the *Synechocystis* ΔP_{II} mutant (Hauf et al., 2016). The Venus fluorescent protein was fused to the C-terminus of P_{II} to avoid sterical hindrance of the T-loop.

When grown in presence of 5 mM ammonium in liquid medium, the *Synechocystis* wild-type, the ΔP_{II} and the P_{II}-Venus-comp. strains showed similar growth rates and ammonium consumption (**Figures 1A,B**). However, with an elevated ammonium concentration of 10 mM, only the wild-type and P_{II}-Venus-comp. strains could maintain normal growth, while the ΔP_{II} mutant arrested growth (**Figure 1C**). Ammonium utilization of wild-type and P_{II}-Venus-comp. were similar under this condition (**Figure 1D**) while the ΔP_{II} strain ceased ammonium utilization (**Figure 1D**). The ammonium-sensitive phenotype of the ΔP_{II} strain, in particular the response toward 10 mM ammonium, resembled the previously reported phenotype of the *Synechocystis* P_{II}(I86N) strain (Watzer et al., 2015). One possibility to explain the inability of the P_{II} mutant strains to grow in 10 mM ammonium-supplemented medium is an increased sensitivity toward toxic effects of ammonium. Although ammonium represents the preferred nitrogen source, it becomes toxic for many photosynthetic organisms at higher concentrations (Drath et al., 2008). To find out whether the reduced growth and impaired ammonium utilization results from ammonium intoxication, we assayed the growth of the various strains in the presence of increasing concentrations of ammonium using the spot assay method (**Figure 2**). Over a range from 5 to 40 mM ammonium, the wild-type and P_{II}-Venus-comp. strains showed a similar growth

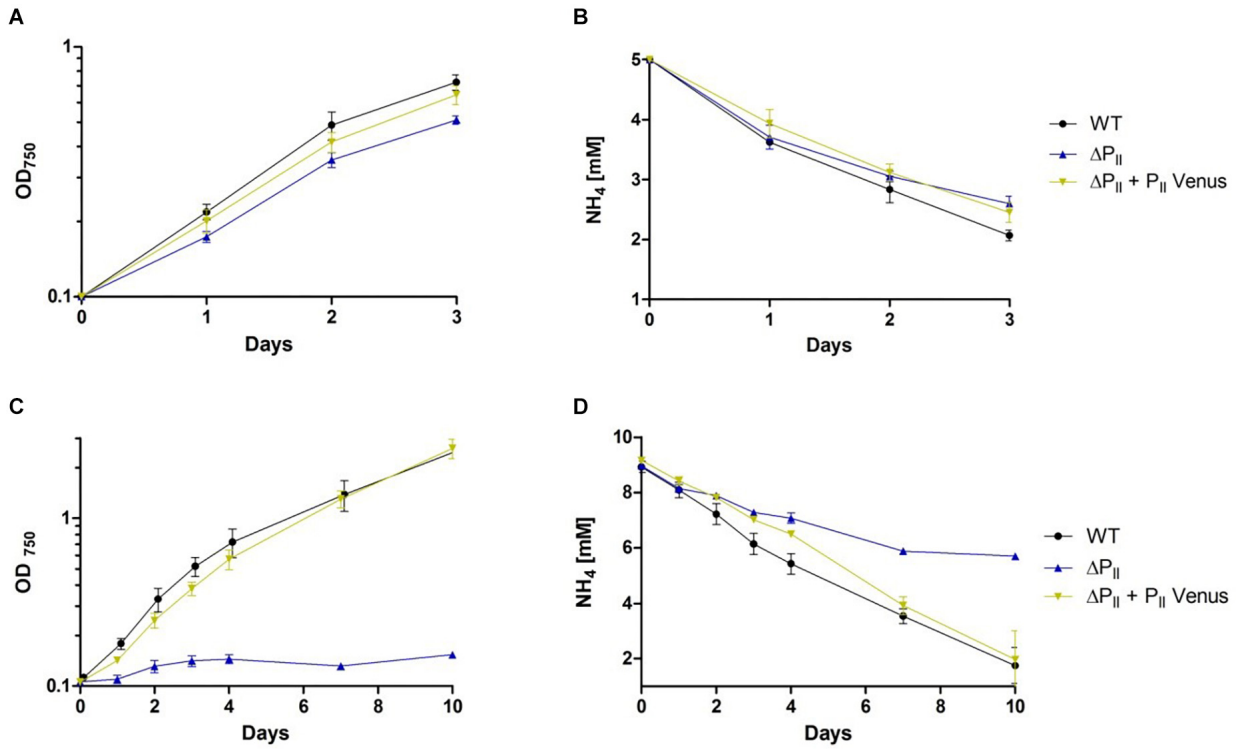

FIGURE 1 | Ammonium supplemented growth and ammonium utilization of *Synechocystis* sp. wild-type, ΔP_{II} and P_{II}-Venus-comp. (ΔP_{II} + P_{II}-Venus) strains. Values are the means of three biological replicates. **(A)** Growth curve in presence of 5 mM ammonium. **(B)** Ammonium concentration in culture supernatants of the various *Synechocystis* strains grown in BG-11 medium with 5 mM ammonium. **(C)** Growth curve in presence of 10 mM ammonium. **(D)** Ammonium concentration in culture supernatants of the various *Synechocystis* strains grown in BG-11 medium with 10 mM ammonium.

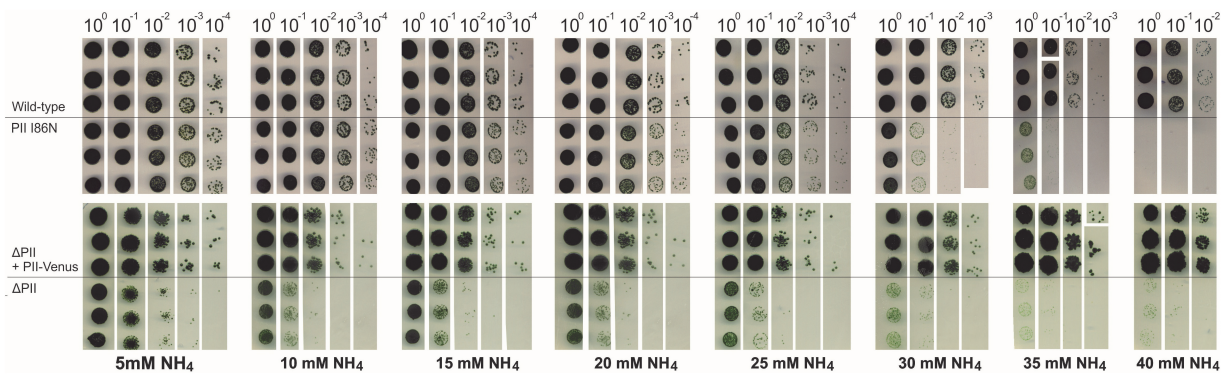

FIGURE 2 | Ammonium sensitivity of the various *Synechocystis* strains (as in **Figure 1**) as determined by the drop plate method with three biological replicates per strain. Starved cultures were adjusted to an OD_{750} of 1.0 and diluted tenfold in series. The dilutions were dropped onto BG-11 agar plates containing increasing concentrations of ammonia (5–40 mM).

and ammonium tolerance. However, the P_{II}(I86N) mutant showed impaired growth at 25 mM while the ΔP_{II} mutant was already strongly affected at a concentration of 10 mM ammonium (**Figure 2**). This demonstrated that P_{II} is indeed required to cope with elevated ammonium concentrations. The P_{II}(I86N) mutant can only partially replace the wild-type P_{II} protein, whereas P_{II}-Venus perfectly complemented the ΔP_{II} strain.

Identification of Novel P_{II} Interaction Partners by FLAG-Tag P_{II} Pull-Down Assays

Uncontrolled influx of ammonium and resulting intoxication of *Synechocystis* ΔP_{II} and P_{II}(I86N) mutants is likely a cause for the elevated ammonium sensitivity in these strains. This suggested the involvement of P_{II} in the regulation of

Synechocystis ammonium permeases. In order to verify such an interaction, we performed pull-down assays using a C-terminal 3xFLAG-tagged P_{II} fusion protein that was expressed in *Synechocystis* under control of the strong *psbA* promoter. Protein extracts were prepared in presence of detergent, to solubilize membrane-bound proteins, and were subjected to anti-FLAG-tag immunoprecipitation. The proteome composition of the immunoprecipitate was subsequently analyzed by MS to reveal the proteins that co-purify with FLAG-tag P_{II}. As an initial experiment, the immunoprecipitation was performed with cells grown in BG-11 medium, containing nitrate as unique nitrogen source. To discriminate between P_{II} interaction partners and unspecific background proteins, the non-transformed wild-type strain was used as an experimental control. Each experiment was further validated by an independent replicate.

As a proof of concept, we were able to identify P_{II} as the most abundant protein in the P_{II} 3xFLAG pull-down (thereafter P_{II} pull-down). Furthermore, some reported interaction partners, such as PipX, were either exclusively identified in the P_{II} pull-down, or, as in the case of the P_{II} phosphatase PphA, were strongly enriched compared to the background control (**Supplementary Figure 2**) (Kloft and Forchhammer, 2005; Espinosa et al., 2007; Forcada-Nadal et al., 2014). The identification of a large number of background proteins in the experiments depends on the wash-stringency, the abundance of individual proteins and the high sensitivity of MS-detection. To distinguish between specific P_{II}-enriched interaction partners and background, we determined relative protein abundance ratios between the P_{II} and control experiments by using label free quantification (LFQ) (Cox et al., 2014). Proteins with a significantly higher abundance in the P_{II} pull-down were identified by significance analysis (p-value = 0.01). Since both independent replicates from nitrate-grown cultures yielded very similar results, we correlated the data (**Figure 3**). Using this approach, the major ammonium permease Amt1 (Montesinos et al., 1998) indeed appeared among the significantly enriched proteins, supporting our suggestion that Amt1 represents a P_{II} binding target in cyanobacteria. Surprisingly, we could also identify subunits of other nitrogen import complexes besides Amt1 among the

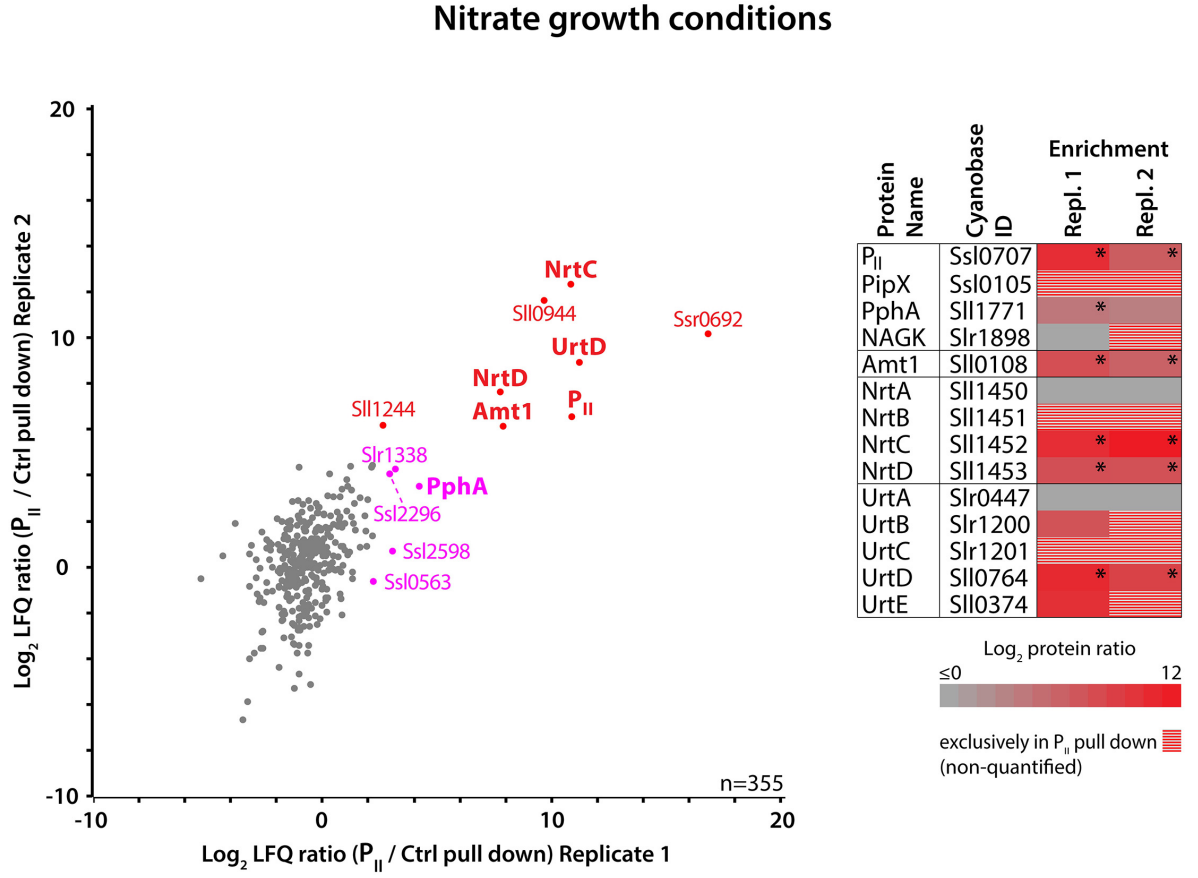

FIGURE 3 | Proteins enriched in anti-FLAG-tag P_{II} immunoprecipitates from nitrate growth conditions. **(Left)** Scatterplot of the $\log_2$ transformed LFQ protein ratios (P_{II}/control pull-down experiment) of 355 quantified proteins detected in two independent replicates. P_{II} pull-down specific outliers which are significantly enriched in both replicates are indicated in red, and significant outliers enriched only in Replicate 1 are indicated in magenta (p-value = 0.01). **(Right)** Heat map representation of the P_{II}-specific enrichment of nitrogen metabolism related proteins. Log_2 transformed LFQ protein ratios from both replicates are color coded and stars indicate significance. Proteins with missing LFQ ratios, detected exclusively in the P_{II} but not in the control pull-down, are striped in red/gray.

significantly enriched proteins, in particular subunits of the bispecific NrtABCD nitrate/nitrite and the UrtABCDE urea transporter complexes. For the NRT and URT transporters, all subunits except the periplasmic substrate binding proteins NrtA and UrtA were either exclusively present or strongly enriched in the P_{II} pull-downs. This suggests that the cytoplasmic components of the transporters together with the pore forming subunit are still associated in a complex, detached from the loosely associated periplasmic binding proteins (NrtA or UrtA).

To further validate a potential interaction between P_{II} and the URT transporter complex, we repeated the experiment with cells grown in urea-supplemented medium. In agreement with the results from the P_{II} pull-down at nitrate growth conditions, we detected an enrichment of the P_{II} target PipX, the ammonium permease Amt1, subunits of the NRT nitrate/nitrite transporter, and most prominent, subunits of the URT urea transporter (**Supplementary Figure 3**). By correlating the data from both independent replicates (**Figure 4**), it became evident that UrtD and UrtE are the strongest enriched proteins under this condition besides P_{II}. This suggests that the presence of urea in the medium influences the interaction of the URT transporter complex with P_{II}.

Besides proteins associated with nitrogen import, we also identified two small hypothetical proteins to be significantly enriched in all experiments, Sll0944 and Ssr0692. Interestingly, both proteins are under transcriptional control of the global nitrogen regulator NtcA (Giner-Lamia et al., 2017), and reveal opposed dynamics in response to nitrogen availability. Under nitrogen-limiting conditions, Sll0944 was found to be strongly up-regulated at transcriptome and proteome levels, whereas Ssr0692 was strongly down-regulated (Spät et al., 2015; Giner-Lamia et al., 2017). Intriguingly, Ssr0692 seems to be up-regulated under carbon limitation (Battchikova et al., 2010) and might be associated to carbon fixation, as it was identified as a potential interactor of NdhH (Sato et al., 2007). The protein Sll0944 is highly conserved in cyanobacteria and possesses a domain of unknown function (DUF1830). Overall, our results imply a direct linkage of Sll0944 and Ssr0692 to nitrogen metabolism with a regulatory involvement of P_{II}. Both proteins are currently under investigation to validate a potential interaction with P_{II} and to determine their function.

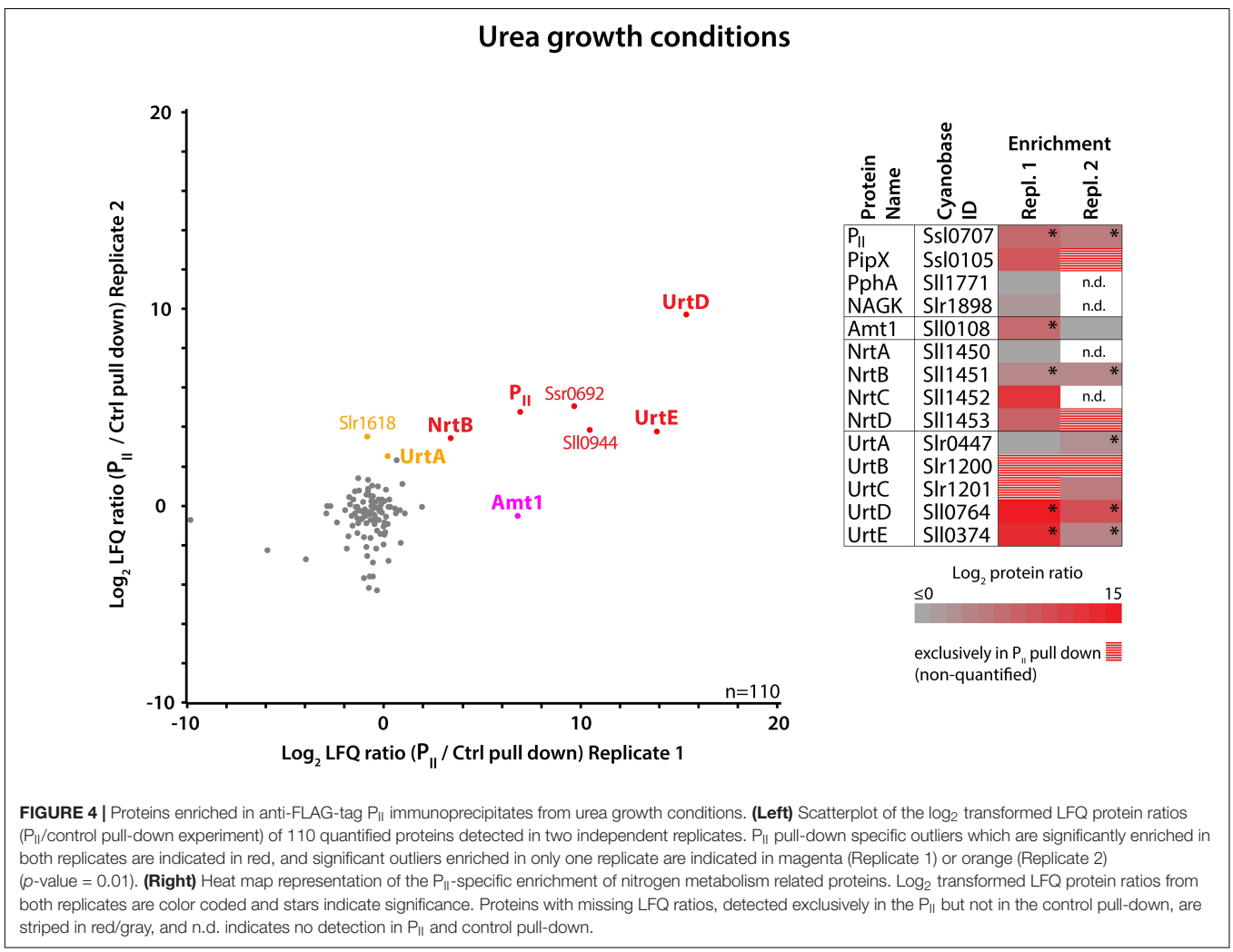

FIGURE 4 | Proteins enriched in anti-FLAG-tag P_{II} immunoprecipitates from urea growth conditions. **(Left)** Scatterplot of the log_2 transformed LFQ protein ratios (P_{II}/control pull-down experiment) of 110 quantified proteins detected in two independent replicates. P_{II} pull-down specific outliers which are significantly enriched in both replicates are indicated in red, and significant outliers enriched in only one replicate are indicated in magenta (Replicate 1) or orange (Replicate 2) (*p*-value = 0.01). **(Right)** Heat map representation of the P_{II}-specific enrichment of nitrogen metabolism related proteins. Log_2 transformed LFQ protein ratios from both replicates are color coded and stars indicate significance. Proteins with missing LFQ ratios, detected exclusively in the P_{II} but not in the control pull-down, are striped in red/gray, and n.d. indicates no detection in P_{II} and control pull-down.

Surprisingly, the well-studied P_{II} interactor NAGK was not clearly enriched in these experiments. A low percentage of P_{II}-NAGK complexes was expected to be present under nitrate or urea growth conditions (Burillo et al., 2004), although the strongest interaction occurs under conditions of nitrogen oversupply. Possibly, the C-terminal 3xFLAG-tag fusion of this P_{II} variant could negatively affect complex formation with NAGK. Therefore, pull-down experiments were also performed with an N-terminal 3xFLAG-tag fusion to P_{II}. There, we could clearly identify NAGK in the pull-down of nitrate grown cells in two independent replicates (**Table 4**). The identification of NAGK in both N-terminal P_{II}-fusion pull-down replicates implies that the localization of the 3xFLAG-tag has an influence on the interaction between P_{II} and its targets. Comparing the results from N- or C-terminal FLAG-tag fused P_{II} pull-down experiments can give additional information to identify potential P_{II} interaction partners. In contrast to the experiments utilizing the C-terminal FLAG-tag, where subunits of the heterotrimeric urease complex UreABC were not enriched, to our surprise, the N-terminal FLAG-tagged P_{II} protein co-purified the entire urease-complex including associated urease accessory proteins D, F, and G. This remarkable finding implies a possible direct interaction between the urease transport complex and the succeeding enzymatic machinery urea metabolism, indicating possible metabolic channeling of urea (Sweetlove and Fernie, 2018).

TABLE 4 | Identified proteins in pull-down experiments at nitrate growth conditions utilizing the N-terminal 3xFLAG-tagged P_{II} fusion protein: Displayed are the identified proteins from two independent replicates (Repl. I and Repl. II).

Protein name/ complex	Cyanobase ID	Mol. weight (kDa)	iBAQ intensity	
			Repl. I	Repl. II
P_{II}/N-3xFLAG P_{II}	Ssl0707	15.43	$4.2*10^7$	$1.1*10^9$
PipX	Ssl0105	10.45	$3.1*10^6$	$9.1*10^7$
PphA	Sll1771	28.47	$4.2*10^4$	$9.1*10^5$
NAGK	Slr1898	31.53	$9.4*10^4$	$6.5*10^5$
Amt1	Sll0108	53.58	$1.2*10^8$	$2.9*10^8$
NrtA	Sll1450	48.97	$1.1*10^5$	$1.4*10^6$
NrtB	Sll1451	29.72	$8.8*10^5$	$5.1*10^6$
NrtC	Sll1452	75.10	$1.4*10^6$	$6.1*10^6$
NrtD	Sll1453	36.56	$1.9*10^5$	$2.9*10^6$
UrtA	Slr0447	48.36	$1.0*10^5$	$2.6*10^5$
UrtB	Slr1200	41.68	$2.4*10^5$	$1.6*10^6$
UrtC	Slr1201	45.08	$3.5*10^5$	$4.9*10^6$
UrtD	Sll0764	41.19	$8.1*10^5$	$3.9*10^6$
UrtE	Sll0374	27.42	$6.5*10^5$	$6.4*10^6$
UreA	Slr1256	11.06	–	$4.9*10^5$
UreB	Sll0420	11.38	$2.0*10^5$	$5.2*10^7$
UreC	Sll1750	61.04	$9.9*10^6$	$3.5*10^7$
UreD	Sll1639	27.16	$1.2*10^5$	$6.4*10^5$
UreF	Slr1899	20.23	$3.1*10^4$	$5.2*10^5$
UreG	Sll0643	22.01	$1.3*10^5$	$1.2*10^6$
Sll0944	Sll0944	18.15	$8.4*10^5$	$9.8*10^7$
Ssr0692	Ssr0692	5.85	$2.8*10^5$	$9.3*10^6$

Protein intensities were calculated using the MaxQuant iBAQ algorithm (Schwanhausser et al., 2011).

Bacterial Two-Hybrid Assay

To further confirm the interaction of P_{II} with the identified nitrogen transporters, we performed bacterial two-hybrid assays using the *Bordetella pertussis* adenylate cyclase two-hybrid system (BACTH) (Battesti and Bouveret, 2012). We tested the cytoplasmic localized ATP-binding proteins of the ABC-type transporters NrtC, NrtD, UrtD, UrtE (Omata et al., 1993; Valladares et al., 2002) as well as Amt1 for possible interactions with various P_{II} proteins. For each interaction candidate, an N- and a C-terminal fusion to the T25 fragment was constructed. In case of a positive interaction with a P_{II}-T18 fusion, cAMP is formed within a cAMP deficient *E. coli* host cell. The interactions were tested by plate assays on X-Gal and MacConkey reporter plates for highest detection sensitivity. The P_{II} – PipX and leucine zipper interactions were used as positive controls. P_{II}-T18 fusions with an empty pKT25 vector were used as negative controls. Next to wild-type P_{II}-T18 fusion, we also included T18 fusions of the P_{II}(I86N), P_{II}(S49D), and P_{II}(R9L) variants to find out how these different P_{II} variants, including a phosphomimetic T-loop variant and variants with different effector binding properties would differ in potential P_{II} interactions. **Figure 5** shows the observed interactions on X-Gal plates in the bacterial two-hybrid assays.

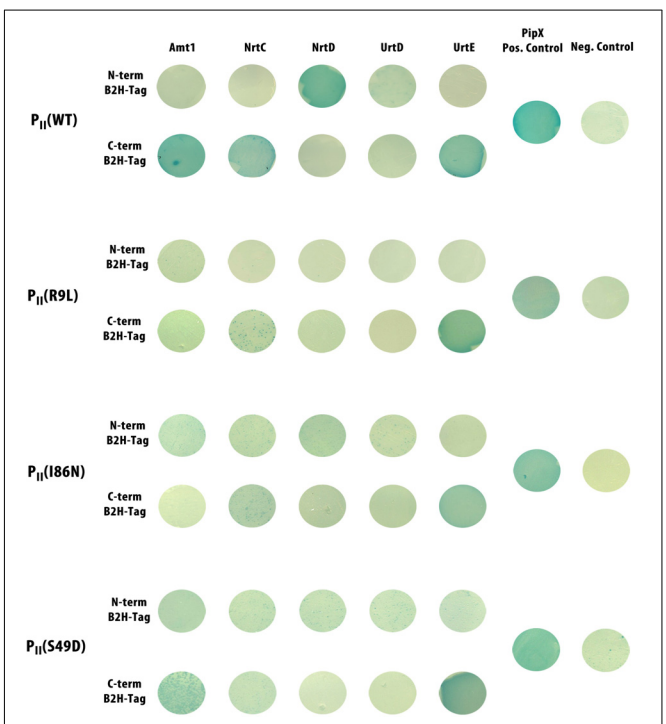

FIGURE 5 | Bacterial-two-hybrid interactions on X-Gal plates of wild-type P_{II} and the P_{II} variants P_{II}(R9L), P_{II}(I86N), P_{II}(S49D) with different transporter subunits. Interaction of P_{II} with C-terminal tagged PipX was used as a positive control. P_{II} with an empty pKT25 vector was used as negative control. Positive interactions are indicated by a blue coloration of the colonies.

All P_{II} variants showed interaction with the known P_{II} interaction partner PipX. Wild-type P_{II} showed clear interaction with Amt1 C-terminally fused to the T25 fragment, while the variants P_{II}(I86N) and P_{II}(R9L) did not interact. The loss of interaction of P_{II}(I86N) is in agreement with our previous conclusions regarding the impaired ammonium utilization of *Synechocystis* sp. strain P_{II}(I86N). The phosphomimetic variant P_{II}(S49D) showed weak interaction with Amt1. In case of the nitrate transport ATP-binding subunits NrtC and NrtD, the BACTH assay revealed clear interaction of wild-type P_{II} with both subunits. Intriguingly, P_{II} interacted only with NrtC when it was fused at its C-terminus with T25, whereas in the case of NrtD, P_{II} interacted with the N-terminal fusion. In contrast to wild-type P_{II}, the P_{II}(R9L) variant was completely unable to interact with any of the Nrt-proteins, while weak interactions were observed with variants P_{II}(S49D) and P_{II}(I86N). With the ATP-binding subunits of the urea transporter, no interaction was observed with the UrtD protein, neither with wild-type P_{II} nor with any of the tested variants. By contrast, the C-terminal T25 fusion of UrtE showed clear interaction with wild-type and all P_{II} variants. The fact that positive interactions only occurred with selective combinations of P_{II} variants and N-or C-terminal T25 fusions of target proteins supports the conclusion that the observed interactions are indeed specific.

P_{II} Deletion Mutant and P_{II}(I86N) Mutant Excrete Nitrite

The pull-down and BACTH assays shown above clearly indicated interaction of wild-type P_{II} protein with components of the uptake systems for ammonium, nitrate, and urea. The interaction with Amt1 likely resembles the known interaction of the P_{II} protein GlnK from heterotrophic bacteria with AmtB (Conroy et al., 2007; Gruswitz et al., 2007) and perfectly explains the physiological response of *Synechococcus* PCC 7942 (hereafter *Synechococcus*) and *Synechocystis* P_{II} mutants toward ammonium. Interaction of P_{II} with components of the NrtABCD nitrate/nitrite transporter had in fact been suggested previously by several physiological studies, which documented altered nitrate utilization properties in various *Synechococcus* and *Synechocystis* P_{II} mutants (Kobayashi et al., 1997; Lee et al., 1998, 2000; Kloft and Forchhammer, 2005). A characteristic phenotype of a P_{II} deletion mutant grown in the presence of nitrate is the uncontrolled uptake of nitrate and subsequent excretion of nitrite into the medium (Kloft and Forchhammer, 2005). Reduction of nitrate requires two electrons whereas six electrons are needed for the reduction of nitrite to ammonium. Because of the lower electron demand for nitrate reduction, nitrite reduction becomes limiting when insufficient reductant is available. Therefore, when nitrate uptake is uncontrolled, nitrite accumulates and is excreted. We wondered if the *Synechocystis* P_{II}(I86N) strain shows a similar nitrite excretion phenotype than the P_{II} deficient mutant when grown on nitrate and if P_{II}-Venus complements the nitrite excretion phenotype of the P_{II}-deficient mutant.

To answer this question, *Synechocystis* wild-type strain, P_{II}(I86N), ΔP_{II} and the P_{II}-Venus comp. strains were grown with nitrate as sole nitrogen source under constant illumination (40 μmol photons m^{-2} s^{-1}) and samples were removed for nitrite determination. Under these conditions, the various strains showed similar growth rates (**Figure 6**). Both mutant strains expected to be impaired in proper control of the NRT complex, the ΔP_{II} mutant and the P_{II}(I86N) strain, indeed excreted nitrite into the medium. Notably, the P_{II}(I86N) mutant excreted much lower nitrite amounts than the P_{II} deletion mutant, in agreement with the partial interaction of the P_{II}(I86N) variant observed in the BACTH assays with NrtC and NrtD subunits. By contrast, P_{II}-Venus perfectly complemented the nitrite excretion phenotype. Together, these results indicated that the BACTH interactions of P_{II} with the NrtC and NtcD subunits are physiologically meaningful.

P_{II} Is Responsible for Inhibition of Nitrate Uptake

To gain further insights in the P_{II}-dependent regulation of nitrate uptake, we measured nitrate consumption rates of the various P_{II}-mutants under different conditions. For this purpose, cells from exponential phase of growth in standard BG-11 medium were washed and subsequently incubated in BG-11^0 medium containing 200 μM NO_3 as nitrogen source. Nitrate utilization was quantified by measuring the nitrate concentration in the culture supernatant over time. Under constant illumination of 40 μmol photons m^{-2} s^{-1}, *Synechocystis* wild-type and the P_{II}-Venus comp. strain showed lower nitrate consumption rates, while both, the P_{II}(I86N) and ΔP_{II} mutant, showed higher nitrate removal (**Figure 7A**). In agreement with our previous results, we observed excretion of nitrite by the P_{II}(I86N) and ΔP_{II} mutants (**Figure 7B**). Interestingly, while the nitrate utilization rate of the P_{II}(I86N) and ΔP_{II} mutant appeared almost identical, the two mutants differed in their rate of nitrite excretion. While nitrite excretion of the ΔP_{II} mutant accelerated over time, the P_{II}(I86N) initially excreted nitrite faster but then slowed it down over time, explaining the lower amounts of nitrite in the exponentially growing culture (**Figure 6**) as compared to the ΔP_{II} mutant.

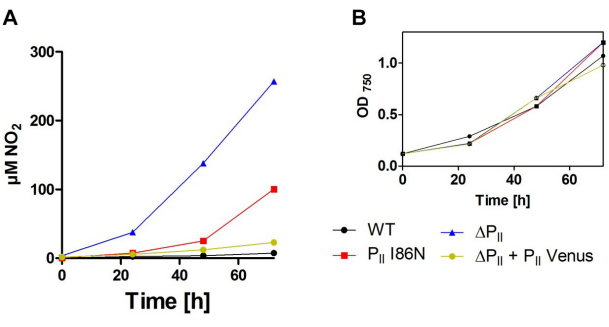

FIGURE 6 | (A) Nitrite excretion of *Synechocystis* sp. wild-type, P_{II}(I86N), ΔP_{II} and P_{II}-Venus-comp. (ΔP_{II} + P_{II}-Venus) complementation grown in BG11 medium supplemented with nitrate. **(B)** Corresponding growth curve to the experiment shown in panel **(A).**

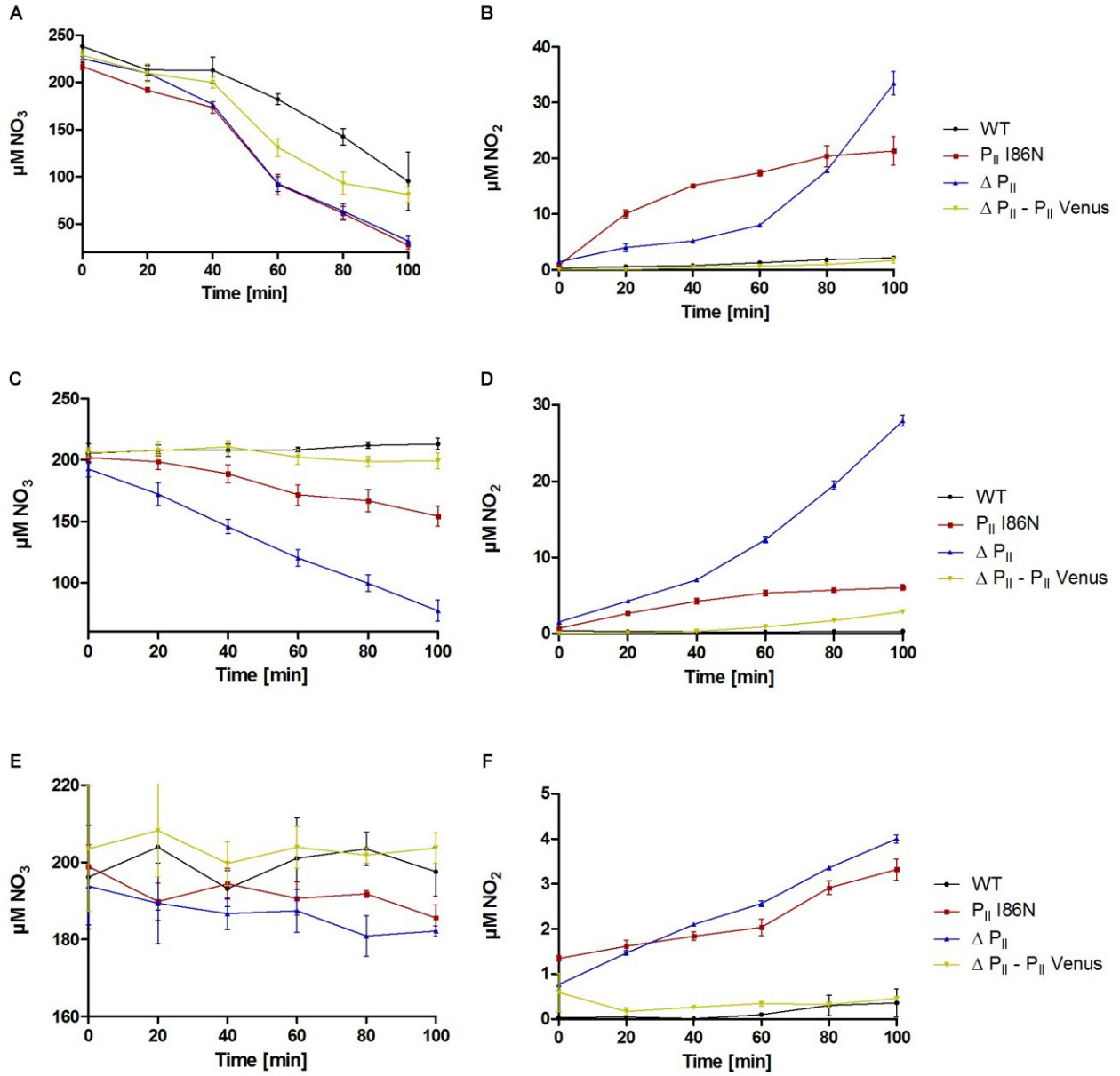

FIGURE 7 | Nitrate utilization and nitrite excretion of various *Synechocystis* strains as indicated. Exponentially growing and nitrate supplemented *Synechocystis* cells were washed and resuspended in a medium containing 200 µM nitrate. Shown are the means of three biological replicates. **(A)** Nitrate utilization and **(B)** nitrite excretion under constant illumination of 40 µmol photons m^{-2} s^{-1}. **(C)** Nitrate utilization and **(D)** nitrite excretion in presence of 2 mM ammonium and under constant illumination of 40 µmol photons m^{-2} s^{-1}. **(E)** Nitrate utilization and **(F)** nitrite excretion in the dark.

Addition of ammonium to nitrate grown cells leads to an immediate inhibition of nitrate uptake. This ammonium-dependent inhibition of nitrate uptake requires the presence of P_{II} protein or P_{II} phosphomimetic variants (Lee et al., 1998). Here, we tested if the P_{II}(I86N) mutant was able to perform the ammonium-dependent nitrate uptake inhibition. For this purpose, nitrate consumption rates were determined after the addition of 2 mM ammonium. Both, *Synechocystis* wild-type and the P_{II}-Venus comp. strains showed a complete inhibition of nitrate uptake in response to ammonium (**Figure 7C**). By contrast, the P_{II}(I86N) and ΔP_{II} mutant strains maintained nitrate uptake after ammonium addition. However, nitrate uptake in the P_{II}(I86N) mutant was clearly diminished as compared to the ΔP_{II} mutant (**Figure 7C**). The uncontrolled nitrate uptake of the P_{II}(I86N) and ΔP_{II} mutant caused excretion of nitrite. Due to the diminished uptake of nitrate by the P_{II}(I86N) mutant, its nitrite excretion was correspondingly lower as compared to the ΔP_{II} mutant (**Figure 7D**).

In addition to the absence of ammonium, active nitrate transport also requires photosynthetic CO_2 fixation

(Romero et al., 1985). Nitrogen assimilation is tightly regulated by light/dark transitions. A transition from light to dark causes an immediate inhibition of nitrate uptake and an inhibition of the ammonium assimilating GS (Romero et al., 1985; Marques et al., 1992). To reveal a role of P_{II} in this response, we tested the dark-switch-off of nitrate uptake in the various P_{II} mutant strains. Although the overall nitrate consumption was very low in darkness (**Figure 7E**) clear differences could be resolved. Notably, the P_{II}(I86N) and ΔP_{II} mutant strains showed slow but constant nitrate uptake as compared to the wild-type and the P_{II}-Venus comp. strain, which did not take up any nitrate. Corresponding to the uptake of nitrate, P_{II}(I86N) and ΔP_{II} mutant excreted small amounts of nitrite (**Figure 7F**), supporting the notion that the P_{II}(I86N) and ΔP_{II} mutants are unable to completely switch-off nitrate uptake in the dark.

P_{II} Signaling Mutants Show Impaired Urea Utilization

To validate the physiological relevance of the interaction of P_{II} with the UrtE subunit of the urea transporter UrtABCDE, we analyzed urea utilization in the different P_{II} mutants. For this purpose, exponentially growing cells were washed and incubated in BG-11^0 medium, containing 150 μM urea as sole nitrogen source with constant illumination of 40 μmol photons m^{-2} s^{-1}. Under these experimental conditions, *Synechocystis* wild-type and P_{II}(I86N) mutant strains utilized similar amounts of urea (**Figure 8A**), whereas both, the ΔP_{II} and P_{II}-Venus comp. strains consumed considerably higher amounts of urea (**Figure 8A**). The wild-type property of the P_{II}(I86N) variant is in agreement with the interaction of the P_{II}(I86N) protein with the UrtE subunit, which appeared to be T-loop independent according to BACTH assays. Urea is hydrolyzed to CO_2 and two molecules of ammonium by the enzyme urease (Mobley and Hausinger, 1989; Esteves-Ferreira et al., 2018). We wondered if an uncontrolled influx of urea could lead to an excretion of ammonium. Therefore, we measured ammonium concentrations in culture supernatant of those cells, which were incubated with 150 μM urea as the sole nitrogen source. Indeed, we detected ammonium excretion of the ΔP_{II} mutant proportional to its urea utilization (**Figure 8B**). In contrast, only minor amounts of ammonium could be detected in the culture supernatant of the *Synechocystis* wild-type, P_{II}(I86N) and P_{II}-Venus comp. strain (**Figure 8B**).

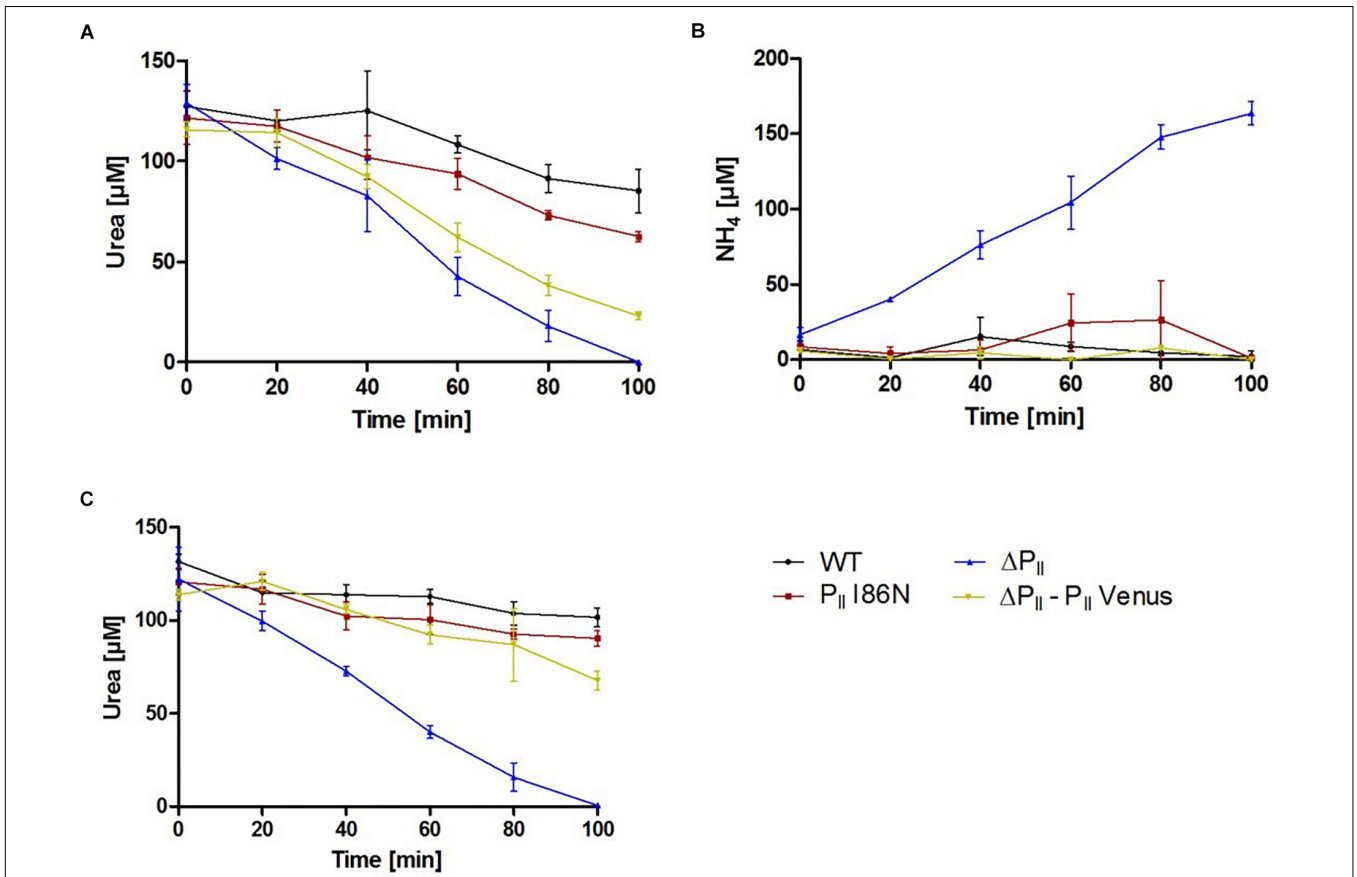

FIGURE 8 | Urea utilization and ammonium excretion of various *Synechocystis* strains as indicated. Exponentially growing and nitrate supplemented *Synechocystis* cells were washed and resuspended in a medium containing 150 μM urea. Shown are the means of three biological replicates. **(A)** Urea utilization and **(B)** ammonium excretion under constant illumination of 40 μmol photons m^{-2} s^{-1}. **(C)** Urea utilization in presence of 2 mM ammonium and under constant illumination of 40 μmol photons m^{-2} s^{-1}.

Synechocystis utilizes available nitrogen sources in a hierarchical order. In presence of ammonium, the uptake of external nitrogen sources is blocked (Muro-Pastor et al., 2005). To test ammonium-dependent inhibition of urea utilization, we determined urea consumption in presence of 2 mM ammonium. The *Synechocystis* wild-type, P_{II}(I86N) and P_{II}-Venus comp. strains showed a clear inhibition in urea utilization in response to the addition of ammonium. In contrast, urea uptake in the ΔP_{II} mutant was completely unaffected by ammonium addition (**Figures 8A,C**). This demonstrates that P_{II} also controls urea uptake, as suggested by the interaction assays.

P_{II} Localization Changes Upon Addition of Nitrate, Ammonium, and Urea

Our previous pull-down experiments and bacterial two-hybrid assays clearly showed interaction of *Synechocystis* P_{II} with Amt1 as well as with nitrate and urea transport components. All interactions appeared to be physiologically relevant. Since all these transporters are localized to the plasma membrane, we suspected that this interaction might affect the cellular localization of P_{II}. Therefore, we monitored P_{II} localization using the *Synechocystis* P_{II}-Venus comp. strain grown under different nitrogen regimes.

Nitrate-replete cells in the mid-exponential growth phase (OD_{750} ~ 0.5) showed heterogeneous distribution of P_{II}-Venus fluorescence in the cell. The majority of cells displayed a strong fluorescence signal in their center and peripheral cell boundary (**Figures 9A,B,D**). The intense signal in the center corresponds to the central cytoplasmic space, inside the multiple thylakoid layers. In this region, P_{II} might interact with different soluble proteins, like NAGK or PipX. The area with low Venus fluorescence is occupied by the thylakoid membranes. The P_{II}-Venus fluorescence at the cell boundary corresponds to the plasma membrane, where Amt1, NrtABCD and UrtABCDE are located (Hahn and Schleiff, 2014) (**Figure 9C**).

When cells are shifted to nitrogen-depleted conditions, they activate the NtcA regulon, including the *glnB* gene and various uptake systems for nitrogen compounds. During prolonged starvation, they undergo chlorosis, which includes a reduction of thylakoid membranes (Forchhammer and Schwarz, 2018). The chlorotic cells rapidly respond to the addition of combined nitrogen sources. Therefore, investigation of P_{II}-Venus fluorescence in chlorotic cells and following the addition of combined nitrogen sources was expected to reveal further insights in the *in vivo* dynamics of P_{II} interactions. To monitor the P_{II} localization in the chlorotic, nitrogen depleted state, cells were grown to an OD_{750} of 0.4–0.6, washed, and resuspended in BG-11^0. After 1 week of nitrogen starvation, the P_{II}-Venus signal was evenly distributed throughout the whole cell and its localization on the plasma membrane was not as distinct as during nitrate-supplemented exponential growth (**Figure 10A**). To test the localization following the addition of different nitrogen sources, 1 week nitrogen starved *Synechocystis* cultures were supplemented with 5 mM NO_3, 5 mM NH_4^+ or 5 mM urea, respectively. Immediately thereafter, a change in the P_{II} localization became visible. The majority of cells showed a clearly visible, distinct plasma membrane localized P_{II}-Venus fluorescence, while the remaining cytosol showed homogenously distributed fluorescence. The re-localization of P_{II} to the plasma

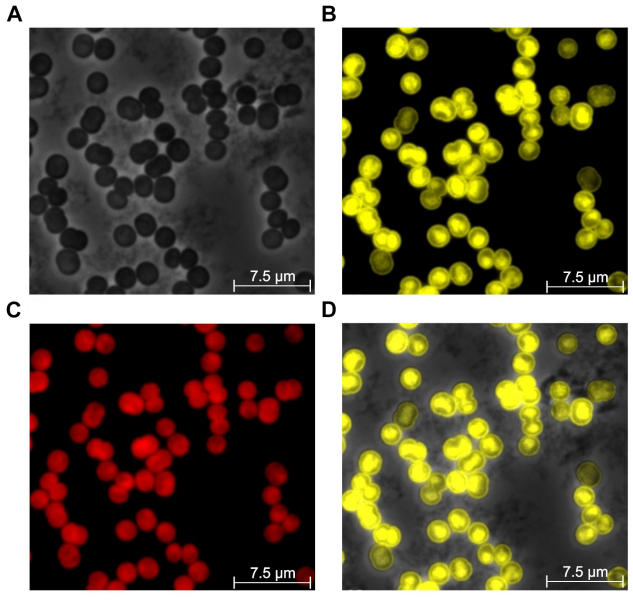

FIGURE 9 | Localization of P_{II}-Venus during exponential growth (OD_{750} of 0.5) of *Synechocystis* **(A)** Phase contrast image of cells. **(B)** Venus fluorescence. **(C)** Autofluorescence of thylakoid membranes. **(D)** Overlay of Venus fluorescence and phase contrast images.

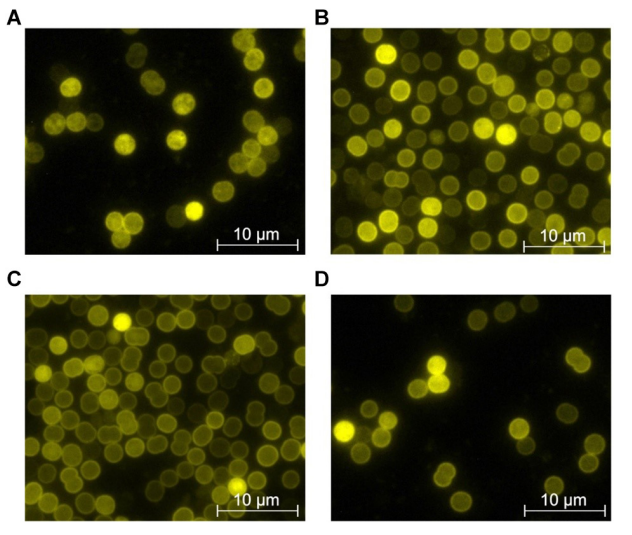

FIGURE 10 | P_{II}-Venus localization under different nitrogen supplemented conditions. **(A)** P_{II}-Venus fluorescence of 1 week nitrogen starved *Synechocystis* cells. **(B–D)** P_{II}-Venus fluorescence of *Synechocystis* during resuscitation from nitrogen starvation. One week nitrogen starved *Synechocystis* cultures were resuscitated by adding 5 mM nitrate **(B)**, 5 mM ammonium **(C)**, or 5 mM urea **(D)**. Fluorescence images were taken 1 h after addition of the nitrogen source.

membrane appeared most clearly in response to ammonium addition as compared to nitrate or urea (**Figures 10B–D**).

Since the fluorescence distribution is subject to a certain degree of heterogeneity with the bulk of single cells observed in the microscope, we attempted to quantitatively describe the average distribution of P_{II}-Venus in a representative set of cells. Therefore, a profile of the fluorescence intensities across median cell sections was determined from 54 individual cells per investigated time point. From these profiles, the relative fluorescence intensity distribution between plasma membrane localized signal to the average cytoplasmic signal was determined and displayed as box-plot (**Figure 11**). Under nitrogen depletion, the majority of the cells showed a higher cytoplasmic P_{II}-Venus localization than plasma membrane localization. Addition of a nitrogen source directly induced a re-localization of P_{II} toward the plasma membrane. In the first 2 h after addition of nitrate or urea, P_{II}-Venus showed a similar localization change (**Figures 11A,C,D**). Two hours after the addition of nitrate, the P_{II}-derived signal from the plasma membrane decreased again and re-appeared in the cytoplasmic space (**Figure 11A**), whereas in urea treated cells, P_{II} continued to accumulate at the plasma membrane (**Figure 11C**). Addition of ammonium induced the most prominent migration of P_{II}-Venus to the plasma membrane in the first hour as compared to nitrate or urea, but thereafter, P_{II}-Venus started to move back to the cytoplasm (**Figure 11B**).

DISCUSSION

The present investigation unraveled a so far unrecognized global function of the cyanobacterial P_{II} signaling protein in controlling the uptake of the major nitrogen sources ammonium, nitrate and urea. Previous studies already suggested occasionally involvement of P_{II} in the regulation of ammonium and nitrate transport (Kobayashi et al., 1997; Lee et al., 1998, 2000; Kloft and Forchhammer, 2005; Conroy et al., 2007), however, this issue was never addressed systematically using a combined biochemical, genetic and physiological approach. Starting from a series of pull-down experiments using FLAG-tagged P_{II} variants, we observed a putative interaction of P_{II} with various nitrogen transport systems. The interactions were verified by bacterial-two hybrid assays and the biological significance of the interaction was validated by physiological

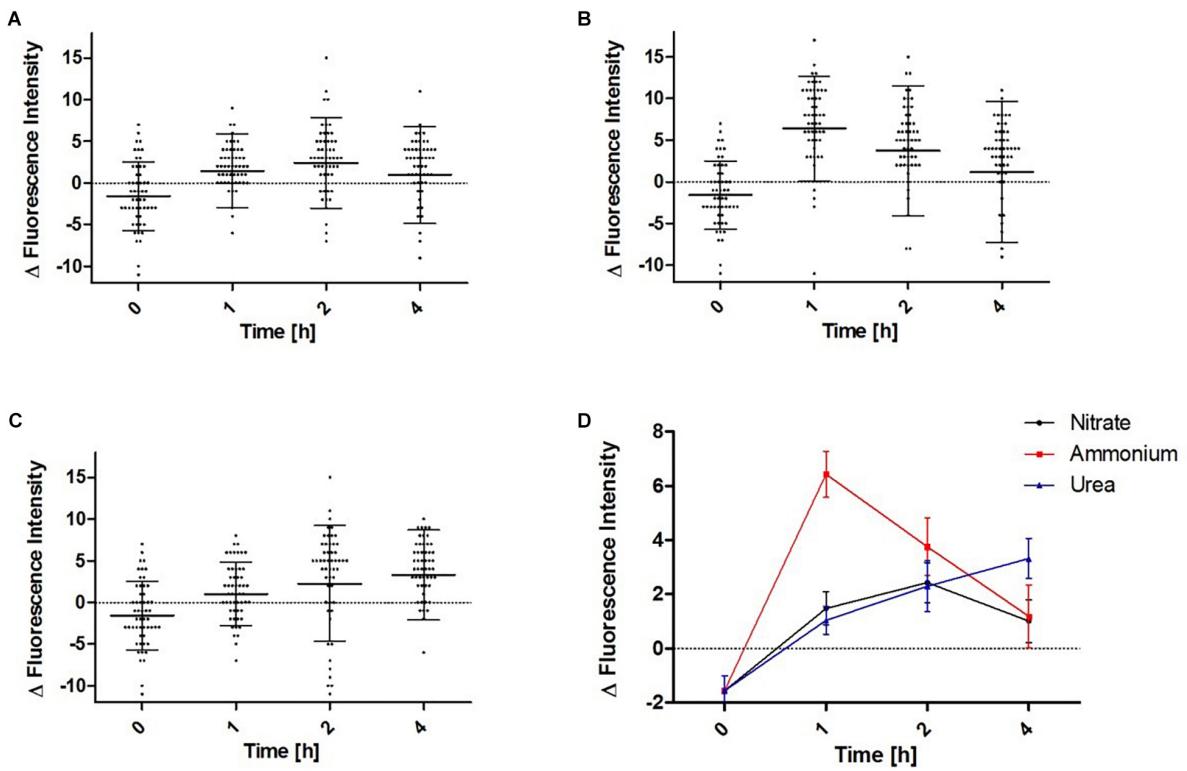

FIGURE 11 | Quantification of the P_{II}-Venus migration toward the plasma membrane in response to the addition of different nitrogen sources to nitrogen starved *Synechocystis* sp. cultures. A linear profile of the fluorescence intensities across midcell was recorded and evaluated as shown in **Supplementary Figure 1**. The maximum fluorescence intensity at the plasma membrane was normalized to the average intensity of the cytoplasm and then, the difference between plasma localized signal and average cytoplasmic signal was calculated (Δ fluorescence intensity). When Δ fluorescence intensity values are below 0, this indicates that the plasma membrane signal is weaker than the average cytoplasmic signal, while values above 0 indicate that the plasma membrane signal is higher than the average cytoplasmic signal. Resuscitation of 1 week nitrogen starved *Synechocystis* sp. cultures were induced by adding either 5 mM NO_3 **(A)**, 5 mM NH_4 **(B)**, or 5 mM urea **(C)**. 50–60 cells were measured per time point. Dots indicate single cell measurements; whiskers showing the standard-deviations; thick black lines show the arithmetic mean. **(D)** Direct comparison of the mean Δ fluorescence intensities from NO_3, NH_4, and urea induced resuscitation.

experiments. Finally, the proposed dynamic interaction of P_{II} with cytoplasmic membrane bound transporters was corroborated by fluorescence microscopy.

Significance Statement

P_{II} signaling proteins play versatile roles in the coordination of carbon- and nitrogen anabolism in prokaryotes and plant chloroplast. In different phylogenetic lineages, P_{II} controls a variety of different target proteins. In cyanobacteria, the P_{II} paralog GlnB has been shown to control global nitrogen-responsive gene expression by interacting with the transcriptional co-activator PipX. Furthermore, P_{II} controls nitrogen storage metabolism in cyanobacteria by regulating the key enzyme of arginine synthesis, *N*-acetylglutamate kinase. Finally, a key enzyme in fatty acid metabolism, the acetyl-CoA carboxylase, was shown to be a target of P_{II}. Several lines of evidences suggested that P_{II} might also be involved in the control of ammonium and nitrate uptake, however, direct involvement of P_{II} has not yet been shown. In this study, we revealed the interactome of P_{II} from the cyanobacterium *Synechocystis* by immunoprecipitating FLAG-tagged P_{II} protein. We found prominent enrichment of components of ammonium, nitrate and urea uptake systems. Direct protein–protein interaction was confirmed by bacterial-two hybrid analysis and the physiological relevance was verified by analyzing ammonium-, nitrate-, and urea-uptake in various P_{II} mutant strains of *Synechocystis*. This study, therefore, demonstrates that P_{II} is the master regulator of the most prominent nitrogen transport systems in cyanobacteria.

Synechocystis P_{II} Regulates Ammonium Uptake by Interacting With the Amt1 Ammonium Permease

In *E. coli*, the P_{II} homolog GlnK regulates AmtB by direct protein–protein interaction to control the influx of ammonium (Conroy et al., 2007). In the GlnK-AmtB complex, the nucleotide binding pockets of GlnK are occupied with ADP and the T-loop of GlnK adopts a vertically extended conformation that closes the ammonium gas channel (Conroy et al., 2007; Maier et al., 2011; Forcada-Nadal et al., 2018). Since the conformation of the T-loop changes upon binding of ATP-Mg^{2+}-2-oxoglutarate, the GlnK-AMT complex only forms under conditions of low 2-OG concentrations, which allows formation of the alternative GlnK-ADP complex (Radchenko et al., 2014).

The present results suggest that in *Synechocystis*, P_{II} regulates the major ammonium permease Amt1 in a similar manner than GlnK the AmtB channel. A weak interaction of Amt1 could still be detected with the phosphomimetic variant S49D. The reduced affinity indicates that the negative charge at position 49 reduces the affinity to Amt1. Therefore, S49 phosphorylated wild-type P_{II} is expected to have an even weaker affinity to Amt1 (two negative charges of phosphoserine as compared to one negative charge of aspartate). In this respect, phosphorylation of S49 would be analogous to uridylylation of Y51 in enterobacterial GlnK proteins, which prevents AmtB interaction (Conroy et al., 2007). Under conditions of strong P_{II} phosphorylation (nitrogen-poor conditions or high CO_2 to nitrate ratio), the Amt1 channel would remain open, allowing unrestricted uptake of ammonium ions. When cells are shifted to excess ammonium conditions, P_{II} becomes dephosphorylated (Ruppert et al., 2002) and diminished 2-OG levels allow formation of the P_{II}-ADP complex, which then can close the Amt1 pores.

In BACTH assays, the P_{II}(R9L) variant was completely impaired in Amt1 interaction. This variant is also unable to interact with NAGK, presumably due to a stabilizing function of the R9 residue at the interface to the binding partner (Fokina et al., 2010a). The failure of this variant to interact with Amt1 indicates that also for Amt1 interaction, the lower face of P_{II} with the protruding T-loops is involved in this protein–protein interaction, in agreement with the structure of the GlnK-AmtB complex.

The failure of the P_{II}(I86N) variant to interact with Amt1 corresponds to the loss of its affinity toward ADP (Fokina et al., 2010b). P_{II}(I86N) has one order of magnitude higher affinity toward ATP than toward ADP and thus, is expected to reside almost exclusively in the ATP-bound state, which would abrogate the interaction with Amt1.

Despite that ammonium uptake in the *Synechocystis* P_{II}(I86N) variant is no more under P_{II} control, this strain exhibits a higher ammonium tolerance than the ΔP_{II} mutant. This difference could be explained by different ammonium assimilation properties. In the P_{II} deletion mutant, the ammonium-scavenging arginine synthesis pathway is not active due to lacking activation of the key enzyme NAGK by P_{II} (Maheswaran et al., 2006). By contrast, *Synechocystis* P_{II}(I86N) highly enhances NAGK activity, resulting in high intracellular arginine concentrations that leads to accumulation of cyanophycin granules (Watzer et al., 2015). This pathway will foster the metabolic removal of excess ammonium and thus results in increased ammonium tolerance.

Analysis of the subcellular localization of P_{II} in response to ammonium stimuli agrees with the above-depicted concept. Only 1 h after the addition of ammonium to chlorotic cells, P_{II} shows a strong migration toward the plasma membrane. Providing ammonium to nitrogen-starved cells should cause a strong decrease of the cellular 2-OG levels. This leads to the observed accumulation of P_{II} to the cytoplasmic membrane, preventing an excess uptake of too much ammonium. After a while, a new equilibrium will be established leading to a partial re-localization of P_{II} to its cytoplasmic targets, such as NAGK. Indeed, *Synechocystis* cells recovering from nitrogen chlorosis start to produce cyanophycin already after a few hours (Watzer and Forchhammer, 2018).

P_{II} Regulates Nitrate Uptake by Interacting With NrtD and NrtC Subunits

Several previous studies documented an involvement of P_{II} in the regulation of nitrate/nitrite uptake. Our data provide novel insights regarding the mechanism of P_{II}-mediated regulation of the NrtABCD transporter. It appears that the NrtABCD complex is directly regulated by interaction of P_{II} with the cytoplasmic ATPase subunits NrtC and NrtD, as indicated by the co-isolation of wild-type P_{II} with both of these proteins. The inability of

the P_{II}(I86N) complemented strain to regulate nitrate utilization as well as the reduced interaction of P_{II}(I86N) with NrtC and NrtD subunits in BACTH assays could in principle be explained by the altered T-loop conformation or by the different ligand binding properties of this variant, discussed above. As shown by BACTH assays and by recent *in vitro* studies (Watzer and Forchhammer, unpublished), the P_{II}(I86N) variant is indeed able to interact with PipX. This interaction requires a vertically extended conformation of the T-loop (Llacer et al., 2010; Forcada-Nadal et al., 2018). Although P_{II}-PipX complexes are favored by the ADP-state of P_{II}, efficient PipX-P_{II} interaction also occurs with the P_{II}-ATP complex. As explained above, the P_{II}(I86N) variant is trapped in the ATP-bound state. The fact that this P_{II} variant binds PipX indicates, that the T-loop of P_{II}(I86N) is flexible enough to adopt various conformations. Therefore, it is likely that formation of the P_{II}-NrtC or NrtD complex requires the ADP-bound state of P_{II}, which is disabled in the P_{II}(I86N) variant. As for NAGK and Amt1, the P_{II}(R9L) variant is unable to interact with any of the NRT subunits, indicating that P_{II} interaction involves the lower part of the P_{II} body, where the T-loop emanates.

The phosphomimetic variant P_{II}(S49D) shows, albeit weaker, interaction with the NRT subunits. This positive interaction explains previous reports, that *Synechocystis* and *Synechococcus* strains expressing these phosphomimetic variants, display a wild-type like regulation of nitrate/nitrite utilization (Lee et al., 2000; Kobayashi et al., 2005). Why the diminished interaction measured by BACTH assays does not properly reflect the physiological behavior of the P_{II}(S49D) expressing strain (full complementation) could be due to different sensitivities of the assays. Kobayashi et al. (2005) used for the complementation of the *Synechocystis* deficient mutant plasmid-borne P_{II} constructs, which cause higher expression levels as in the wild-type genotype. Therefore, a weaker interaction of P_{II} with the NRT subunits could still be sufficient to inhibit NRT. The mechanism of NRT inhibition by P_{II} still awaits structure-functional explanation. Our BACTH assays indicate that P_{II} interacts with both ATPase subunits of NRT. Of these, the NrtC subunit seems to play a particular role: Truncation of the regulatory domain of NrtC results in an ammonium-insensitive NRT, despite the presence of a functional P_{II} system. The regulatory domain of NrtC possesses a putative binding site for nitrate (Koropatkin et al., 2006). Probably P_{II}, through binding to NrtC and NrtD, must act in concert with the regulatory NrtC domain, to stop nitrate uptake. If one of the two regulators is missing, ammonium inhibition would not work. It is tempting to speculate that the regulatory domain of NrtC directly senses the nitrate-state of the cells (Koropatkin et al., 2006) to prepare NRT for inhibition by the P_{II}-ADP complex, whereas P_{II} in the 2-OG-Mg-ATP complex (signaling high C/low N state) would not interact and, therefore, not inhibit NRT. This dual regulatory model combines information from the nitrate status with the global C/N and energy state sensing of P_{II} to tune NRT activity to the actual need. This model also explains the light-response of NRT: Low energy conditions favor the ADP-complex of P_{II}, explaining why in the dark, complete switch-off of NRT requires P_{II}.

P_{II} Regulates Urea Uptake by Interacting With the UrtE Subunit

In addition to Amt1 and NRT, our data also identified the ABC-type urea transporter (UrtABCDE) as a novel P_{II} target, with the UrtE subunit being the direct interaction partner of P_{II}. No BACTH interaction was observed for UrtD. This implies that the UrtD protein identified in the FLAG-tag pull-down resulted from pull-down of the entire URT complex. As deduced from the urea-utilization phenotype of the different P_{II} variant strains, as well as form the properties of BACTH interactions, the interaction of P_{II} with UrtE is distinct from the mode of Amt1 or NrtC and NrtD interaction. P_{II} interaction with UrtE seems to be T-loop independent, since the phosphomimetic S49D variant as well as the P_{II}(I86N) and P_{II}(R9L) variants interacted in BACTH assays like wild-type P_{II}. The ability of P_{II}(R9L) to interact with UrtE indicates that the interaction may involve a region of P_{II} distinct from the usual interaction face used by NAGK, PipX or Amt1.

In agreement with a different binding mode between P_{II} and UrtE, the P_{II}(I86N) variant could substitute wild-type P_{II} regarding the control of urea utilization. This suggests that the P_{II}-ATP complex is able to interact with UrtE in a non-conventional manner. The control of urea uptake prevents its futile hydrolysis and the consequent release of ammonium. Although the P_{II}-Venus variant displayed higher urea uptake rates than the P_{II} deficient mutant, it could prevent concomitant ammonium excretion, indicating that also the P_{II}-Venus variant successfully regulates urea utilization. Consistently, all the tested P_{II} variant strains (wild-type, I86N and P_{II}-Venus) were able to carry out ammonium inhibition of urea uptake. Careful examination of the data shows that the P_{II}-Venus strain displayed slightly higher urea uptake rates than the other two strains. It is possible that due to the bulky fluorescent proteins fused to P_{II} the interaction with P_{II} does not tune down urea uptake as efficient as in the case of the non-tagged P_{II} variants. Nevertheless, the P_{II}-Venus construct is functional, which also agrees with the re-localization of P_{II}-Venus to the plasma membrane upon addition of urea to nitrogen-starved cells. Under certain conditions, the entire multisubunit urease complex appeared in P_{II}-FLAG-tag pull-down experiments. This observation deserves further investigation. It suggests either a direct interaction of the urease complex with P_{II} or a possible metabolic channeling between the urea uptake system and the multisubunit urease complex, leading to a co-immunoprecipitation of the entire super-complex. Further studies are required to reveal the molecular mechanism of urea metabolism and the involvement of P_{II} in this process.

CONCLUSION

All together, the present study has expanded the insights in P_{II} regulatory interactions in *Synechocystis*. According to this study, the P_{II} regulatory network includes all relevant nitrogen uptake systems in *Synechocystis*. It is highly probable that the same holds true for other cyanobacteria. In *Synechococcus elongatus*, (Chang et al., 2013) genetic and physiological studies suggested that in addition to NRT, P_{II} is likely involved in the control of a cyanate ABC transporter (CynABC), which is not

present in *Synechocystis*. Localization of P_{II}-YFP fusions to the cytoplasmic membrane could also be seen in fluorescent images from *S. elongatus* (Espinosa et al., 2018). Control of transport proteins appears to be a highly conserved property of the P_{II} family members, as exemplified by the widely distributed GlnK-Amt interaction. Recently, a more distantly related member of the P_{II} superfamily, SbtB, an accessory component of the sodium-dependent bicarbonate transporter SbtA, was shown to be involved in regulation of bicarbonate metabolism in *Synechocystis* (Selim et al., 2018). Moreover, many putative non-characterized P_{II} family members are genetically linked to transport and channel proteins. However, except for GlnK-AmtB, no structures are known for P_{II}-protein complexes with membrane channel proteins. Whether the interactions of the P_{II} members with the channels follow a universal mode, or whether different types of interaction exist, remains to be demonstrated. However, the differences observed between the interactions of P_{II} variants with UrtE, NrtC/D and Amt1 suggest that the interactions could be as versatile as observed for the various soluble P_{II} interactors (Forcada-Nadal et al., 2018).

DATA AVAILABILITY

The datasets generated for this study can be found in the PRIDE ProteomeXchange consortium, PXD013411.

AUTHOR CONTRIBUTIONS

BW designed, conducted, and evaluated the cyanobacterial growth experiments, quantifications of nitrate, nitrite, ammonium, and urea utilization and carried out the microscopic experiments. RS constructed *Synechocystis* strains expressing tagged P_{II}. PS and OH carried out anti-FLAG pull-down experiments. PS and BM carried out and evaluated nanoLC-MS/MS analyses. MK designed and constructed bacterial two-hybrid vectors. NN carried out and evaluated bacterial two-hybrid assays. KF designed and supervised the study and wrote the manuscript with BW. All authors gave input and approved the manuscript.

FUNDING

This work was supported by grants from the DFG (Fo195/9-2) and the research training group GRK 1708. RS was supported by the project LO1416 of the Czech Ministry of Education.

SUPPLEMENTARY MATERIAL

The Supplementary Material for this article can be found online at: https://www.frontiersin.org/articles/10.3389/fmicb.2019.01428/full#supplementary-material

REFERENCES

Baker, K. M., Gobler, C. J., and Collier, J. L. (2009). Urease gene sequences from algae and heterotrophic bacteria in axenic and nonaxenic phytoplankton cultures. *J. Phycol.* 45, 625–634. doi: 10.1111/j.1529-8817.2009.00680.x

Battchikova, N., Vainonen, J. P., Vorontsova, N., Keranen, M., Carmel, D., and Aro, E. M. (2010). Dynamic changes in the proteome of *Synechocystis* 6803 in response to CO_2 limitation revealed by quantitative proteomics. *J. Proteome Res.* 9, 5896–5912. doi: 10.1021/pr100651w

Battesti, A., and Bouveret, E. (2012). The bacterial two-hybrid system based on adenylate cyclase reconstitution in *Escherichia coli*. *Methods* 58, 325–334. doi: 10.1016/j.ymeth.2012.07.018

Burillo, S., Luque, I., Fuentes, I., and Contreras, A. (2004). Interactions between the nitrogen signal transduction protein PII and *N*-acetyl glutamate kinase in organisms that perform oxygenic photosynthesis. *J. Bacteriol.* 186, 3346–3354. doi: 10.1128/jb.186.11.3346-3354.2004

Caldovic, L., and Tuchman, M. (2003). N-acetylglutamate and its changing role through evolution. *Biochem. J.* 372(Pt 2), 279–290. doi: 10.1042/BJ20030002

Chang, Y., Takatani, N., Aichi, M., Maeda, S.-I., and Omata, T. (2013). Evaluation of the effects of PII deficiency and the toxicity of PipX on growth characteristics of the PII-less mutant of the cyanobacterium *Synechococcus elongatus*. *Plant Cell Physiol.* 54, 1504–1514. doi: 10.1093/pcp/pct092

Cheah, E., Carr, P. D., Suffolk, P. M., Vasudevan, S. G., Dixon, N. E., and Ollis, D. L. (1994). Structure of the *Escherichia coli* signal transducing protein PII. *Structure* 2, 981–990.

Chellamuthu, V. R., Alva, V., and Forchhammer, K. (2013). From cyanobacteria to plants: conservation of PII functions during plastid evolution. *Planta* 237, 451–462. doi: 10.1007/s00425-012-1801-0

Chidgey, J. W., Linhartova, M., Komenda, J., Jackson, P. J., Dickman, M. J., Canniffe, D. P., et al. (2014). A cyanobacterial chlorophyll synthase-HliD complex associates with the Ycf39 protein and the YidC/Alb3 insertase. *Plant Cell* 26, 1267–1279. doi: 10.1105/tpc.114.124495

Conroy, M. J., Durand, A., Lupo, D., Li, X. D., Bullough, P. A., Winkler, F. K., et al. (2007). The crystal structure of the *Escherichia coli* AmtB-GlnK complex reveals how GlnK regulates the ammonia channel. *Proc. Natl. Acad. Sci. U.S.A.* 104, 1213–1218. doi: 10.1073/pnas.0610348104

Cox, J., Hein, M. Y., Luber, C. A., Paron, I., Nagaraj, N., and Mann, M. (2014). Accurate proteome-wide label-free quantification by delayed normalization and maximal peptide ratio extraction, termed MaxLFQ. *Mol. Cell. Proteomics* 13, 2513–2526. doi: 10.1074/mcp.M113.031591

Cox, J., and Mann, M. (2008). MaxQuant enables high peptide identification rates, individualized p.p.b.-range mass accuracies and proteome-wide protein quantification. *Nat. Biotechnol.* 26, 1367–1372. doi: 10.1038/nbt.1511

Dai, G. Z., Qiu, B. S., and Forchhammer, K. (2014). Ammonium tolerance in the cyanobacterium *Synechocystis* sp. strain PCC 6803 and the role of the psbA multigene family. *Plant Cell Environ.* 37, 840–851. doi: 10.1111/pce.12202

Drath, M., Kloft, N., Batschauer, A., Marin, K., Novak, J., and Forchhammer, K. (2008). Ammonia triggers photodamage of photosystem II in the cyanobacterium *Synechocystis* sp strain PCC 6803. *Plant Physiol.* 147, 206–215. doi: 10.1104/pp.108.117218

Espinosa, J., Forchhammer, K., Burillo, S., and Contreras, A. (2006). Interaction network in cyanobacterial nitrogen regulation: PipX, a protein that interacts in a 2-oxoglutarate dependent manner with PII and NtcA. *Mol. Microbiol.* 61, 457–469. doi: 10.1111/j.1365-2958.2006.05231.x

Espinosa, J., Forchhammer, K., and Contreras, A. (2007). Role of the *Synechococcus* PCC 7942 nitrogen regulator protein PipX in NtcA-controlled processes. *Microbiology* 153, 711–718.

Espinosa, J., Labella, J. I., Cantos, R., and Contreras, A. (2018). Energy drives the dynamic localization of cyanobacterial nitrogen regulators during diurnal cycles. *Environ. Microbiol.* 20, 1240–1252. doi: 10.1111/1462-2920.14071

Espinosa, J., Rodriguez-Mateos, F., Salinas, P., Lanza, V. F., Dixon, R., de la Cruz, F., et al. (2014). PipX, the coactivator of NtcA, is a global regulator in cyanobacteria. *Proc. Natl. Acad. Sci. U.S.A.* 111, E2423–E2430. doi: 10.1073/pnas.1404097111

Esteves-Ferreira, A. A., Inaba, M., Fort, A., Araujo, W. L., and Sulpice, R. (2018). Nitrogen metabolism in cyanobacteria: metabolic and molecular control,

growth consequences and biotechnological applications. *Crit. Rev. Microbiol.* 44, 541–560. doi: 10.1080/1040841X.2018.1446902

Fiddler, R. N. (1977). Collaborative study of modified AOAC method of analysis for nitrite in meat and meat products. *J. Assoc. Off. Anal. Chem.* 60, 594–599.

Flores, E., and Herrero, A. (1994). "Assimilatory nitrogen metabolism and its regulation," in *The Molecular Biology of Cyanobacteria*, ed. D. A. Bryant (Dordrecht: Springer), 487–517.

Fokina, O., Chellamuthu, V. R., Forchhammer, K., and Zeth, K. (2010a). Mechanism of 2-oxoglutarate signaling by the *Synechococcus elongatus* PII signal transduction protein. *Proc. Natl. Acad. Sci. U.S.A.* 107, 19760–19765. doi: 10.1073/pnas.1007653107

Fokina, O., Chellamuthu, V. R., Zeth, K., and Forchhammer, K. (2010b). A novel signal transduction protein PII variant from *Synechococcus elongatus* PCC 7942 indicates a two-step process for NAGK-PII complex formation. *J. Mol. Biol.* 399, 410–421. doi: 10.1016/j.jmb.2010.04.018

Forcada-Nadal, A., Forchhammer, K., and Rubio, V. (2014). SPR analysis of promoter binding of *Synechocystis* PCC6803 transcription factors NtcA and CRP suggests cross-talk and sheds light on regulation by effector molecules. *FEBS Lett.* 588, 2270–2276. doi: 10.1016/j.febslet.2014.05.010

Forcada-Nadal, A., Llacer, J. L., Contreras, A., Marco-Marin, C., and Rubio, V. (2018). The PII-NAGK-PipX-NtcA regulatory axis of cyanobacteria: a tale of changing partners, allosteric effectors and non-covalent interactions. *Front. Mol. Biosci.* 5:91. doi: 10.3389/fmolb.2018.00091

Forchhammer, K. (2004). Global carbon/nitrogen control by PII signal transduction in cyanobacteria: from signals to targets. *FEMS Microbiol. Rev.* 28, 319–333. doi: 10.1016/j.femsre.2003.11.001

Forchhammer, K. (2008). PII signal transducers: novel functional and structural insights. *Trends Microbiol.* 16, 65–72. doi: 10.1016/j.tim.2007.11.004

Forchhammer, K., and Hedler, A. (1997). Phosphoprotein PII from cyanobacteria-analysis of functional conservation with the PII signal-transduction protein from *Escherichia coli*. *Eur. J. Biochem.* 244, 869–875.

Forchhammer, K., IrmLer, A., Kloft, N., and Ruppert, U. (2004). PII signalling in unicellular cyanobacteria: analysis of redox-signals and energy charge. *Physiol. Plant.* 120, 51–56. doi: 10.1111/j.0031-9317.2004.0218.x

Forchhammer, K., and Luddecke, J. (2016). Sensory properties of the PII signalling protein family. *FEBS J.* 283, 425–437. doi: 10.1111/febs.13584

Forchhammer, K., and Schwarz, R. (2018). Nitrogen chlorosis in unicellular cyanobacteria - a developmental program for surviving nitrogen deprivation. *Environ. Microbiol.* 21, 1173–1184. doi: 10.1111/1462-2920.14447

Forchhammer, K., and Tandeau de Marsac, N. (1995). Phosphorylation of the PII protein (glnB gene product) in the cyanobacterium *Synechococcus* sp. strain PCC 7942: analysis of in vitro kinase activity. *J. Bacteriol.* 177, 5812–5817.

Gibson, D. G., Young, L., Chuang, R. Y., Venter, J. C., Hutchison, C. A. III, and Smith, H. O. (2009). Enzymatic assembly of DNA molecules up to several hundred kilobases. *Nat. Methods* 6, 343–345. doi: 10.1038/nmeth.1318

Giner-Lamia, J., Robles-Rengel, R., Hernández-Prieto, M. A., Muro-Pastor, M. I., Florencio, F. J., and Futschik, M. E. (2017). Identification of the direct regulon of NtcA during early acclimation to nitrogen starvation in the cyanobacterium *Synechocystis* sp. PCC 6803. *Nucleic Acids Res.* 45, 11800–11820. doi: 10.1093/nar/gkx860

Gruswitz, F., O'Connell, J., and Stroud, R. M. (2007). Inhibitory complex of the transmembrane ammonia channel, AmtB, and the cytosolic regulatory protein, GlnK, at 1.96 A. *Proc. Natl. Acad. Sci. U.S.A.* 104, 42–47. doi: 10.1073/pnas.0609796104

Hahn, A., and Schleiff, E. (2014). "The cell envelope," in *The Cell Biology of Cyanobacteria*, eds E. Flores and A. Herrero (Norfolk: Caister Academic Press), 29–87.

Hauf, W., Schmid, K., Gerhardt, E. C., Huergo, L. F., and Forchhammer, K. (2016). Interaction of the nitrogen regulatory protein GlnB PII with biotin carboxyl carrier protein (BCCP) controls acetyl-CoA levels in the cyanobacterium *Synechocystis* sp. PCC 6803. *Front. Microbiol.* 7:1700. doi: 10.3389/fmicb.2016.01700

Heinrich, A., Maheswaran, M., Ruppert, U., and Forchhammer, K. (2004). The *Synechococcus elongatus* PII signal transduction protein controls arginine synthesis by complex formation with N-acetyl-L-glutamate kinase. *Mol. Microbiol.* 52, 1303–1314. doi: 10.1111/j.1365-2958.2004.04058.x

Herrero, A., and Flores, E. (2008). *The Cyanobacteria: Molecular Biology, Genomics, and Evolution*. Norfolk: Caister Academic Press.

Hisbergues, M., Jeanjean, R., Joset, F., de Marsac, N. T., and Bedu, S. (1999). Protein PII regulates both inorganic carbon and nitrate uptake and is modified by a redox signal in *Synechocystis* sp PCC 6803. *FEBS Lett.* 463, 216–220.

Hollingshead, S., Kopečná, J., Jackson, P. J., Canniffe, D. P., Davison, P. A., Dickman, M. J., et al. (2012). Conserved chloroplast open-reading frame ycf54 is required for activity of the magnesium protoporphyrin monomethylester oxidative cyclase in *Synechocystis* PCC 6803. *J. Biol. Chem.* 287, 27823–27833. doi: 10.1074/jbc.M112.352526

Huergo, L. F., Pedrosa, F. O., Muller-Santos, M., Chubatsu, L. S., Monteiro, R. A., Merrick, M., et al. (2012). PII signal transduction proteins: pivotal players in post-translational control of nitrogenase activity. *Microbiology* 158(Pt 1), 176–190. doi: 10.1099/mic.0.049783-0

Jiang, P., Peliska, J. A., and Ninfa, A. J. (1998). Enzymological characterization of the signal-transducing uridylyltransferase/uridylyl-removing enzyme (EC 2.7.7.59) of *Escherichia coli* and its interaction with the PII protein. *Biochemistry* 37, 12782–12794. doi: 10.1021/bi980667m

Karimova, G., Ullmann, A., and Ladant, D. (2001). Protein-protein interaction between *Bacillus stearothermophilus* tyrosyl-tRNA synthetase subdomains revealed by a bacterial two-hybrid system. *J. Mol. Microbiol. Biotechnol.* 3, 73–82.

Kloft, N., and Forchhammer, K. (2005). Signal transduction protein PII phosphatase PphA is required for light-dependent control of nitrate utilization in *Synechocystis* sp. strain PCC 6803. *J. Bacteriol.* 187, 6683–6690. doi: 10.1128/JB.187.19.6683-6690.2005

Kobayashi, M., Rodriguez, R., Lara, C., and Omata, T. (1997). Involvement of the C-terminal domain of an ATP-binding subunit in the regulation of the ABC-type nitrate/nitrite transporter of the cyanobacterium *Synechococcus* sp. PCC 7942. *J. Biol. Chem.* 272, 27197–27201. doi: 10.1074/jbc.272.43.27197

Kobayashi, M., Takatani, N., Tanigawa, M., and Omata, T. (2005). Posttranslational regulation of nitrate assimilation in the cyanobacterium *Synechocystis* sp. strain PCC 6803. *J. Bacteriol.* 187, 498–506. doi: 10.1128/JB.187.2.498-506.2005

Koropatkin, N. M., Pakrasi, H. B., and Smith, T. J. (2006). Atomic structure of a nitrate-binding protein crucial for photosynthetic productivity. *Proc. Natl. Acad. Sci. U.S.A.* 103, 9820–9825. doi: 10.1073/pnas.0602517103

Lee, H. M., Flores, E., Forchhammer, K., Herrero, A., and de Marsac, N. T. (2000). Phosphorylation of the signal transducer PII protein and an additional effector are required for the PII mediated regulation of nitrate and nitrite uptake in the cyanobacterium *Synechococcus* sp PCC 7942. *Eur. J. Biochem.* 267, 591–600. doi: 10.1046/j.1432-1327.2000.01043.x

Lee, H. M., Flores, E., Herrero, A., Houmard, J., and de Marsac, N. T. (1998). A role for the signal transduction protein PII in the control of nitrate/nitrite uptake in a cyanobacterium. *FEBS Lett.* 427, 291–295.

Llacer, J. L., Contreras, A., Forchhammer, K., Marco-Marin, C., Gil-Ortiz, F., Maldonado, R., et al. (2007). The crystal structure of the complex of PII and acetylglutamate kinase reveals how PII controls the storage of nitrogen as arginine. *Proc. Natl. Acad. Sci. U.S.A.* 104, 17644–17649. doi: 10.1073/pnas.0705987104

Llacer, J. L., Espinosa, J., Castells, M. A., Contreras, A., Forchhammer, K., and Rubio, V. (2010). Structural basis for the regulation of NtcA-dependent transcription by proteins PipX and PII. *Proc. Natl. Acad. Sci. U.S.A.* 107, 15397–15402. doi: 10.1073/pnas.1007015107

Luque, I., Flores, E., and Herrero, A. (1994). Nitrate and nitrite transport in the cyanobacterium *Synechococcus* sp PCC 7942 are mediated by the same permease. *Biochim. Biophys. Acta Bioenerg.* 1184, 296–298.

Luque, I., and Forchhammer, K. (2008). "Nitrogen assimilation and C/N balance sensing," in *The Cyanobacteria. Molecular Biology, Genomics and Evolution*, eds A. Herrero and E. Flores (Norfolk: Caister Academic Press), 335–382.

Maeda, S. I., and Omata, T. (1997). Substrate-binding lipoprotein of the cyanobacterium *Synechococcus* sp strain PCC 7942 involved in the transport of nitrate and nitrite. *J. Biol. Chem.* 272, 3036–3041. doi: 10.1074/jbc.272.5.3036

Maheswaran, M., Urbanke, C., and Forchhammer, K. (2004). Complex formation and catalytic activation by the PII signaling protein of N-acetyl-L-glutamate kinase from *Synechococcus elongatus* strain PCC 7942. *J. Biol. Chem.* 279, 55202–55210. doi: 10.1074/jbc.M410971200

Maheswaran, M., Ziegler, K., Lockau, W., Hagemann, M., and Forchhammer, K. (2006). PII-regulated arginine synthesis controls accumulation of cyanophycin in *Synechocystis* sp strain PCC 6803. *J. Bacteriol.* 188, 2730–2734. doi: 10.1128/Jb.188.7.2730-2734.2006

Maier, S., Schleberger, P., Lu, W., Wacker, T., Pfluger, T., Litz, C., et al. (2011). Mechanism of disruption of the Amt-GlnK complex by PII-mediated sensing of 2-oxoglutarate. *PLoS One* 6:e26327. doi: 10.1371/journal.pone.0026327

Manzano, C., Candau, P., Gomez-Moreno, C., Relimpio, A. M., and Losada, M. (1976). Ferredoxin-dependent photosynthetic reduction of nitrate and nitrite by particles of *Anacystis nidulans*. *Mol. Cell. Biochem.* 10, 161–169.

Marques, S., Merida, A., Candau, P., and Florencio, F. J. (1992). Light-mediated regulation of glutamine-synthetase activity in the unicellular cyanobacterium *Synechococcus* sp PCC6301. *Planta* 187, 247–253.

Merrick, M. (2014). Post-translational modification of PII signal transduction proteins. *Front. Microbiol.* 5:763. doi: 10.3389/fmicb.2014.00763

Mobley, H. L. T., and Hausinger, R. P. (1989). Microbial ureases - significance, regulation and molecular characterization. *Microbiol. Rev.* 53, 85–108.

Montesinos, M. L., Muro-Pastor, A. M., Herrero, A., and Flores, E. (1998). Ammonium/methylammonium permeases of a cyanobacterium. Identification and analysis of three nitrogen-regulated amt genes in *Synechocystis* sp. PCC 6803. *J. Biol. Chem.* 273, 31463–31470.

Muro-Pastor, M. I., Reyes, J. C., and Florencio, F. J. (2001). Cyanobacteria perceive nitrogen status by sensing intracellular 2-oxoglutarate levels. *J. Biol. Chem.* 276, 38320–38328.

Muro-Pastor, M. I., Reyes, J. C., and Florencio, F. J. (2005). Ammonium assimilation in cyanobacteria. *Photosynth. Res.* 83, 135–150.

Nakao, M., Okamoto, S., Kohara, M., Fujishiro, T., Fujisawa, T., Sato, S., et al. (2010). CyanoBase: the cyanobacteria genome database update 2010. *Nucleic Acids Res.* 38, D379–D381. doi: 10.1093/nar/gkp915

Ohashi, Y., Shi, W., Takatani, N., Aichi, M., Maeda, S., Watanabe, S., et al. (2011). Regulation of nitrate assimilation in cyanobacteria. *J. Exp. Bot.* 62, 1411–1424. doi: 10.1093/jxb/erq427

Olsen, J. V., de Godoy, L. M. F., Li, G. Q., Macek, B., Mortensen, P., Pesch, R., et al. (2005). Parts per million mass accuracy on an orbitrap mass spectrometer via lock mass injection into a C-trap. *Mol. Cell. Proteomics* 4, 2010–2021. doi: 10.1074/mcp.T500030-MCP200

Omata, T., Andriesse, X., and Hirano, A. (1993). Identification and characterization of a gene-cluster involved in nitrate transport in the cyanobacterium *Synechococcus* sp PCC 7942. *Mol. Gen. Genet.* 236, 193–202. doi: 10.1007/Bf00277112

Radchenko, M., and Merrick, M. (2011). The role of effector molecules in signal transduction by PII proteins. *Biochem. Soc. Trans.* 39, 189–194. doi: 10.1042/BST0390189

Radchenko, M. V., Thornton, J., and Merrick, M. (2014). Association and dissociation of the GlnK-AmtB complex in response to cellular nitrogen status can occur in the absence of GlnK post-translational modification. *Front. Microbiol.* 5:731. doi: 10.3389/fmicb.2014.00731

Rappsilber, J., Mann, M., and Ishihama, Y. (2007). Protocol for micro-purification, enrichment, pre-fractionation and storage of peptides for proteomics using StageTips. *Nat. Protoc.* 2, 1896–1906. doi: 10.1038/nprot.2007.261

Rees, A. P., Woodward, E. M. S., and Joint, I. (2006). Concentrations and uptake of nitrate and ammonium in the Atlantic ocean between 60 degrees N and 50 degrees S. *Deep Sea Res. Part II Top. Stud. Oceanogr.* 53, 1649–1665. doi: 10.1016/j.dsr2.2006.05.008

Rippka, R., Deruelles, J., Waterbury, J. B., Herdman, M., and Stanier, R. Y. (1979). Generic assignments, strain histories and properties of pure cultures of cyanobacteria. *J. Gen. Microbiol.* 111, 1–61.

Romero, J. M., Lara, C., and Guerrero, M. G. (1985). Dependence of nitrate utilization upon active CO_2 fixation in *Anacystis nidulans* - a regulatory aspect of the interaction between photosynthetic carbon and nitrogen-metabolism. *Arch. Biochem. Biophys.* 237, 396–401.

Ruppert, U., IrmLer, A., Kloft, N., and Forchhammer, K. (2002). The novel protein phosphatase PphA from *Synechocystis* PCC 6803 controls dephosphorylation of the signalling protein PII. *Mol. Microbiol.* 44, 855–864.

Sakamoto, T., Inoue-Sakamoto, K., and Bryant, D. A. (1999). A novel nitrate/nitrite permease in the marine cyanobacterium *Synechococcus* sp. strain PCC 7002. *J. Bacteriol.* 181, 7363–7372.

Sato, S., Shimoda, Y., Muraki, A., Kohara, M., Nakamura, Y., and Tabata, S. (2007). A large-scale protein–protein interaction analysis in *Synechocystis* sp. PCC6803. *DNA Res.* 14, 207–216. doi: 10.1093/dnares/dsm021

Schindelin, J., Arganda-Carreras, I., Frise, E., Kaynig, V., Longair, M., Pietzsch, T., et al. (2012). Fiji: an open-source platform for biological-image analysis. *Nat. Methods* 9, 676–682. doi: 10.1038/Nmeth.2019

Schwanhausser, B., Busse, D., Li, N., Dittmar, G., Schuchhardt, J., Wolf, J., et al. (2011). Global quantification of mammalian gene expression control. *Nature* 473, 337–342. doi: 10.1038/nature10098

Selim, K. A., Haase, F., Hartmann, M. D., Hagemann, M., and Forchhammer, K. (2018). PII-like signaling protein SbtB links cAMP sensing with cyanobacterial inorganic carbon response. *Proc. Natl. Acad. Sci. U.S.A.* 115, E4861–E4869. doi: 10.1073/pnas.1803790115

Solomon, C. M., Collier, J. L., Berg, G. M., and Glibert, P. M. (2010). Role of urea in microbial metabolism in aquatic systems: a biochemical and molecular review. *Aquat. Microb. Ecol.* 59, 67–88. doi: 10.3354/ame01390

Soo, R. M., Hemp, J., Parks, D. H., Fischer, W. W., and Hugenholtz, P. (2017). On the origins of oxygenic photosynthesis and aerobic respiration in cyanobacteria. *Science* 355, 1436–1439. doi: 10.1126/science.aal3794

Spät, P., Macek, B., and Forchhammer, K. (2015). Phosphoproteome of the cyanobacterium *Synechocystis* sp PCC 6803 and its dynamics during nitrogen starvation. *Front. Microbiol.* 6:248. doi: 10.3389/fmicb.2015.00248

Sweetlove, L. J., and Fernie, A. R. (2018). The role of dynamic enzyme assemblies and substrate channelling in metabolic regulation. *Nat. Commun.* 9:2136. doi: 10.1038/s41467-018-04543-8

Valladares, A., Montesinos, M. L., Herrero, A., and Flores, E. (2002). An ABC-type, high-affinity urea permease identified in cyanobacteria. *Mol. Microbiol.* 43, 703–715. doi: 10.1046/j.1365-2958.2002.02778.x

Vegapalas, M. A., Flores, E., and Herrero, A. (1992). NtcA, a global nitrogen regulator from the cyanobacterium *Synechococcus* that belongs to the Crp family of bacterial regulators. *Mol. Microbiol.* 6, 1853–1859. doi: 10.1111/j.1365-2958.1992.tb01357.x

Vitousek, P. M., and Howarth, R. W. (1991). Nitrogen limitation on land and in the sea - how can it occur. *Biogeochemistry* 13, 87–115.

Vizcaino, J. A., Cote, R. G., Csordas, A., Dianes, J. A., Fabregat, A., Foster, J. M., et al. (2013). The proteomics identifications (PRIDE) database and associated tools: status in 2013. *Nucleic Acids Res.* 41, D1063–D1069. doi: 10.1093/nar/gks1262

Vogel, A. I., Furniss, B. S., and Vogel, A. I. (1989). *Vogel's Textbook of Practical Organic Chemistry*. New York, NY: Longman Scientific & Technical.

Watzer, B., Engelbrecht, A., Hauf, W., Stahl, M., Maldener, I., and Forchhammer, K. (2015). Metabolic pathway engineering using the central signal processor PII. *Microb. Cell Fact.* 14:192. doi: 10.1186/s12934-015-0384-4

Watzer, B., and Forchhammer, K. (2018). Cyanophycin synthesis optimizes nitrogen utilization in the unicellular cyanobacterium *Synechocystis* sp. PCC 6803. *Appl. Environ. Microbiol.* 84:e01298-18. doi: 10.1128/AEM.01298-18

Whitton, B. A. (2012). *Ecology of Cyanobacteria II: Their Diversity in Space and Time*. New York, NY: Springer.

Wirén, N. V., and Merrick, M. (2004). "Regulation and function of ammonium carriers in bacteria, fungi, and plants," in *Molecular Mechanisms Controlling Transmembrane Transport*, eds E. Boles and R. Krämer (Berlin: Springer), 95–120.

Xu, Y. B., Carr, P. D., Clancy, P., Garcia-Dominguez, M., Forchhammer, K., Florencio, F., et al. (2003). The structures of the PII proteins from the cyanobacteria *Synechococcus* sp PCC 7942 and *Synechocystis* sp. PCC 6803. *Acta Crystallogr. D Biol. Crystallogr.* 59(Pt 12), 2183–2190. doi: 10.1107/S0907444903019589

Zeth, K., Fokina, O., and Forchhammer, K. (2014). Structural basis and target-specific modulation of ADP sensing by the *Synechococcus elongatus* PII signaling protein. *J. Biol. Chem.* 289, 8960–8972. doi: 10.1074/jbc.M113.536557

Zhao, M. X., Jiang, Y. L., Xu, B. Y., Chen, Y., Zhang, C. C., and Zhou, C. Z. (2010). Crystal structure of the cyanobacterial signal transduction protein PII in complex with PipX. *J. Mol. Biol.* 402, 552–559. doi: 10.1016/j.jmb.2010.08.006

Conflict of Interest Statement: The authors declare that the research was conducted in the absence of any commercial or financial relationships that could be construed as a potential conflict of interest.

Supplementary Figures

The signal transduction protein P_{II} controls ammonium, nitrate and urea uptake in cyanobacteria

Björn Watzer [1§], Philipp Spät [1, 2§], Niels Neumann [1], Moritz Koch [1], Roman Sobotka [3], Boris Macek [2], Oliver Hennrich [1] and Karl Forchhammer [1*]

[1] Interfaculty Institute of Microbiology and Infection Medicine Tuebingen, Department of Organismic Interactions, Eberhard Karls Universität Tübingen, Tübingen 72076, Germany

[2] Interfaculty Institute for Cell Biology, Department of Quantitative Proteomics, Eberhard Karls Universität Tübingen, Tübingen 72076, Germany

[3] Centre Algatech, Institute of Microbiology, Academy of Sciences of the Czech Republic, Třeboň 379 01, Czech Republic

§ contributed equally

*** Correspondence:**
Karl Forchhammer
karl.forchhammer@uni-tuebingen.de

Supplementary Figure 1

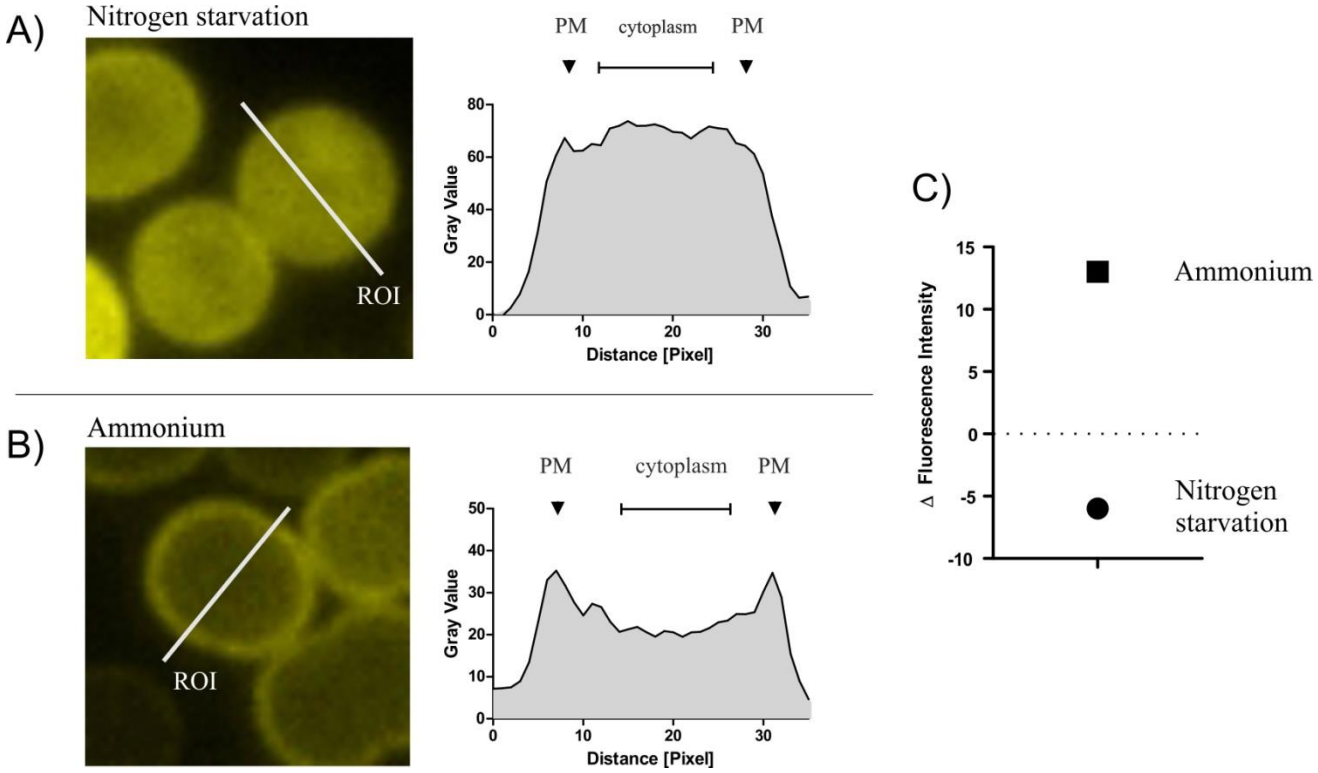

Supplementary Figure 1: Example of image evaluation of a nitrogen starved (A) and ammonium supplemented (B) *Synechocystis* cell. The fluorescents intensities of every pixel in a linear region of interest (ROI) across the cell were determined. The maximum gray value of the plasma membrane (PM) was subtracted from the average gray value of the cytoplasm (Δ Fluorescence intensity). (C) shows the final representation of the Δ Fluorescence intensity values. Values < 0 indicate a stronger cytoplasmic localized signal, while values > 0 show a stronger plasma membrane association.

Supplementary Figure 2

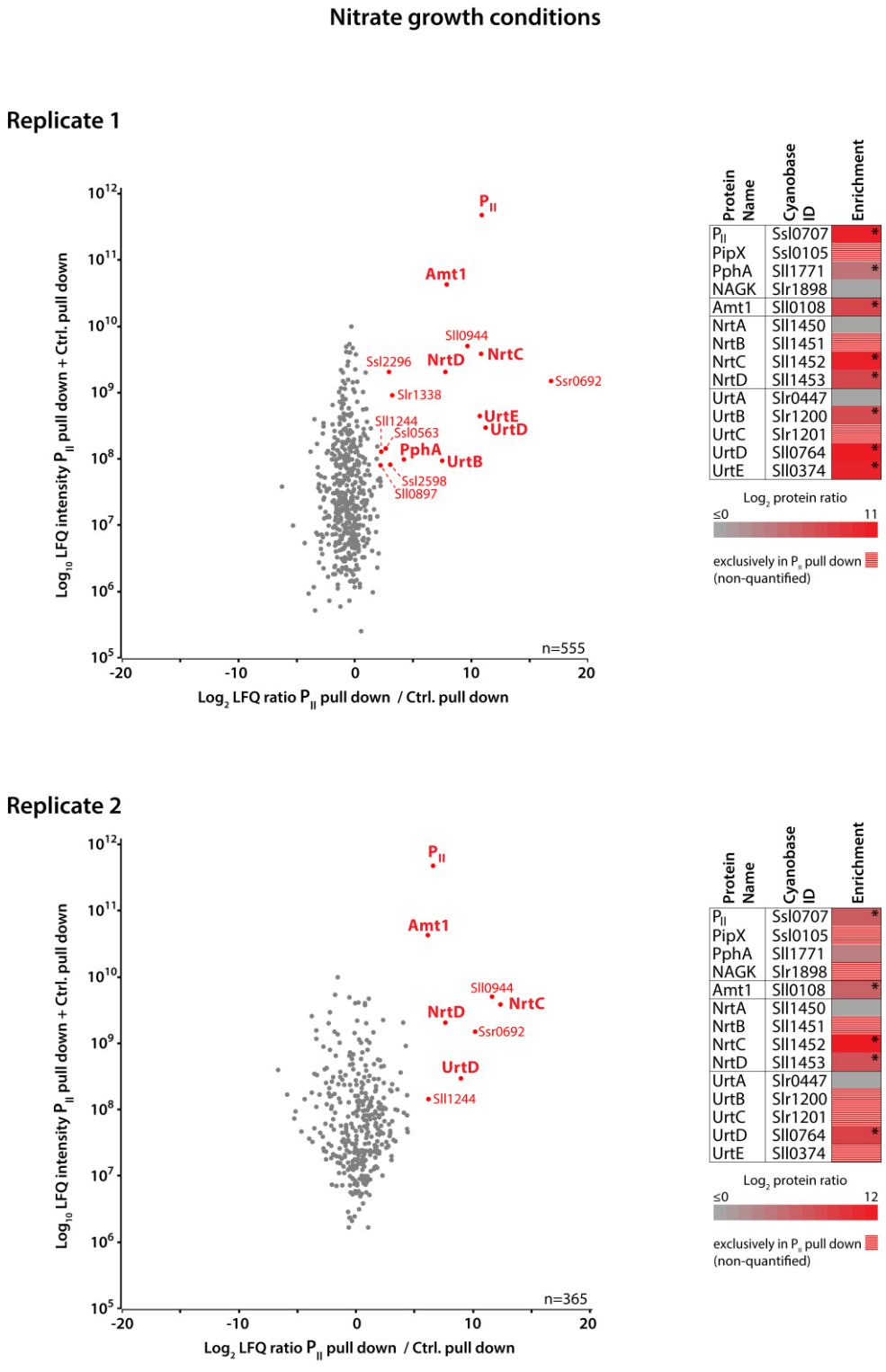

Supplementary Figure 2: Scatterplot of quantified proteins from two independent replicates at nitrate growth conditions (17.5 mM). Left: Log_2 transformed LFQ protein ratios (P_{II}/control pull down experiment) are plotted against the log_{10} transformed sum of protein intensities. Significant outliers in P_{II} pull down experiments (p value=0.01) are indicated in red. Right: Heat map representation of the P_{II}-specific enrichment of nitrogen metabolism related proteins. Log_2 transformed LFQ protein ratios are color coded with stars indicating significance. Proteins with missing LFQ ratios, detected exclusively in the P_{II} but not in the control pull down, are displayed by red/grey stripes.

Supplementary Figure 3

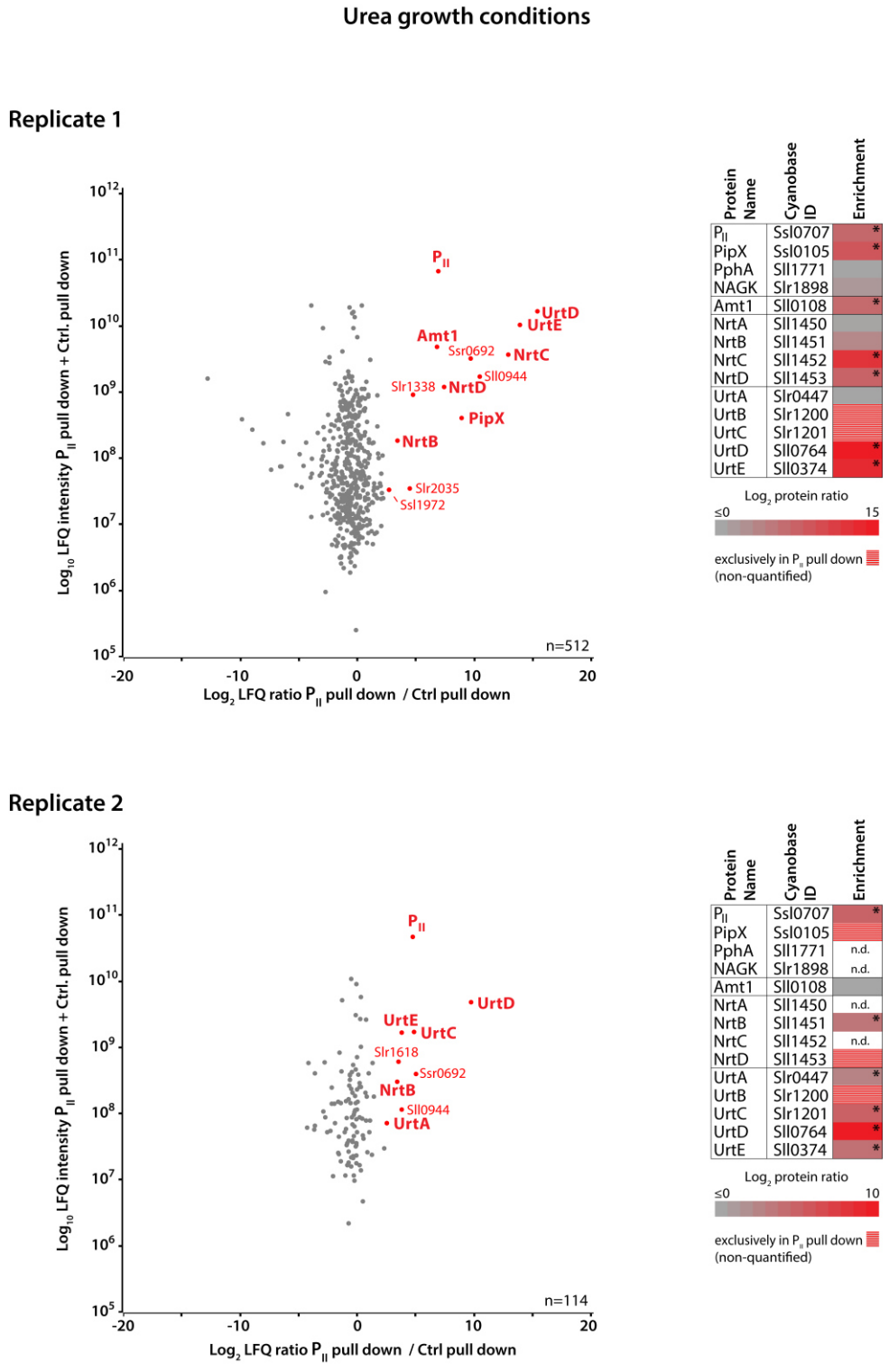

Supplementary Figure 3: Scatterplot of quantified proteins from two independent replicates at urea growth conditions (5 mM). Left: Log_2 transformed LFQ protein ratios (P_{II}/control pull down experiment) are plotted against the log_{10} transformed sum of protein intensities. Significant outliers in P_{II} pull down experiments (p value=0.01) are indicated in red. Right: Heat map representation of the P_{II}-specific enrichment of nitrogen metabolism related proteins. Log_2 transformed LFQ protein ratios are color coded with stars indicating significance. Proteins with missing LFQ ratios, detected exclusively in the P_{II} but not in the control pull down, are displayed by red/grey stripes, and n.d. indicates no detection in the P_{II} and control pull down.

Publication 2: Review

Neumann N., Doello S., Forchhammer K.

Recovery of Unicellular Cyanobacteria from Nitrogen Chlorosis: A Model for Resuscitation of Dormant Bacteria.

Microb Physiol. 2021;31(2):78-87.

Microbial Physiology

Review Article

Microb Physiol 2021;31:78–87
DOI: 10.1159/000515742

Received: January 8, 2021
Accepted: March 6, 2021
Published online: April 20, 2021

Recovery of Unicellular Cyanobacteria from Nitrogen Chlorosis: A Model for Resuscitation of Dormant Bacteria

Niels Neumann Sofia Doello Karl Forchhammer

Interfaculty Institute of Microbiology and Infection Medicine Tübingen, Eberhard Karls University Tübingen, Tübingen, Germany

Keywords
Metabolic quiescence · Cell cycle arrest · Glycogen metabolism · ATP homeostasis · Starvation

Abstract
Nitrogen starvation induces developmental transitions in cyanobacteria. Whereas complex multicellular cyanobacteria of the order Nostocales can differentiate specialized cells that perform nitrogen fixation in the presence of oxygenic photosynthesis, non-diazotrophic unicellular strains, such as *Synechococcus elongatus* or *Synechocystis* PCC 6803, undergo a transition into a dormant non-growing state. Due to loss of pigments during this acclimation, the process is termed chlorosis. Cells maintain viability in this state for prolonged periods of time, until they encounter a useable nitrogen source, which triggers a highly coordinated awakening process, termed resuscitation. The minimal set of cellular activity that maintains the viability of cells during chlorosis and ensures efficient resuscitation represents the organism's equivalent of the BIOS, the basic input/output system of a computer, that helps "booting" the operation system after switching on. This review summarizes the recent research in the resuscitation of cyanobacteria, representing a powerful model for the awakening of dormant bacteria.

Introduction

Nutrient starvation can be detrimental to organisms when it leads to metabolic disorder that impairs vital cellular processes. A successful strategy to survive such periods of nutrient deprivation that is particularly widespread in prokaryotes is the transition into a dormant state. In this state, the metabolic processes are reduced to an absolute minimum. The remaining activities just ensure survival and enable the dormant cells to awake and resume growth once the limiting nutrient becomes available again. It is assumed that in natural environments a majority of the bacteria reside in a dormant state, and these cells comprise a "seed bank" – a reservoir – that can be resuscitated when favourable conditions occur. This mechanism is largely responsible for the fitness of bacterial populations and contributes to the sudden appearance of bacteria in the environment and the spreading of antibiotic resistances and bacterial pathogens. An example of dormant bacteria acting as a reservoir of antibiotic resistance is presented in the study by Udikovic-Kolic et al. [2014], where manure supplementation of soil is shown to result in proliferation of diverse soil-resident bacteria, some carrying antibiotic resistance genes.

The ways in which the cells enter dormancy and recover from the dormant stage are rather diverse. Some bacteria form endospores or exospores, others create en-

karger@karger.com
www.karger.com/mip

Correspondence to:
Karl Forchhammer, karl.forchhammer@uni-tuebingen.de

capsulated cysts or even generate apparently non-differentiated persister cells, which is the case in *Mycobacterium tuberculosis* [Keren et al., 2011]. Despite the differences among these quiescent states, a common requirement in this survival strategy is the ability to reactivate metabolism upon encountering permissive conditions.

Studying the molecular mechanisms supporting these cellular processes is complicated for several reasons. A bacterial population that has undergone the transition into a dormant state is usually highly heterogeneous, since phenotypical variation can be beneficial in the emergence from starvation-induced growth arrest [Moreno-Gámez et al., 2020]. In many cases, including populations of nutrient-starved *Flavobacterium columnare* and *Brucella suis* cells, only a small proportion of the cells remain viable [Arias et al., 2012; AlDahouk et al., 2013]; in others, such as the germination of akinetes of filamentous heterocyst-forming cyanobacteria, re-activation of metabolism is highly asynchronous [Perez et al., 2018]. This heterogeneity precludes the employment of powerful molecular methods that rely on homogenous populations, such as metabolomics, proteomic or transcriptomic studies. Therefore, in many cases, the behaviour of dormant cells can only be studied using single-cell analysis, which still has many limitations. One of the rare cases where transition into and out of the dormant state occurs in a population-wide coherent manner is the case of nitrogen starvation-induced chlorosis in some unicellular cyanobacterial strains, such as *Synechococcus elongatus* and *Synechocystis* PCC 6803. Following a brief description of nitrogen starvation-induced chlorosis, the present article provides a consolidated review of our current knowledge on the resuscitation of these cyanobacteria from prolonged nitrogen chlorosis.

Entry into Chlorosis

That nitrogen starvation leads to bleaching of cyanobacterial cultures was already described in 1910 and this process was termed "chlorosis" [Boresch, 1910]. Only about 70 years later, studies in *S. elongatus* showed that the rapid bleaching caused by nitrogen starvation, a colour change from deep blue-green to yellowish-greenish, was mainly caused by the degradation of the blue phycobiliproteins [Allen and Smith, 1969]. These proteins constitute the light-harvesting antenna system for the photosynthetic reaction centres, the phycobilisomes (PBS) [Grossman et al., 1993]. By screening for mutants with a non-bleaching phenotype on nutrient-deficient plates in the 1990s, *nbl* (non-bleaching) genes were identified in the laboratory of A. Grossman [Collier and Grossman, 1994]. These *nbl*-genes are responsible for phycobiliprotein degradation upon various stress conditions, including nitrogen starvation or high-light stress. Until the mid-1990s, it was assumed that the chlorotic cells lost viability, until a study by Görl et al. [1998] showed that chlorotic *Synechococcus* cells maintain viability for extended periods of time [reviewed in Schwarz and Forchhammer, 2005]. This study revealed a gradual decline in cellular activities following the initial phycobiliprotein degradation, until the cells entered a dormant-like state with almost no detectable metabolic activity. Based on these observations, the chlorosis process could be divided into 3 phases, with phase 1 being the rapid degradation of phycobiliprotein occurring within 1–2 days, followed by phase 2, the gradual decline of metabolic activity (concomitant with a decline in chlorophyll *a*) within the following 8–14 days, and finally, the terminal phase 3, the dormant state with a low basal level of photosynthetic activity [Görl et al., 1998]. Concomitant with the gradual decline of metabolic activity, the cells undergo substantial intracellular re-organization through proteolysis, in particular with respect to the degradation of the intracellular membrane system, the thylakoids, which accommodate the molecular machines of the photosynthetic electron transport chain including photosystem I and II. However, a low level of photosynthetic activity involving PSI and PSII activity is preserved during prolonged chlorosis, which was shown to be required to maintain long-term cell viability [Sauer et al., 2001]. Since no net yield of photosynthesis could be determined, it was suggested that the photosynthetic electrons are recycled through a water-to-water cycle, where oxygen, produced through water splitting at PSII, serves as electron acceptor for PSI-reduced ferredoxin [Sauer et al., 2001]. Considering the severe decomposition of intracellular structures after long-term chlorosis, it is astonishing that cells readily re-green within 2 days and resume growth following the addition of a nitrogen source [Görl et al., 1998; Sauer et al., 1999; Sauer et al., 2001; reviewed in Schwarz and Forchhammer, 2005].

Synechocystis sp. 6803 is a unicellular cyanobacterium only distantly related to *S. elongatus* [Robertson et al., 2001]. It is metabolically more versatile than *S. elongatus* as it is not strictly photoautotrophic and is able to synthesize various reserve polymers not present in *S. elongatus*, such as the nitrogen storage compound cyanophycin (CP) [Stephan et al., 2000] or the polymer polyhydroxybutyrate (PHB) [Hauf et al., 2013; reviewed in Koch et al., 2020]. Despite these differences, the basic nitrogen-star-

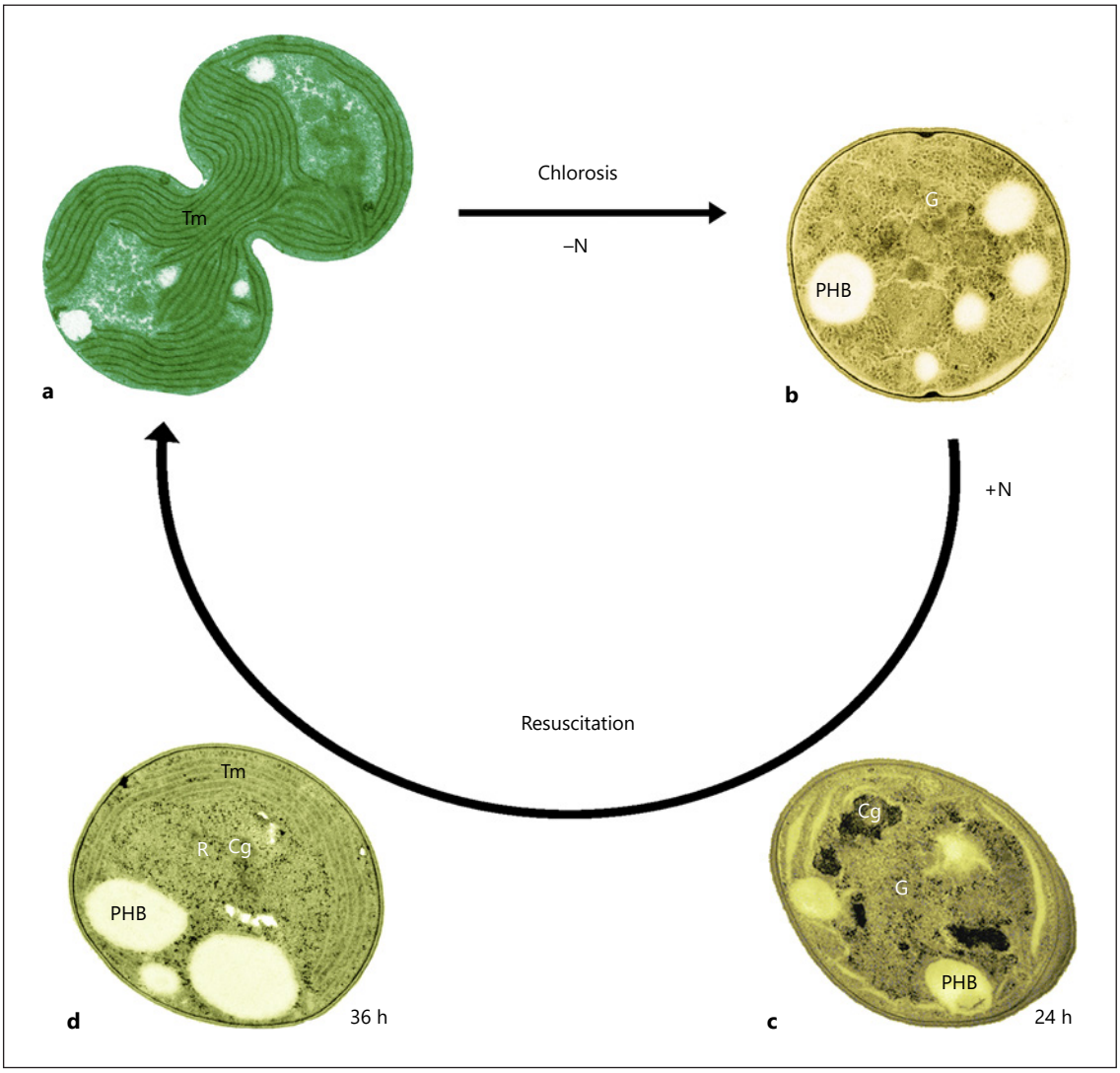

Fig. 1. *Synechocystis* cells during developmental transitions through nitrogen starvation and resuscitation. **a** Cell in exponential growth phase. **b** Chlorotic cell starved for 1 month. **c** Cells during the first 24 h of resuscitation. **d** Cells after 36 h of resuscitation. G, glycogen granules; PHB, polyhydroxybutyrate granules; Cg, cyanophycin granules; Tm, thylakoid membrane; R, ribosomes.

vation acclimation response seems to be highly conserved. Similar to *S. elongatus*, *Synechocystis* employs a set of *nbl* genes under the control of a conserved sensor kinase (Hik33/NblS) to degrade phycobiliproteins, which degrades the photosynthetic apparatus and tunes down metabolic activity until a dormant-like state is attained, from which it rapidly recovers after supplementation with combined nitrogen [reviewed in Schwarz and Forchhammer, 2005]. A distinguishing feature of the strains is the accumulation of large amounts of PHB in *Synechocystis* during prolonged chlorosis [Schlebusch and Forchhammer, 2010; Hauf et al., 2013; Damrow et al., 2016]. However, mutants defective in PHB synthesis are neither impaired in the chlorosis response, nor in the ability to recover from nitrogen starvation [Klotz et al., 2016; Koch et al., 2020], indicating that PHB metabolism is not directly involved in surviving nitrogen deprivation. Unlike PHB, glycogen seems to be a major carbon polymer supporting nitrogen starvation; both *Synechocystis* and *S. elongatus* rapidly accumulate large amounts of this polymer upon nitrogen limitation or upon inhibition of glutamine synthetase (GS) activity [Klotz et al., 2015]. However, mutants that are defective in glycogen synthesis (*glgC* mutants or *glgA1/glgA2* double mutants) display

metabolic deficiencies during nitrogen starvation and are impaired in phycobiliprotein degradation and, therefore, show a non-bleaching phenotype. After a few days under nitrogen-deficient medium, they lose viability [Gründel et al., 2012; Hickman et al., 2013]. The synthesis of glycogen is accompanied by the concomitant induction of expression of glycogen catabolic genes, for which the SigE and Rre37 regulators are responsible [Azuma et al., 2011; Osanai et al., 2014]. Although this appears paradoxical, it illustrates that a genetic program exists that "anticipates" the recovery from nitrogen starvation (see below).

Resuscitation from Chlorosis: A Global Analysis

A first global and comprehensive analysis of the resuscitation of chlorotic *Synechocystis* cells was performed by Klotz et al. [2016]. When fully developed, long-term chlorotic *Synechocystis* cells were supplied with nitrate, and it could be shown that they started to re-green and regain photosynthetic activity after about 24 h. After about 2 days, photosynthetic performance was almost completely restored, and after 3 days, cell division was resumed. Figure 1 provides a graphical representation of these developmental transitions. At a first glance, the retarded appearance of photosynthetic pigments might give the impression that the cells only respond to the addition of a nitrogen source with a delay of approximately a day. However, examination at the molecular level reveals that the apparent 24-h lag phase is in fact a highly dynamic period. As shown by transcriptomic and proteomic analysis, the basic operating system of the cells, which during chlorosis has been turned down to a minimum, must be re-established before the cells are able to re-green and rebuild the complex intracellular machineries of photosynthesis [Klotz et al., 2016; Spat et al., 2018]. It transpired that the entire process follows a highly orchestrated genetically encoded program, evident at all levels of cellular activity.

At the metabolic level, resuscitation can be divided into two principal phases. In the first phase, immediately after nitrate addition, cells turn on a heterotrophic-like metabolism, based on glycogen consumption and oxygen-dependent respiration. In the second phase, after about 24 h, when the photosystems reappear, cells switch to a mixotrophic metabolism, where glycogen utilization co-occurs with CO_2 fixation and oxygenic photosynthesis. Only in the fully recovered state do they finally resume the classical photoautotrophic metabolism and return to vegetative growth. A key to the understanding of the resuscitation program is the underlying glycogen metabolism, which provides the cells with energy and metabolic precursors (see Fig. 2 for an overview of the principal pathways of glycogen metabolism in *Synechocystis*). Therefore, glycogen is pivotal to the viability of chlorotic cells. The *Synechocystis* genome harbours two paralogous genes for glycogen synthetases, *glgA1* (sll0945) and *glgA2* (sll1393). Knockout of only one of the two *glgA* paralogues results in mutants that synthesize the same amount of glycogen as the wild type following nitrogen step down. Nevertheless, these two mutants display striking phenotypic differences upon nitrogen starvation. Whereas the *glgA2* mutants are able to carry a wild-type response to chlorosis, the *glgA1* mutants as well as the *glgA1/glgA2* double mutants show impaired chlorosis: instead of a step-wise degradation of the photosynthetic pigments, the mutants do not initially respond to nitrogen depletion, but after a while they turn white and lose viability [Koch et al., 2019]. This suggests that only glycogen produced by GlgA1 is relevant for survival. The molecular basis of this difference is unclear and is currently under investigation.

Similar non-redundant pairs of glycogen metabolic genes are found for the paralogues of glycogen phosphorylase, *glgP1* (sll1356) and *glgP2* (slr1367), as well as for the paralogues for glycogen-debranching enzyme *glgX1* (slr0237) and *glgX2* (slr1857). The analysis of the respective mutants showed that only GlgP2 supports the resuscitation program. The *glgP2* mutants (still able to produce GlgP1), as well as the *glgP1/glgP2* double knockout mutants, are unable to be resuscitated from chlorosis, although the initial process of chlorosis proceeds normally, as deduced from the ordered degradation of pigments [Doello et al., 2018]. The poor resuscitation of the various *glgA* and *glgP* mutants is depicted in Figure 2b. The glycogen phosphorylase reaction releases Glc-1P, which is further converted by phosphoglucomutase (PGM, sll0726) to generate Glc-6P (see Fig. 2a). This metabolite can either enter the Embden-Meyerhof-Parnas pathway (EMP), or it can be oxidized by glucose-6P dehydrogenase (encoded by the *zwf* gene) to 6P-gluconate, which is further metabolized by the oxidative pentose phosphate (OPP) cycle or the Entner-Doudoroff (ED) pathway. Whereas mutants with a deficient EMP pathway recover almost like the wild type from the chlorotic state, *zwf* knockout mutants are strongly impaired in resuscitation. A mutant deficient in only the ED pathway is less severely affected than a mutant with an impairment in the OPP pathway, showing that the latter is the most important glycogen catabolic pathway in recovering chlorotic cells [Doello et al., 2018].

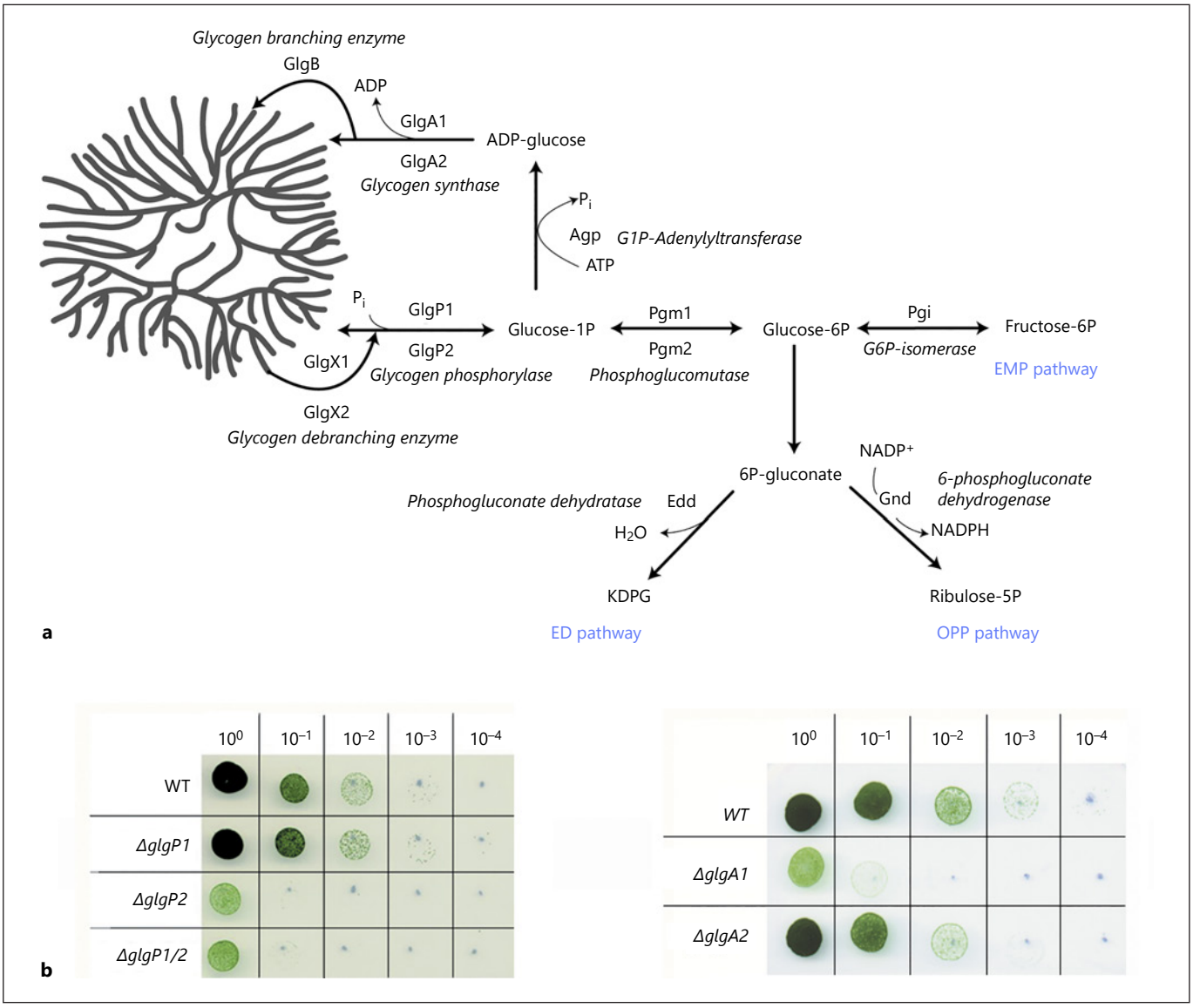

Fig. 2. Schematic representation of glycogen metabolism in *Synechocystis* and its involvement in chlorosis and resuscitation. **a** Depiction of reactions in glycogen metabolism and glycogen catabolic pathways in *Synechocystis*. **b** Resuscitation of chlorotic cells tested by drop plate assay. From a serial dilution of chlorotic cultures (0–10^{-4} dilution as indicated), 5 µL were dropped on nitrate-supplied BG11 plates and incubated until colonies appeared. Resuscitation efficiency of wild type (WT) is compared to various mutants deficient in glycogen phosphorylase (Δ*glgP1*, Δ*glgP2*, Δ*glgP1/2*) or glycogen synthase (Δ*glgA1*, Δ*glgA2*).

When the cells started to respire and to degrade glycogen upon the addition of nitrate to chlorotic cultures, the low level of photosynthetic activity, which is still measurable in the chlorotic state, is completely shut down. Photosynthetic oxygen evolution only reappears at the end of the first phase of resuscitation, indicating a switch to a mixotrophic metabolism. During this period, which takes place about 1 day after addition of the nitrogen source, re-greening becomes visible, indicating the re-installation of the photosynthetic machinery. Electron micrographs reveal that in this second phase of resuscitation, the cells reconstruct the thylakoid system de novo (see Fig. 1d). After about 2 days, most of the cells have recovered their photosynthetic machineries and are able to switch metabolism toward vegetative growth. With the onset of cell division, 2–3 days after the addition of a ni-

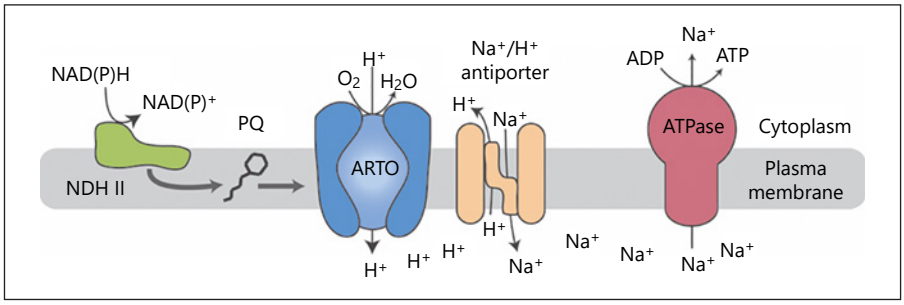

Fig. 3. Sodium-dependent bioenergetic processes in nitrogen-starved cells. Depiction of the components of the respiratory chain and the ATP synthesis machinery in the plasma membrane of *Synechocystis*.

trogen source, the resuscitation program is complete, and the cells exhibit typical vegetative growth. During chlorosis, the cells apparently become arrested in a pre-divisional state; they contain on average double the amount of chromosomal DNA than actively growing cells. At the end of the resuscitation program, the average cell size, as well as the average chromosome copy number, decrease to half the values of chlorotic cells, which is indicative of ongoing cell division [Klotz et al., 2016].

The Start of Resuscitation

Bioenergetics of Awakening

During chlorosis, metabolic reactions are reduced to a minimum and the intracellular energy charge is kept low; the ATP content is maintained at a basal level, which constitutes the minimum to maintain cell survival. Thus, the ATP levels in nitrogen-starved cells are reduced by up to 25% of the value in vegetatively growing cells. Upon addition of a nitrogen source to chlorotic cells, the first detected cellular response is a rapid increase in the ATP content. However, the extent of this increase is dependent on the form in which nitrogen is provided. Addition of sodium nitrate to chlorotic cells triggers a 100% increase in the ATP content within 20 min, whereas supplementation with potassium nitrate leads to a slower increase in the ATP levels (approximately 20–30% less compared to sodium nitrate). Doello et al. [2021] investigated this peculiar phenomenon and have discovered a so far unrecognized and unique bioenergetic strategy in nitrogen-starved cells.

During prolonged chlorosis, the thylakoid membranes, which accommodate the majority of the F-type ATPase complexes, are degraded. Consequently, chlorotic cells rely on the ATP synthases located in the plasma membrane, which are able to use a sodium motive force to power ATP synthesis. When resuscitation is started by the addition of sodium nitrate, the sudden rise of the extracellular sodium concentration leads to an increased sodium motive force, which causes an instantaneous increase in the ATP levels. When potassium nitrate is used to induce resuscitation, the concentration of sodium remains constant, and the increase in the ATP content results from a metabolically regulated response to the availability of a nitrogen source.

When nitrogen assimilation initiates, the cellular ATP demand dramatically increases due to the high turnover rate of the energy-consuming GS reaction. A concomitant increase in ATP synthesis is, therefore, essential to ensure efficient nitrogen assimilation and to avoid drainage of the cellular ATP levels. How cells achieve this tight control of the ATP homeostasis has not yet been entirely deciphered; however, it has been shown that activation of the GS reaction is involved in this regulatory mechanism, because the increase in ATP levels in response to the availability of nitrogen is sensitive to MSX, a specific GS inhibitor. Additionally, upon addition of a nitrogen source, ATP synthesis requires glycogen degradation and respiration. This was demonstrated by the lack of an increase in the ATP content in a GlgP-negative mutant, which is impaired in glycogen catabolism, and in wild-type cells when they are treated with potassium cyanide (KCN), an inhibitor of the respiration. Moreover, specific inhibition of electron transfer from the plastoquinone pool (PQ) to the cytochrome b_6f complex, which is exclusively found in the thylakoid membranes, reveals that respiration takes place at the plasma membrane in chlorotic cells undergoing the early steps of resuscitation [Doello et al., 2021]. It is, therefore, tempting to speculate that nitrogen assimilation through the GS reaction initiates glycogen breakdown, thereby generating reducing equivalents, which then activate respiration at the cytoplasmic membrane. The plasma membrane is equipped with an alternative respiratory chain consisting of a type II NADH:quinone oxidoreductase (NDH II) and an alternative respiratory terminal oxidase (ARTO) [Baers et al., 2019]. In fact, we could show that NDH II is one of the most highly accumulated proteins in the chlorotic state

Microb Physiol 2021;31:78–87
DOI: 10.1159/000515742

[Spat et al., 2018]. In vegetative cells, this respiratory system is coupled to the generation of a sodium motive force to energize sodium-dependent bicarbonate uptake [Pils and Schmetterer, 2001]. In nitrogen-starved cells, where inorganic carbon fixation is arrested, this bioenergetic system ensures energy provision in the standby mode and to support the initial phase of resuscitation (Fig. 3).

Resumption of Nitrogen Assimilation

The activity of GS is subject to tight regulation. In cyanobacteria, GS activity is controlled by the inhibitory proteins IF7 and IF17, whose synthesis is under global nitrogen control and is strongly downregulated during nitrogen starvation [Bolay et al., 2018]. Moreover, the cells express a second, nitrogen starvation-specific GS gene, *glnN* [Reyes and Florencio, 1994]. In *S. elongatus*, GlnN helps recovery of the cells from long-term nitrogen starvation [Sauer et al., 1999]. Thus, the cells maintain highly active nitrogen assimilation capacity during chlorosis. As soon as nitrogen becomes available again, GS starts working, thereby initiating the resuscitation program. Nitrogen assimilation then operates at full capacity, with the inhibitory peptides IF7 and IF187 only being induced toward the end of resuscitation [Spat et al., 2018]. In agreement with these findings is the observation that the noncoding regulatory RNA NsiR4, which prevents expression of IF7, remains highly expressed in the initial phase of resuscitation. The assimilation of combined nitrogen initially exceeds the pace of protein synthesis, since the entire translational machinery first has to be re-installed. The excess of assimilated nitrogen is transiently stored as CP [Watzer and Forchhammer, 2018], which is deposited as a granular structure in the cytoplasm (see Fig. 1c; structures indicated by Cg). When the protein synthesis machinery is fully operational, the CP material is recycled for synthesis of cellular building blocks. This strategy enables cells to store any available nitrogen for subsequent utilization in an environment with fluctuating and transient nitrogen supply. Physiological comparison of mutants deficient in CP synthase (cphA) with wild-type cells demonstrated that in the absence of CP synthesis cells are unable to recover completely when nitrogen is only transiently available to the cells. By contrast, wild-type cells can resuscitate successfully and return to vegetative growth [Watzer and Forchhammer, 2018].

Early Events in Transcriptional Regulation

To reveal the molecular events occurring during the process of resuscitation, a detailed transcriptome study has been performed [Klotz et al., 2016]. To achieve this, a high-density microarray covering the entire chromosome and the 7 plasmids was used, probing all 8,916 transcripts of coding and non-coding RNA. RNA was extracted at 5 different time points (after 0, 4, 12, 24 and 48 h after nitrate addition), starting with fully developed chlorotic cells and finishing with completely re-greened cells. A total of 1,570 differentially regulated genes were detected, which corresponds to 17.6% of the entire transcriptome. Of these genes, approximately one-third comprises non-coding RNA. The changes in the transcriptome during the resuscitation process perfectly reflect the chronological order of cellular processes. The majority of the differentially regulated genes belong to the early responding genes, whose expression changes after about 4 h. They comprise 425 and 626 up- or downregulated genes, respectively, compared with the dormant state. The upregulated group of genes includes the entire set of genes encoding the translational apparatus, as well as metabolic genes, particularly those involved in nitrate/nitrite assimilation, genes encoding enzymes for co-factor biosynthesis, ATP synthesis and CO_2 fixation. The latter finding is striking, as it hints at a role for CO_2 fixation prior to the onset of photosynthesis. In agreement with this suggestion, Doello et al. [2018] detected CO_2 fixation activity as soon as 10 h after the initiation of resuscitation, well before the onset of oxygen evolution. Surprisingly, the genes encoding the enzymes required for glycogen catabolism are not strongly upregulated at the transcriptional level. In fact, the glycogen catabolic genes are already upregulated in response to the nitrogen step down, concomitant with the synthesis of glycogen. Proteome analyses confirm that the respective proteins are maintained at elevated levels throughout the chlorotic state. This demonstrates an "anticipatory principle" in the acclimation toward nitrogen starvation. The decisive catabolic enzymes are prepared in standby mode, awaiting the availability of nutrient. This necessarily implies that the enzymes, such as glycogen phosphorylase, have to be kept in an inactive state, in order to prevent premature glycogen consumption. Preliminary data indicate a key role for PGM in the control of glycogen breakdown [unpubl. data].

As deduced from the dynamics of the transcriptome, the early responses reflect the re-installation of the basic operation system of the cells, the core anabolic reactions, energy metabolism and the translational apparatus, enabling the cells to re-configure the complex cellular structures that were degraded during chlorosis. As deduced from this study, the transcriptional machinery itself, in particular the components of the RNA polymerase, does

not change in expression as strongly as the translational machinery. The changes are more subtle and affect specific regulatory components. During nitrogen starvation, the transcriptional machinery switches from use of the house-keeping SigA-dependent RNA polymerase to use of alternative sigma factors, in particular, SigB, SigC and SigE [Imamura and Asayama, 2009; Heilmann et al., 2017]. In particular, SigC has been shown to promote late-stage gene expression and nitrogen promoter recognition [Asayama et al., 2004]. SigE mediates induced expression of various carbon catabolic genes during nitrogen starvation (see above). During resuscitation, however, the transcriptional machinery has to be re-wired toward SigA-dependent transcription, which is responsible for the expression of the core operating system of the cell. The extensive re-organization of the transcriptome agrees with a dominant role for different sigma factors that affect global transcriptional patterns [Srivastava et al., 2020]. The small non-coding 6S RNA may have a key role in sigma factor transition. The 6S RNA is widely distributed in prokaryotes and acts as a global regulatory RNA involved in growth control. *Synechocystis* mutants with mutations in *ssaA* show delayed recovery from the chlorotic state [Heilmann et al., 2017]. The authors of that work also performed in vivo pull-down analysis of the RNA polymerase complex, and the data suggest that the 6S RNA promotes the recruitment of the housekeeping sigma factor SigA to the RNA polymerase core complex, concurrently supporting displacement of group 2 sigma factors, such as SigB, C and E. An early transition back to SigA-dependent transcription explains the extensive transcriptional response observed at the onset of resuscitation in the study by Klotz et al. [2016].

The Second Phase of Resuscitation: Restoration of Photosynthesis

Only after the re-launch of the basic components of the metabolic machinery can the cells afford to re-install the photosynthetic machinery. This is because it imposes a high metabolic burden on the cells through the coordinated synthesis of lipids for thylakoid membranes, the large amounts of tetrapyrroles and all the proteins required for the photosynthetic complexes, from the PBS antenna to the reaction centres. The timing of chlorophyll biosynthesis is especially crucial, because free chlorophyll is toxic to the cells. All these processes must, therefore, occur in a highly coordinated manner. How this is achieved is still poorly understood. The two aforementioned transcriptome and proteome studies [Klotz et al., 2016; Spat et al., 2018], however, provide preliminary insights into this process. Remarkably, the first cellular response upon nitrogen addition is in fact to suppress any residual photosynthetic activity. This early negative impact on photosynthesis is in good agreement with the observation that the function of some of the early regulated gene products is to prevent premature synthesis of photosynthetic components. For example, transient expression of the non-coding RNA PsrR1 supresses chlorophyll biosynthesis and PBS gene expression [Georg et al., 2014] and expression of several PSII-related and chlorophyll biosynthesis-related genes are repressed in the early stage of resuscitation. The logic of this strategy might also be related to the diurnal lifestyle of cyanobacteria. In nature, the cyanobacteria are constantly subjected to the daily availability of light energy for a certain length of time. The awakening of the cells relies exclusively on glycogen-dependent energy metabolism, which allows utilization of nitrogen sources independent of light availability. This ensures a secure progression of resuscitation until the entire basic operation system is completely re-installed. Only then do the cells start to reconstitute the photosynthetic apparatus. The corresponding process works extremely precisely and is finely tuned at all levels. This is clearly illustrated for chlorophyll biosynthesis [Spat et al., 2018], whereby a decisive step in chlorophyll biosynthesis is the conversion of protochlorophyllide to chlorophyllide, for which light-dependent and light-independent isoenzymes exist in *Synechocystis*. At the proteome level, the enzymes are undetectable in the chlorotic state and in the early phase of resuscitation. The light-dependent protochlorophyllide reductase (Por) only becomes detectable in the middle phase of resuscitation [Spat et al., 2018], whereas the light-independent isoenzymes ChlB and ChlL are still absent. In agreement with this, the expression of the corresponding genes is repressed during the early phase of resuscitation (see above). This strategy ensures that chlorophyll biosynthesis can start as soon as the basic operation system is re-installed and light is available. The final biosynthetic enzyme, chlorophyll synthase (ChlG) is already present prior to the induction of Por synthesis, so that using this strategy the cells are prepared to convert the highly toxic chlorophyllide molecule into chlorophyll *a*, which is then incorporated into chlorophyll-binding proteins, which have to be synthesized simultaneously.

Another crucial step in the re-installation of the photosynthetic machinery is the assembly of the photosynthetic protein complexes in newly synthesized thylakoid membranes. Here, quantitative analyses of the phosphoproteome have yielded first intriguing insights into what

is occurring. Among the phosphoproteins whose degree of phosphorylation changed dynamically over the time course of resuscitation, the largest functional group is indeed the proteins related to photosynthesis [Spat et al., 2018]. These proteins can be grouped in 5 classes according to the pattern of phosphorylation change. The few residual proteins of the PBS rods are highly phosphorylated during chlorosis and the phosphorylation level gradually decreases during resuscitation. Phosphorylation of the phycobiliproteins could be related to protein stability and turnover. Other photosynthetic proteins, such as PBS core proteins or some components of PSI and PSII, show a transient increase in phosphorylation. The Vipp1 proteins, for example, which play a decisive role in thylakoid membrane biogenesis [Heidrich et al., 2017], show a particularly complex phosphorylation pattern with 8 detected phosphorylation sites, occurring on 2 clustered regions of the protein. The phosphorylation level remains high during the initial resuscitation phase, with some sites even showing initially increased phosphorylation, until time point 24 h. Subsequently, phosphorylation of all sites decreases, which occurs concomitantly with the accumulation of newly synthesized Vipp1 protein and the emergence of stacked thylakoid membranes. Vipp1 was shown to form large multimeric structures that form rings and rods [Theis et al., 2019] and control the formation of thylakoid membranes [Westphal et al., 2001]. Phosphorylation of Vipp1 might thus keep this protein in an inactive state, until the progression of resuscitation advances to the stage where Vipp1 activity comes into play. Based on this study, protein phosphorylation has thus emerged to add another layer of regulator complexity controlling the timing of resuscitation.

Conclusions

The analysis of the nitrogen starvation-induced transition of *Synechocystis* into a dormant-like chlorotic state and resuscitation form this state has revealed new insights into dormancy and awakening. Organisms from most diverse origins tune down cellular activities to a minimum in order to survive extended periods of adverse environmental conditions, such as nutrient starvation. Under these circumstances, they all need to find the answer to a major issue: What is the minimal activity necessary to maintain viability?

In order to resuscitate cells from the dormant state, a minimal initial energy is necessary, and a minimal set of the most fundamental cellular functions has to be maintained; in order to make new protein, at least some ribosomes and translation factors need to be in place. This minimal set of cellular activities represents the organism's equivalent of the BIOS, the basic input/output system of a computer, that helps re-boot the operation system after being switched on. In analogy, the same tasks have to be performed when resuscitation from the dormant state is executed. We have learned by using chlorosis in *Synechocystis* as a model system that evolution has prepared cells with a sophisticated genetic program to achieve this task. Moreover, it appears that already at the stage when the cells enter the dormant state, they anticipate the future awakening and prepare essential components to allow rapid resuscitation. The revival of nutrient starvation-induced *Bacillus subtilis* spores is another example of the existence of a highly organized developmental program to awaken from dormancy and reconstruct a cell [Sinai et al., 2015]. Another lesson learned from these investigations is the identification of the functions of genes that have been annotated as "hypothetical," since their roles appear only under extreme conditions, and some of these may even belong to the cellular BIOS.

Conflict of Interest Statement

The authors have no conflicts of interest to declare.

Funding Sources

Work in the Forchhammer laboratory was funded by the RTG 1708 "Molecular principles of bacterial survival strategies" and by DFG-funded Research Unit SCyCode (FOR2816). We further acknowledge support by Open Access Publishing Fund of University of Tübingen and Infrastructural Funding from the Cluster of Excellence EXC 2124 "Controlling Microbes to Fight Infections."

Author Contributions

Conceptualization: K.F.; writing, original draft preparation: K.F.; review and editing: N.N., S.D. and K.F.

References

Al Dahouk S, Jubier-Maurin V, Neubauer H, Köhler S. Quantitative analysis of the Brucella suis proteome reveals metabolic adaptation to long-term nutrient starvation. BMC Microbiol. 2013;13(1):199.

Allen MM, Smith AJ. Nitrogen chlorosis in blue-green algae. Arch Mikrobiol. 1969;69(2):114–20.

Arias CR, LaFrentz S, Cai W, Olivares-Fuster O. Adaptive response to starvation in the fish pathogen Flavobacterium columnare: cell viability and ultrastructural changes. BMC Microbiol. 2012;12(1):266.

Asayama M, Imamura S, Yoshihara S, Miyazaki A, Yoshida N, Sazuka T, et al. SigC, the group 2 sigma factor of RNA polymerase, contributes to the late-stage gene expression and nitrogen promoter recognition in the cyanobacterium Synechocystis sp. strain PCC 6803. Biosci Biotechnol Biochem. 2004;68(3):477–87.
Azuma M, Osanai T, Hirai MY, Tanaka K. A response regulator Rre37 and an RNA polymerase sigma factor SigE represent two parallel pathways to activate sugar catabolism in a cyanobacterium Synechocystis sp. PCC 6803. Plant Cell Physiol. 2011;52(2):404–12.
Baers LL, Breckels LM, Mills LA, Gatto L, Deery MJ, Stevens TJ, et al. Proteome mapping of a cyanobacterium reveals distinct compartment organization and cell-dispersed metabolism. Plant Physiol. 2019;181(4):1721–38.
Bolay P, Muro-Pastor MI, Florencio FJ, Klähn S. The distinctive regulation of cyanobacterial glutamine synthetase. Life (Basel). 2018;8(4).
Boresch K. Zur Physiologie der Blaualgenfarbstoffe. Lotos (Prag). 1910;58:344–345.
Collier JL, Grossman AR. A small polypeptide triggers complete degradation of light-harvesting phycobiliproteins in nutrient-deprived cyanobacteria. EMBO J. 1994;13(5):1039–47.
Damrow R, Maldener I, Zilliges Y. The multiple functions of common microbial carbon polymers, glycogen and PHB, during stress responses in the non-diazotrophic cyanobacterium Synechocystis sp. PCC 6803. Front Microbiol. 2016;7:966.
Doello S, Burkhardt M, Forchhammer K. The essential role of sodium bioenergetics and ATP homeostasis in the developmental transitions of a cyanobacterium. Curr Biol. 2021.
Doello S, Klotz A, Makowka A, Gutekunst K, Forchhammer K. A specific glycogen mobilization strategy enables rapid awakening of dormant cyanobacteria from chlorosis. Plant Physiol. 2018;177(2):594–603.
Georg J, Dienst D, Schürgers N, Wallner T, Kopp D, Stazic D, et al. The small regulatory RNA SyR1/PsrR1 controls photosynthetic functions in cyanobacteria. Plant Cell. 2014;26(9):3661–79.
Görl M, Sauer J, Baier T, Forchhammer K. Nitrogen-starvation-induced chlorosis in Synechococcus PCC 7942: adaptation to long-term survival. Microbiology. 1998;144(9):2449–58.
Grossman AR, Schaefer MR, Chiang GG, Collier JL. The phycobilisome, a light-harvesting complex responsive to environmental conditions. Microbiol Rev. 1993;57(3):725–49.
Gründel M, Scheunemann R, Lockau W, Zilliges Y. Impaired glycogen synthesis causes metabolic overflow reactions and affects stress responses in the cyanobacterium Synechocystis sp. PCC 6803. Microbiology. 2012;158(Pt 12):3032–43.
Hauf W, Schlebusch M, Hüge J, Kopka J, Hagemann M, Forchhammer K. Metabolic changes in Synechocystis PCC6803 upon nitrogen-starvation: excess NADPH sustains polyhydroxybutyrate accumulation. Metabolites. 2013;3(1):101.
Heidrich J, Thurotte A, Schneider D. Specific interaction of IM30/Vipp1 with cyanobacterial and chloroplast membranes results in membrane remodeling and eventually in membrane fusion. Biochim Biophys Acta. 2017;1859(4):537–49.
Heilmann B, Hakkila K, Georg J, Tyystjärvi T, Hess WR, Axmann IM, et al. 6S RNA plays a role in recovery from nitrogen depletion in Synechocystis sp. PCC 6803. BMC Microbiol. 2017a;17(1):229.
Hickman JW, Kotovic KM, Miller C, Warrener P, Kaiser B, Jurista T, et al. Glycogen synthesis is a required component of the nitrogen stress response in Synechococcus elongatus PCC 7942. Algal Res. 2013;2(2):98–106.
Imamura S, Asayama M. Sigma factors for cyanobacterial transcription. Gene Regul Syst Bio. 2009;3:65–87.
Keren I, Minami S, Rubin E, Lewis K. Characterization and transcriptome analysis of Mycobacterium tuberculosis persisters. mBio. 2011;2(3):e00100–11.
Klotz A, Georg J, Bučinská L, Watanabe S, Reimann V, Januszewski W, et al. Awakening of a dormant cyanobacterium from nitrogen chlorosis reveals a genetically determined program. Curr Biol. 2016;26(21):2862–72.
Klotz A, Reinhold E, Doello S, Forchhammer K. Nitrogen starvation acclimation in Synechococcus elongatus: redox-control and the role of nitrate reduction as an electron sink. Life (Basel). 2015;5(1):888.
Koch M, Berendzen KW, Forchhammer AK. On the role and production of polyhydroxybutyrate (PHB) in the cyanobacterium Synechocystis sp. PCC 6803. Life (Basel). 2020;10(4).
Koch M, Doello S, Gutekunst K, Forchhammer K. PHB is produced from glycogen turn-over during nitrogen starvation in Synechocystis sp. PCC 6803. Int J Mol Sci. 2019;20(8):1942.
Moreno-Gámez S, Kiviet DJ, Vulin C, Schlegel S, Schlegel K, van Doorn GS, et al. Wide lag time distributions break a trade-off between reproduction and survival in bacteria. Proc Natl Acad Sci USA. 2020;117(31):18729–36.
Osanai T, Oikawa A, Numata K, Kuwahara A, Iijima H, Doi Y, et al. Pathway-level acceleration of glycogen catabolism by a response regulator in the cyanobacterium Synechocystis species PCC 6803. Plant Physiol. 2014;164(4):1831–41.
Perez R, Wörmer L, Sass P, Maldener I. A highly asynchronous developmental program triggered during germination of dormant akinetes of filamentous diazotrophic cyanobacteria. FEMS Microbiol Ecol. 2018;94(1). https://doi.org/10.1093/femsec/fix131.
Pils D, Schmetterer G. Characterization of three bioenergetically active respiratory terminal oxidases in the cyanobacterium Synechocystis sp. strain PCC 6803. FEMS Microbiol Lett. 2001;203(2):217–22.
Reyes JC, Florencio FJ. A mutant lacking the glutamine synthetase gene (glnA) is impaired in the regulation of the nitrate assimilation system in the cyanobacterium Synechocystis sp. strain PCC 6803. J Bacteriol. 1994;176(24):7516–23.
Robertson BR, Tezuka N, Watanabe MM. Phylogenetic analyses of Synechococcus strains (cyanobacteria) using sequences of 16S rDNA and part of the phycocyanin operon reveal multiple evolutionary lines and reflect phycobilin content. Int J Syst Evol Microbiol. 2001;51(Pt 3):861–71.
Sauer J, Gorl M, Forchhammer K. Nitrogen starvation in Synechococcus PCC 7942: involvement of glutamine synthetase and NtcA in phycobiliprotein degradation and survival. Arch Microbiol. 1999;172(4):247–55.
Sauer J, Schreiber U, Schmid R, Völker K, Forchhammer K. Nitrogen starvation-induced chlorosis in Synechococcus PCC 7942. Low-level photosynthesis as a mechanism of long-term survival. Plant Physiol. 2001;126(1):233–43.
Schlebusch M, Forchhammer K. Requirement of the nitrogen starvation-induced protein Sll0783 for polyhydroxybutyrate accumulation in Synechocystis sp. strain PCC 6803. Appl Environ Microbiol. 2010;76(18):6101–7.
Schwarz R, Forchhammer K. Acclimation of unicellular cyanobacteria to macronutrient deficiency: emergence of a complex network of cellular responses. Microbiology (Reading, Engl). 2005;151(Pt 8):2503–14.
Sinai L, Rosenberg A, Smith Y, Segev E, Ben-Yehuda S. The molecular timeline of a reviving bacterial spore. Mol Cell. 2015;57(4):695–707.
Spat P, Klotz A, Rexroth S, Macek B, Forchhammer K. Chlorosis as a developmental program in cyanobacteria: the proteomic fundament for survival and awakening. Mol Cell Proteomics. 2018.
Srivastava A, Summers ML, Sobotka R. Cyanobacterial sigma factors: current and future applications for biotechnological advances. Biotechnol Adv. 2020 May-Jun;40:107517.
Stephan DP, Ruppel HG, Pistorius EK. Interrelation between cyanophycin synthesis, L-arginine catabolism and photosynthesis in the cyanobacterium Synechocystis sp. strain PCC 6803. Z Naturforsch C J Biosci. 2000;55(11⁄12):927–42.
Theis J, Gupta TK, Klingler J, Wan W, Albert S, Keller S, et al. VIPP1 rods engulf membranes containing phosphatidylinositol phosphates. Sci Rep. 2019;9(1):8725.
Udikovic-Kolic N, Wichmann F, Broderick NA, Handelsman J. Bloom of resident antibiotic-resistant bacteria in soil following manure fertilization. Proc Natl Acad Sci USA. 2014;111(42):15202–7.
Watzer B, Forchhammer K. Cyanophycin synthesis optimizes nitrogen utilization in the unicellular cyanobacterium Synechocystis sp. strain PCC 6803. Appl Environ Microbiol. 2018;84(20).
Westphal S, Heins L, Soll J, Vothknecht UC. Vipp1 deletion mutant of Synechocystis: a connection between bacterial phage shock and thylakoid biogenesis?. Proc Natl Acad Sci USA. 2001;98(7):4243–8.

Publication 3: Research article

Selim KA., Haffner M., Burkhardt M., Mantovani O., **Neumann N.**, Albrecht R., Seifert R., Krüger L., Stülke J., Hartmann MD., Hagemann M., Forchhammer K.

Diurnal metabolic control in cyanobacteria requires perception of second messenger signaling molecule c-di-AMP by the carbon control protein SbtB.

Science Advances 2021 • Vol 7, Issue 50

SIGNAL TRANSDUCTION

Diurnal metabolic control in cyanobacteria requires perception of second messenger signaling molecule c-di-AMP by the carbon control protein SbtB

Khaled A. Selim[1,2]*†, Michael Haffner[1]†, Markus Burkhardt[1], Oliver Mantovani[3], Niels Neumann[1], Reinhard Albrecht[2], Roland Seifert[4], Larissa Krüger[5], Jörg Stülke[5], Marcus D. Hartmann[2], Martin Hagemann[3], Karl Forchhammer[1]*

Because of their photosynthesis-dependent lifestyle, cyanobacteria evolved sophisticated regulatory mechanisms to adapt to oscillating day-night metabolic changes. How they coordinate the metabolic switch between autotrophic and glycogen-catabolic metabolism in light and darkness is poorly understood. Recently, c-di-AMP has been implicated in diurnal regulation, but its mode of action remains elusive. To unravel the signaling functions of c-di-AMP in cyanobacteria, we isolated c-di-AMP receptor proteins. Thereby, the carbon-sensor protein SbtB was identified as a major c-di-AMP receptor, which we confirmed biochemically and by x-ray crystallography. In search for the c-di-AMP signaling function of SbtB, we found that both SbtB and c-di-AMP cyclase–deficient mutants showed reduced diurnal growth and that c-di-AMP–bound SbtB interacts specifically with the glycogen-branching enzyme GlgB. Accordingly, both mutants displayed impaired glycogen synthesis during the day and impaired nighttime survival. Thus, the pivotal role of c-di-AMP in day-night acclimation can be attributed to SbtB-mediated regulation of glycogen metabolism.

INTRODUCTION

Aerobic life on Earth evolved about 2.7 to 3.2 billion years ago with the evolution of oxygenic photosynthesis by cyanobacteria. Because photosynthesis uses energy provided by sunlight, cyanobacteria have evolved intricate circadian timing machinery to fine-tune photosynthesis and other metabolic activity to successive day-night cycles of different length (*1*). The recent discovery of a true circadian clock in the nonphotosynthetic bacterium *Bacillus subtilis* suggests that circadian rhythms may be widespread among other prokaryotes as well (*2*). All eukaryotic organisms independently evolved a circadian clock to acclimate to different diurnal cycles. In humans, the disruption of circadian timing correlates with diverse health problems including cancer and cardiovascular diseases (*3*).

Photoautotrophic organisms are constantly exposed to alternating day-night light regimes, which requires a permanent metabolic switch between autotrophic CO_2 fixation via Calvin-Benson cycle during the day and heterotrophic-like carbon catabolism during the night. During the day, newly fixed CO_2 is used for anabolic reactions, producing the building blocks for cell growth, and, in addition, for building up organic carbon reserves such as glycogen in cyanobacteria or starch in plants. During the night, glycogen is metabolized mainly using the oxidative pentose-phosphate (OPP) pathway, to provide reduction equivalents for energy conserving respiration (*4*, *5*). The constant switch between autotrophic and heterotrophic metabolism is operated by a sophisticated network of regulatory processes, which we only begin to understand. It involves sensing of the redox, energy, carbon, and nitrogen status as well as a specific timing machinery, the circadian clock (*1*, *3*, *6*). Although it is clear that the diurnal rhythm affects central carbon metabolism, mainly of glycogen anabolism and catabolism (*3*, *7*, *8*), our understanding of the signaling cascades regulating central carbon and nitrogen metabolisms under diurnal growth is still very preliminary.

Recent investigations pointed toward additional regulatory circuits, whose connection to the circadian clock is unclear. For instance, these reports revealed a noncanonical role of the second messengers cyclic di-adenosine monophosphate [3′,5′-c-di–adenosine 5′-monophosphate; hereafter c-di-AMP] and of the alarmone guanosine penta- and tetraphosphate ppGpp(p) in the diurnal photosynthetic lifestyle of cyanobacteria (*9*–*11*). Since its discovery in 2008, the second messenger c-di-AMP came into focus of research, owing to its essentiality in many organisms (*12*–*14*). This cyclic nucleotide has been implicated in regulating several biological processes, mainly related to cell wall and osmotic homeostasis in Firmicutes and, to a lesser extent, in Actinobacteria. In these heterotrophic bacteria, the main c-di-AMP targets are ion and osmolyte transporters, including those of K^+, Na^+, and Mg^{2+} ions, glycine betaine, and amino acids (*12*–*14*). Binding of c-di-AMP has also been demonstrated for a protein of the PII superfamily, termed DarA in *B. subtilis* (*15*) or PstA in *Staphylococcus aureus* (*16*); however, the physiological role of those signaling proteins remains unclear. In cyanobacteria, c-di-AMP has been recently described to be required for nocturnal dormancy of *Synechococcus elongatus*, because mutants of the c-di-AMP cyclase were impaired in nighttime survival. However, the molecular mechanism underlying the function of c-di-AMP in nocturnal dormancy has remained unresolved (*11*). In addition, the analysis of *Synechocystis* sp. mutants in which

[1]Organismic Interactions Department, Interfaculty Institute for Microbiology and Infection Medicine, Cluster of Excellence 'Controlling Microbes to Fight Infections', Tübingen University, Auf der Morgenstelle 28, 72076 Tübingen, Germany. [2]Department of Protein Evolution, Max Planck Institute for Developmental Biology, Tübingen, Germany. [3]Plant Physiology Department, Institute of Biological Sciences, Rostock University, Rostock, Germany. [4]Institute of Pharmacology, Hannover Medical School, Hannover, Germany. [5]Department of General Microbiology, Göttingen Center for Molecular Biosciences (GZMB), Göttingen University, Göttingen, Germany.
*Corresponding author. Email: khaled.selim@uni-tuebingen.de (K.A.S.); karl.forchhammer@uni-tuebingen.de (K.F.)
†These authors shared co-first authorship.

the c-di-AMP concentration was elevated or reduced implied a role for c-di-AMP in acclimation to abiotic stress and osmotic homeostasis (*17*). These findings agreed with the prediction of c-di-AMP–dependent riboswitches upstream of genes involved in ion homeostasis and osmolyte transport (*18*). Furthermore, expression of the *sll0505* gene, encoding the *Synechocystis* di-adenylate cyclase, showed a strong correlation with the acclimation to long-term nitrogen starvation. Upon resuscitating the chlorotic *Synechocystis* cells from nitrogen starvation, *sll0505* belonged to the strongest early up-regulated genes, implying a role of c-di-AMP in the awakening from dormancy (*19*). Although several c-di-AMP receptor proteins were identified in heterotrophic bacteria (*12*, *14*), the c-di-AMP targets and its signaling role in cyanobacteria remain elusive.

Another second messenger nucleotide that returned into the focus of interest is cyclic AMP (3′,5′-cAMP; hereafter cAMP), as it was revealed as effector molecule for the PII-like signaling protein SbtB. We identified SbtB as a unique component of the cyanobacterial carbon-concentrating mechanism (CCM), required for efficient acclimation to varying inorganic carbon (C_i) regimes (*20*). HCO_3^-/CO_2 metabolism is also strictly regulated by the diurnal metabolic status of the cells, with active C_i accumulation during the autotrophic day mode and arrest of HCO_3^- transport during nocturnal dormancy (*21*). Recently, it has been shown that the diurnal switch of C_i transport activity is regulated via phytochromes involving SbtB (*21*). The *sbtB* gene is located in an operon with the gene for the sodium-dependent bicarbonate transporter SbtA. A similar genetic arrangement is frequently found in proteins of the PII family, which cluster with the transport proteins they regulate. Accordingly, SbtB was proven as a regulator of SbtA transport activity (*20*, *22*, *23*). Similar to canonical PII proteins (*24*, *25*), SbtB perceives energy signals by binding adenosine 5′-triphosphate (5′-ATP) or adenosine 5′-diphosphate (5′-ADP), but unlike canonical PII proteins, SbtB also senses 5′-AMP and preferentially binds the second messenger cAMP (*20*). The cAMP concentration was correlated with the CO_2 supply of the cells, implying an evolutionary conserved role of the second messenger cAMP as an indicator of the cellular carbon status via SbtB signaling (*20*, *26*). Furthermore, structural analysis of SbtB revealed a putative redox-sensitive motif at the C terminus (*20*), suggesting that SbtB may play a role in controlling HCO_3^- transport in response to light/dark-mediated redox stimuli.

The binding of a broad range of adenine nucleotides suggested that SbtB may also bind c-di-AMP. Because our preliminary data confirmed this assumption, we set out to verify the physiological relevance of c-di-AMP binding to SbtB in the cyanobacterial model organism *Synechocystis* sp. PCC 6803 (hereafter *Synechocystis*). The c-di-AMP pull-down experiment to fish in vivo c-di-AMP receptors notably retrieved SbtB as the most enriched protein. The SbtB-c-di-AMP complex could pull down another target of central carbon metabolism, the glycogen-branching enzyme GlgB. C-di-AMP signaling via SbtB turned out to be pivotal for the diurnal lifestyle of *Synechocystis* through regulation of glycogen metabolism via GlgB.

RESULTS

SbtB is the major c-di-AMP receptor protein in *Synechocystis*

The SbtB signaling proteins are highly conserved in cyanobacteria and act as C_i-sensing module using energy and carbon signal inputs through binding of the adenine nucleotides ATP, ADP, and AMP as well as cAMP (*20*, *23*, *27*). This unique ability of SbtB to bind a wide variety of adenine-based nucleotides made it likely that SbtB could also bind the second messenger c-di-AMP. Using isothermal titration calorimetry (ITC), we tested the ability of recombinant SbtB protein from *Synechocystis* (*Sc*SbtB) to bind c-di-AMP. The trimeric *Sc*SbtB was able to bind with high affinity to c-di-AMP (Fig. 1A) with dissociation constant (K_d) values (K_{d1} of 2.3 μM, K_{d2} of 12.2 μM, and K_{d3} of 35.9 μM for the first, second, and third binding site of trimeric *Sc*SbtB, respectively) comparable to that of cAMP but stronger than that of ATP, ADP, and AMP (*20*). Moreover, the binding enthalpy for c-di-AMP was almost equivalent or higher than that of ATP, ADP, and AMP at a lower concentration of c-di-AMP (fig. S1), which indicates preferential binding to c-di-AMP over standard adenine nucleotides. To test whether binding to c-di-AMP is a common trait among SbtB proteins in cyanobacteria, we examined the ability of the SbtB protein from the filamentous cyanobacterium *Nostoc* sp. PCC 7120 (*Ns*SbtB) to bind c-di-AMP. Similar to *Sc*SbtB protein, ITC analysis revealed that *Ns*SbtB is able to bind c-di-AMP as well.

To reveal whether c-di-AMP binding to SbtB proteins is of physiological relevance, we performed a pull-down experiment with a crude cell extract from *Synechocystis* using immobilized c-di-AMP as a bait and searched for protein preys that specifically bound to c-di-AMP (Fig. 1B). The *Sc*SbtB protein, encoded by *slr1513*, was the highest enriched protein in the pull-down fraction (Fig. 1B), confirming that *Sc*SbtB is a real target of c-di-AMP signaling. In addition to *Sc*SbtB, we identified several transporters, among them the major potassium transporters in *Synechocystis* KtrA (*sll0493*), TrkA (*slr0773*), and MthK (*sll0993*). Moreover, the magnesium transporter MgtE (*slr1216*), the sodium/H^+ antiporters NhaS2 and NhaS5 (*sll0273* and *slr0415*, respectively), and the glutamate-Na^+ symporter (*slr0625*) were identified as c-di-AMP–binding proteins. In addition to SbtB, the identification of these potential c-di-AMP–dependent transporters implied that c-di-AMP may play a major role in regulating ionic and osmotic homeostasis of *Synechocystis*. KtrA, TrkA, and MgtE are also well-known c-di-AMP target proteins in Gram-positive bacteria (*12*, *14*, *28*); their successful identification here validated our pull-down assay. None of the c-di-AMP target proteins was identified in the negative control experiment.

Collectively, these results established SbtB as yet another PII-like protein interacting with c-di-AMP. Because the function of c-di-AMP sensing by this protein family remains obscure, we focused our investigation on the detailed characterization of the SbtB:c-di-AMP molecular interaction and its physiological consequences.

Structural basis of c-di-AMP binding to SbtB

To gain deeper insight into the structural basis of c-di-AMP binding by *Sc*SbtB, we aimed to obtain the crystal structure of the *Sc*SbtB:c-di-AMP complex. To this end, we used crystals that we previously obtained in different ligandation states from several cocrystallization trials of *Sc*SbtB (*20*). These crystals contain one *Sc*SbtB trimer in the asymmetric unit in space group $P3_2$, such that the three monomers and the three ligand binding sites, which are situated between the subunits, are involved in different crystal contacts (*20*). We now used apo crystals of this form in soaking experiments with c-di-AMP, resulting in a 2.0 Å crystal structure of the *Sc*SbtB:c-di-AMP complex (Fig. 1, C to F). However, only two of the binding sites turned out to be occupied by c-di-AMP (Fig. 1C), both with clear electron density for c-di-AMP in full occupancy (Fig. 1D). In these two sites,

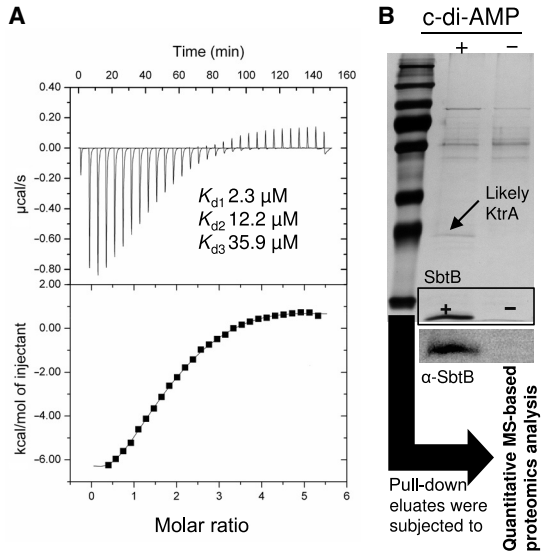

Gene (protein name)	Predicted function	Score	Sequence coverage (%)
slr1513 (SbtB)	PII-like protein; Regulator of HCO_3^- transporter SbtA	128.8	66.4
sll0493 (KtrA)	NAD^+-binding subunit (with RCK_C domain) of K^+ transporter KtrABE	70.3	19.3
slr0415 (NhaS5)	Na^+/H^+ antiporter	43.3	4.0
sll0993 (MthK)	K^+ channel	34.2	10.4
slr1216 (MgtE)	Mg^{2+} transporter (with CBS domain)	32.5	2.2
slr0773 (TrkA)	ATPase subunit (with RCK_C domain) of K^+ ABC transporter TrKAB	28.3	9.3
slr0615	ABC transporter	19.6	1.6
sll0273 (NhaS2)	Na^+/H^+ antiporter	16.8	1.7
sll1581 (gumB)	Sugar ABC transporter; substrate-binding protein	14.7	3.6
sll1730	NUDIX hydrolases	14.3	9
slr1149	ABC transporter	13.5	1.5
sll1618	Hypothetical protein	12.4	8.0
slr1124 (MalK)	Cytoplasmic membrane protein for maltose uptake	12.3	3.7
sll1837	Hypothetical protein	12.2	15.2
slr1470	Hypothetical protein	12.1	6.9
Slr0625 (GltS)	Glutamate:sodium symporter	10.8	2.7
sll0615 (GDT1-like protein)	Sugar-like permease	10.7	6.3

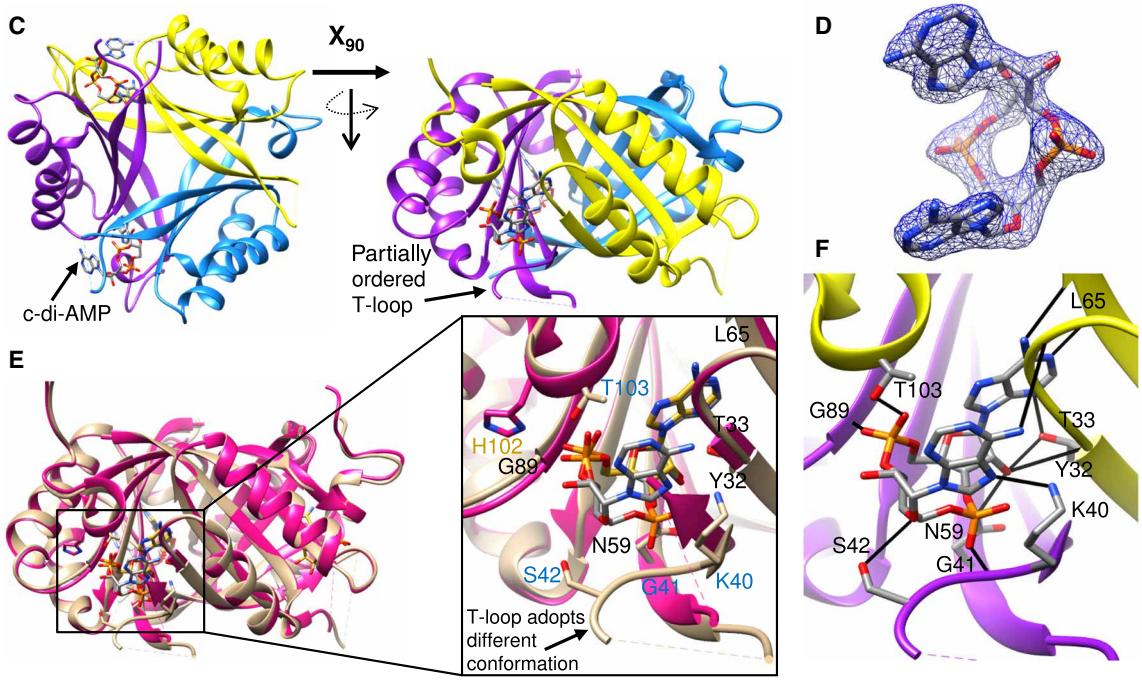

Fig. 1. Identification of SbtB as a major c-di-AMP receptor protein in cyanobacteria. (**A**) ITC analysis shows that SbtB binds c-di-AMP in an anticooperative manner with K_d values as indicated. Top: The raw ITC data in the form of the heat produced during the titration of 33.3 µM SbtB (trimeric concentration) with 0.5 mM c-di-AMP. Bottom: The binding isotherms and the best-fit curves according to the three sequential binding site model. (**B**) SDS–polyacrylamide gel electrophoresis analysis of c-di-AMP pull-down elution fraction and Western blot detection of SbtB, using α-SbtB antibodies. Samples were analyzed with quantitative MS-based proteomics analysis. Identified proteins are sorted by their scores. NAD^+, nicotinamide adenine dinucleotide; ATPase, adenosine triphosphatase; ABC, ATP-binding cassette; NUDIX hydrolases cleave nucleoside diphosphates linked to any ("x") moiety. (**C** to **F**) Structural and binding properties of the *Sc*SbtB protein. (C) Overall architecture of the trimeric SbtB:c-di-AMP complex with nucleotide-binding pockets located in the intersubunit clefts and shown in ribbon representation with different color for each monomer. (D) The electron density of c-di-AMP is shown as an F_o-F_c omit map contoured at 2.5 σ. (E) Superposition of *Sc*SbtB:c-di-AMP (brown) with *Sc*SbtB:AMP (pink; PDB: 5O3R), yielding an root mean square deviation of 0.33 Å and showing that the T-loop in the SbtB:c-di-AMP complex is partially ordered and adopts a different conformation than in the SbtB:AMP structure. (F) Close-up of the c-di-AMP binding site with relevant residues for nucleotide binding shown as sticks, and H bonds indicated by thin lines. (*E*) Inset: Highlighting the superposition of the nucleotide binding sites, with residues specific for c-di-AMP binding labeled in blue and those for AMP in orange.

as compared to the AMP- or cAMP-bound complexes, the base of the T-loop was found in a different conformation (Fig. 1E), forming additional interactions with the ligand (Fig. 1F), while the third site remained in apo-state due to limitations of the crystal packing. To exclude that also the folding of the T-loop or other binding-induced conformational changes were possibly restrained by crystal contacts during the soaking experiment, we also performed cocrystallization trials with c-di-AMP. Unexpectedly, these again yielded the same

crystal form resulting in a dataset of similar resolution, with the same two sites occupied and no noticeable structural differences.

All three subunits of the *Sc*SbtB:c-di-AMP complex are essentially in the same conformation as in the apo-*Sc*SbtB coordinates, and the whole *Sc*SbtB:c-di-AMP complex superimposes with a Cα–root mean square deviation value of 0.26 Å on the apo-*Sc*SbtB trimer [Protein Data Bank (PDB): 5O3P] (fig. S2). While there were no major differences between the *Sc*SbtB:c-di-AMP complex and apo-*Sc*SbtB, a comparison with the AMP- or cAMP-bound complexes revealed several additional unique interactions between c-di-AMP and the base of the T-loop (Fig. 1, E and F, and fig. S2), which caused a partial ordering and restructuring of the loop (Fig. 1, C to F). Structural alteration of the T-loop is a characteristic mechanism by which effector molecules modulate the interaction of canonical PII proteins with their receptors (*25*, *29*). The effect of c-di-AMP binding on the T-loop conformation strengthened the above results on the specificity of c-di-AMP binding to SbtB and suggested that c-di-AMP signaling via SbtB is functionally relevant and affects SbtB interaction with diverse interaction partners.

Physiological role of SbtB as a c-di-AMP receptor protein

Next, to search for a functional link between SbtB as a c-di-AMP receptor protein and c-di-AMP signaling cascade, we aimed to compare the phenotype of a *sbtB*-deficient mutant (encoded by *slr1513*) with a mutant deficient in *dacA*, which encodes for the only identified di-adenylate cyclase A (DacA; encoded by *sll0505*) in *Synechocystis*. To create a c-di-AMP free mutant, we first attempted the generation of a deletion or insertion Δ*dacA* mutant in a glucose-sensitive background (GS-strain). The insertion attempt aimed to avoid a polar effect on the expression of the downstream gene *sll0506* (encoding for undecaprenyl phosphate synthetase), because the *sll0505* gene overlaps with *sll0506* and is predicted to contain a possible promoter region for *sll0506* (*17*). However, we only achieved partial segregation by both attempts (fig. S3). In contrast, complete segregation was obtained in the background of glucose-tolerant *Synechocystis* strain (GT-strain), as revealed by the absence of the wild-type (WT) gene fragment through polymerase chain reaction (PCR) amplification (fig. S3). This implies that DacA is not essential for the viability of the GT-*Synechocystis* under standard, glucose-free conditions but it is, for unknown reasons, essential for the lifestyle of GS-*Synechocystis*. Unless mentioned otherwise, the following results were generated using the fully segregated Δ*dacA* insertion mutant in GT-*Synechocystis* background. However, we were able to reproduce all these results using the Δ*dacA* deletion mutant in GT-*Synechocystis* as well.

Measurements of the intracellular c-di-AMP concentration confirmed that the completely segregated Δ*dacA* mutant was free of c-di-AMP, while the WT cells contained around 4.6 μmol per cell of c-di-AMP under photoautotrophic growth conditions (Fig. 2A). To further confirm that *dacA* gene (*sll0505*) encodes an active di-adenylate cyclase able to synthesize c-di-AMP, *Escherichia coli*, which does not synthesize c-di-AMP naturally, was transformed with a plasmid expressing a *sll0505*–green fluorescent protein (GFP) fusion protein under the control of the isopropyl-β-D-thiogalactopyranoside (IPTG)–inducible T7 promoter. High concentration of c-di-AMP was detected in *E. coli* cells upon induction as compared to un-induced cells (fig. S3), confirming the annotation of DacA.

In cyanobacteria, c-di-AMP signaling was previously linked to osmoregulation, to the resuscitation from long-term chlorosis under nitrogen starvation condition, and to day-night rhythms (*11*, *17*, *19*), whereas SbtB was shown to be important for C_i acclimation (*20*). It was therefore obvious to assume that c-di-AMP perception by SbtB could be involved in one or more of those c-di-AMP–linked processes by comparing the phenotypes of the mutants Δ*dacA* and Δ*sbtB* under different growth conditions.

First, *Synechocystis* WT, Δ*dacA*, and Δ*sbtB* mutants were subjected to osmotic stress by treating them with increasing concentrations of sorbitol (50 to 600 mM) (fig. S4). In agreement with a previous study (*17*), the growth of Δ*dacA* was strongly impaired in the presence of high osmolyte concentrations, with 300 mM sorbitol completely preventing growth. By contrast, the Δ*sbtB* mutant was not affected by osmotic stress (fig. S4), implying that c-di-AMP sensing by SbtB is not involved in osmoregulation. This clear phenotype of Δ*dacA* supports the notion that c-di-AMP has a key role in osmoregulation and maintenance of the intracellular turgor pressure within cyanobacteria. Moreover, this phenotype agrees with the identification of several ion and osmolyte transporters in the c-di-AMP pull-down experiment, including those for K^+, Na^+, and Mg^{2+} ions, glutamate, and maltose (Fig. 1B).

Second, the recovery from nitrogen starvation–induced chlorosis of the mutant strains was tested by resupplementation with a nitrogen source. The Δ*dacA* mutant was neither able to properly enter chlorosis nor to recover from chlorosis nearly as efficiently as the WT cells, which is consistent with high expression of the *dacA* gene under resuscitation conditions (fig. S5) (*19*). In contrast, the Δ*sbtB* mutant did not show any phenotypic difference to WT during these treatments (fig. S5). This suggests that SbtB is not required for entering and exiting from chlorosis, whereas c-di-AMP plays an important role in this process perhaps due to interaction with as yet unknown receptor protein.

Third, we wanted to test whether c-di-AMP might be involved in primary C_i acquisition, because our previous study revealed that Δ*sbtB* is impaired in proper C_i acclimation (*20*). Therefore, the photosynthetic HCO_3^--dependent oxygen evolution of the Δ*dacA* mutant was compared to WT in high C_i (HC)– and low C_i (LC)–acclimated cells (Fig. 2B and fig. S6). Both WT and Δ*dacA* cells showed the expected acclimation to HC conditions by lowering affinity for HCO_3^- as estimated by an increase of HCO_3^- K_m to about 300 μM (Fig. 2B). Under LC conditions, the affinity toward HCO_3^- increased markedly in both Δ*dacA* mutant and WT cells (Fig. 2B). Although the initial rise of the photosynthetic activity at low C_i concentrations was similar, the maximal photosynthetic rates (V_{max}) in the Δ*dacA* mutant was lower than in WT cells under LC-acclimated condition. The decreased V_{max} indicates a lower activity of the Calvin-Benson cycle (fig. S6), at saturating C_i amounts. Despite this difference, this experiment indicated that, in contrast to the Δ*sbtB* mutant, operation of the CCM was not affected in the Δ*dacA* mutant (*20*).

Last, we investigated the involvement of DacA and SbtB in diurnal growth by exposing the cells to 12-hour light/12-hour dark cycles. Similar to *S. elongatus* (*11*), the *Synechocystis* Δ*dacA* mutant showed a strong growth defect under day-night conditions (Fig. 2, C and D, and fig. S7). Unexpectedly, the Δ*sbtB* mutant showed a similar diurnal growth impairment (Fig. 2, C and D, and fig. S7). SbtB is known to regulate the HCO_3^- transporter SbtA through direct protein-protein interaction in response to the energy state of the cell and the second messenger cAMP (*20*, *22*, *23*, *27*), raising several questions of either an involvement of SbtA or cAMP in impaired

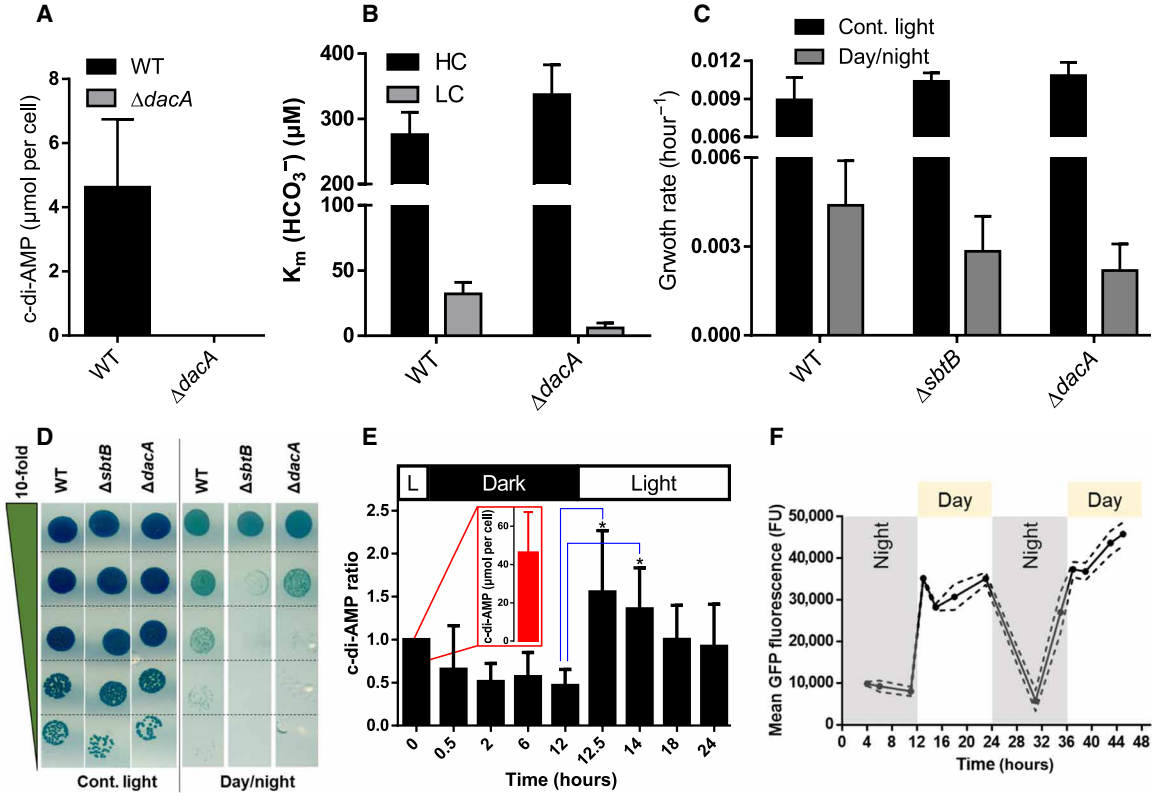

Fig. 2. Physiological characterization of Δ*sbtB* and Δ*dacA* mutants. (**A**) c-di-AMP concentration shown in μmol per cell within vegetative photoautotrophic growing *Synechocystis* sp. PCC 6803 WT (black bar) and the di-adenylate cyclase deficient mutant Δ*dacA* (gray bar; undetectable). (**B**) Bicarbonate affinity represented by the K_m (HCO_3^-) values of *Synechocystis* WT and the Δ*dacA* mutant under either high carbon (HC; black bars) or low carbon (LC; gray bars) regimes. (**C**) Specific growth rate of *Synechocystis* WT, Δ*sbtB*, and Δ*dacA* cells under either continuous light (black bars) or a 12-hour diurnal rhythm (gray bars). (**D**) Growth test by drop plate assay of *Synechocystis* WT, Δ*sbtB*, and Δ*dacA* cells as indicated under either continuous light (left) or a 12-hour diurnal rhythm (right). Cells were normalized to an optical density at 750 nm (OD_{750}) of 1.0 and serial diluted in 10-fold steps (top to bottom; depicted by a green triangle). (**E**) Relative c-di-AMP concentration within *Synechocystis* WT cells throughout a 12-hour diurnal rhythm. Statistically significant differences ($P < 0.05$) are indicated by asterisk (*) for the transition from the end of the night phase (12 hours) to early day-phase (12.5 and 14 hours). Values are means ± SD; $n = 5$ to 6 independent measurements. The c-di-AMP was not detectable within Δ*dacA* cells. The *x* axis shows the time in hours; the *y* axis shows the relative amount of c-di-AMP normalized to the first time point at the end of the day phase (indicated by 0.0 hours). (E) Inset: c-di-AMP concentration shown in micromoles per cell for the first measurable time point (0.0 hours). (**F**) Mean of in vivo SbtB-sfGFP expression throughout a 12-hour diurnal rhythm, as indicated. The *x* axis shows the time in hours; the *y* axis shows the mean GFP fluorescence in fluorescence units (FU).

diurnal growth. However, the Δ*sbtA* and Δ*cya1* (encodes for the major cAMP cyclase in *Synechocystis*) mutants grew almost like WT cells under 13 successive day-night cycles (fig. S7D). Together, these results indicated that the common growth defect of the Δ*sbtB* and Δ*dacA* mutants under diurnal cycles (Fig. 2, C and D) was not mediated by neither cAMP nor by a defect in primary C_i acquisition via SbtA (Figs. 2B and figs. S6 and S7). Rather, it pointed toward a specific/unidentified c-di-AMP–controlled process, involving signal perception by SbtB.

Diurnal cycling of c-di-AMP correlates with SbtB

To gain insight into the mechanism that makes c-di-AMP and SbtB indispensable for diurnal growth, we first looked for *sbtB* (*slr1513*) and *dacA* (*sll0505*) expression in the transcriptome dataset of diurnally grown *Synechocystis* cells (*30*). Both *sbtB* and *dacA* transcripts showed a diurnal dynamic, with a sharp increase at the beginning of the day and a decline in the dark phase (fig. S8). To reveal whether the changes in *dacA* transcript levels correlated with the c-di-AMP levels, the intracellular concentration of c-di-AMP was determined in WT *Synechocystis* cells under diurnal growth at different time points during day-night cycles. The first sampling point was taken at the end of the light phase, and four samples were taken during the following 12 hours of dark phase and four samples in the following 12 hours of light phase (Fig. 2E). While the c-di-AMP concentration dropped during the dark period, a rapid two to fourfold increase in c-di-AMP concentration was observed 30 min after onset of light (Fig. 2E). The maximum c-di-AMP concentration was reached in the early light phase and then declined throughout the remaining light phase (Fig. 2E), correlating well with the expression pattern of *dacA* (fig. S8). Because SbtB is known to bind the second messenger cAMP as well and to further exclude any possible role for cAMP in day-night metabolism (fig. S7E), we checked for intracellular concentration of cAMP under the same cycling condition in the WT and Δ*dacA* cells. The intracellular concentration of cAMP did not change markedly between day-night cycle within both of WT and Δ*dacA* cells (fig. S8C), which further supports the specificity of c-di-AMP in regulating *Synechocystis* diurnal metabolism. Moreover, we monitored SbtB expression using as a reporter the fluorescently

labeled fusion protein SbtB–super-folded GFP (sfGFP) (*20*). The SbtB-sfGFP fluorescence showed the same cycling pattern as the c-di-AMP concentration, dropping during the dark phase and peaking during the day (Fig. 2F). Last, to examine whether there might be a regulatory connection between *sbtB* and *dacA* at the level of transcription, we checked for the expression profile of *sbtB* (*slr1513*) in Δ*dacA* and for *dacA* (*sll0505*) in Δ*sbtB* mutant in comparison to WT cells using microarray technology (fig. S8, D and E). The *sbtB* mutation had negligible effect on the expression of *dacA*, while the *dacA* mutation led to partial down-regulation of *sbtB*, which could explain the inability of *dacA* mutant to fully activate the Calvin-Benson cycle (fig. S6), consistent with the proposed role for SbtB in regulating the entire CCM (*20*). Notably, the expression of the genes situated upstream (*sll0504*) and downstream (*sll0506*) of *dacA* was similar in both the Δ*dacA* and Δ*sbtB* mutants and very close to that of the WT cells, which confirmed that *dacA* mutation has no polar effects on the transcription of neighboring genes.

SbtB regulates glycogen metabolism via interaction with the glycogen-branching enzyme GlgB

Because the proteins of the PII superfamily, to which SbtB belongs, are known to exert their regulatory functions via direct protein-protein interaction (*29*), we hypothesized that SbtB binds to yet unknown target(s) in a c-di-AMP–dependent manner, thereby affecting diurnal growth.

To identify potential SbtB interaction partners, we characterized the global SbtB interactome using several mass spectrometry-based pull-down approaches and screened for hits that could be involved in day-night acclimation. First, coimmunoprecipitation (CoIP) experiments were performed with WT *Synechocystis* crude cell extracts using α-SbtB–specific antibodies. As negative control, we used crude cell extracts from Δ*sbtB* cells. Compared to the negative control, the immunoprecipitate contained five to ninefold enriched enzymes related to glycogen metabolism (fig. S9A). In particular, we identified glycogen synthase (GlgA2, *sll1393*), glycogen phosphorylase (GlgP2, *slr1367*), glycogen-branching enzyme (GlgB, *sll0158*), and glycogen-debranching enzyme (GlgX1, *slr0237*) as potential SbtB interacting partners. Because glycogen metabolism is of primary importance for day-night acclimation in cyanobacteria (*3*, *8*), the observed enrichment of glycogen metabolic enzymes would fit into the proposed c-di-AMP–related function of SbtB in diurnal growth.

To further elucidate c-di-AMP–dependent SbtB interactions, we performed several pull-down assays by immobilizing recombinant C-terminal His_8- or strep-tagged *Sc*SbtB protein on Ni^{2+} magnetic beads or streptavidin magnetic beads, respectively, and incubating them with *Synechocystis* crude cell extracts either in the presence or absence of c-di-AMP, followed by successive washes to remove the unbound proteins. In several pull-down experiments, the known SbtB-target SbtA was identified, which validated the procedure. With the His_8-tagged *Sc*SbtB protein on Ni^{2+} magnetic beads, in addition to SbtA, we identified again GlgA2, GlgP2, GlgB, GlgX, and furthermore the second glycogen-debranching enzyme (GlgX2, *slr1857*) and glucose-1-phosphate adenylyltransferase (GlgC, *slr1176*). Notably, GlgB and GlgA2 were more than 20-fold enriched in the presence of c-di-AMP (fig. S9B), implying that they could be of particular importance. When strep-tagged *Sc*SbtB protein was used as affinity bait, a cleaner pull-down with a low background due to higher specificity of streptavidin beads was obtained. Using this attempt, only the glycogen-branching enzyme GlgB was enriched as specific interaction partner (Fig. 3A and fig. S9, C and D). In the presence of c-di-AMP, GlgB was 14 times more abundant as compared to the pull-down in the absence of effector molecules (Fig. 3A). This enrichment was specific for c-di-AMP and not observed in the presence of cAMP (fig. S9, C and D). GlgB was not identified in the negative control (empty streptavidin beads) as well.

To further validate the specificity of SbtB-GlgB interaction and examine possible interactions with other glycogen-related enzymes by an independent method, we carried out interaction assays using the bacterial adenylate cyclase two-hybrid (BACTH) system. The BACTH system relies on the reconstitution of a functional adenylate cyclase (Cya) upon positive interaction of the proteins of interest fused to the T25 and T18 subunits of Cya, which can be detected by color change on X-Gal reporter plates. Here, we fused the T25 subunit of Cya N-terminally to SbtB, while the T18 subunit of Cya was fused either N- or C-terminally to the glycogen-related enzymes GlgA1, GlgA2, GlgP1, GlgP2, GlgB, and GlgC (fig. S10). The T25-SbtB fusion with an empty pUT18 vector was used as negative control, while the leucine zipper interaction was used as positive control. A clear interaction was observed only between T25-SbtB and GlgB N-terminally tagged with a T18 subunit (Fig. 3B), whereas no interaction was obtained with C-terminally tagged GlgB and the other glycogen metabolic enzymes (fig. S10). This result strongly indicated that SbtB is a specific interactor of GlgB.

To gain further insights into SbtB-GlgB complex formation, we studied the SbtB-GlgB interaction using microscale thermophoresis (MST). We titrated SbtB against labeled GlgB in the presence or absence of c-di-AMP. SbtB was able to bind GlgB with a K_d of 0.22 ± 0.07 μM (Fig. 3C); however, the presence of c-di-AMP (100 μM) did not change the binding constant markedly (K_d of 0.43 ± 0.10 μM).

Molecular basis for diurnal, c-di-AMP–dependent control of GlgB by SbtB

The photosynthetic synthesis of glycogen as carbohydrate reserve during the day is crucial for cyanobacterial survival in the night (*3*, *7*, *31*). To confirm the involvement of GlgB in this process, we tested diurnal growth of a Δ*glgB* mutant. The Δ*glgB* mutant was impaired in diurnal growth in a similar manner to the Δ*sbtB* and Δ*dacA* mutants (Fig. 3D), confirming the importance of glycogen metabolism and GlgB in diurnal growth. To obtain further evidence of a functional link between SbtB and the regulation of glycogen metabolism via GlgB in a c-di-AMP–dependent manner, we determined the intracellular glycogen concentration at the mid of the day phase. As compared to *Synechocystis* WT cells, glycogen levels were significantly reduced in all three mutants (Δ*sbtB*, Δ*dacA*, and Δ*glgB*) (Fig. 3E), with Δ*dacA* showing the lowest amount of glycogen with about 14.7%, Δ*sbtB* with 28.2%, and Δ*glgB* with 26.7% (Fig. 3E). Complementation of Δ*sbtB* by introducing copy of *slr1513* under the control of the *psbA2* promoter restored the growth of the mutant under day-night rhythm and restored the glycogen content to the levels of WT cells (fig. S11, A and B). Moreover, addition of glucose to BG_{11} medium rescued the diurnal growth defect of Δ*sbtB* (fig. S11C).

Because glycogen catabolism is the major source for respiration in the dark, supporting a heterotrophic mode of metabolism (*32*), we measured oxygen evolution and respiration during three successive day-night cycles. During the day, both Δ*sbtB* and Δ*dacA* mutants showed 50% less oxygen evolution than WT cells (Fig. 3F), in agreement with the inability of both mutants to fully activate the

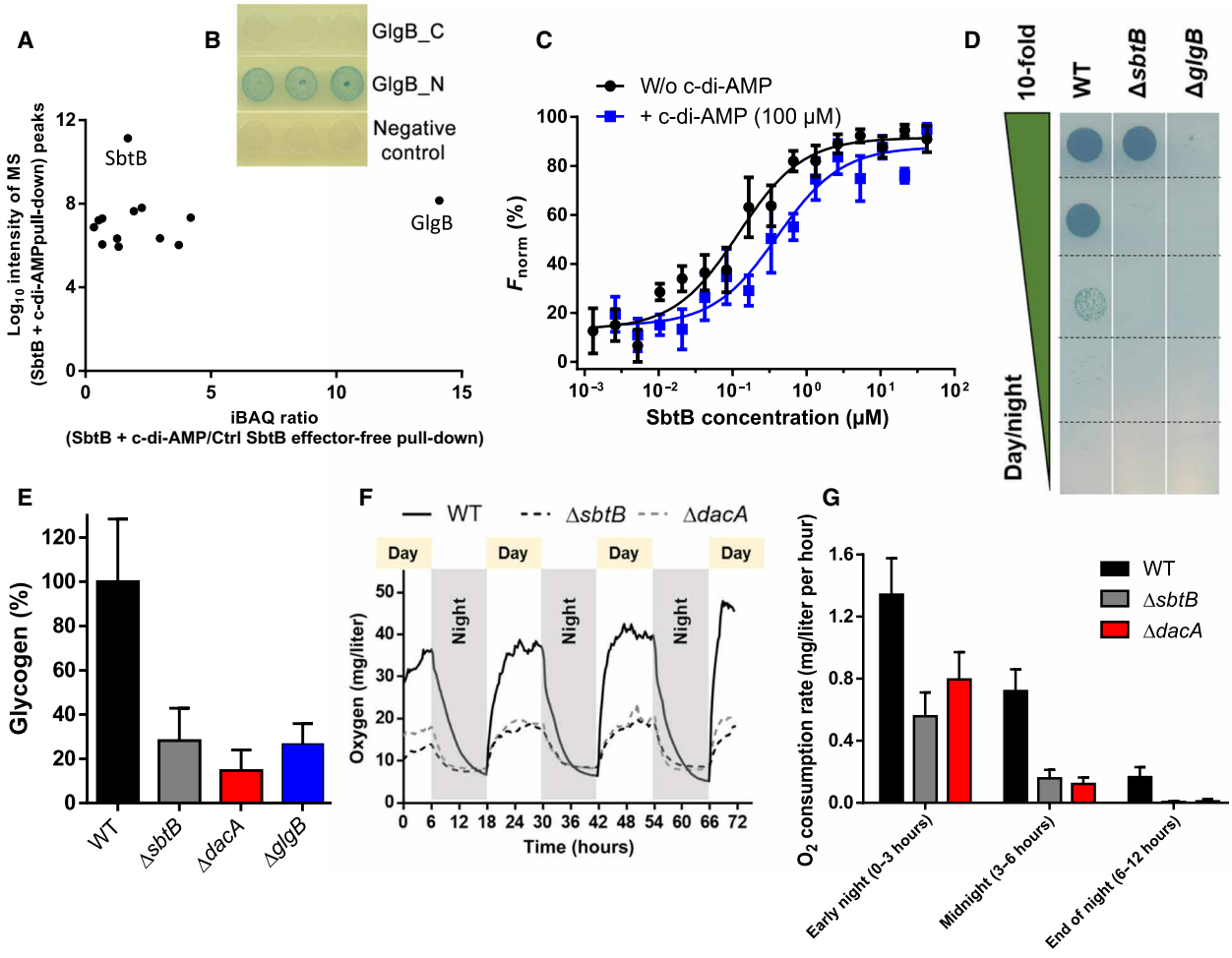

Fig. 3. Regulation of glycogen metabolism via c-di-AMP dependent SbtB signaling. (**A**) Streptavidin magnetic bead-based pull-downs using strep-tagged *Sc*SbtB protein in the absence or presence of c-di-AMP. The c-di-AMP enriched SbtB-GlgB interaction. (**B**) BACTH assay was performed using *E. coli* cells expressing T25-SbtB fusion together with either C-terminal (GlgB_C) or N-terminal (GlgB_N) T18-GlgB fusion, or empty Cya-T18 (negative control). SbtB-GlgB interaction is evidenced by appearance of a blue color on X-Gal reporter plates (middle). (**C**) MST analysis of the SbtB-GlgB interaction in either presence (blue line) or absence (black line) of 100 µM c-di-AMP, as indicated. The *y* axis shows the relative, normalized fluorescence units. (**D**) Growth test by drop plate assay of *Synechocystis* WT, Δ*sbtB*, and Δ*glgB* cells, as indicated in a 12-hour diurnal rhythm. Cells were normalized to an OD_{750} of 1.0 and serial diluted in 10-fold steps (up to down). (**E**) Relative glycogen levels of *Synechocystis* WT (black bar), Δ*sbtB* (gray bar), Δ*dacA* (red bar), and Δ*glgB* (blue bar) cells in the midday of a 12-hour diurnal rhythm. The glycogen content was normalized to 100% of WT cells. (**F**) Photosynthetic oxygen production and respiration of *Synechocystis* WT (black line) in comparison to Δ*sbtB* (black, dashed line) and Δ*dacA* (gray, dashed line) throughout a 12-hour diurnal rhythm for 72 hours, as indicated. The *y* axis shows the oxygen levels in parts per million (milligrams per liter). (**G**) Oxygen consumption rates in milligrams per liter per hour based on the data from (F). Oxygen consumption rates for WT (black bars), Δ*sbtB* (gray bars), and Δ*dacA* (red bars) were calculated for the early night (first 3 hours), midnight (next 3 to 6 hours), and the end of the night (last 6 to 12 hours).

Calvin-Benson cycle (fig. S6) (*20*). Upon onset of darkness, all strains started respiration, with WT cells displaying approximately twofold higher oxygen consumption than the mutants. Whereas WT cells kept on the respiration process for the whole night (12 hours), the Δ*sbtB* and Δ*dacA* cells ceased respiration after 6 hours (fig. 3FG). This result suggests that both mutants were unable to maintain respiration throughout a 12-hour night period and, therefore, were impaired in diurnal growth. To confirm this assumption, we determined the viability of the mutants compared to the WT cells during a prolonged dark incubation for 5 days. As revealed by drop plate assay, both mutants showed a marked loss of viability after 2 days of darkness. After 5 days of darkness, Δ*sbtB* cells were completely unviable (fig. S11D). Moreover, all strains retained a comparable efficiency of photosystem II (PSII) and photosynthetic pigmentations over 3 days of darkness, implying that the loss of viability of the mutants was not due to an alteration in the photosynthetic machinery (fig. S11, E and F). Again, all of those results indicate that the low glycogen levels in both mutants are the main cause of the growth defect under the day-night rhythm. However, it should be mentioned that Δ*dacA* cells showed about 25% reduction of apparent PSII quantum yield [determined by pulse-amplitude modulation (PAM) fluorescence] in the absence of actinic light as compared to WT cells (fig. S11E).

DISCUSSION

Here, we revealed that the PII-like signaling protein SbtB binds the second messenger c-di-AMP in addition to the standard adenine

nucleotides (AMP, ADP, and ATP) and to the carbon status reporting second messenger nucleotide cAMP. To our knowledge, this is the first signaling protein known to interact with both cAMP and c-di-AMP. This highlights the central role of SbtB as a switch point in cyanobacterial cell physiology, integrating not only signals from the energy state and carbon supply through adenine nucleotide and cAMP binding (*20*, *23*, *27*), respectively, but also from the diurnal state by binding to c-di-AMP. We were able to confirm the ability of SbtB to bind c-di-AMP from two distinct cyanobacterial species of unicellular *Synechocystis* sp. PCC 6803 and filamentous filamentous *Nostoc* sp. PCC 7120, which emphasizes a general role for c-di-AMP signaling via SbtB. In Gram-positive bacteria, c-di-AMP synthesis is related to cell wall homeostasis, potassium homeostasis, and osmotic control (*12*–*14*). Previous data indicated that, in cyanobacteria too, c-di-AMP might also control osmoregulation (*17*), which we were able to confirm in our study as well (Fig. 1B). We linked the c-di-AMP signaling with cyanobacterial osmoregulation by identifying several c-di-AMP target transporters in the c-di-AMP–dependent pull-down experiment, including transporters for K^+, Na^+, and Mg^{2+} ions, glutamate, and maltose. Furthermore, a link between c-di-AMP and nighttime survival was reported in *S. elongatus* as suggested by loss of viability of the Δ*dacA* mutant under dark conditions by a cryptic mechanism (*11*). Here, we revealed the exact mechanism by which c-di-AMP contributes to the regulation of the day-night rhythm in cyanobacteria.

Our data indicate that binding of c-di-AMP to SbtB modulates the interaction of SbtB with enzymes of glycogen synthesis, particularly with the glycogen-branching enzyme GlgB (Fig. 4), which we were able to confirm by different independent methods. In the *sbtB*-deficient mutant, the accumulation of glycogen during daytime is severely diminished and to a similar degree in the Δ*dacA* or Δ*glgB* mutants, which are unable to synthesize c-di-AMP or branched glycogen, respectively. Further support for a correlation between c-di-AMP concentration and glycogen synthesis comes from the diurnal cycling of c-di-AMP concentration, high during the day, when glycogen is synthesized, and low in the night, when glycogen is consumed. In *Synechocystis*, the daily c-di-AMP cycling levels correlate well with the expression of the diadenylate cyclase-encoding gene *sll0505* (*dacA*) under day-night cycles. In agreement, the SbtB-encoding gene *slr1513* was found to follow the same expression pattern as *sll0505* (*30*). Furthermore, the interaction between SbtB and GlgB was enriched in the presence of c-di-AMP, at least in the in vivo pull-down experiments; however, such influence was not observed using the recombinant purified proteins from *E. coli* in the in vitro MST experiment. The reason for that is presently ambiguous, but one possibility is that other components in the *Synechocystis* crude extract contribute to enhancing the affinity of SbtB for GlgB, perhaps other components of the glycogen metabolic enzymes, such as GlgA2 and/or GlgP2. Of note, GlgA2 and GlgP2 were enriched in the CoIP and His-tag SbtB pull-downs; however,

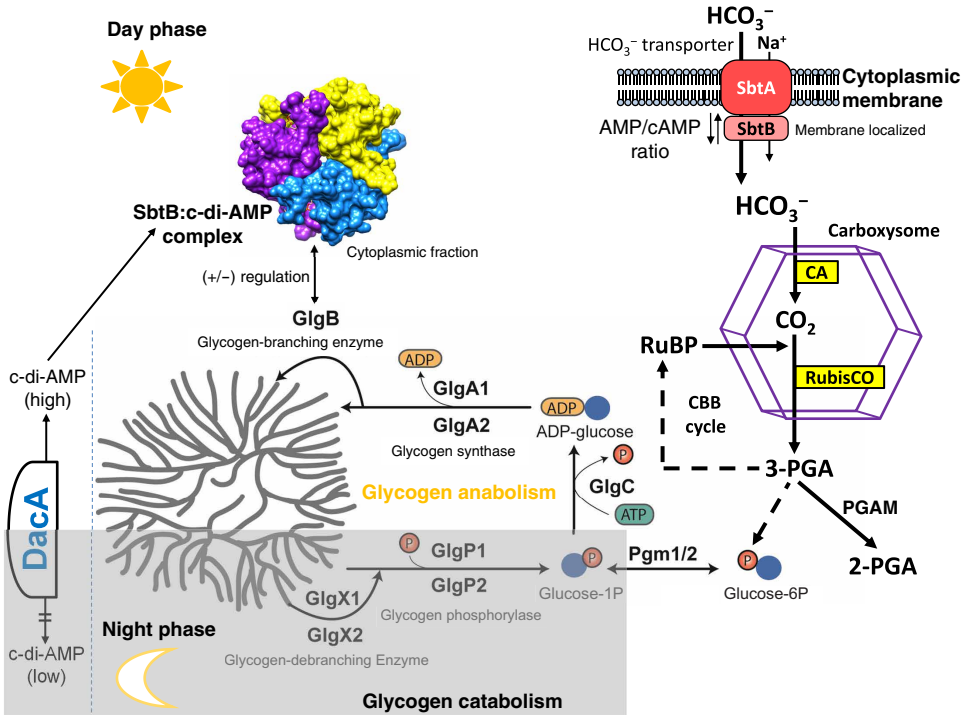

Fig. 4. Model of regulation of day-night switch of glycogen metabolism via c-di-AMP sensing by SbtB. During the day, cyanobacteria use an active carbon concentrating mechanism, which composes of several C_i uptake systems (among them the HCO_3^- transporter SbtA), and the carboxysome, where HCO_3^- is dehydrated to CO_2 by carbonic anhydrase (CA) and then CO_2 fixation occurs by RubisCO. Via the activity of Calvin-Benson (CBB) cycle, a part of the newly fixed carbon is redirected toward synthesis of carbon storage compound (glycogen). Simultaneously, the concentration of the second messenger nucleotide c-di-AMP increases in the day due to di-adenylate cyclase (DacA) activity. The soluble fraction of SbtB protein, not sequestered by SbtA, interacts with c-di-AMP and promotes glycogen synthesis by interacting with the glycogen-branching enzyme GlgB. After nightfall, c-di-AMP concentration decreases, and the catabolism of glycogen, which produced in the day, is the resource for nighttime survival.

we were not able to confirm such interaction with BACTH, implying that they could be indirectly involved in modulating SbtB-GlgB interaction. Nevertheless, a genome-wide fitness assessment of *S. elongatus* revealed that mutations in genes encoding for GlgB (*Synpcc7942_1085*) and SbtB (*Synpcc7942_1476*) and, to a less extent, for DacA (*Synpcc7942_0263*) cause a strong decrease in the bacterium fitness under diurnal rhythms (*3*) but not for SbtA (*Synpcc7942_1475*) or the putative cAMP synthases (*Synpcc7942_2195* or *Synpcc7942_0663*), which further support the specificity notion of SbtB and c-di-AMP signaling for the fitness of cyanobacterial diurnal metabolism.

However, c-di-AMP concentration oscillated in the opposite direction in *S. elongatus*, with high concentration in the night and low concentration during the day (*11*). The reasons for the discrepancy are now unclear, although both strains show a clear phenotypic defect under diurnal rhythm in the absence of the c-di-AMP cyclase, confirming the essentiality of c-di-AMP for cyanobacterial growth under day-night rhythm. It is known that *S. elongatus* uses a precisely operating circadian clock machinery to tune metabolism in a diurnal manner (*1*, *3*, *8*). Although components of this clock are conserved in *Synechocystis*, the overall process appears to be distinct owing to the emergence of multiple paralogs of the oscillator proteins (*6*, *33*). However, to comprehensively understand the control of the diurnal cycling of SbtB and c-di-AMP concentration, detailed analysis of the clock influence on SbtB and on c-di-AMP specific cyclase and phosphodiesterase activities is required. Notably, *sbtB* expression was strongly deregulated in the mutant of the circadian clock output regulator RpaA (*6*), which cannot survive the day-night rhythm as well (*8*).

In contrast to Δ*sbtB* (Fig. 3E), the Δ*rpaA* mutant is not impaired in glycogen synthesis during daytime (*8*, *34*). In this case, the inability of Δ*rpaA* to grow under day-night regime is due to the failure of this mutant to activate, in the night, carbon catabolic genes, including components of the OPP pathway, glycolysis, and glycogen degradation via GlgP (*1*, *6*, *8*, *34*). Apparently, SbtB and RpaA are working in opposite directions on glycogen anabolism and catabolism, respectively. Nevertheless, it appears that RpaA is involved in regulation of *sbtB*-gene expression in the day phase by yet unknown mechanism (*6*).

In addition to a role in regulating glycogen synthesis, c-di-AMP appears to regulate numerous ion transporters and osmotic responses, as deduced from the identification of several K^+ transporters, including KtrA (*sll0493*), TrkA (*slr0773*), and MthK (*sll0993*) as c-di-AMP targets. This highlights a conserved role for c-di-AMP in controlling osmotic homeostasis and K^+ transport (*12*–*14*), which is of particular importance, since K^+ is the major inorganic cation in the cytoplasm, acting as counter-ion of glutamate. In agreement with our identification of KtrA as a potential c-di-AMP target, the Na^+-dependent K^+ uptake system KtrABE was previously shown to be required for regulation of cell turgor and the adaptation to hyperosmotic stress elicited by either sorbitol or NaCl (*35*, *36*). However, osmotic control by c-di-AMP appears to act independently of SbtB, because the Δ*sbtB* mutant was not impaired in its responses to osmotic stress conditions like Δ*dacA* (fig. S4). Moreover, it seems also that the Mg^{2+} transporter MgtE is a conserved c-di-AMP target among different bacterial phyla (*12*, *14*, *28*). Of note, Mg^{2+} is of particular importance for the photosynthetic lifestyle of cyanobacteria as it is the central ion in the chlorophylls and required for the maintenance of the thylakoid membranes (*37*).

Cross-talk between second messenger nucleotides is perhaps a more common phenomenon than so far realized. Recently, it was found that the second messengers c-di-GMP and (p)ppGpp reciprocally control *Caulobacter crescentus* growth by competitive binding to a metabolic switch protein, SmbA (*38*). With this in mind, SbtB might play a similar role in cyanobacterial physiology. As is typical for signaling proteins of the PII family (*29*, *39*), SbtB seems to simultaneously perform multiple tasks in controlling cyanobacterial carbon metabolism: controlling bicarbonate uptake via SbtA interaction in response to cAMP and energy state of the cell (*20*, *22*, *23*, *27*) and controlling glycogen synthesis via interaction with glycogen-branching enzyme GlgB in response to c-di-AMP. Accordingly, SbtB would link the control of glycogen synthesis to bicarbonate availability. Under low carbon conditions, SbtB was preferentially found associated to the membrane fraction, presumably due to binding to SbtA (*20*, *23*). Thereby, less SbtB would be available for activation of glycogen synthesis, which takes place in the cytoplasmic space. More SbtB would become available under elevated C_i conditions, when SbtB is enriched in the soluble fraction (*20*). This hypothesis agrees with the fact that the glycogen levels in cells grown under atmospheric CO_2 concentration are low but increase at elevated C_i conditions (*40*, *41*). But, apparently, SbtB integrates the cellular information of both second messengers c-di-AMP and cAMP independently of each other, in agreement with distinct phenotype of Δ*dacA* and Δ*cya1* mutants (fig. S7). Whereas, cAMP acts as an indicator for cellular carbon status (*20*, *26*) and c-di-AMP is a specific indicator of day-night transition (Fig. 2E), and possibly they compete for SbtB available sites. The fact that c-di-AMP binding to SbtB affects the conformation of the T-loop is in perfect agreement with this scenario. The T-loop represents the major protein-interaction motif of PII signaling proteins (*39*). In complex with c-di-AMP, we have found the T-loop in a new conformation that is distinct from the cAMP or linear adenine nucleotide complex forms (Fig. 1E and fig. S2), a conformation that is seemingly driving the interaction with the newly identified GlgB and possibly yet to be identified receptors. The precise structural and regulatory mechanisms of these interactions, especially between SbtB:c-di-AMP and GlgB, await further biochemical and structural elucidation.

MATERIALS AND METHODS

Generation and purification of recombinant proteins

All the plasmids and primers used in this study are listed in (table S1). The recombinant C-terminal StrepII-tagged *Sc*SbtB was expressed and purified as previously described (*20*). Recombinant C-terminal StrepII-tagged SbtB protein from the filamentous *NsSbtB* was constructed as described in (*20*) using the primer pairs compatible for *Ns*SbtB. For generation of recombinant C-terminal His_8-tagged *Sc*SbtB, the SbtB encoding gene *slr1513* was amplified from *Synechocystis* sp. PCC 6803 and inserted via Gibson cloning in linearized pET28a vector. For generation of recombinant N-terminal His_6-tagged GlgB, the GlgB encoding gene *sll0158* was amplified from *Synechocystis* sp. PCC 6803 and inserted via Gibson cloning in linearized pET15b vector. The recombinant StrepII-tagged proteins were purified as previously described (*20*, *24*), while the His-tagged proteins were purified as described previously (*24*, *42*). For the recombinant C-terminal GFP-tagged DacA, which was used for quantification of c-di-AMP in *E. coli*, the DacA encoding gene

sll0505 was amplified from *Synechocystis* sp. PCC 6803 and inserted via Gibson cloning in linearized pET28a-eGFP–based vector.

Crystallization, crystal handling, data collection, and structure elucidation

For soaking experiments, crystals of the trigonal apo crystal form were reproduced as described previously (*20*). These crystals were grown with a reservoir solution composed of 0.1 M phosphate-citrate (pH 4.2) and 40% (w/v) polyethylene glycol (PEG) 300 and were soaked in a droplet of reservoir solution supplemented with 0.33 mM c-di-AMP (cyclic di-3′,5′-adenylate sodium salt; catalog no. C088, BioLoG, Germany) for 4 hours. For cocrystallization, 2.5 mM c-di-AMP was added to the protein solution, and crystallization trials were performed as described (*20*). Cocrystals were grown with a reservoir solution of 0.1 M tris-sodium citrate (pH 5.6), 10% (w/v) PEG 4000, and 10% (w/v) isopropanol, and 20% PEG 400 was used for cryo-protection. All crystals were flash-cooled in liquid nitrogen, and diffraction data were collected at 100 K on a PILATUS 6M-F detector at beamline X10SA of the Swiss Light Source (PSI, Villigen, Switzerland). All data were indexed, integrated, and scaled using the XDS software package (*43*). The structures were solved using difference Fourier methods based on the trigonal apo-*Sc*SbtB structure (PDB: 5O3P). After initial rigid body refinement with REFMAC5 (*44*), it became apparent that the cocrystal structure was essentially identical to the costructure obtained by soaking and not regarded further. The structure of the *Sc*SbtB:c-di-AMP complex was rebuilt and completed by cyclic manual modeling with Coot program and refinement with REFMAC5 based on the data obtained from the soaking experiment. Data collection and refinement statistics are shown in (table S2). Structural representations were prepared using UCSF Chimera.

Generation of mutants

The nonmotile unicellular, freshwater cyanobacterium *Synechocystis sp*. PCC 6803 (glucose-tolerant Tübingen substrain; called here GT-strain) was used as a reference WT strain in this study. Our laboratory "Tübingen" substrain of the glucose-tolerant WT *Synechocystis sp*. PCC 6803 is originally derived from the parental strain *Synechocystis sp*. PCC-M (*45*). While the glucose-sensitive strain of *Synechocystis* sp. PCC 6803 (called here GS-strain) was obtained from Rostock cyanobacterial culture collection and adapted to grow under our standard cultivation conditions in Tübingen for almost 14 years. All constructs used in this study were generated via Gibson assembly, unless specified otherwise. All knockout mutants were generated with homolog recombination using the natural competence of *Synechocystis* sp. PCC 6803, as described previously (*20*). All plasmids and primers used in this study are listed in (table S1).

For generation of knockout deletion mutants in either GT-strain or GS-strain, the mutants were constructed by deleting the ORFs *slr1513*, *sll0505*, and *sll0158* (designated *sbtB*, *dacA*, and *glgB*, respectively) and replaced with the erythromycin, spectinomycin, and chloramphenicol resistance cassette, respectively. The cAMP-free mutant was created by knocking out *slr1991* (designated Δ*cya1*), which encodes the soluble adenylyl cyclase in *Synechocystis sp*., as described previously (*20*). For the generation of the *sbtA* knockout mutant, the *sbtA* upstream sequence was obtained using the primer combination SbtAB_Apa5 and DelSbtA_Bam5, whereas the *sbtA* downstream sequence was obtained using the primer combination SbtAB_Sac3 and DelSbtA_Bam3. First, the two fragments were cloned each in a single pGEMT vector (Promega), and then, the two fragments were combined into one vector by transferring the downstream fragment as Sac I/Bam HI fragment into the vector containing the upstream fragment. Into the central Bam HI restriction site, either a kanamycin or a streptomycin resistance cassette was inserted. The Δ*dacA* insertion mutant was generated by inserting a kanamycin resistance cassette into the region encoding for the active center of DacA. All the plasmids used to generate the mutants were verified by sequencing and then transformed in *Synechocystis* sp. PCC6803, as described (*20*). All mutants were selected on BG_{11} plates supplemented with proper antibiotics and verified by PCR.

For complementation, SbtB-sfGFP strain was generated by introducing the *sbtB* gene (*slr1513*) fused to the gene encoding sfGFP under the control of the native promoter of *sbtB* gene into Δ*sbtB* backgrounds using the self-replicating plasmid pVZ322, as described previously (*20*). For inducible complementation of Δ*sbtB*, the *sbtB* gene (*slr1513*) was reinserted in the genome under the control of the light inducible promotor *psbA2*.

Cultivation conditions

All cyanobacterial growth experiments were performed in nitrate supplemented BG_{11} medium (BG_{11}^{n}) with addition of 5 mM $NaHCO_3$ to avoid C_i limitation. Precultures were grown in shaking conditions at 28°C under continuous light (~50 μE) until mid of logarithmic growth phase before each experiment started. Cells were always normalized to their optical density at 750 nm using a Helios Gamma UV-Vis Spectrophotometer (Thermo Fisher Scientific). Experiments in day-night conditions were performed in a separate day-night chamber, providing 12-hour light phase (~50 μE) followed by a 12-hour darkness phase.

Nitrogen starvation was induced by shifting the cells to nitrogen-free BG_{11} medium (BG_{11}^{0}) with an initial optical density at 750 nm (OD_{750}) of 0.5 and kept under constant light of 50 to 100 μE. For resuscitation assays, samples were taken after 7 and 14 days of nitrogen starvation, and the resuscitation was induced by shifting the cultures back to BG_{11}^{n}, as described previously (*19*, *46*). The osmotic stress was generated by addition of 50 to 600 mM sorbitol to BG_{11}^{n}, as indicated.

To generate long dark conditions, cultures were inoculated to a final OD_{750} of 0.4 and covered from light immediately using dark aluminum foil for 5 days and kept shaking at 28°C. To determine the recovery after prolonged darkness, samples were taken directly before shift to darkness (T_{zero}) and after 1, 2, 3, and 5 days of dark treatment and were recovered by shifting to 50 μE of white continuous light.

The agar drop assays were performed on BG_{11} agar plates containing 1.5% Bacto Agar (Thermo Fisher Scientific) in serial dilutions of OD_{750} ranging from 10^{0} to 10^{-4}, as described previously (*46*). To protect the freshly dropped cells from the photoinhibition, the agar plates were covered with white tissues for 24 hours after dropping, before they were exposed to the required conditions.

Oxygen measurements

To estimate oxygen levels in liquid cultures during 24 hours of diurnal rhythm, cultures were inoculated to a final OD_{750} of 0.4. Oxygen levels were measured in those cultures each 15 min using an Oxy-1 SMA (PreSens GmbH, Regensburg, Germany) device in combination with SP-PSt3-NAU-D5-YOP Oxygen Sensor Spots (PreSens GmbH). In contrast, the rate of C_i-dependent oxygen

evolution (oxygenic photosynthesis) as a function of increasing HCO_3^- concentration was determined using a Clark-type oxygen electrode (Hansatech), as previously described (*20*). All measurements were performed at least three times.

Estimation of intracellular glycogen concentration

Intracellular glycogen concentration was estimated as previously described (*7*) with modifications from (*19*). Cells were first exposed to two successive day-night cycles, followed by harvest of 40 ml of each culture within the mid of the third day phase.

Measurement of PSII activity by WATER-PAM chlorophyll fluorescence and the whole-cell spectra

On the basis of chlorophyll a fluorescence, PSII activity was determined using PAM fluorometry using a PAM control (Heinz Walz GmbH), as described previously (*20*, *47*), at a wavelength of 650 nm (measuring light). Shortly, the measurements were performed by diluting 20 µl of cells in H_2O to a final volume of 2 ml, followed by measuring every 30 s with the saturating pulse at either zero or 56 µE of actinic light. Samples were normalized to a fluorescence level of unexcited cells (F) that remained between 400 and 500 (*47*). The apparent PSII activity was determined with the saturation pulse method using the F_v/F_m ratio, where F_v defined as $F_m - F_0$.

Whole-cell spectra (320 to 750 nm; 5 nm s^{-1}) were recorded using a SPECORD 205 (Analytik Jena AG). Cultures were diluted 1:5 to a final volume of 1 ml.

Determination of intracellular c-di-AMP concentration

Samples for c-di-AMP measurement were taken throughout 24 hours. The first sample was taken immediately before the dark phase, the second sample 30 min after the onset of darkness, and subsequent samples every 2 hours afterward were harvested. The samples of the day phase were harvested in the same manner as for the night phase. Samples were taken from *Synechocystis sp.* PCC 6803 WT and Δ*dacA* cells. Illumination during light phase was at approximately 40 to 50 µE and during dark below 1 µE. Centrifugation steps were done at 20.800*g*, 4°C, and for 10 min. For sampling, 10 ml of cultures was filtered on a glass fiber prefilter (Merck Millipore Ltd., Cork, Ireland) with a pore size of 1.6 µm. Filters were then put in 2-ml reaction tubes, frozen in liquid nitrogen, and stored at −80°C until further processing. Samples were thawed in 700 µl of ice cold extraction solvent [acetonitrile/methanol/water (2/2/1, v/v/v)] and incubated in ice for 15 min. Afterward, they were heated for 10 min at 95°C, cooled on ice, and centrifuged, and the supernatant was transferred into a new tube. These steps, without the heating, were repeated twice with another 200 µl of extraction solvent. The combination of the supernatants from the three extractions was stored over night at −20°C. The next day, samples were centrifuged once more, supernatants were transferred to new tubes, and liquid were evaporated using a vacuum evaporator (Martin Christ Gefriertrocknungsanlagen GmbH, Osterode am Harz, Germany). The dried samples were resuspended in 200 µl of H_2O of which 40 µl was transferred into mass spectrometry vials filled with 40 µl of H_2O with $^{13}C_{20}{}^{15}N_{10}$-c-di-GMP and $^{13}C_{20}{}^{15}N_{10}$-c-di-AMP (200 ng/ml each). Further dilution, if necessary, was done with a solution of H_2O with $^{13}C_{20}{}^{15}N_{10}$-c-di-GMP and $^{13}C_{20}{}^{15}N_{10}$-c-di-AMP (100 ng/ml each). Calibrator preparation for mass spectrometry measurement was done with either 10 µl of cdiNMP-cGAMP calibrator cdZ0-13 or 10 µl of cdiNMP metabolites calibrator cdM0, 4-13. ddH_2O (40 µl) and ddH_2O (50 µl) with $^{13}C_{20}{}^{15}N_{10}$-c-di-GMP and $^{13}C_{20}{}^{15}N_{10}$-c-di-AMP (200 ng/ml each) were added and vortexed. Samples were heated at 95°C for 10 min, cooled on ice and frozen over night at −20°C. Samples were thawed, centrifuged, and transferred into MS vials with inserts.

Pull-down assays

Cell pellets of logarithmic growing *Synechocystis* WT or Δ*sbtB* cells were resuspended in 1 ml of detergent-free lysis buffer [50 mM tris-HCl, 50 mM NaCl, 50 mM KCl, 1 mM EDTA, 0.5 mM phenylmethylsulfonyl fluoride (pH 7.4)] and transferred into 1.5-ml microtubes containing 0.1 ml of glass beads (0.1 mm). Samples were lysed by using a FastPrep-24 Ribolyser (five cycles; 7.0 m s^{-1}; 30 s per cycle; 5-min break between each cycle; 4°C) and spun down at 10.000*g* and 4°C for 10 min. The supernatant was transferred into a fresh 1.5-ml reaction tube and kept on ice. The cyclic-di-AMP target fishing was performed as described (*48*), by passing the whole crude cell extract from WT *Synechocystis* sp. PCC 6803 cells growing under continuous illumination over 2′-AHC-c-diAMP agarose (catalog no. A183, BioLoG, Germany), while EtOH-NH agarose (catalog no. E010, BioLoG, Germany) was used as a negative control. The detection of SbtB in the c-di-AMP pull-down was confirmed by Western blot analysis using specific *Sc*SbtB-polyclonal antibodies as described previously (*20*).

For the strep-tag pull-down, 10 µM purified strep-tagged *Sc*SbtB was incubated with Δ*sbtB* crude cell extract (normalized to 3 mg of protein) of cells growing under continuous illumination, on 150 µl of MagStrep "type3" XT Beads (IBA GmbH) in the presence of either 2 mM cAMP (3′,5'-cAMP; Sigma-Aldrich, Germany) or 2 mM c-di-AMP (catalog no. C088, BioLoG, Germany) or without effector molecule in 1.5-ml reaction tubes at 28°C for 15 min. As a negative control, the same reaction was performed without purified *Sc*SbtB, to eliminate the proteins which could bind nonspecifically to the Strep beads. After discarding the supernatant, the column was washed three times with 1 ml of washing buffer [100 mM tris-HCl (pH 8.0), 150 mM NaCl, and 1 mM EDTA]. The elution was performed two times with 50 µl of BXT elution buffer (Biotin Elution Buffer, IBA GmbH), and both elution fractions were combined in a fresh 1.5-ml reaction tube. After measuring protein concentration by using a BCA Kit (Thermo Fisher Scientific), the whole sample was sent to liquid chromatography–mass spectrometry.

For the His_8-tag pull-down, 10 µM purified His-tagged SbtB was incubated with WT *Synechocystis* sp. PCC 6803 crude cell extract (normalized to 3 mg of protein) of cells growing under continuous illumination, on 150 µl of Ni-NTA MagBeads (Genaxxion) with either 0.1 mM c-di-AMP or without effector molecules in 1.5-ml reaction tubes at 28°C for 15 min. After discarding the supernatant, the column was washed five times with 1 ml of washing buffer [50 mM Na_2HPO_4 (pH 8.0), 300 mM NaCl, and 10 mM imidazole]. The elution was performed with 20 µl of elution buffer [50 mM Na_2HPO_4 (pH 8.0), 300 mM NaCl, and 250 mM imidazole].

For the SbtB, CoIP cell pellets of 300 ml logarithmic growing *Synechocystis* sp. PCC 6803 WT and Δ*sbtB* cells growing under continuous illumination (day condition) were resuspended in 1 ml of detergent-free lysis buffer [50 mM tris-HCl and 5 mM EDTA (pH 7.4)] and transferred into 1.5-ml microtubes containing 0.1 ml of glass beads (0.1 mm). Samples were lysed by using a FastPrep-24 Ribolyser (five cycles; 7.0 m s^{-1}; 30 s per cycle; 5-min break between

each cycle; 4°C) and spun down at 16.000*g* and 4°C for 5 min. The supernatant was transferred into a fresh 1.5-ml reaction tube and kept on ice. Aliquots of 150 µl of Protein G magnetic beads (Merck/Millipore PureProteome) were washed twice with 1 ml of lysis buffer and incubated with 60 µl of rabbit *Synechocystis* α-SbtB antiserum for 10 min at room temperature. After three additional washing steps, the beads were incubated under the previous coupling conditions with 3 mg of crude cell extract of either WT or Δ*sbtB*. After another three washing steps, elution was performed in two consecutive steps with each 60 µl of elution buffer (200 mM glycine buffer at pH 2.5). Both fractions were combined, shock-frozen in liquid nitrogen, and stored at −80°C until further analysis. As control for nonspecific binding, WT crude cell extract was incubated with rabbit *B. subtilis* α-TnrA antiserum coupled with Protein G magnetic beads.

For all of pull-down experiments, the eluted protein fractions were first subjected to the short SDS–polyacrylamide gel electrophoresis purification step, where the proteins were migrated into 12% gels for 1.5 cm and then stained with Coomassie blue, followed by in-gel digestion with Trypsin for the stained/isolated pieces of the gel-containing proteins. Trypsin-digested peptides were analyzed by liquid chromatography–tandem mass spectrometry on a Proxeon Easy-nLC coupled to Q Exactive HF, using linear gradient for 60 min. The spectra were searched against *Synechocystis* sp. PCC6803 database (UP000001425_1111708_complete_2019-02-13) and sequences for different versions of SbtB proteins (His-tagged or Strep-tagged). Label-free quantification was used to calculate intensities and iBAQ values that give semiquantitative quantifications of protein enrichment. The number of unique identified peptides/protein, sequence coverage, and score were considered to select proteins of interest.

GFP fluorescence quantification

The total amount of GFP fluorescence in the whole cells was determined as described previously in (*20*) for the Δ*sbtB* strain that expresses sbtB-sfGFP construct under the control of the native promoter of *sbtB* gene in successive day-night cycles. The emission of GFP fluorescence at 525 nm was determined for normalized cells of OD_{750} of 0.1, after excitation at 485 nm, using a Tecan multimode microplate reader (SparK 10M).

BACTH assay

Plasmid construction, cell cultivation, and experimental procedure of BACTH assay were performed as described previously (*49*) only on X-Gal plates supplemented with X-Gal (40 µg/ml), kanamycin (50 µg/ml), ampicillin (100 µg/ml), and IPTG (1 mM). We tested only the N-terminal fusion of T25 subunit of Cya to SbtB, while the T18 subunit of Cya was fused either N- or C-terminally to the glycogen-related enzymes GlgA1, GlgA2, GlgP1, GlgP2, GlgB, and GlgC. Primers used to generate T25-SbtB fusion protein are listed in (table S1). The T25-SbtB fusion with an empty pUT18 vector was used as negative control, while the leucine zipper interaction was used as positive control. The *E. coli* BTH101 (Euromedex) was used for BACTH assays. The BACTH assays were performed at least three-times with three independent *E. coli* colonies to confirm the reproducibility and the specificity of the SbtB-GlgB interaction.

Microscale thermophoresis

MST experiments were carried out as previously described (*20*) using a Monolith NT.115 (NanoTemper Technologies GmbH) with uncoated Monolith NT.115 Capillaries (NanoTemper Technologies GmbH). Primary amines (lysine residues) of His-tagged GlgB were fluorescent labeled using the Monolith Protein Labeling Kit RED-NHS (NanoTemper Technologies GmbH). Titration series of StrepII-tagged *Sc*SbtB in the range of 1.3 nM to 42.5 µM were incubated with 10 nM fluorescent labeled His-tagged GlgB in 50 mM phosphate buffer (pH 8.0). All runs were performed in triplicate with 40% MST power and 60% light-emitting diode power. Single-site fitting was done using the NanoTemper data analysis software.

Isothermal titration calorimetry

ITC experiments were performed as previously described (*20*, *50*) using a VP-ITC microcalorimeter (MicroCal) in 50 mM sodium-potassium phosphate buffer (pH 8.0) supplemented with 0.5 mM EDTA, at 20°C. For determination of binding isotherms of small effector molecules binding to *Sc*SbtB, the protein (33.3 µM trimer concentration) was titrated against 0.5 or 1.0 mM c-di-AMP sodium salt (catalog no. C088, BioLoG, Germany).

SUPPLEMENTARY MATERIALS

Supplementary material for this article is available at https://science.org/doi/10.1126/sciadv.abk0568

View/request a protocol for this paper from *Bio-protocol*.

REFERENCES AND NOTES

1. D. G. Welkie, B. E. Rubin, S. Diamond, R. D. Hood, D. F. Savage, S. S. Golden, A hard day's night: Cyanobacteria in diel cycles. *Trends Microbiol.* **27**, 231–242 (2019).
2. Z. Eelderink-Chen, J. Bosman, F. Sartor, A. N. Dodd, Á. T. Kovács, M. Merrow, A circadian clock in a nonphotosynthetic prokaryote. *Sci. Adv.* **7**, eabe2086 (2021).
3. D. G. Welkie, B. E. Rubin, Y. G. Chang, S. Diamond, S. A. Rifkin, A. LiWanga, S. S. Golden, Genome-wide fitness assessment during diurnal growth reveals an expanded role of the cyanobacterial circadian clock protein KaiA. *Proc. Natl. Acad. Sci. U.S.A.* **115**, E7174–E7183 (2018).
4. N. Wan, D. M. DeLorenzo, L. He, L. You, C. M. Immethun, G. Wang, E. E. K. Baidoo, W. Hollinshead, J. D. Keasling, T. S. Moon, Y. J. Tang, Cyanobacterial carbon metabolism: Fluxome plasticity and oxygen dependence. *Biotechnol. Bioeng.* **114**, 1593–1602 (2017).
5. A. Makowka, L. Nichelmann, D. Schulze, K. Spengler, C. Wittmann, K. Forchhammer, K. Gutekunst, Glycolytic Shunts Replenish the Calvin–Benson–Bassham Cycle as Anaplerotic Reactions in Cyanobacteria. *Mol. Plant* **13**, 471–482 (2020).
6. C. Köbler, S. J. Schultz, D. Kopp, K. Voigt, A. Wilde, The role of the *Synechocystis* sp. PCC 6803 homolog of the circadian clock output regulator RpaA in day–night transitions. *Mol. Microbiol.* **110**, 847–861 (2018).
7. M. Gründel, R. Scheunemann, W. Lockau, Y. Zilliges, Impaired glycogen synthesis causes metabolic overflow reactions and affects stress responses in the cyanobacterium *Synechocystis* sp. PCC 6803. *Microbiology* **158**, 3032–3043 (2012).
8. S. Diamond, D. Jun, B. E. Rubin, S. S. Golden, The circadian oscillator in *Synechococcus elongatus* controls metabolite partitioning during diurnal growth. *Proc. Natl. Acad. Sci. U.S.A.* **112**, E1916–E1925 (2015).
9. R. D. Hood, S. A. Higgins, A. Flamholz, R. J. Nichols, D. F. Savage, The stringent response regulates adaptation to darkness in the cyanobacterium *Synechococcus elongatus*. *Proc. Natl. Acad. Sci. U.S.A.* **113**, E4867–E4876 (2016).
10. A. M. Puszynska, E. K. O'Shea, ppGpp controls global gene expression in light and in darkness in *S. elongatus*. *Cell Rep.* **21**, 3155–3165 (2017).
11. B. E. Rubin, T. N. Huynh, D. G. Welkie, S. Diamond, R. Simkovsky, E. C. Pierce, A. Taton, L. C. Lowe, J. J. Lee, S. A. Rifkin, J. J. Woodward, S. S. Golden, High-throughput interaction screens illuminate the role of c-di-AMP in cyanobacterial nighttime survival. *PLOS Genet.* **14**, e1007301 (2018).
12. J. He, W. Yin, M. Y. Galperin, S. H. Chou, Cyclic di-AMP, a second messenger of primary importance: Tertiary structures and binding mechanisms. *Nucleic Acids Res.* **48**, 2807–2829 (2020).
13. W. Yin, X. Cai, H. Ma, L. Zhu, Y. Zhang, S. H. Chou, M. Y. Galperin, J. He, A decade of research on the second messenger c-di-AMP. *FEMS Microbiol. Rev.* **44**, 701–724 (2020).
14. J. Stülke, L. Krüger, Cyclic di-AMP Signaling in Bacteria. *Annu. Rev. Microbiol.* **74**, 159–179 (2020).
15. J. Gundlach, A. Dickmanns, K. Schröder-Tittmann, P. Neumann, J. Kaesler, J. Kampf, C. Herzberg, E. Hamemr, F. Schwede, V. Kaever, K. Tittmann, J. Stülke, R. Ficner,

Identification, characterization, and structure analysis of the cyclic di-AMP-binding PII-like signal transduction protein DarA. *J. Biol. Chem.* **290**, 3069–3080 (2015).
16. I. Campeotto, Y. Zhang, M. G. Mladenov, P. S. Freemont, A. Gründling, Complex structure and biochemical characterization of the staphylococcus aureus Cyclic Diadenylate Monophosphate (c-di-AMP)-binding Protein PstA, the Founding Member of a New Signal Transduction Protein Family. *J. Biol. Chem.* **290**, 2888–2901 (2015).
17. M. Agostoni, A. R. Logan-Jackson, E. R. Heinz, G. B. Severin, E. L. Bruger, C. M. Waters, B. L. Montgomery, Homeostasis of Second Messenger Cyclic-di-AMP Is Critical for Cyanobacterial Fitness and Acclimation to Abiotic Stress. *Front. Microbiol.* **9**, 1121 (2018).
18. J. W. Nelson, N. Sudarsan, K. Furukawa, Z. Weinberg, J. X. Wang, R. R. Breaker, Riboswitches in eubacteria sense the second messenger c-di-AMP. *Nat. Chem. Biol.* **9**, 834–839 (2013).
19. A. Klotz, J. Georg, L. Bučinská, S. Watanabe, V. Reimann, W. Januszewski, R. Sobotka, D. Jendrossek, W. R. Hess, K. Forchhammer, Awakening of a Dormant Cyanobacterium from Nitrogen Chlorosis Reveals a Genetically Determined Program. *Curr. Biol.* **26**, 2862–2872 (2016).
20. K. A. Selim, F. Haase, M. D. Hartmann, M. Hagemann, K. Forchhammer, PII-like signaling protein SbtB links cAMP sensing with cyanobacterial inorganic carbon response. *Proc. Natl. Acad. Sci. U.S.A.* **115**, 4861–4869 (2018).
21. N. Oren, S. Timm, M. Frank, O. Mantovani, O. Murik, M. Hagemann, Red/far-red light signals regulate the activity of the carbon-concentrating mechanism in cyanobacteria. *Sci. Adv.* **7**, eabg0435 (2021).
22. J. Du, B. Förster, L. Rourke, S. M. Howitt, G. D. Price, Characterisation of Cyanobacterial Bicarbonate Transporters in *E. coli* Shows that SbtA Homologs Are Functional in This Heterologous Expression System. *PLOS ONE* **9**, 12 (2014).
23. S. Fang, X. Huang, X. Zhang, M. Zhang, Y. Hao, H. Guo, L. N. Liu, F. Yu, P. Zhang, Molecular mechanism underlying transport and allosteric inhibition of bicarbonate transporter SbtA. *Proc. Natl. Acad. Sci. U.S.A.* **118**, e2101632118 (2021).
24. T. Lapina, K. A. Selim, K. Forchhammer, E. Ermilova, The PII signaling protein from red algae represents an evolutionary link between cyanobacterial and Chloroplastida PII proteins. *Sci. Rep.* **8**, 790 (2018).
25. K. A. Selim, E. Ermilova, K. Forchhammer, From cyanobacteria to Archaeplastida: New evolutionary insights into PII signalling in the plant kingdom. *New Phytol.* **227**, 722–731 (2020).
26. Y. Chen, M. J. Cann, T. N. Litvin, V. Iourgenko, M. L. Sinclair, L. R. Levin, J. Buck, Soluble adenylyl cyclase as an evolutionarily conserved bicarbonate sensor. *Science* **289**, 625–628 (2000).
27. J. A. Kaczmarski, N. S. Hong, B. Mukherjee, L. T. Wey, L. Rourke, B. Förster, T. S. Peat, G. D. Price, C. J. Jackson, Structural Basis for the Allosteric Regulation of the SbtA Bicarbonate Transporter by the PII-like Protein, SbtB, from *Cyanobium* sp. PCC7001. *Biochemistry* **58**, 5030–5039 (2019).
28. J. Gundlach, L. Krüger, C. Herzberg, A. Turdiev, A. Poehlein, I. Tascón, M. Weiss, D. Hertel, R. Daniel, I. Hänelt, V. T. Lee, J. Stülke, Sustained sensing in potassium homeostasis: Cyclic di-AMP controls potassium uptake by KimA at the levels of expression and activity. *J. Biol. Chem.* **294**, 9605–9614 (2019).
29. K. Forchhammer, K. A. Selim, Carbon/nitrogen homeostasis control in cyanobacteria. *FEMS Microbiol. Rev.* **44**, 33–53 (2020).
30. R. Saha, D. Liu, A. Hoynes-O'Connor, M. Liberton, J. Yu, M. Bhattacharyya-Pakrasi, A. Balassy, F. Zhang, T. Seok Moon, C. D. Maranas, H. B. Pakrasi, Diurnal regulation of cellular processes in the cyanobacterium *Synechocystis* sp. Strain PCC 6803: Insights from transcriptomic, fluxomic, and physiological analyses. *MBio* **7**, e00464-16 (2016).
31. E. Suzuki, H. Ohkawa, K. Moriya, T. Matsubara, Y. Nagaike, I. Iwasaki, S. Fujiwara, M. Tsuzuki, Y. Nakamura, Carbohydrate metabolism in mutants of the cyanobacterium *Synechococcus elongatus* PCC 7942 defective in glycogen synthesis. *Appl. Environ. Microbiol.* **76**, 3153–3159 (2010).
32. S. Doello, A. Klotz, A. Makowka, K. Gutekunst, K. Forchhammer, A specific glycogen mobilization strategy enables rapid awakening of dormant cyanobacteria from chlorosis. *Plant Physiol.* **177**, 594–603 (2018).
33. A. Wiegard, C. Köbler, K. Oyama, A. K. Dörrich, C. Azai, K. Terauchi, A. Wilde, I. M. Axmann, *Synechocystis* KaiC3 displays temperature- and KaiB-dependent ATPase activity and is important for growth in darkness. *J. Bacteriol.* **202**, e00478-19 (2020).
34. H. Iijima, T. Shirai, M. Okamoto, A. Kondo, M. Y. Hirai, T. Osanai, Changes in primary metabolism under light and dark conditions in response to overproduction of a response regulator RpaA in the unicellular cyanobacterium *Synechocystis* sp. PCC 6803. *Front. Microbiol.* **6**, 888 (2015).
35. S. Berry, B. Esper, I. Karandashova, M. Teuber, I. Elanskaya, M. Rögner, M. Hagemann, Potassium uptake in the unicellular cyanobacterium *Synechocystis* sp. strain PCC 6803 mainly depends on a Ktr-like system encoded by slr1509 (ntpJ). *FEBS Lett.* **548**, 53–58 (2003).
36. N. Matsuda, H. Kobayashi, H. Katoh, T. Ogawa, L. Futatsugi, T. Nakamura, E. P. Bakker, N. Uozumi, Na^+-dependent K^+ Uptake Ktr System from the Cyanobacterium *Synechocystis* sp. PCC 6803 and Its Role in the Early Phases of Cell Adaptation to Hyperosmotic Shock. *J. Biol. Chem.* **279**, 54952–54962 (2004).
37. A. C. Pohland, D. Schneider, D, Mg^{2+} homeostasis and transport in cyanobacteria - at the crossroads of bacterial and chloroplast Mg^{2+} import. *Biol. Chem.* **400**, 1289–1301 (2019).
38. V. Shyp, B. N. Dubey, R. Böhm, J. Hartl, J. Nesper, J. A. Vorholt, S. Hiller, T. Schirmer, U. Jenal, Reciprocal growth control by competitive binding of nucleotide second messengers to a metabolic switch in *Caulobacter crescentus*. *Nat. Microbiol.* **6**, 59–72 (2021).
39. K. Forchhammer, J. Lüddecke, Sensory properties of the PII signalling protein family. *FEBS J.* **283**, 425–437 (2016).
40. M. Eisenhut, E. A. von Wobeser, L. Jonas, H. Schubert, B. W. Ibelings, H. Bauwe, H. C. Matthijs, M. Hagemann, Long-term response toward inorganic carbon limitation in wild type and glycolate turnover mutants of the cyanobacterium *Synechocystis* sp. strain PCC 6803. *Plant Physiol.* **144**, 1946–1959 (2007).
41. J. K. Gupta, P. Rai, K. K. Jain, S. Srivastava, Overexpression of bicarbonate transporters in the marine cyanobacterium *Synechococcus* sp. PCC 7002 increases growth rate and glycogen accumulation. *Biotechnol. Biofuels* **13**, 17 (2020).
42. K. A. Selim, L. Tremiño, C. Marco-Marín, V. Alva, J. Espinosa, A. Contreras, M. D. Hartmann, K. Forchhammer, V. Rubio, Functional and structural characterization of PII-like protein CutA does not support involvement in heavy metal tolerance and hints at a small-molecule carrying/signaling role. *FEBS J.* **288**, 1142–1162 (2021).
43. W. Kabsch, XDS. *Acta Crystallogr. D Biol. Crystallogr.* **66**, 125–132 (2010).
44. G. N. Murshudov, P. Skubák, A. A. Lebedev, N. S. Pannu, R. A. Steiner, R. A. Nicholls, M. D. Winn, F. Long, A. A. Vagin, REFMAC5 for the refinement of macromolecular crystal structures. *Acta Crystallogr. D Biol. Crystallogr.* **67**, 355–367 (2011).
45. D. Trautmann, B. Voss, A. Wilde, S. Al-Babili, W. R. Hess, Microevolution in cyanobacteria: Re-sequencing a motile substrain of Synechocystis sp. PCC 6803. *DNA Res.* **19**, 435–448 (2012).
46. K. A. Selim, M. Haffner, Heavy Metal Stress Alters the Response of the Unicellular Cyanobacterium *Synechococcus elongatus* PCC 7942 to Nitrogen Starvation. *Life* **10**, 275 (2020).
47. A. M. Acuna, J. J. Snellenburg, M. Gwizdala, D. Kirilovsky, R. Van Grondelle, I. H. M. Van Stokkum, Resolving the contribution of the uncoupled phycobilisomes to cyanobacterial pulse-amplitude modulated (PAM) fluorometry signals. *Photosynth. Res.* **127**, 91–102 (2016).
48. J. Kampf, J. Gundlach, C. Herzberg, K. Treffon, J. Stülke, Identification of c-di-AMP-Binding Proteins Using Magnetic Beads, in *c-di-GMP Signaling: Methods and Protocols. Methods in Molecular Biology* (Springer, Science+Business Media LLC, Berlin, 2017), pp. 347–359.
49. B. Watzer, P. Spät, N. Neumann, M. Koch, R. Sobotka, B. Macek, O. Hennrich, K. Forchhammer, The signal transduction protein P_{II} controls ammonium, nitrate and urea uptake in cyanobacteria. *Front. Microbiol.* **10**, 1428 (2019).
50. K. A. Selim, M. Haffner, B. Watzer, K. Forchhammer, Tuning the *in vitro* sensing and signaling properties of cyanobacterial PII protein by mutation of key residues. *Sci. Rep.* **9**, 18985 (2019).

Acknowledgments: We are grateful to A. Klotz and H. Grenzendorf (IMIT, Tübingen University) for the excellent assistance, the staff of beamline X10SA/SLS, the Proteome Center (Tübingen University), W. R. Hess (Freiburg University) for the microarray data, and L. Lo-Presti for critical scientific and linguistic editing of the manuscript. Furthermore, we would like to acknowledge the infrastructural support by the Cluster of Excellence "Controlling Microbes to Fight Infections" (EXC 2124–390838134) of the DFG. K.A.S. would like to dedicate this research to the memory of A. Selim, a distinguished father and medical doctor, for the continued support. **Funding:** This work was supported by the German research foundation (DFG) within the priority program SPP1879 to (K.F., M.Hag., M.Haf., and O.M.) and by institutional funds of the Max Planck Society. DFG-Cluster of Excellence (EXC 2124) "Controlling Microbes to Fight Infections" to (K.A.S.). **Author contributions:** K.A.S. and K.F. conceived, initiated, and supervised the whole project. K.A.S. designed the experiments. M.Haf. and K.A.S. performed most of the physiological and biochemical experiments, except for c-di-AMP quantification by M.B. with help of R.S., photosynthetic HCO_3^--dependent oxygen evolution by O.M. under supervision of M.Hag., and BACTH by N.N. L.K. and J.S. helped M.Haf. for performing c-di-AMP pull-down. R.A. performed crystallographic sample preparation and diffraction data collection, K.A.S. solved the crystal structure, and M.D.H. supervised the structural analysis. K.A.S. evaluated and interpreted the results, prepared the figures, and wrote the manuscript. K.A.S., M.D.H., M.Hag., and K.F. commented and edited on the manuscript. All authors approved the final version of the manuscript. **Competing interests:** The authors declare that they have no competing interests. **Data and materials availability:** Crystallography, atomic coordinates, and structure factors have been deposited in the Protein Data Bank, www.wwpdb.org (PDB ID code: 7OBJ).

Submitted 18 June 2021
Accepted 18 October 2021
Published 8 December 2021
10.1126/sciadv.abk0568

Science Advances
AAAS

Supplementary Materials for

Diurnal metabolic control in cyanobacteria requires perception of second messenger signaling molecule c-di-AMP by the carbon control protein SbtB

Khaled A. Selim*, Michael Haffner, Markus Burkhardt, Oliver Mantovani, Niels Neumann, Reinhard Albrecht, Roland Seifert, Larissa Kruger, Jorg Stulke, Marcus D. Hartmann, Martin Hagemann, Karl Forchhammer*

*Corresponding author. Email: khaled.selim@uni-tuebingen.de (K.A.S.); karl.forchhammer@uni-tuebingen.de (K.F.)

Published 8 December 2021, *Sci. Adv.* **7**, eabk0568 (2021)
DOI: 10.1126/sciadv.abk0568

This PDF file includes:

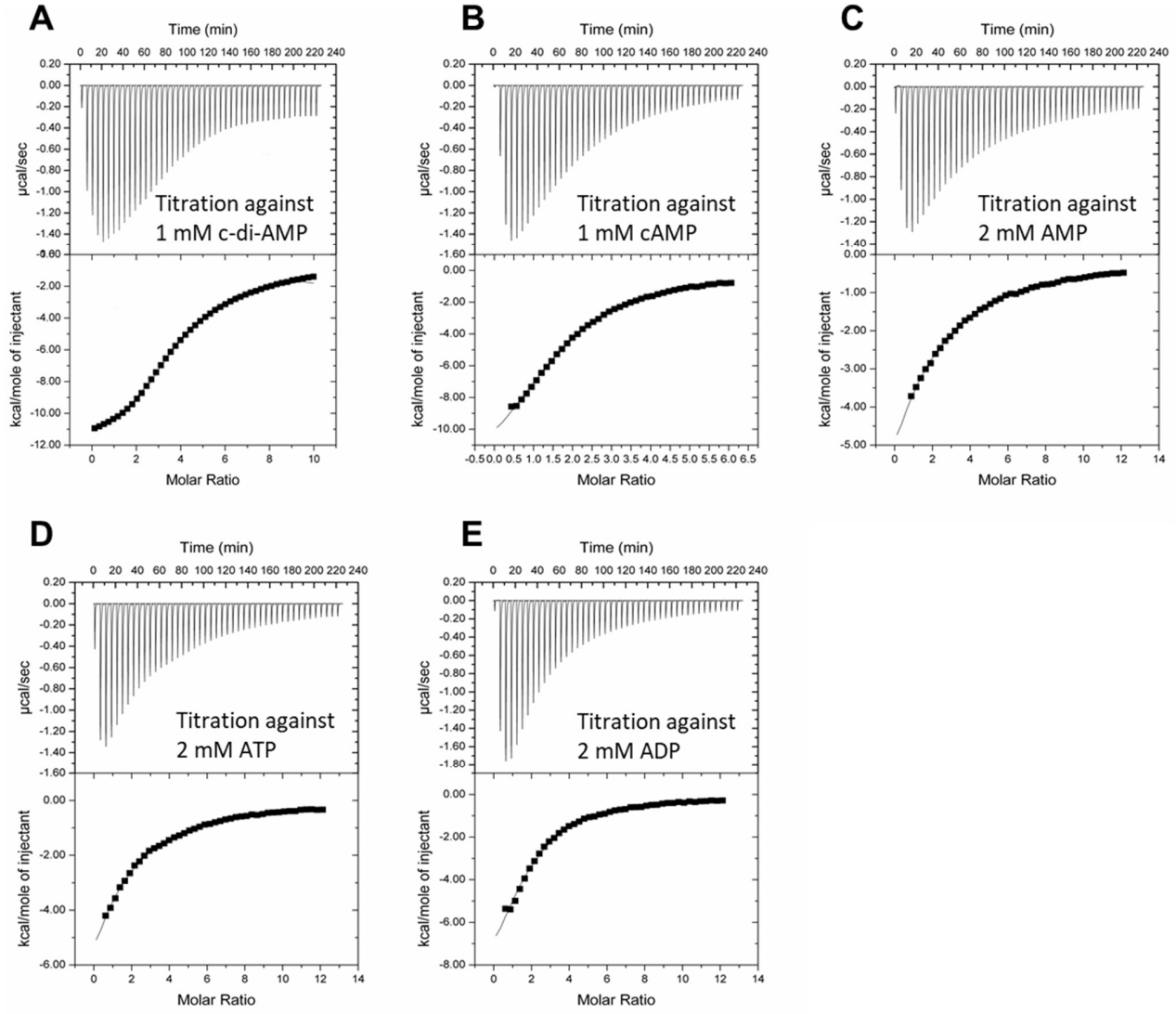

Fig. S1. ITC analysis of ligand binding properties of the *Sc*SbtB protein. Binding of various adenosine nucleotides to the *Sc*SbtB protein with strong binding isotherm. ITC titration against (A) 1 mM c-di-AMP, (B) 1 mM cAMP, (C) 2 mM AMP, (D) 2 mM ATP, and (E) 2 mM ADP. The binding enthalpy for c-di-AMP was almost equivalent or higher than that of AMP, ATP, ADP and cAMP at a lower concentration of c-di-AMP. Upper panels show the raw ITC data in the form of the heat produced during the titration of 33.3 µM SbtB (trimeric concentration) with different effector molecules; lower panels show the binding isotherms and the best-fit curves according to the three sequential binding site models for trimeric SbtB.

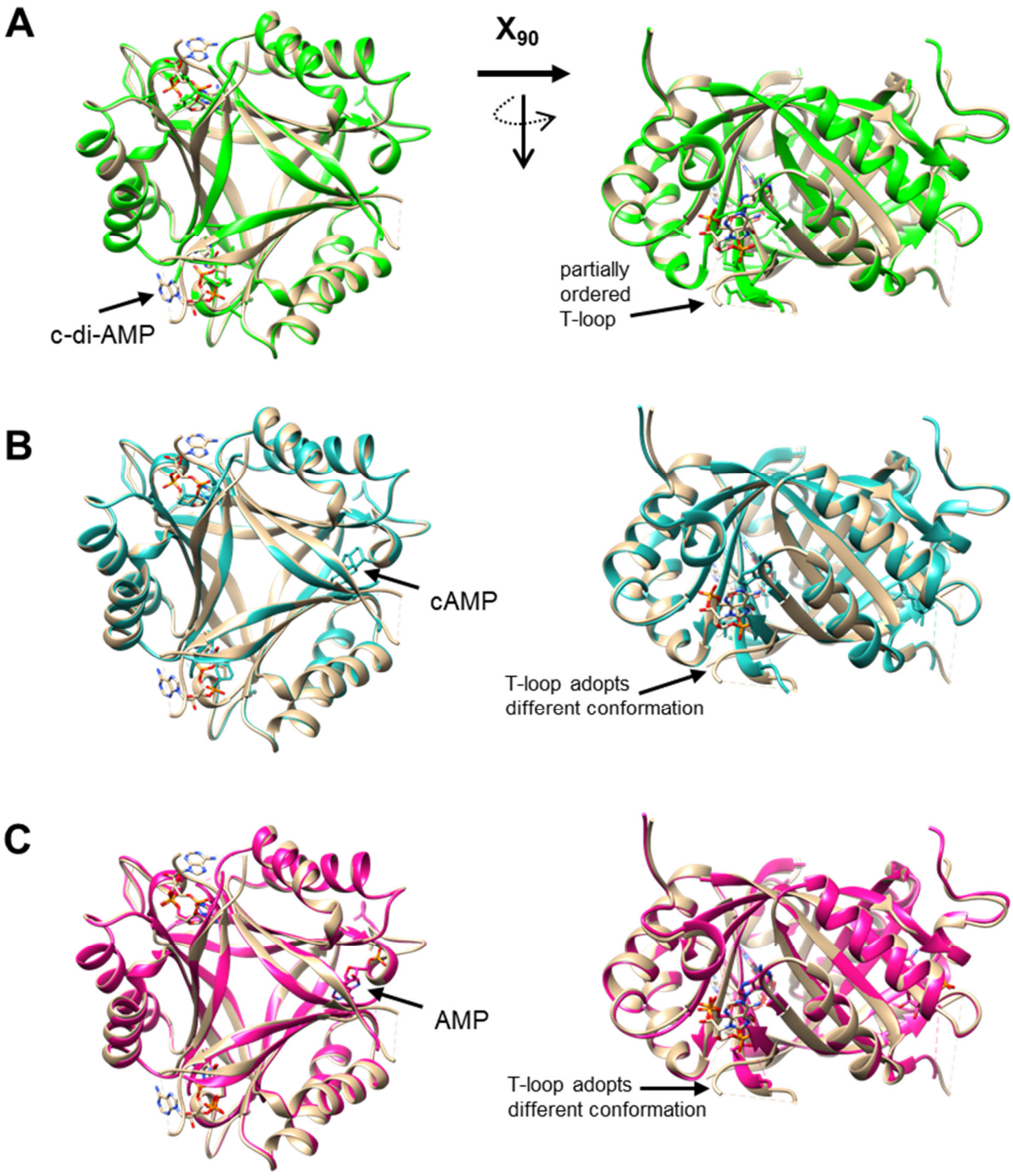

Fig. S2. Structural superpositions of *Sc*SbtB:c-di-AMP complex with different *Sc*SbtB structures. Superposition of *Sc*SbtB:c-di-AMP complex (brown) with (A) apo-*Sc*SbtB trimer (green; PDB: 5O3P), (B) *Sc*SbtB:cAMP complex (blue; PDB: 5O3Q), and *Sc*SbtB:AMP complex (pink; PDB: 5O3R), yielded RMSD values of 0.26 Å, 0.31 Å and 0.33 Å, respectively. Structural representations were prepared using UCSF Chimera (http://www.rbvi.ucsf.edu/chimera).

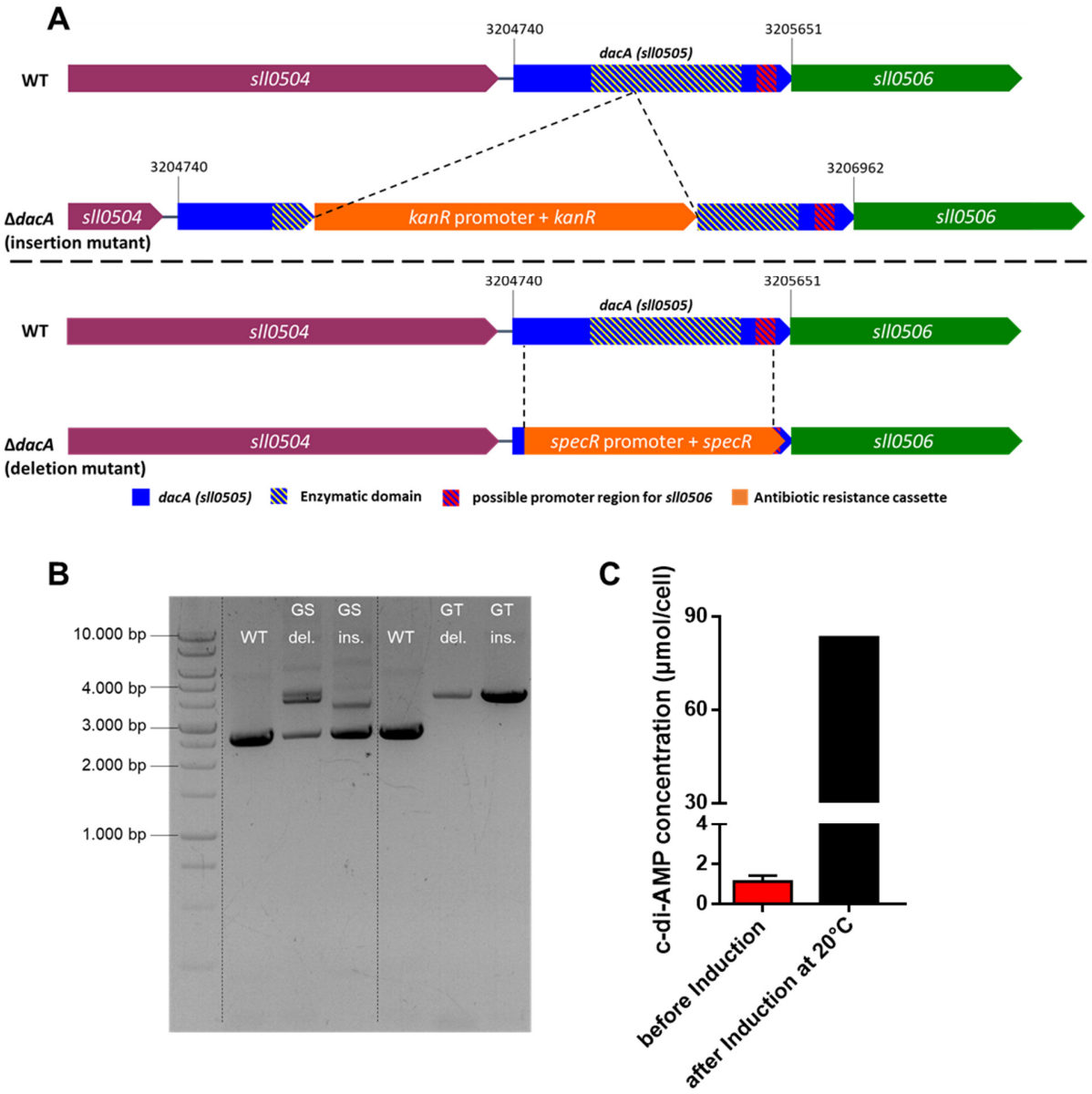

Fig. S3. Generation of the Δ*dacA* mutant in glucose tolerant (GT) and glucose sensitive *Synechocystis* sp. PCC 6803 wild-type cells. (A) Schematic overview of the strategies to generate a Δ*dacA* mutant either by inserting a kanamycin resistance cassette in the enzymatic domain-encoding region of the *sll0505* gene (Δ*dacA* insertion mutant); or by deleting almost the entire *sll0505* gene using a spectinomycin resistance cassette (Δ*dacA* deletion mutant), as indicated. Notably, cyanobacteria show a conserved operon organization for DacA encoding-gene (*sll0505*), where the diaminopimelate decarboxylase (*lysA; sll0504*) and the undecaprenyl pyrophosphate synthase (*uppS; sll0506*) encoding-genes are constantly up- and down-stream of the *sll0505* gene, respectively. (B) segregation level of either Δ*dacA* insertion mutant or the Δ*dacA* deletion mutant in both glucose tolerant (GT) and glucose sensitive (GS) *Synechocystis* backgrounds. (C) c-di-AMP concentration in *E. coli* cells before and after induction of the DacA encoding gene with 0.1 mM IPTG.

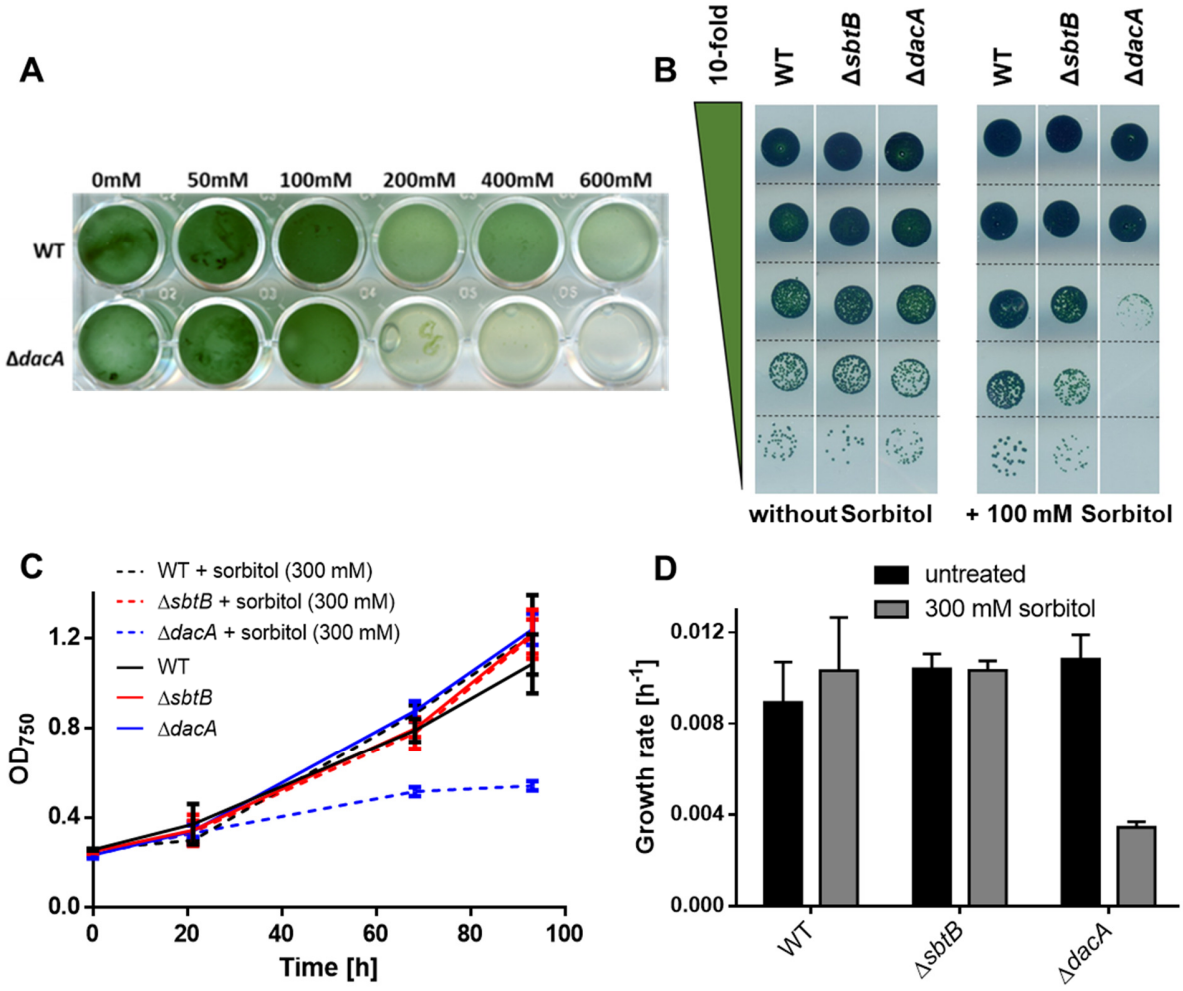

Fig. S4. Sensitivity of the Δ*dacA* mutant to osmotic stress. (A) *Synechocystis* WT and Δ*dacA* cells were exposed to osmotic stress generated by increasing concentrations of sorbitol (ranging from 0 mM – 600 mM). Cells were inoculated to a final OD_{750} of 0.25, and pictures were taken 6 days after inoculation. (B) Growth test by drop-plate assay of *Synechocystis* WT, Δ*dacA*, and Δ*sbtB* cells on BG_{11} agar (left) and BG_{11} agar supplemented with 100 mM sorbitol (right). Cells were normalized to an OD_{750} of 1.0 and serial diluted to an OD_{750} of 1 x 10^{-4} (from top to down). (C and D) Growth curves and rates of *Synechocystis* WT, Δ*dacA*, and Δ*sbtB* cells in the presence and absence of 300 mM sorbitol, as indicated. Notably, the osmotic stress effect of sorbitol was more pronounced in the BG_{11} agar plats in (B) than in liquid culture (A) due to the limitation of gas-exchange and therefore the cells on BG_{11} agar plats are strictly C_i-dependent (i.e. low carbon acclimated).

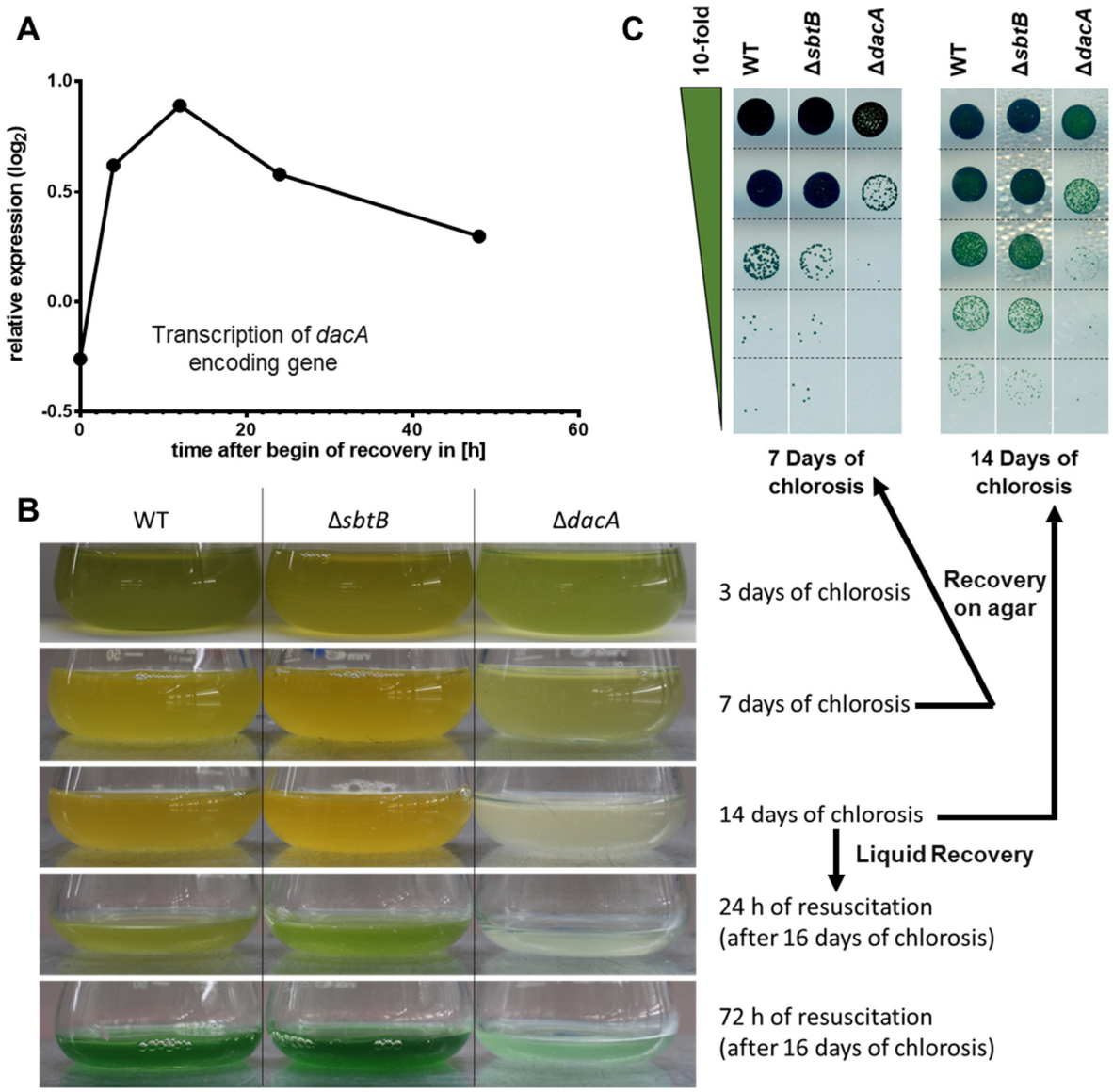

Fig. S5. Characterization of the Δ*sbtB* and Δ*dacA* mutants during recovery from nitrogen starvation. (A) Transcription levels of *sll0505* (encoding for DacA) during 48 hours of resuscitation from nitrogen chlorosis. The expression levels of *sll0505* was extracted from our previous microarray data; published previously in (*19*). X-axis shows the time in hours after the addition of combined nitrogen sources to the media; Y-axis shows the relative gene expression in a logarithmic scale. (B) Nitrogen chlorosis and resuscitation of *Synechocystis* WT, Δ*sbtB* and Δ*dacA* cells as indicated. Pictures were taken after 3, 7, and 14 days of chlorosis (first three pictures; up to down) and at 24 hours as well as 72 hours of resuscitation (last two pictures; up to down). (C) Resuscitation test by drop-plate assay of WT, Δ*sbtB* and Δ*dacA* cells that had been nitrogen starved for 7 and 14 days (samples from [B]). Cells were normalized to an OD_{750} of 1 and serial diluted in 10-fold steps (up to down; depicted by a green triangle).

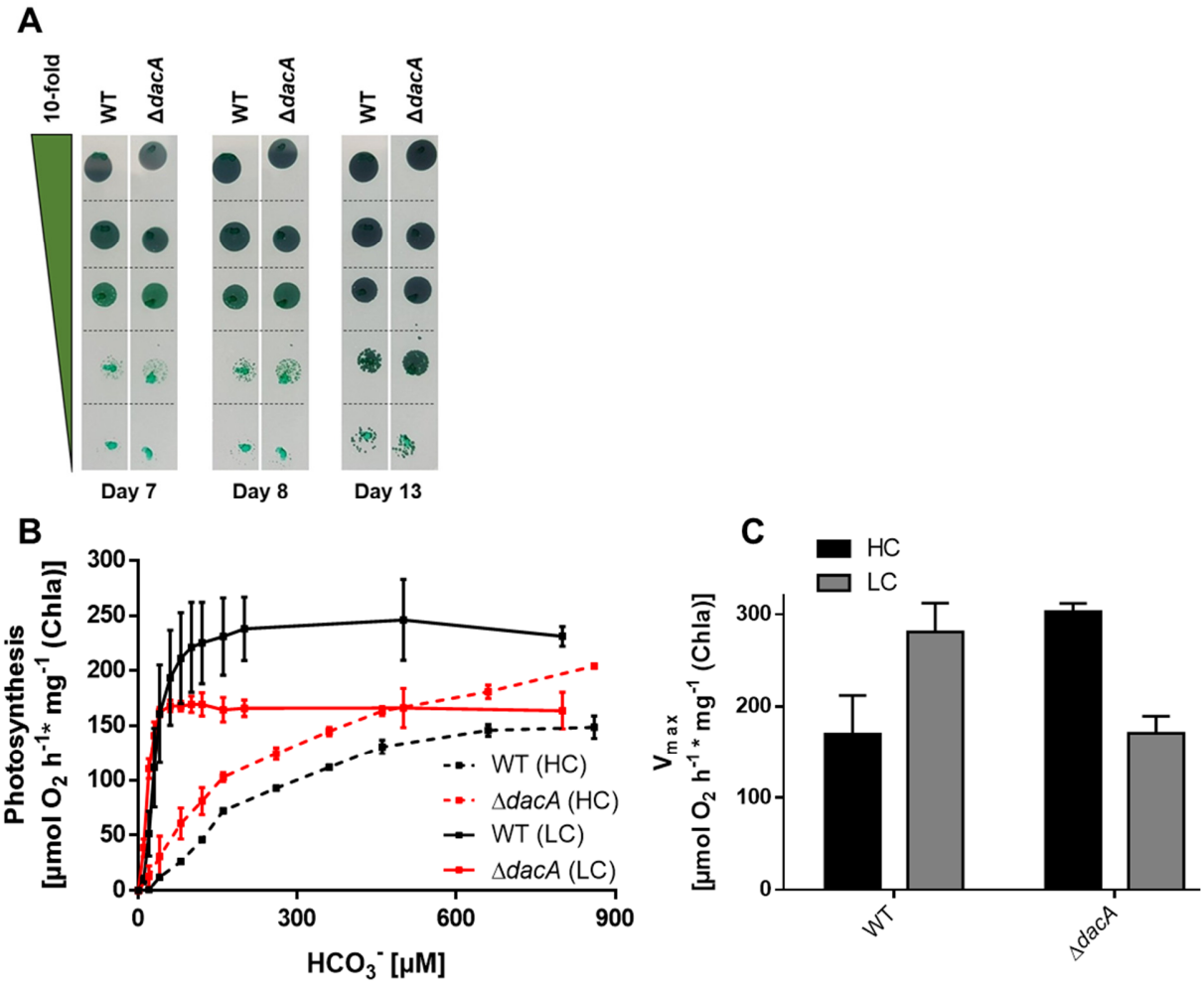

Fig. S6. Characterization of the Δ*dacA* mutant under low carbon conditions. (A) Growth test by drop-plate assay of *Synechocystis* WT and Δ*dacA* cells on carbon-free BG_{11} plates (pH 8.0). Cells were normalized to an OD_{750} of 1 and serial diluted in 10-fold steps (up to down; depicted by a green triangle). (B) *In vivo* bicarbonate uptake (as indicated by oxygen evolution) of *Synechocystis* WT (black lines) and Δ*dacA* (red lines) cells adapted either to high carbon (HC; dashed lines) or to low carbon (LC; solid lines) conditions. X-axis shows bicarbonate dependent oxygen evolution in µmol O_2/h per mg chlorophyll a. Y-axis shows increasing concentrations of bicarbonate in µM. (C) Calculated V_{max} values of bicarbonate uptake in *Synechocystis* WT and Δ*dacA* cells adapted either to high carbon conditions (HC; black bars) or to low carbon conditions (LC; grey bars), based on the data shown in (B).

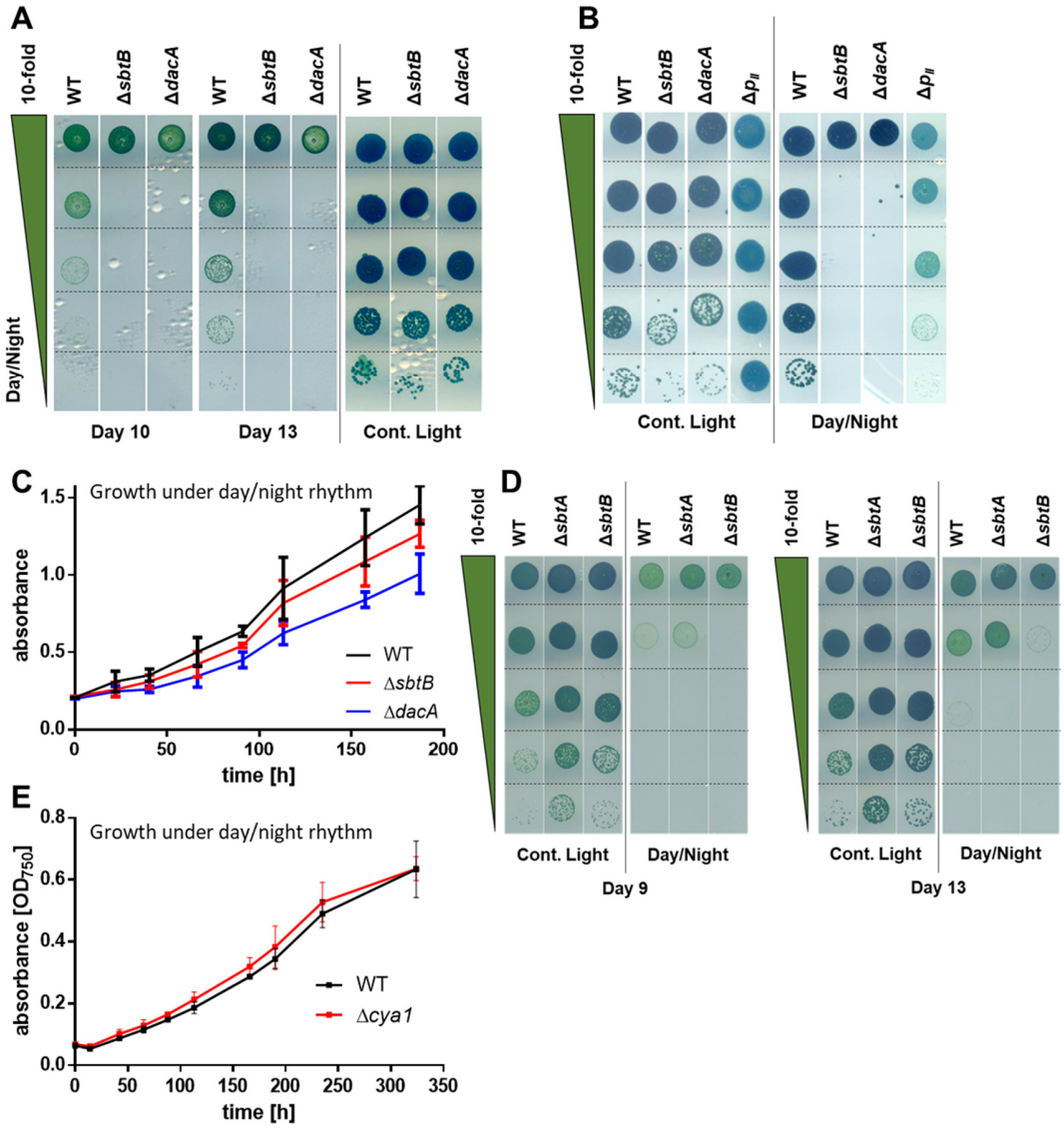

Fig. S7. Characterization of the Δ*sbtB* and Δ*dacA* mutants under diurnal rhythm. (A) Growth test by drop-plate assay of *Synechocystis* WT, Δ*sbtB* and Δ*dacA* (insertion mutant) cells under either continuous light (left) or a 12 h diurnal rhythm (right). (B) Growth test by drop-plate assay of *Synechocystis* WT, Δ*sbtB*, Δ*dacA* (deletion mutant), and Δ*glnB* (Δp_{II}; which encodes for canonical PII protein was used as a negative control) cells under either continuous light (left picture) or a 12 h diurnal rhythm (right picture). (C) Growth curve of *Synechocystis* WT (black line), Δ*sbtB* (red line) and Δ*dacA* (blue line) cells throughout a 12 h diurnal rhythm. (D) Growth test by drop-plate assay of *Synechocystis* WT, Δ*sbtA* and Δ*sbtB* cells under either continuous light or a 12 h diurnal rhythm, as indicated, for 9 and 13 days. (E) Growth curve of *Synechocystis* WT (black line) and Δ*cya1* (red line) cells throughout a 12 h diurnal rhythm. For (A, B and D), the cells were normalized to an OD_{750} of 1.0 and serial diluted in 10-fold steps (up to down; depicted by a green triangle). For (C, E) X-axis shows the time in hours; Y-axis shows the absorbance at 750 nm.

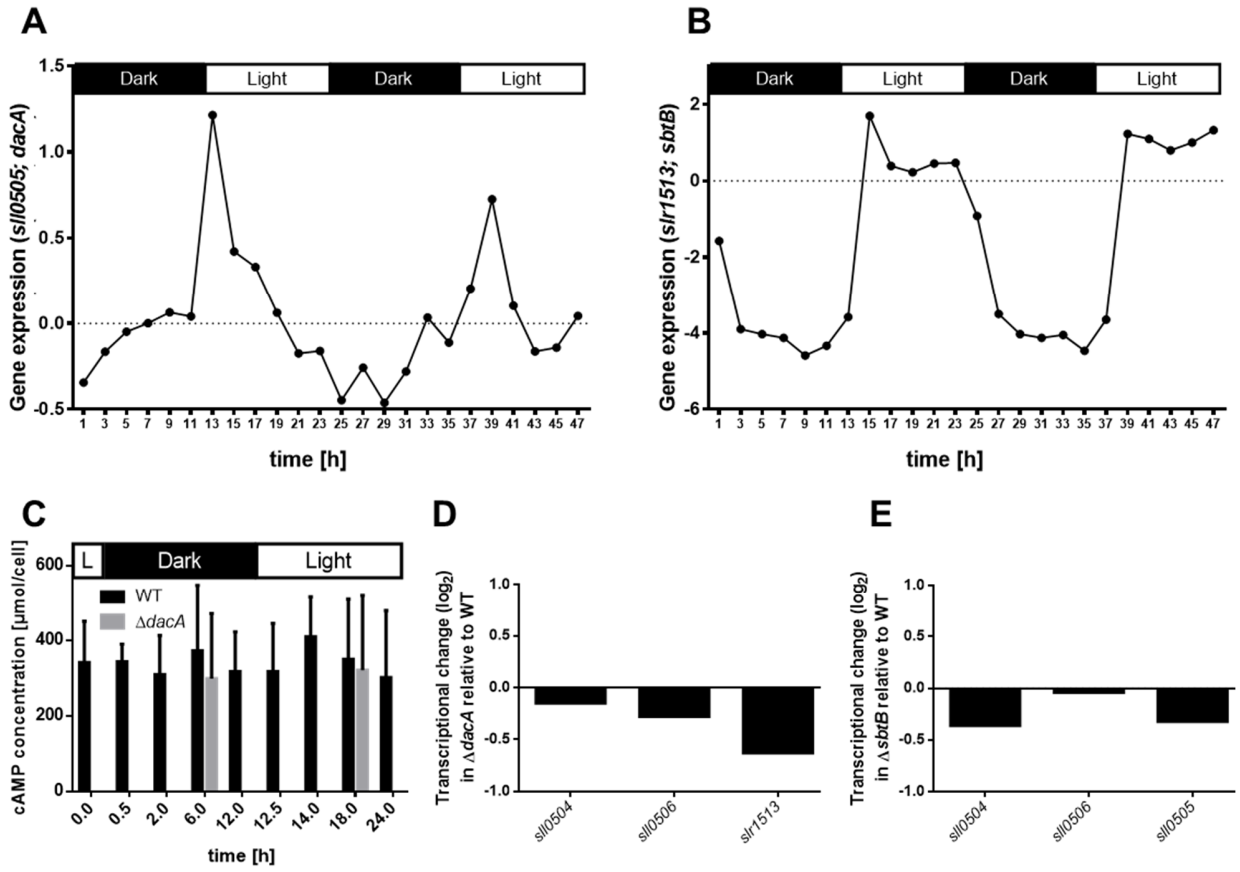

Fig. S8. *dacA* and *sbtB* expression profile and intracellular levels of cAMP. Gene expression profile of (A) *dacA* (*sll0505*) and (B) *sbtB* (*slr1513*) in *Synechocystis* WT throughout a 12 h diurnal rhythm; published previously in (*30*). For (A, B) X-axis shows the time in hours; Y-axis shows the relative gene expression. (C) cAMP concentration throughout a 12 h diurnal rhythm within *Synechocystis* WT (black bars) and Δ*dacA* cells (gray bars), as indicated. X-axis shows the time in hours; Y-axis shows the intracellular concentrations of cAMP. For (A, B, and C) The night phases are depicted by black bars; the day phases are depicted by white bars. (D, E) Expression of the genes situated up- (*sll0504*) or down-stream (*sll0506*) of *dacA* (*sll0505*), and for the SbtB encoding gene (*slr1513*) in Δ*dacA* mutant (D) and for the *dacA* encoding operon (*sll0504-sll0505-sll0506*) in Δ*sbtB* mutant (E), relative to their expression in WT cells under standard cultivation conditions.

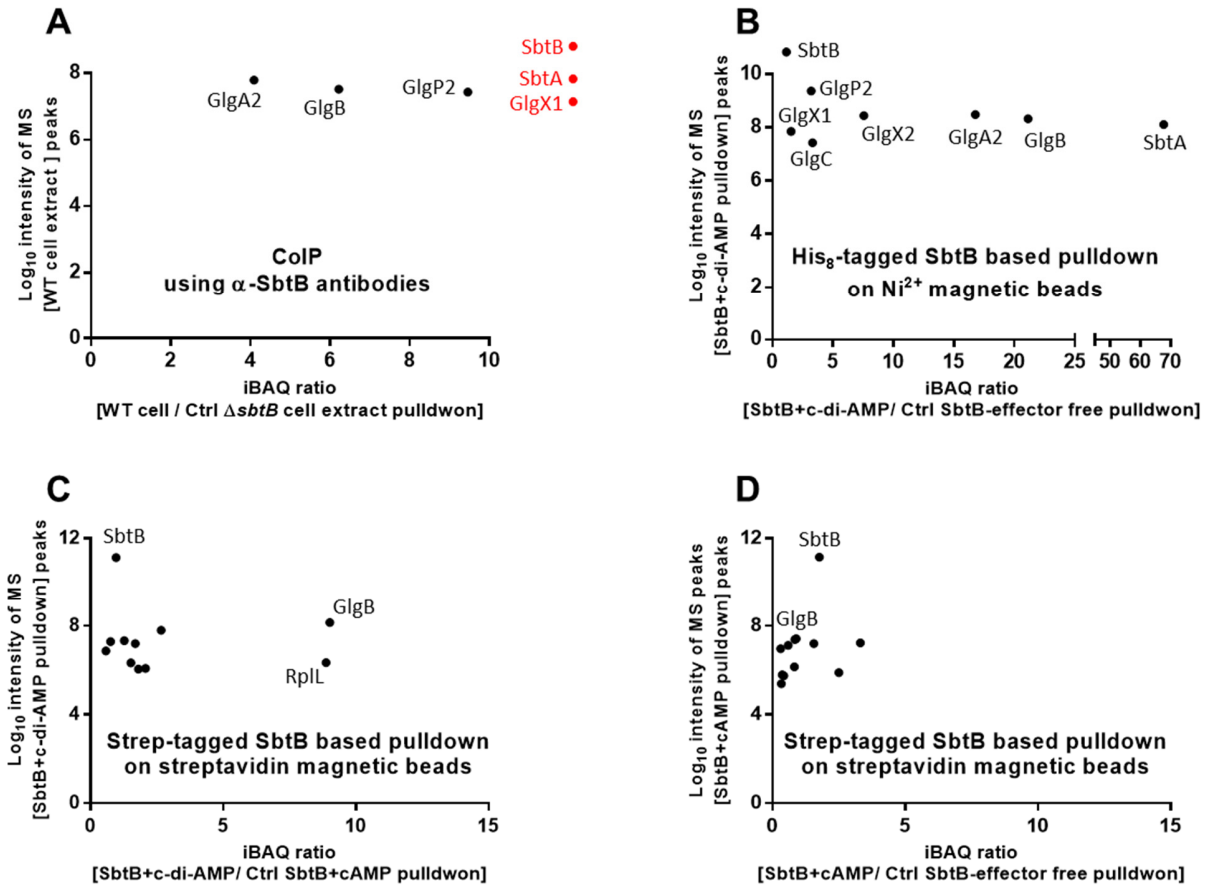

Fig. S9. SbtB interactome and proteins enrichment in different SbtB-based pull-downs. (A) CoIP pull-down using α-SbtB specific antibodies from crude cell extracts from WT cells and Δ*sbtB* mutant (as a control). The red dots were not identified in the Δ*sbtB*-based pull-down. (B) Ni^{2+} magnetic beads-based pull-down using His_8-tagged *St*SbtB protein. The pull-downs were done either in presence or absence of c-di-AMP (0.1 mM). Incubation of SbtB with c-di-AMP enriched the co-elution of glycogen-associated enzymes, in practically GlgB. (C-D) Streptavidin magnetic beads-based pull-downs using strep-tagged *St*SbtB protein. The pull-downs were done either in absence or presence of 2 mM effector molecules (c-di-AMP or cAMP). In contrast to cAMP, the presence of c-di-AMP enriched GlgB interaction with SbtB (compare Fig. 3A with S9C and S9C with S9D). (A-C) Eluates were analyzed by high accuracy LC-MS/MS to calculate protein enrichment ratios. The identified proteins were sorted by score and refined manually to remove unspecific binning proteins. Significantly enriched proteins were calculated based on iBAQ values and plotted against the intensity of MS peaks of the identified/defined peptides. The known SbtB-interacting partner SbtA was identified in (A) and (B), which validated our pull-down approach in general.

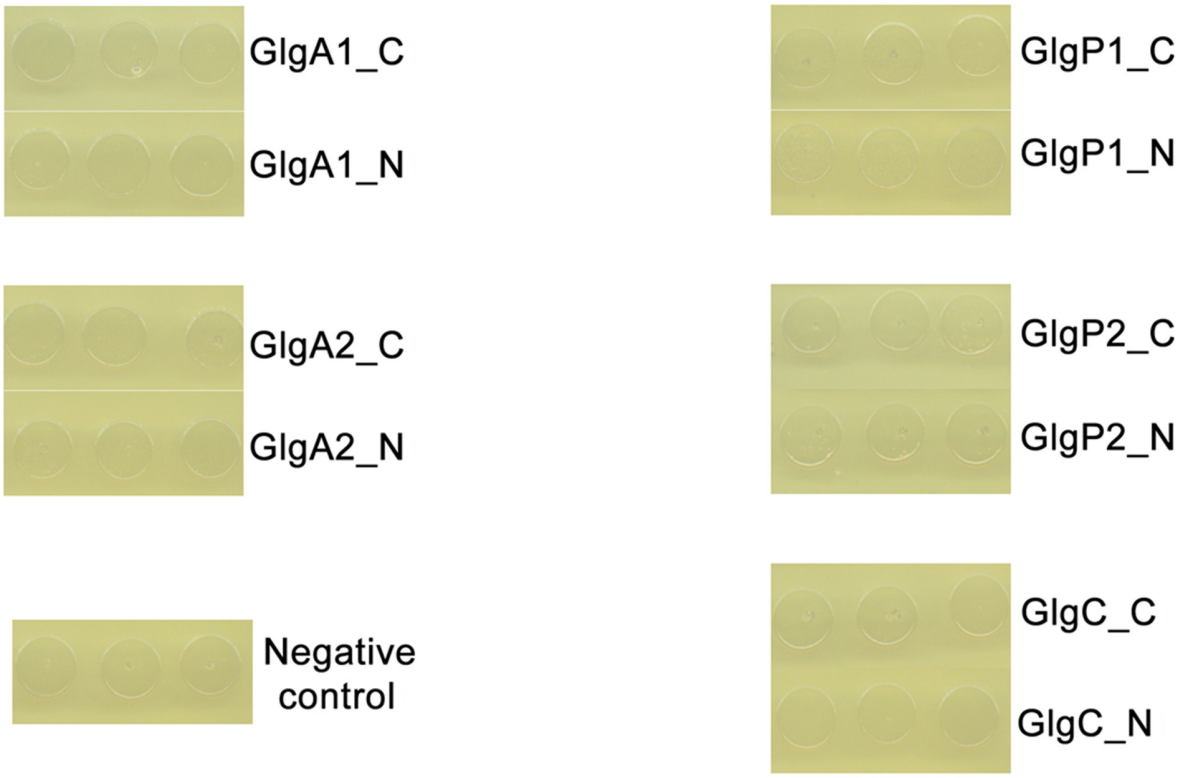

Fig. S10. Analysis of the interaction between glycogen-related enzymes and SbtB via bacterial two hybrid assay. The assay was performed using *E. coli* cells expressing N-terminally fusion of Cya-T25 subunit with SbtB (SbtB_N) together with GlgA1 (left, top), GlgA2 (left, middle), GlgP1 (right, top), GlgP2 (right, middle) or GlgC (right, bottom). Each glycogen related enzyme was either C-terminally (depicted by "_C") or N-terminally (depicted by "_N") fusion of Cya-T18 subunit to the enzyme. Empty Cya-T18 was used as a negative control (left, bottom). No interaction was observed between for GlgA1, GlgA2, GlgP1, GlgP2, and GlgC with SbtB. The assay was done using 3-independent/freshly transformed *E. coli* cells.

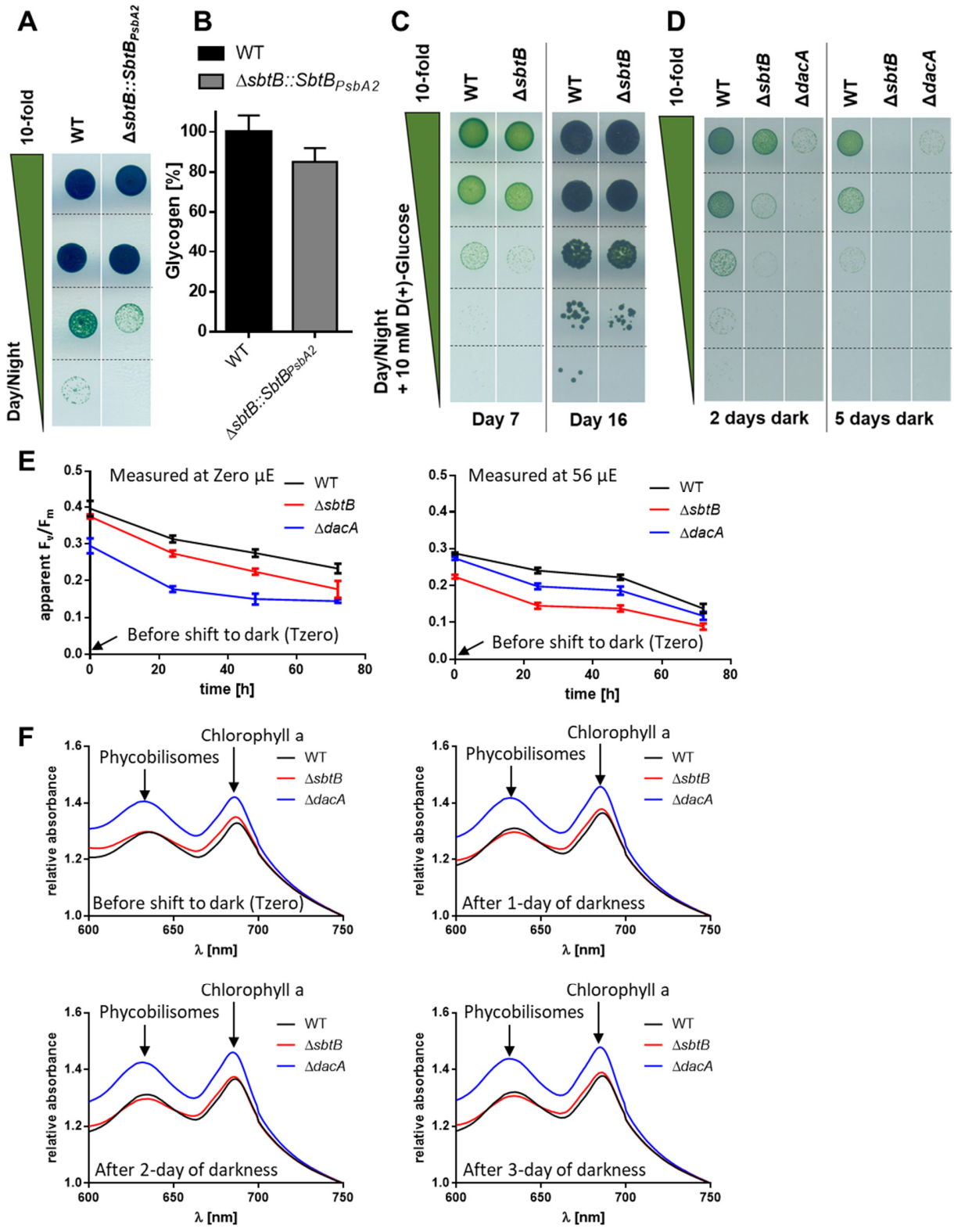

Fig. S11. Complementation and growth defect under prolonged dark conditions of the Δ*sbtB* mutant.

(A) Growth test by drop-plate assay of *Synechocystis* WT and complemented Δ*sbtB*:SbtB$_{PsbA2}$ (right) cells

throughout a 12 h diurnal rhythm. The Δ*sbtB* complementation strain Δ*sbtB*::$SbtB_{PsbA}$ complements the phenotype of Δ*sbtB* that is shown in figures 2D and S6. (B) Glycogen levels of the complemented Δ*sbtB*::$SbtB_{PsbA2}$ cells (grey bar) relative to WT (black bar) at midday of a 12 h diurnal rhythm. The Δ*sbtB*::$SbtB_{PsbA2}$ regained almost wild-type levels of glycogen when compared to the Δ*sbtB* that is shown in figure 3D. (C) Complementation of Δ*sbtB* mutant by addition of 10 mM D(+)-glucose under a 12 h diurnal rhythm, as indicated. Pictures were taken after 7 (left) and 16 (right) days of growth. (D) Viability test using the drop-plate assay of *Synechocystis* WT, Δ*sbtB* and Δ*dacA* cells after 2 (left) and 5 (right) days of incubation in complete darkness, as indicated. Cells were normalized to an OD_{750} of 1.0 and serial diluted in 10-fold steps (top to bottom; depicted by a green triangle). Pictures were taken after 7 days of incubation in continuous light. (E) Pulse-amplitude modulation (PAM) fluorometry of *Synechocystis* WT (black line) in comparison to Δ*sbtB* (red line) and Δ*dacA* (blue line) cells before and after 1, 2, and 3 days of prolonged dark treatment. PAM fluorometry was either measured in absence (left; zero μE) or at constant 56 μE of actinic light (right). (F) Whole cell spectra of *Synechocystis* WT (black line) in comparison to Δ*sbtB* (red line) and Δ*dacA* (blue line) before (top, left) and after 1 (top, right), 2 (bottom, left), and 3 (bottom, right) days of dark treatment. The peak representing phycobilisomes at 620 nm as well as the peak representing chlorophyll a at 680 nm are depicted by black arrows. Cultures were mathematically normalized to similar OD_{750}.

Table S1. List of plasmids and primers used in this study

Primers/ amplification	Sequence (5′→3′)	Note/ Ref.
Creation of Δ*dacA* insertion mutant (pUC19-DacA_ins. plasmid)		
Downstream of *sll0505*	FW_Down-sll0505 ATATGTGATGGGTTAAAAAGGATCGATCCTCTAGCTAGAGGACGTAAATTTCGGCGTAGG	This study
	RV_Down-sll0505 TAGCTATAAATTATTTAATAAGTAAGTTAAGGGATGCAGGTACTCAG GCGTTTGCTTTGG	This study
Upstream of *sll0505*	FW_Up-sll0505 TGCACGGATCTGCCCTGGCTTCAGGAGATCGGAAGACCTCGAAAGC CCGACATGGGTAAG	This study
	RV_Up-sll0505 CACTTCATCCGGGGTCAGCACCACCGGCAAGCGCCGCGACTACCAA AGGCTTGACCTACG	This study
Kanamycin resistance cassette	KanRpVZ_0505down_fw ATGCTCGATGAGTTTTTCTAACGCCCTCATGGTGATGGAAG	This study
	KanRpVZ_0505_up_rv GCTCGAATTGACATAAGCCTGTTCCCAATCCGATTTTGGGACAGTTCC	This study
	0505up_KanRpVZ_fw CTGTCCCAAAATCGGATTGGGAACAGGCTTATGTCAATTCGAGCTCG	This study
	0505down_KanRpVZ_rv CATCACCATGAGGGCGTTAGAAAAACTCATCGAGCATCAAATGAAAC TGC	This study
Up- and downstream of *sll0505* + KanR	pUC19_05up_fw CAATTTCACACAGGAAACAGCTATGACCATGATTACGCCAATGTCGG GCTTTCCCCC	This study
	pUC19_0505down_rv TTTTCCCAGTCACGACGTTGTAAAACGACGGCCAGTGAATTTCATTTT TTGTCGTTTTGGGCAGTTGAG	This study
Creation of Δ*dacA* deletion mutant (pUC19-DacA_del. plasmid)		
Upstream of *sll0505*	1670: Fw_Up-sll0505-DacA TGCACGGATCTGCCCTGGCTTCAGGAGATCGGAAGACCTCGAAAGCCCGACATGGGTAAG	This study
	1671: Rv_Up-sll0505-DacA CACTTCATCCGGGGTCAGCACCACCGGCAAGCGCCGCGACTACCAAAGGCTTGACCTACG	This study
Downstream of *sll0505*	1672: Fw_Down-sll0505-DacA ATATGTGATGGGTTAAAAAGGATCGATCCTCTAGCTAGAGGACGTAAATTTCGGCGTAGG	This study
	1673: Rv_Down-sll0505-DacA TAGCTATAAATTATTTAATAAGTAAGTTAAGGGATGCAGGTACTCAGGCGTTTGCTTTGG	This study
Up- and downstream of *sll0505* + spectinomycin resistance cassette	1777: Fw_Down-sll0505-DacA_pUC19 TGTAAAACGACGGCCAGTGAATTCGAGCTCGGTACCCGGGGACGTAAATTTCGGCGTAGG	This study
	1778: Rv_Up-sll0505-DacA_pUC19 ATGACCATGATTACGCCAAGCTTGCATGCCTGCAGGTCGATACCAAAGGCTTGACCTACG	This study
Creation of Δ*sbtB* deletion mutant (pRL270-SbtB_del. plasmid)		
Upstream of *slr1513*	1275_Fw: GAATAAATAAATCCTGGTGTCCCTGTTGATACCGGGAAGCCATCAA CAATAACTAGGCTTGTTTC	(20)
	1276_Rv:CCATATTGGCCACGTTTAAATCAAAACTGGTGAAACTCACCGGCCA TCATCGAAGTGGAAG	(20)
Downstream of *slr1513*	1277_Fw:AGGTATATGTGATGGGTTAAAAAGGATCGATCCTCTAGAGCTGCTG CTGCTAGTATTGAG	(20)
	1278_Rv: TAGCTATAAATTATTTAATAAGTAAGTTAAGGGATGCAGGTTTGTT TATCTCCTAGAAGTATGTAAG	(20)
Creation of Δ*glgB* deletion mutant (pUC19-GlgB_del. plasmid)		
Upstream of *sll0158*	glgB_US_fw: GACCATGATTACGCCAAGCTTGCATGCCTGCAGGTCGACTAACCCCCGTCATTGGCATCAAT ATC	This study
	glgB_US_rev: GGATTTATTTATTCTGCGAATCGGCTATGGTGATTTTTTG	This study
Downstream of *sll0158*	glgB_DS_fw: ATCAGCAGGGAAGAAATTGGTTATAACTGAGTTAGCGATAATTTTC	This study
	glgB_DS_rev: CGGCCAGTGAATTCGAGCTCGGTACCCGGGGATCCTCTAGGACGATCAACCAGCCCAGGAG	This study
Cm resistance cassette	CmR_fw: CAAAAAATCACCATAGCCGATTCGCAGAATAAATAAATCC	This study
	CmR_rev: GAAAATTATCGCTAACTCAGTTATGAGTTTGTAGAAACGCAAAAAG	This study

Creation of Δ*sbtA* deletion mutant (pUC19-SbtA_del. plasmid)		
Downstream of *slr1512*	SbtAB_Apa5 GGGCCCTTTCATCCCGCTCAATCAGG	This study
	SbtAB_Sac3 GAGCTCTCAAACCGGCCAGTATTGAC	This study
Upstream of *slr1512*	DelSbtA_Bam_5 GGATCCGGACAAAAAATCCATAATG	This study
	DelSbtA_Bam_3 GGATCCCCAATAGTTTATGGTC	This study
Complementation of Δ*sbtB* by re-introducing *slr1513* under the control of *psbA2* promoter (pFLAG-SbtB_psbA2 plasmid)		
	FW_pFLAG-SbtB CAATCTGAACATCGACAAATACATAAGGAATTATAACCATATGGCTAA ACCAGCGAACAAG	This study
	RV_pFLAG-SbtB GTTGAATAAATCGAACTTTTGCTGAGTTGAAGGAAGATCTTTAACAGC CCTCAGGGCCA	This study
Generation of SbtB-sfGFP under the native promotor of *slr1513* (pVZ322-SbtB-sfGFP)		
SbtB-sfGFP	pVZ-Seq_Fw: CAGCTCCATAGGCCGCTTTC	(20)
	pVZ-Seq_Rv: GCTGCCCGGATTACAGATC	(20)
Recombinant proteins		
StrepII-tagged *Sl*SbtB (*slr1513*); (pASK-*Sl*SbtB-strep plasmid)	1256_Fw: GTGAAATGAATAGTTCGACAAAAATCTAGATAACGAGGGCAAAAAATG GCTAAACCAGCGAACAAGCTCG	(20)
	1257_Rv: AAGCTTATTATTTTTCGAACTGCGGGTGGCTCCAAGCGCTACAGCCCT CAGGGCCACAGAAAG	(20)
StrepII-tagged *Ns*SbtB (*all2133*); (pASK-*Ns*SbtB-strep plasmid)	1664: Fw_all2133_CT strep GTGAAATGAATAGTTCGACAAAAATCTAGATAACGAGGGCAAAAAATGGCCAAGCCAGCCA AAAAG	This study
	1665: Rv_all2133_CT strep CAAGCTTATTATTTTTCGAACTGCGGGTGGCTCCAAGCGCTACAGCCGTCTGGTCCGC	This study
His8-tagged *Sl*SbtB (*slr1513*); (pET28a-*Sl*SbtB-His8 plasmid)	FW_pET28a-SbtB CTAGAAATAATTTTGTTTAACTTTAAGAAGGAGATATACCATGG CTAAACCAGCGAACAA	This study
	RV_pET28a-SbtB CAGCCGGATCTCAGTGGTGGTGGTGGTGGTGGTGGTGCGAACA GCCCTCAGGGCCACAG	This study
His_6-tagged GlgB (*sll0158*); (pET15b-GlgB-His_6 plasmid)	Fw_GlgB-N-His ATCATCATCACAGCAGCGGCCTGGTGCCGCGCGGCAGCCATATGAC CTACACCATCAACGC	This study
	Rv_GlgB-N-His TCAGCTTCCTTTCGGGCTTTGTTAGCAGCCGGATCCTCGAGCTAAGCT ATGTTGCTAGCCTCTTC	This study
DacA-GFP (sll0505); (pET28a-DacA-eGFP plasmid)	1762: Fw_DacA-eGFP CTAGAAATAATTTTGTTTAACTTTAAGAAGGAGACTCGAGATGTCGGGCTTTCCCCCG	This study
	1763: RV_DacA-eGFP CTCCTTTGCTGAATTGACCCTGGAAGTACAGGTTTTCGGATTTTTTGTCGTTTTGGGCAGTT GAGG	This study
BACTH constructs		
SbtB-BACTH; (pKT25_SbtB plasmid)	pKT25_sbtb_fw: CGATTACCTGGCGCGCACGCGGCGGGCTGCAGGGTCGACTATGGCTAAACCAGCGAACAA G	This study
	pKT25_sbtb_rev: GGCCGAATTCTTAGTTACTTAGGTACCCGGGGATCCTCTAGTTAACAGCCCTCAGGGCCAC	This study
GlgB-N (*sll0158*_N); (pUT18_GlgB_N plasmid)	pUT18 glgB sll0158 fw GACCATGATTACGCCAAGCTTGCATGCCTGCAGGTCGACTATGACCTACACCATCAACG	This study
	pUT18 glgB sll0158 rev CCTCGCTGGCGGCTGAATTCGAGCTCGGTACCCGGGGATCAGCTATGTTGCTAGCCTCTTC	This study
GlgB-C (*sll0158*_C); (pUT18_GlgB_C plasmid)	pUT18c glgB sll0158 fw GCCGTCGCTGGGCGCAGTGGAACGCCACTGCAGGTCGACTATGACCTACACCATCAACG	This study
	pUT18c glgB sll0158 rev TTAGTTATATCGATGAATTCGAGCTCGGTACCCGGGGATCAGCTATGTTGCTAGCCTCTTC	This study

Table S2: Crystallographic data collection and refinement statistics

Structure	*St*SbtB:c-di-AMP complex
PDB code	7OBJ
Data collection	
Space group	$P3_2$
Cell parameters	a = b = 63.2 Å, c = 81.7 Å
Wavelength (Å)	1.00
Resolution limits (Å)[a]	32.74 – 2.00 (2.12 – 2.00)
Unique reflections	24685 (3942)
Completeness (%)	99.7 (98.3)
I/σI	20.61 (1.03)
Redundancy	10.3 (10.1)
R_{merge} (%)	6.4 (223.1)
CC(1/2)	100 (43.1)
Refinement	
Resolution limits (Å)	32.74 – 2.00 (2.05 – 2.00)
R_{cryst}(%)	17.8 (37.6)
R_{free} (%)	21.5 (38.7)
Protein molecules per asymmetric unit cell	3
Mean B value (Å^2)	58.0
Ramachandran statistics	
Core regions (%)	95.0

[a]Values in parentheses refer to the highest-resolution shell.

Publication 4: Research article

Doello, S.; **Neumann, N.**; Forchhammer, K.

Regulatory phosphorylation event of Phosphoglucomutase 1 tunes its activity to regulate glycogen metabolism.

FEBS Journal • Vol 289, No. 19

The FEBS Journal

FEBS PRESS science publishing by scientists

Regulatory phosphorylation event of phosphoglucomutase 1 tunes its activity to regulate glycogen metabolism

Sofía Doello, Niels Neumann and Karl Forchhammer

Interfaculty Institute of Microbiology and Infection Medicine, University of Tübingen, Germany

Keywords
carbon metabolism; cyanobacteria; glycogen; phosphoglucomutase; phosphorylation

Correspondence
K. Forchhammer, Interfaculty Institute of Microbiology and Infection Medicine, University of Tübingen, Auf der Morgenstelle 28, 72076 Tübingen, Germany
Tel: +4970712972096
E-mail: karl.forchhammer@uni-tuebingen.de

(Received 17 December 2021, revised 25 March 2022, accepted 3 May 2022)

doi:10.1111/febs.16471

Regulation of glycogen metabolism is of vital importance in organisms of all three kingdoms of life. Although the pathways involved in glycogen synthesis and degradation are well known, many regulatory aspects around the metabolism of this polysaccharide remain undeciphered. Here, we used the unicellular cyanobacterium *Synechocystis* as a model to investigate how glycogen metabolism is regulated in nitrogen-starved dormant cells, which entirely rely on glycogen catabolism to resume growth upon nitrogen repletion. We identified phosphoglucomutase 1 (PGM1) as a key regulatory point in glycogen metabolism, and post-translational modification as an essential mechanism for controlling its activity. We could show that PGM1 is phosphorylated ata residue in the regulatory latch domain (Ser 47) during nitrogen starvation, which inhibits its activity. Inactivation of PGM1 by phosphorylation at Ser 47 prevents premature degradation of the glycogen stores and appears to be essential for survival of *Synechocystis* in the dormant state. Remarkably, this regulatory mechanism seems to be evolutionary conserved in PGM1 enzymes, from bacteria to humans.

Introduction

Glycogen is the major carbohydrate storage compound in a broad range of organisms, from bacteria to humans. This polysaccharide is composed of glucose molecules connected by α,1-4 linkages and branched via α,1-6 linkages, and it is generally considered a carbon sink with energy-storage function. In humans, glycogen is mainly accumulated in the liver and skeletal muscle, and it constitutes a rapid and accessible form of energy that can be supplied to tissues on demand [1]. In many bacteria, glycogen plays a crucial role in survival to an ever-changing environment. It is usually synthesized and accumulated inside the cells under growth-limiting conditions at excess of a carbon source, and degraded when the supply of energy or carbon is not enough to maintain growth or viability, thus allowing cell survival in transient starvation conditions [2]. In cyanobacteria, which generally sustain cell growth by performing oxygenic photosynthesis, glycogen is synthesized towards the end of the day, when photosynthetically fixed carbon is in excess and cells need to prepare to survive the night [3]. Glycogen accumulation also occurs as a response to nutrient limitation. In fact, the greatest amount of glycogen accumulation in non-diazotrophic cyanobacteria, which are unable to fix atmospheric N_2, occurs under nitrogen starvation conditions [4].

Nitrogen deprivation activates a genetically determined survival program in non-diazotrophic cyanobacteria, which has been extensively studied in the unicellular cyanobacterial strains *Synechococcus elongatus* and *Synechocystis* sp. PCC 6803 (from now *Synechocystis*) [5,6]. When *Synechocystis* encounters nitrogen depletion, the intracellular carbon/nitrogen balance is disturbed, and growth can no longer be

Abbreviations
COBALT, Constraint-based Multiple Alignment Tool; PAGM, phosphoacetylglucosamine mutase; PGM/PMM, phosphogluco/phosphomanno mutase; PGM1, phosphoglucomutase 1; PGM2/PGM2L1, phosphopentomutase/glucose-1,6-bisphosphate synthase; PMM, phosphomannomutase; PNGM, phosphoglucosamine mutase; α-D-PHM, α-D-phosphohexomutase.

supported. This metabolic situation leads to rapid accumulation of glycogen, which serves as a sink for the excess of carbon [5]. To survive these starvation conditions, cells undergo an adaptation process termed chlorosis that involves the degradation of the light-harvesting complexes to avoid an excess of energy and reduction equivalents that are no longer consumed by anabolic reactions. As a result of the metabolic and morphological changes induced by nitrogen starvation, cells enter a dormant state, which allows them to survive adverse conditions for a prolonged period of time [6]. Upon nitrogen availability, the glycogen stores accumulated in dormant cells play a key role in the restoration of vegetative growth [7]. When dormant cells have access to a nitrogen source, their metabolism switches towards a glycolytic phase. They turn off residual photosynthesis,while the production of energy and metabolic intermediates now entirely relies on glycogen catabolism [8]. This extraordinary situation, in which carbohydrate degradation can be completely separated from photosynthetic processes even in the presence of light, makes awakening *Synechocystis* cells an excellent model to study the regulation of glycogen catabolism.

Although the metabolic pathways involved in glycogen synthesis and degradation are well known, many regulatory aspects around the metabolism of this polysaccharide remain to be deciphered. In nitrogen-starved *Synechocystis* cells, glycogen degradation is known to start soon after addition of a nitrogen source, and the enzymes responsible for this process have been identified (Fig. 1) [7]. However, how glycogen catabolism is induced in dormant cells has not yet been elucidated. The enzymes involved in glycogen metabolism are conserved from bacteria to humans. The glycogen phosphorylase and debranching enzyme are responsible for the excision of glucose molecules from the glycogen granule, releasing glucose-1-phosphate (glucose-1P) and glucose, respectively. Glucose-1P is then converted to glucose-6-phosphate (glucose-6P) by the phosphoglucomutase (PGM), an evolutionary conserved enzyme that also catalyzes the reverse reaction, while glucose is converted to glucose-6P by the glucokinase. Glucose-6P can then enter different catabolic pathways to produce glyceraldehyde-3-phosphate. Intriguingly, most of the glycogen catabolic enzymes are up-regulated during nitrogen starvation, although glycogen degradation does not start until a nitrogen source is available. This suggests that the activity of these enzymes must be tightly regulated: They must remain inactive when cells are dormant and be activated upon nitrogen availability. An exception to the abundance pattern of most glycogen catabolic enzymes is PGM1, the expression of which is

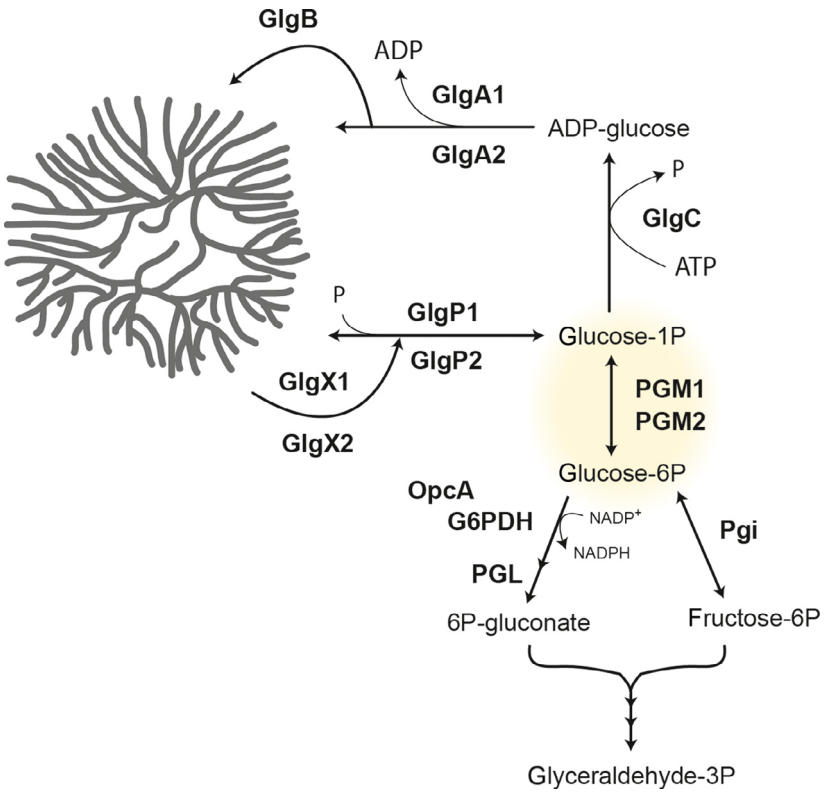

Fig. 1. Schematic representation of the glycogen metabolic hub in *Synechocystis*. Glycogen is synthesized by the glycogen synthases (GlgAs) and branching enzyme (GlgB) from ADP-glucose, which is obtained from glucose-1-phosphate (glucose-1P) through the reaction catalyzed by the glucose-1-phosphate adenylyltransferase (GlgC). Glycogen catabolism starts with the glycogen phosphorylases (GlgPs) and debranching enzymes (GlgXs). The glucose-1P released by GlgPs is converted to glucose-6-phosphate (glucose-6P) by the phosphoglucomutases (PGMs). Glucose-6P can be metabolized by the phosphoglucoisomerase (Pgi) to enter the Embden-Meyerhof-Parnas pathway or by the glucose-6P dehydrogenase (G6PDH), which requires the activator protein OpcA, to enter the oxidative pentose phosphate pathway and the Enter-Doudoroff pathway. Ultimately, all pathways generate glyceraldehyde-3-phosphate (glyceraldehyde-3P).

suppressed under nitrogen starvation and activated during resuscitation [8,9]. Although *Synechocystis* possesses two PGM isoenzymes, PGM1 (*sll0726*) has been shown to be responsible for almost 97% of the PGM activity [10], while PGM2 (*slr1334*) serves as glucose-1,6-bisphosphate synthase [11]. PGM1 was recently identified as a phosphoprotein with two localized serine phosphorylation sites: Ser 47 and Ser 152. Ser 152 corresponds to the catalytically active serine residue, which mediates the phosphoryl transfer between the sugar and the enzyme. Initial phosphorylation of this catalytic serine residue is provided by the activator glucose-1,6-bisphosphate [11]. During chlorosis, the degree of phosphorylation of this residue decreases. On the contrary, the phosphorylation of Ser 47 strongly increases during nitrogen starvation, representing one of the most strongly induced phosphorylation events [9]. The function of this serine residue is so far unknown; previous studies have not considered it to be involved in catalysis or regulation of PGM1 activity [12,13]. These findings prompted us to investigate the possible involvement of PGM1 in the regulation of glycogen metabolism, leading to the identification of a key regulatory mechanism in glycogen catabolism, which seems to be conserved from bacteria to humans.

Results

PGM1 is activated during resuscitation from nitrogen starvation

Our previous studies suggested the occurrence of an unknown mechanism controlling the activity of glycogen catabolic enzymes in *Synechocystis*: The transcription of most glycogen catabolic genes is highly up-regulated during nitrogen deprivation when glycogen is synthesized, but turned down during resuscitation when glycogen is catabolized [7,14]. In agreement, a proteomic study showed increased abundance of these enzymes in the dormant state and return to normal levels during resuscitation (Fig. 2A) [9]. One exception to this expression pattern is PGM1, the abundance of which is low during nitrogen starvation and increases during resuscitation (Fig. 2A). In the same study, a quantitative analysis of the phosphorylation events during nitrogen starvation and resuscitation revealed that PGM1 can be phosphorylated at two different serine residues. Due to an incorrect annotation of PGM1 in CyanoBase [15], the residues previously designated as Ser 63 and Ser 168 [9] correspond to the residues Ser 47 and Ser 152 of PGM1 (see below, Fig. 3). Interestingly, Ser 47 is one of the most strongly phosphorylated residues in chlorotic cells, being 13 times more phosphorylated under nitrogen starvation than during vegetative growth (Fig. 2B). These findings suggested that PGM1 might be a regulatory point, ensuring that glycogen catabolism is arrested in the chlorotic state until nitrogen becomes available again.

To test whether there was any change in the activity of PGM1 upon addition of a nitrogen source to dormant cells, we assayed PGM1 activity in cell extracts from chlorotic and resuscitating cells (Fig. 2C). While some PGM1 activity was detectable in nitrogen-starved cells, the measured activity was three times higher in cells supplemented with nitrate 24 h before. These results suggested an activation of PGM1 upon addition of nitrogen to chlorotic cells. Analysis of the levels of glucose-phosphates during nitrogen starvation and resuscitation supported this idea because higher levels of glucose-1P and glucose-6P, the substrates of PGM1, were detected in chlorotic than in recovering cells (Fig. 2D). Given the significant phosphorylation changes detected in PGM1 during nitrogen starvation, we hypothesized this post-translational modification could regulate enzyme activity in the different developmental stages.

PGM1 has two phosphorylation sites with opposite phosphorylation dynamics

According to homology modeling of PGM1, Ser 152 is the catalytic serine residue involved in the phosphor-exchange reaction. This residue is highly conserved in the members of the α-D-phosphohexomutase (α-D-PHM) superfamily, and it is located in the active site of PGM1 (marked in green in Fig. 4A). This catalytic serine is poorly phosphorylated during nitrogen starvation, and it progressively becomes more phosphorylated during resuscitation (Fig. 2B). As phosphorylation of the catalytic serine is required for catalysis, the phosphorylation dynamics of this residue corresponds to its state of catalytic activity, with PGM1 being inactive in chlorotic cells and becoming activated during resuscitation. Ser 47 follows the opposite pattern: The high level of phosphorylation of this residue under nitrogen starvation progressively decreases during resuscitation (Fig. 2B). As deduced from homology modeling, Ser 47 is located on the surface of the enzyme, in a loop known as 'the latch' (marked in red in Fig. 4A). The phosphorylation dynamics of Ser 47 was confirmed using clear native PAGE – immunoblot analysis. Because Ser 47 is on the surface of the enzyme, the addition of a phosphate group to this residue affects the net charge of the protein and influences its migration in a native gel, whereas phosphorylation of

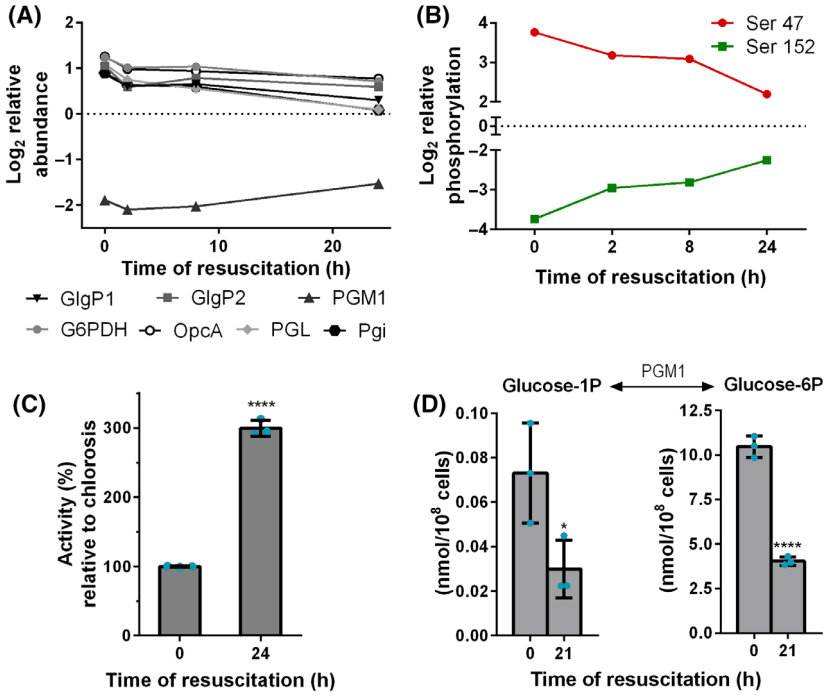

Fig. 2. Abundance, phosphorylation and activity of PGM1 during nitrogen starvation and resuscitation. (A) Protein abundance ratios of GlgP1, GlgP2, PGM1, G6PDH, OpcA, PGL, and Pgi during resuscitation from nitrogen starvation. Ratios were calculated comparing the protein abundance during nitrogen starvation and resuscitation with their abundance during vegetative growth. Relative abundance is shown as the $\log_2$ of the calculated ratios. Positive values indicate up-regulation and negative values down-regulation compared to protein levels during vegetative growth (normalized to zero, dotted line) [9]. (B) Phosphorylation events of the two phosphorylation sites in PGM1 at the indicated time points during resuscitation from nitrogen starvation. Ratios were calculated comparing the abundance of phosphorylated and unphosphorylated peptides at different time points during resuscitation to their abundance during vegetative growth. Relative phosphorylation is shown as the $\log_2$ of the calculated ratios [9]. (C) Relative enzyme activity of PGM1 in cell extracts from chlorotic and resuscitating cells. The activity in chlorotic cells (53.87 U·mg^{-1}) was considered as 100%. (D) Glucose-1P and glucose-6P content normalized to 10^8 cells during nitrogen starvation and resuscitation. For (C) and (D) at least three biological replicates were measured. Error bars represent the standard deviation (SD). Asterisks represent the statistical significance: one asterisk represents $P \leq 0.05$, two asterisks $P \leq 0.01$, three asterisks $P \leq 0.001$, and four asterisks $P \leq 0.0001$.

Ser 152, which is buried in the catalytic center, does not. As shown in Fig. 4B, after 24 h of nitrogen starvation a lower band appeared in the gel, which represents PGM1 phosphorylated at Ser 47 (PGM1^2). After 7 days of chlorosis, only the lower band is observed. The upper band, which represents PGM1 dephosphorylated at Ser 47 (PGM1^1), is only observed again 8 h after resuscitation was initiated. To confirm that the different bands correspond to different phosphorylation states of PGM1, cell extracts from chlorotic cells were prepared in the absence of phosphatase inhibitors and treated with alkaline phosphatase. Under these conditions, most of PGM1 was detected in the upper band, corresponding to the non-phosphorylated state (Fig. 4B).

While the residue Ser 152 in *Synechocystis* PGM1 is conserved throughout the α-D-PHM superfamily, since it directly participates in catalysis, Ser 47 appears to be subfamily-specific. The α-D-PHM superfamily comprises different classes of enzymes, which share a common structure and mechanism of catalysis [16]. The Conserved Domain Database (CDD) classifies the members of the α-D-PHM superfamily into different subfamilies according to their domain architecture [17]. Based on their substrate specificities, these subfamilies can be grouped into: phosphoglucomutases or PGM1 (cd03085 and cd05801), phosphomannomutases or PMM (cd03088), bifunctional phosphogluco/phosphomanno mutases or PGM/PMM (cd03089), phosphoglucosamine mutases or PNGM (cd05802), phosphoacetylglucosamine mutases or PAGM (cd03086), phosphopentomutases/glucose-1,6-bisphosphate synthases or PGM2/PGM2L1 (cd05799), and enzymes of unknown function (cd03087, cd05800, and cd05803). The residue Ser 47 is located in the latch loop and as shown in the phylogenetic tree in Fig. 4C, it is conserved in the members of the subfamilies cd05801 and cd03085, which are PGM1 enzymes. According to

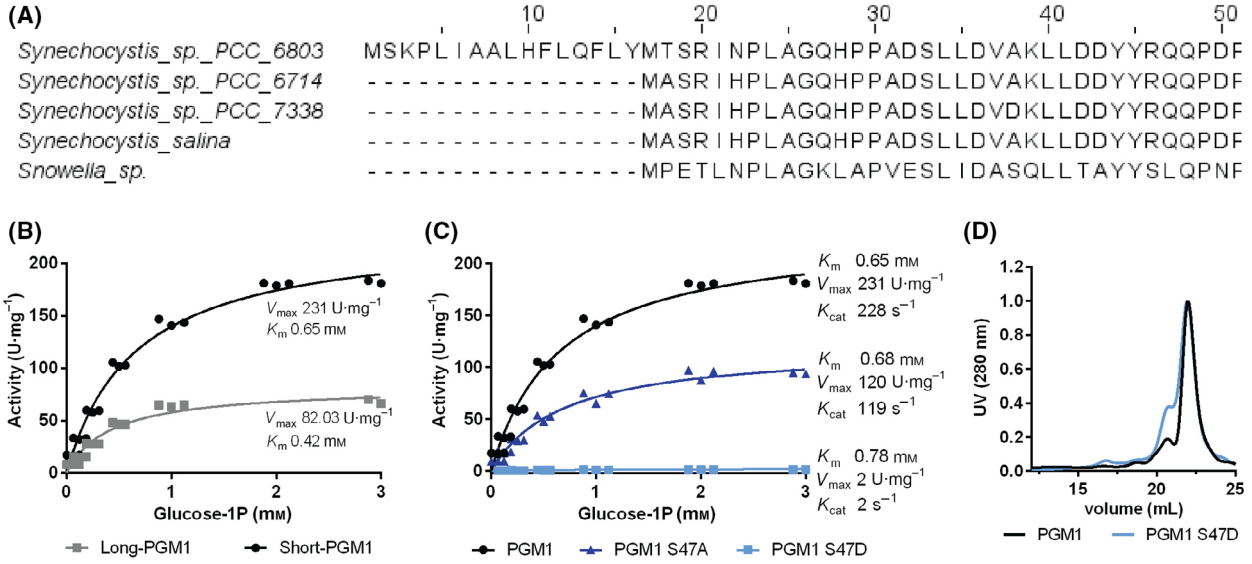

Fig. 3. *In vitro* characterization of wild type PGM1 and phosphomimetic variants. (A) Alignment of PGM1 sequences from different *Synechocystis* strains. Sequences were aligned using NCBI COBALT and edited with Jalview [46]. (B) Enzymatic characterization of the two versions of PGM1. Long-PGM1 and Short-PGM1 represent the enzyme from *Synechocystis* sp. PCC 6803 with or without the 16-amino acid N-terminal extension that is absent in the annotation of the other strains, respectively. (C) Michaelis-Menten kinetics of wild type (WT) PGM1, PGM1 S47A, and PGM1 S47D. Three replicates were measured for each data-point. (D) Size exclusion chromatography of PGM1 and PGM1 S47D. The UV signal at 280 nm is shown.

structural studies on enzymes from the cd05801 and cd03089 subfamilies, this loop participates in a conformational change required for catalysis and in stabilization of the substrate through interaction with the phosphorylated end of the sugar [18–21]. The presence of a residue with a phosphorylatable hydroxyl group in its side chain at the position of Ser 47 might be a determinant for phosphoglucomutase reaction velocity since the subfamilies that have high phosphoglucomutase activity (cd03085, cd05801, cd03088 and cd03089) [13,19,21–24] present Ser or Tyr at this site, while the subfamilies presenting Ala (cd03086, and cd05799) or Asp (cd05802) at this position possess low phosphoglucomutase activity [11,25–27].

Phosphorylation of PGM1 at Ser 47 inhibits its activity

To gain more insights into the role of Ser 47 in catalysis, we created different recombinant PGM1 variants with site-specific amino acid substitutions. Analysis of the sequences of PGM1 from several *Synechocystis* strains revealed a different annotation for *Synechocystis* sp. PCC 6803, which included a 16-amino acid N-terminal extension that is missing in the other strains (Fig. 3A). Additionally, the experimentally validated transcriptional start site from *Synechocystis* sp. PCC 6803 suggests a shorter open reading frame for PGM1, with Met 17 as putative translational start site [28]. To clarify if the N-terminal extension is an annotation error, we prepared as recombinant proteins the PGM1 as annotated in Cyanobase [15] (Long-PGM1) and a version without the 16-amino acid N-terminal extension (Short-PGM1). We then measured their activity *in vitro*, assuming that the native version exhibits higher activity. Although both versions showed a similar substrate affinity, as deduced from the calculated Michaelis-Menten constant (K_m), the maximal velocity(V_{max}) of the reaction was almost three-fold higher for the short version (Fig. 3B), substantiating that the short version likely represents the physiologically relevant protein. The different PGM1 variants were therefore created from the Short-PGM1 version (hereafter referred to as PGM1). To elucidate the importance of the interactions of the hydroxyl group of Ser 47 in catalysis, this residue was replaced by Ala (PGM1 S47A), a smaller and hydrophobic residue. Comparison of the kinetic parameters of the wild-type (WT) PGM1 and PGM1 S47A showed that the substitution of Ser for Ala at position 47 affected the V_{max} of the reaction, which decreased almost two-fold, but it did not decrease substrate affinity, as shown by the K_m value (Fig. 3C). These results indicate that the interactions in which Ser 47 is involved are not essential but play a modulating rolein catalysis. Phosphorylation of this residue could therefore disturb these interactions and inhibit PGM1 activity. To estimate the effect of phosphorylation of this residue on enzyme activity, Ser 47 was substituted by Asp (PGM1

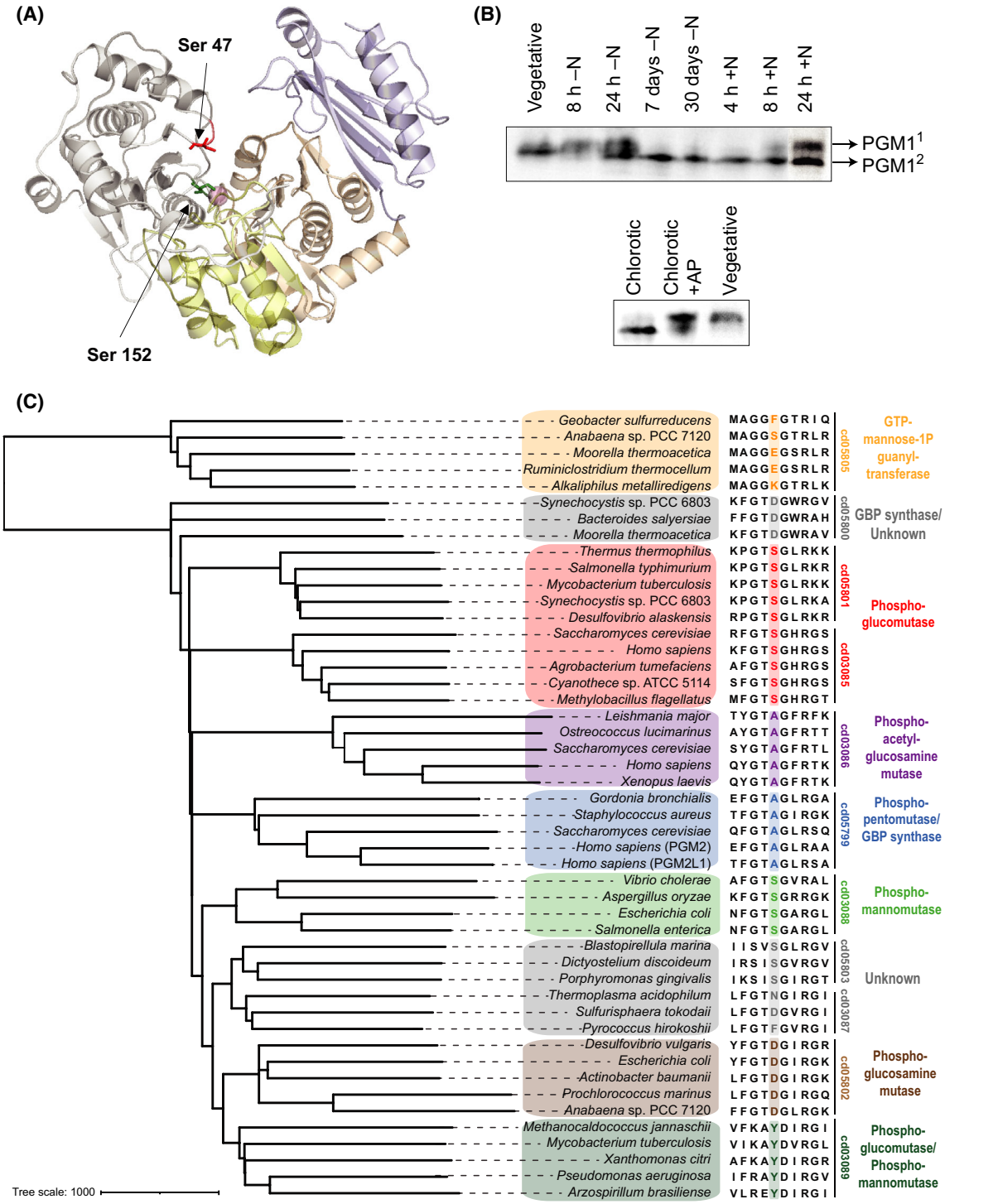

Fig. 4. Location and conservation of phosphorylation sites. (A) Structure of *Synechocystis* PGM1 obtained from Swiss Model using *Salmonella typhimurium*'s PGM1 as a template (Protein Data Bank code 3OLP). The two colored residues shown in a stick model represent the two phosphorylation sites: Ser 47 (and the latch domain) in red and Ser 152 in green. The Mg^{+} ion required for catalysis is shown as a pink sphere. Domain 1 is colored in grey, domain 1 in yellow, domain 3 in orange, and domain 4 in blue. (B) Clear native PAGE – immunoblot validation of PGM1 phosphorylation dynamics during nitrogen starvation, resuscitation, and after treatment with 1 $U{\cdot}mL^{-1}$ of alkaline phosphatase (AP) for 10 min. $PGM1^{1}$ and $PGM1^{2}$ represent PGM1 dephosphorylated and phosphorylated at Ser 47, respectively. Representative of $N = 3$. (C) Phylogenetic tree of the α-D-PHM superfamily showing conservation of the residue Ser 47 of *Synechocystis*.

S47D), a larger and negatively charged amino acid that resembles a phosphorylated Ser. The purified PGM1 S47D seemed to be correctly folded, as deduced from its size exclusion chromatography elution profile (Fig. 3D), but presented very low activity *in vitro* (0.86% of the WT activity, Fig. 3C), showing that phosphorylation of Ser 47 inactivates PGM1.

Phosphorylation of PGM1 at Ser 47 is essential for survival under nitrogen starvation

To determine the physiological significance of phosphorylation of Ser 47 during nitrogen starvation in *Synechocystis*, we created and characterized various PGM1 mutant strains. A PGM1 knockout strain (Δ*pgm1*) could not properly acclimate to nitrogen-depletion and presented a so-called non-bleaching phenotype: Cells did not degrade their photosynthetic pigments and turned yellow, but stayed greenish instead, progressively looking paler (Fig. 5A). Quantitatively, the absorbance at 680/440 nm (indicative of chlorophyll *a*) and at 625 nm (indicative of phycobiliproteins) in the Δ*pgm1* strain did not significantly decrease during the first days of nitrogen starvation, in contrast to the WT (Fig. 5B). After 6 days of chlorosis, when the WT still shows residual peaks at the mentioned wavelengths, almost no pigment absorbance could be measured in the Δ*pgm1* strain. After 7 days of nitrogen starvation, a very reduced proportion of Δ*pgm1* cells could recover when they were dropped on an agar plate containing nitrate in comparison to the WT (Fig. 5C). Such a phenotype was previously observed in mutants that were

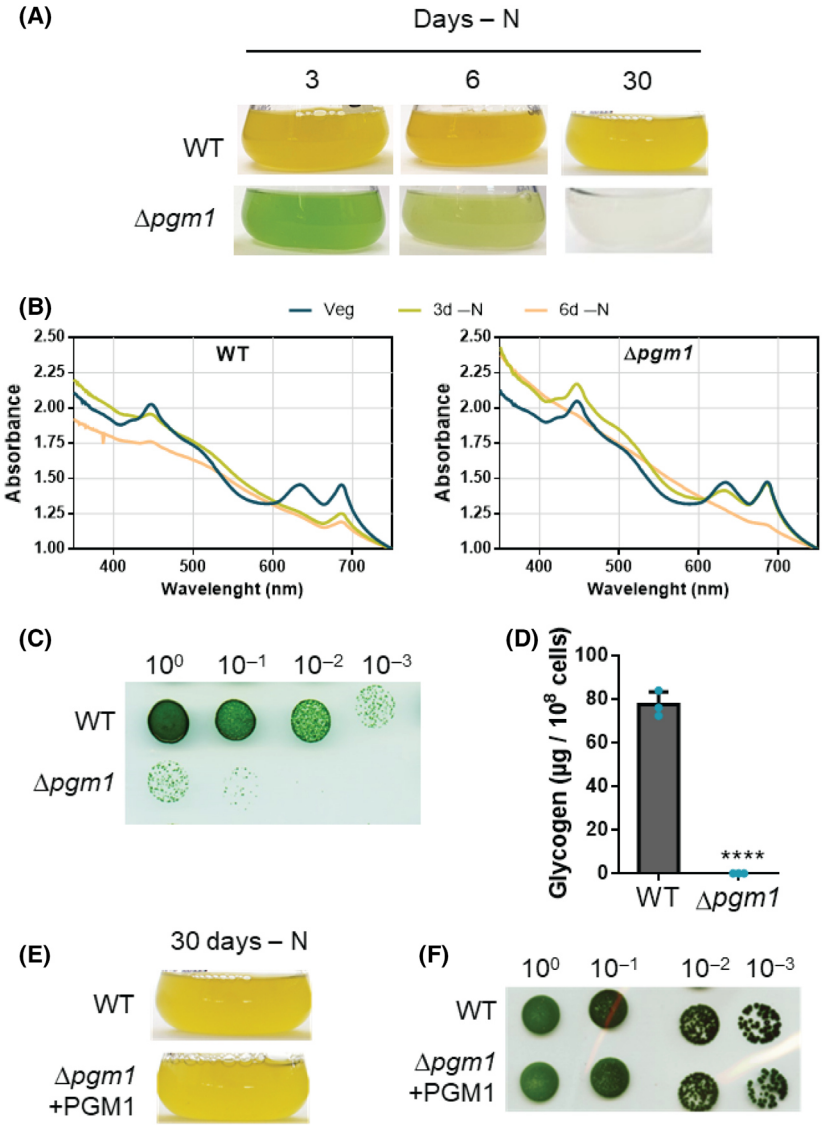

Fig. 5. Characterization of PGM1 knockout (Δ*pgm1*) and complementation strains (Δ*pgm1*+PGM1). (A) Pictures of WT and Δ*pgm1* cultures after 3, 6, and 30 days of nitrogen starvation. (B) Absorption spectra of WT and Δ*pgm1* during nitrogen starvation. (C) Recovery assay on a BG_{11}-agar plate of WT and Δ*pgm1* after 7 days of nitrogen starvation. Numbers on top represent the dilution factor, starting with an OD_{750} of 1. Pictures were taken 5 days after dropping chlorotic cells on the plate. (D) Glycogen content of WT and Δ*pgm1* after 7 days of nitrogen starvation. Three biological replicates were measured. Error bars represent the SD. Asterisks represent the statistical significance: one asterisk represents $P \leq 0.05$, two asterisks $P \leq 0.01$, three asterisks $P \leq 0.001$, and four asterisks $P \leq 0.0001$.(E) Pictures of WT and Δ*pgm1*+PGM1 cultures after 30 days of nitrogen starvation. (F) Recovery assay on a BG_{11}-agar plate of WT and Δ*pgm1*+PGM1. Numbers on top represent the dilution factor, starting with an OD_{750} of 1. Pictures were taken 7 days after dropping chlorotic cells on the plate.

impaired in glycogen synthesis[29], as accumulation of this polymer has been shown to be indispensable for adaptation to nitrogen-starvation. This phenotype was expected, given that PGM1 catalyzes the interconversion between glucose-1P and glucose-6P and is therefore involved in glycogen synthesis. Indeed, no glycogen was detected in seven-days-starved Δ*pgm1* cells (Fig. 5D), indicating that PGM1 activity is essential for glycogen synthesis under nitrogen deprivation and that the activity of PGM2 does not compensate the lack of PGM1. This is consistent with the fact that phosphorylation of Ser 47 is only detected after 24 h of nitrogen depletion (Fig. 3B), when synthesis of the glycogen stores has already taken place. Consequently, a strain with an inactive PGM1 variant, such as the PGM1 S47D, would not be able to enter the chlorotic state due to its inability to synthesize glycogen. To study the physiological consequences of the lack of PGM1 inactivation via phosphorylation, we complemented the Δ*pgm1* strain with the WT PGM1 (Δ*pgm1*+PGM1) and with the partially active PGM1 S47A variant (Δ*pgm1*+PGM1S47A), which lacks the phosphorylation site. Complementation with the WT protein rescued the phenotype: The Δ*pgm1*+PGM1 strain showed a similar behavior than the WT under nitrogen starvation (Fig. 5E,F). Conversely, the Δ*pgm1*+PGM1S47A strain could not successfully enter chlorosis. Although it seemed to induce pigment degradation upon nitrogen starvation (in contrast to the Δ*pgm1* strain), these cultures did not acquire the same characteristic yellowish colour than the WT, but a pale colour instead (Fig. 6A,B) and showed very poor recovery on nitrate-containing agar plates (Fig. 6C,D). This strain could not accumulate the same amount of glycogen than the WT (Fig. 6E), presumably due to the lower activity of the PGM1 S47A variant, which was not enough to meet the cellular demand. As the Δ*pgm1*+PGM1S47A strain failed to properly acclimate to nitrogen deprivation, we transformed WT cells with PGM1 S47A (WT+PGM1S47A) to study the impact of the presence of a PGM1 variant lacking phosphorylation of residue 47 on long-term nitrogen starvation. As expected,this strain could initially acclimate to nitrogendepletion like the WT (Fig. 6A,B), since it contains the WT version of PGM1. After 6 days of chlorosis, WT+PGM1S47A cells could recover as efficiently as WT cells on nitrate-containing agar plates (Fig. 6C). However, after prolonged exposure to nitrogen deprivation, when the WT version of PGM1 would be highly phosphorylated, the cultures of the WT+PGM1S47A strain progressively lost their yellowish color (Fig. 6A). After 1 month of starvation, only a reduced number of cells could recover following nitrogen repletion (Fig. 6D). WT+PGM1S47A cells could synthesize a similar amount of glycogen than WT cells upon nitrogen depletion, but after 1 week of starvation their glycogen content began to gradually decrease (Fig. 6E). These findings imply that inactivation of PGM1 via phosphorylation is crucial for preventing premature glycogen degradation during prolonged nitrogen starvation, which appears to be essential for survival of these conditions.

PGM1 regulation seems to be conserved from bacteria to humans

Regulation of PGM1 activity is crucial for the survival of a wide range of organisms to many different conditions. As all PGM1 enzymes present a phosphorylatable Ser residue at the site of Ser 47 of *Synechocystis*, the regulation of PGM1 activity via phosphorylation of this residue might not be exclusive to *Synechocystis*, but widespread among the cd05801 and cd03085 subfamilies. Indeed, phosphorylation of this residue has been detected in the PGM1 from mammals (Fig. 7A) [30,31]. In humans, PGM1 deficiency leads to glycogenosis, a metabolic disorder that causes the abnormal use and storage of glycogen, and congenital disorders of glycosylation. Despite the importance of the correct activity of this enzyme on human health, little is known regarding its regulation. Although Ser 20 of the human PGM1 (HPGM1), which is the homologous residue of *Synechocystis* PGM1 Ser 47 in the human enzyme, has been identified as a phosphorylation site [30], the role of phosphorylation of this residue has not been investigated. Lee et al. [32] investigated the effects of mutations present in patients suffering from PGM1 deficiency on the *in vitro* activity of the PGM1 enzyme and identified six mutations that compromised catalysis and six mutations that caused folding defects (Fig. 7B). Interestingly, a mutation in the latch loop (T19A) (Fig. 7C) severely affected the catalytic activity of the enzyme [32], suggesting that addition of a phosphate group to an adjacent residue in this loop (i.e. S20) might also inhibit catalysis, as we observed for *Synechocystis* PGM1. To ascertain this, we prepared recombinant HPGM1 along with a mutant variant in which Ser 20 had been substituted by Asp (HPGM1 S20D) and measured their activities *in vitro*. As presented in Fig. 7D, no enzyme activity was detected for the HPGM1 S20D variant, indicating that the phosphorylated form of the human enzyme is likely inactive.

Discussion

Regulation of glycogen metabolism is of vital importance in organisms of all three kingdoms of life. In

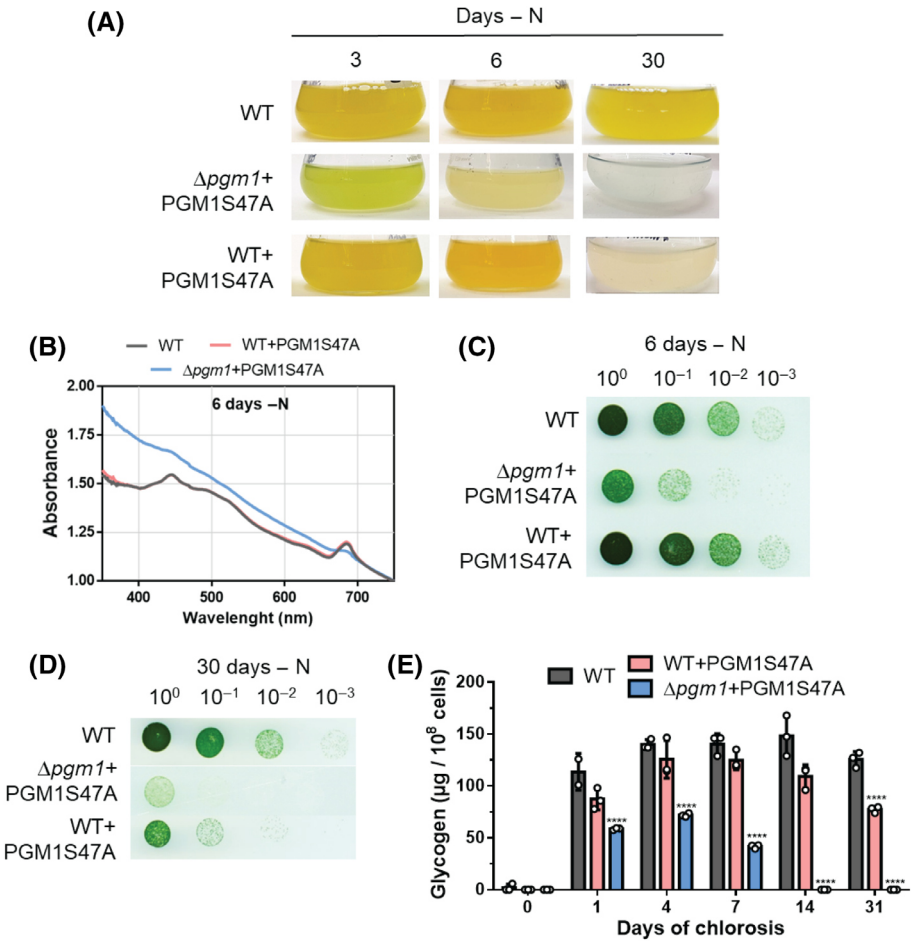

Fig. 6. Characterization of Δ*pgm1*+PGM1S47A and WT+PGM1S47A strains. (A) Pictures of WT, Δ*pgm1*+PGM1S47A, and WT+PGM1S47A cultures after 3, 6, and 30 days of nitrogen starvation. (B) Absorption spectra of WT Δ*pgm1*+PGM1S47A, and WT+PGM1S47A 6 days after nitrogen starvation. (C) Recovery assay on a BG_{11}-agar plate of WT, Δ*pgm1*+PGM1S47A, and WT+PGM1S47A after 6 days of nitrogen starvation. Numbers on top represent the dilution factor, starting with an OD_{750} of 1. Pictures were taken 5 days after dropping chlorotic cells on the plate. (D) Recovery assay on a BG_{11}-agar plate of WT, Δ*pgm1*+PGM1S47A, and WT+PGM1S47A after 30 days of nitrogen starvation. Numbers on top represent the dilution factor, starting with an OD_{750} of 1. Pictures were taken 5 days after dropping chlorotic cells on the plate. (E) Glycogen content of WT, Δ*pgm1*+PGM1S47A and WT+PGM1S47A at the indicated time points during nitrogen starvation. In all experiments, three biological replicates were measured. Error bars represent the SD. Asterisks represent the statistical significance: one asterisk represents $P \leq 0.05$, two asterisks $P \leq 0.01$, three asterisks $P \leq 0.001$, and four asterisks $P \leq 0.0001$.

bacteria, proper control of glycogen synthesis and degradation determines the ability to survive transient periods of nutrient starvation. In mammals, deficiencies in glycogen metabolism produce a variety of different metabolic disorders, some of them very severe [32]. In this study, we used the unicellular cyanobacterium *Synechocystis* to investigate the regulation of glycogen metabolism. During nitrogen starvation, the activity of the glycogen catabolic enzymes must be regulated to prevent premature glycogen degradation, so that cells can use this reserve polymer once the conditions are favourable for resuscitation. We could show that phosphorylation of PGM1 at a peripheral residue regulates its activity and is required to prevent premature glycogen degradation.

PGM1 is an evolutionary conserved enzyme that mediates one of the most important reactions incarbohydrate metabolism: It catalyzes the interconversion between glucose-1P and glucose-6P, being thereby involved in both, glycogen synthesis and degradation [33]. Despite its important role in sugar metabolism, PGM1 activity has only recently started to be considered as a target for metabolic control [34–37]. At the onset of nitrogen starvation, the activity of PGM1 is required for glycogen synthesis, as shown by the inability of a PGM1 knock-out mutant to synthesize

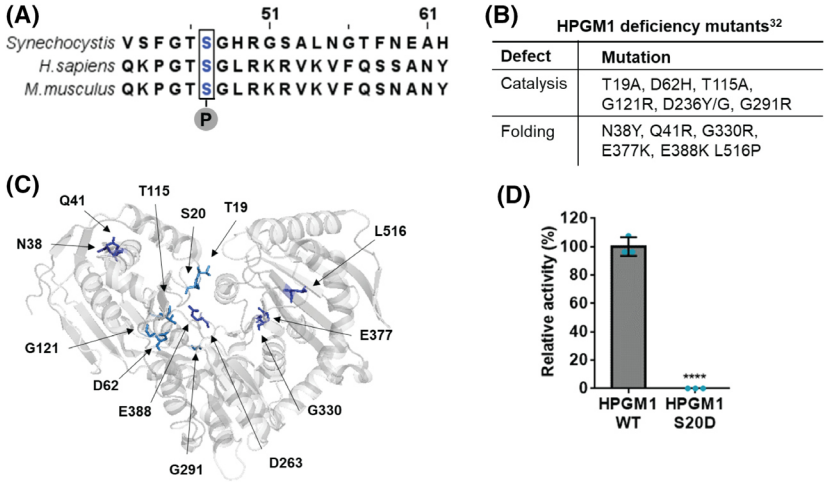

Fig. 7. Regulation of PGM1 by phosphorylation is conserved in mammals. (A) Alignment of the sequence of PGM1 from *Synechocystis*, *Homo sapiens*, and *Mus musculus*. The conserved phosphorylation site is marked in blue. Sequences were aligned using NCBI COBALT and edited with Jalview [46]. (B) List of human PGM1 (HPGM1) deficiency mutants and their associated defects [32]. (C) Structure of HPGM1 (Protein Data Bank code 5EPC) with relevant residues highlighted. (D) Relative *in vitro* activity of HPGM1 and HPGM1 S20D. The activity of WT PGM1 (170.9 U·mg^{-1}) was considered to be 100%. At least three replicates were measured. Error bars represent the SD. Asterisks represent the statistical significance: one asterisk represents $P \leq 0.05$, two asterisks $P \leq 0.01$, three asterisks $P \leq 0.001$, and four asterisks $P \leq 0.0001$.

glycogen. Hence, during the first hours of nitrogen starvation, PGM1 remains dephosphorylated at Ser 47, a residue located in the so-called latch loop. Once enough glycogen has been accumulated, PGM1 activity is inhibited by phosphorylation of Ser 47. This residue is highly phosphorylated in long-term-chlorotic cells, and *in vitro* characterization of a phosphomimetic variant of PGM1 (PGM1 S47D) indicates that the phosphorylated version of the enzyme is inactive. When a non-phosphorylated PGM1 S47A variant is present in chlorotic cells, glycogen is degraded after prolonged nitrogen starvation, leading to loss of viability. This highlights the pivotal role of Ser 47 phosphorylation for controlling glycogen metabolism.

Analysis of the PGM1 S47A variant indicated that the interactions in which Ser 47 is involved are important for modulating catalysis, as the V_{max} was two-fold lower in the PGM1 S47A variant than in WT PGM1, without impairing the substrate affinity. This is in line with structural studies of the reaction mechanism on related proteins, which suggested a role of Ser 47 in a conformational change occurring during catalysis [18–21]. When the enzyme is in its open conformation, its catalytic cleft is easily accessible for phosphorylated sugars. When the substrate enters the catalytic site, its dephosphorylated end interacts with the phosphorylated catalytic serine, and the phosphorylated end of the phosphor-sugar must interact with a group of residues from domain 4 (the phosphate-binding loop, colored in blue in Fig. 3A). In order for these residues to come in contact with the substrate, the enzyme must undergo a conformational change that involves a rotation of domain 4 and changes the active site from an open cleft to a closed pocket. This conformational change requires the interaction of a group of residues from the phosphate-binding loop with the residues from the latch loop (colored in red in Fig. 3A) [13,16,18,20,38]. When the hydroxyl group in the side chain of Ser 47 is eliminated by replacing it with Ala, the interactions that allow such conformational change and stabilization of the substrate are partially disturbed, which affects the velocity of the catabolic reaction. In the absence of the WT PGM1, a *Synechocystis* strain containing a non-phosphorylated PGM1 S47A variant accumulated only a reduced amount of glycogen, showing that the anabolic reaction is also affected with the substitution of Ser for Ala. When the site of Ser 47 is occupied by a negatively charged residue, as in the phosphomimetic variant or when the serine residue is phosphorylated, these interactions are completely disrupted, and catalysis is almost entirely inhibited.

Interestingly, Ser 47 is conserved among PGM1 enzymes (cd03085 and cd05801 subfamilies), and also in PMM enzymes (cd03088). In agreement with the finding that this residue is in volved in modulating K_{cat}, subfamilies that generally have high PGM1 activity [13,19,21–24] present a phosphorylatable amino acid (Ser or Tyr) at this site, while those subfamilies

that show low PGM1 activity and preferably catalyze the interconversion of other phosphor-sugars/amino sugars (cd05802, cd03086, and cd05799) [11,25–27] contain Asp or Ala at this position. The Ser residue in the latch loop has also been identified as a phosphorylation site in the PGM1 from mammals, which belong to the cd03085 subfamily. Even though PGM1 deficiency can cause severe disease in humans, its regulation remains under-investigated. HPGM1 is known to be phosphorylated and thereby activated by the p21-activated signaling kinase 1 (Pak1) on Thr 466 [33]. However, although Ser 20, the homologous of *Synechocystis* Ser 47, had previously been reported as a phosphorylation site in HPGM1 [30], the role of this phosphorylation on enzyme activity had not been characterized. We were able to demonstrate that, as in *Synechocystis*, HPGM1 is also inactivated by replacement of Ser 20 with a phosphomimetic residue. In agreement with our results, a study involving human patients suffering from PGM1 deficiency showed that introduction of a hydrophobic residue in the latch loop in HPGM1 led to a reduced enzyme activity (3.3% of the control) and caused disease in heterozygote patients [39]. These findings are in line with our physiological characterization of the Δ*pgm1*+PGM1S47A strain and suggest that the regulatory mechanism discovered in this study is conserved in PGM1 enzymes.

This work contributes to the understanding of the regulation of PGM1 activity, which plays a pivotal role in the central carbohydrate metabolism. We showed the existence of a phosphorylation event that modulates PGM1 activity to control glycogen synthesis and degradation, a regulatory mechanism that seems to be essential for survival of nutrient deprivation and evolutionary conserved from bacteria to humans. The molecular mechanisms that lead to this post-translational modification remain, nevertheless, to be deciphered.

Materials and methods

Cyanobacterial cultivation

The cyanobacterial strains used in this study are listed in Table 1. All strains were grown in BG_{11} supplemented with 5 mM $NaHCO_3$ for vegetative growth, as described previously [40]. Nitrogen starvation was induced as previously described by a 2-step wash with $BG_{11\text{-}0}$ medium supplemented with 5 mM $NaHCO_3$, which contains all BG_{11} components except for $NaNO_3$ [7,41]. Resuscitation was induced by addition of 17 mM $NaNO_3$ to cells residing in $BG_{11\text{-}0}$. Cultivation was performed with continuous illumination (50–60 μmol photons·m^{-2}·s^{-1}) and shaking (130–140 rpm) at 27 °C. Mutant strains were cultivated with the appropriate concentration of antibiotics [8]. All strains used for this study are shown in Table 1. Biological replicates were inoculated from the same pre-cultures, but propagated, nitrogen-starved and resuscitated independently in different flasks under identical conditions.

Table 1. List of used strains.

Strain	Genotype	Purpose
E. coli NEB10β	Δ(ara-leu) 7697 araD139 fhuAΔlacX74 galK16 galE15 e14-Φ80dlacZΔM15 recA1 relA1 endA1 nupGrpsL(StrR) rphspoT1 Δ(mrr-hsdRMS-mcrBC)	Molecular cloning
E. coli Rosetta gami (DE3)	Δ(ara-leu)7697 ΔlacX74 ΔphoA PvuII phoR araD139 ahpC galE galK rpsL (DE3) F′[lac^+ $lacI^q$ pro] gor522:: Tn10 trxB pLysSRARE (Cam^R, Str^R, Tet^R)	Protein expression
Synechocystis sp. PCC 6803 GT	Wild-type	Control strain
Δ*pgm*	*Sll0726::Spec^R*	Characterization
Δ*pgm* + PGM1	Δ*pgm pVZ322(sll0726) Kan^R, Gen^R*	Characterization
Δ*pgm* + PGM1S47A	Δ*pgm pVZ322(sll0726(S47A)) Kan^R, Gen^R*	Characterization
WT+PGM1S47A	*pVZ322(sll0726(S47A)) Kan^R, Gen^R*	Characterization

Protein overexpression and purification

Escherichia coli Rosetta-gami (DE3) was used for the overexpression of all proteins. All primers and plasmids used for protein overexpression are shown in Table 2 and Table 3, respectively. All enzymes were Strep-tagged at the C-terminus. Cells were cultivated in 2xYT (1 L of culture in 5 L flasks) at 37 °C until they reached exponential growth (OD_{600} 0.6–0.8) and protein overexpression was then induced by adding 75 μg·L^{-1} anhydrotetracycline, followed by incubation at 20 °C for 16 h. Cells were harvested by centrifugation at 4000 g for 10 min at 4 °C, and disrupted by sonication in 40 mL of lysis buffer [100 mM Tris-HCl pH 7.5, 150 mM KCl, 5 mM $MgCl_2$, DNAse, and cOmplete™ protease inhibitor cocktail (Roche, Basel, Switzerland)]. The cell lysates were centrifuged at 20 000 g for 1 h at 4 °C and the supernatants were filtered with a 0.22 μM filter.

The cell extracts were loaded onto a five-milliliter Ni-NTA Strep-tactin® superflow column (Qiagen, Germantown, MD, USA), washed with wash buffer (100 mM Tris-HCl pH 7.5 and 150 mM KCl), and eluted with elution buffer (100 mM Tris-HCl pH 7.5, 150 mM KCl, and 2.5 mM desthiobiotin). The buffer of all purified proteins was exchanged via dialysis using dialysis buffer (100 mM Tris-

Table 2. List of used primers.

Primer	Sequence (5′ - 3′)
pASKC Lpgm1 fw	TAGAAATAATTTTGTTTAACTTTAAGAAGGAGATATACAAGTGTCTAAGCCCCTGATCGC
pASKC Lpgm1 rev	GTCTTATTTTTCGAACTGCGGGTGGCTCCAGCTAGCCATGCCCAAAGCCGAGGTAACAATG
pASKC Spgm1 fw	TAGAAATAATTTTGTTTAACTTTAAGAAGGAGATATACAAATGACAAGCAGAATTAATCC
pASKC Spgm1 rev	TCTTATTTTTCGAACTGCGGGTGGCTCCAGCTAGCCATGCCCAAAGCCGAGGTAACAATG
Pgm1 S47A fw	CTTTGGTACCgctGGCCATCGGG
Pgm1 S47A rev	CTCACTAACTGGGCGGGATTTTC
Pgm1 S47D fw	CTTTGGTACCgatGGCCATCGGGG
Pgm1 S47D rev	CTCACTAACTGGGCGGGA
pUC19-DSpgm1 fw	CCATGATTACGCCAAGCTTGCATGCCTGCAGGTCGACTGGCACAGCCATAGCCTAAAG
SmR-DSpgm1 rev	GTTTCTACAAACTCCATATGTCGACCCGGTCAATGTTCCG
DSpgm1-SmR fw	CGGAACATTGACCGGGTCGACATATGGAGTTTGTAGAAACG
USpgm1 SmR rev	CCTTTTTGGCTAGGATTTGGGAGCTCTTGACCGAACGCAG
SmR-USpgm1 fw	CTGCGTTCGGTCAAGAGCTCCCAAATCCTAGCCAAAAAGG
pUC19-USpgm1 rev	AAACGACGGCCAGTGAATTCGAGCTCGGTACCCGGGGATCCAGGCAATCAATCCGCTCAG
pVZ322 pgm1 fw	GCTTCCAGATGTATGCTCTTCTGCTCCTGCAGGTCGACTTTAGCCCAAAGCCGAGGTAAC
pVZ322 pgm1 rev	TGAATGTTCCGTTGCGCTGCCCGGATTACAGATCCTCTAGCAGGCAATCAATCCGCTCAG
Hpgm S20D fw	ACCGGGTACCGATGGTCTGCGTAAAC
Hpgm S20D rev	TTCTGGTCCTGGTACGCC

Table 3. List of used plasmids.

Plasmid	Purpose
pASK IBA5C-LongPgm1	Expression of C-terminus Strep-tagged *Synechocystis* (long) PGM1 in *E. coli*
pASK IBA5C-ShortPgm1	Expression of C-terminus Strep-tagged *Synechocystis* (short) PGM1 in *E. coli*
pASK IBA5C - pgm1S47A	Expression of C- terminus Strep-tagged *Synechocystis* PGM1 S47A in *E. coli*
pASK IBA5C - pgm1S47D	Expression of C- terminus Strep-tagged *Synechocystis* PGM1 S47D in *E. coli*
pASK IBA5C-HPgm1	Expression of C- terminus Strep-tagged *H. sapiens* PGM1 in *E. coli*
pASK IBA5C-HPgm1S20D	Expression of C- terminus Strep-tagged *H. sapiens* PGM1 S20D in *E. coli*
pUC19-pgm1	Replacement of *pgm1* for $Spec^R$ in *Synechocystis* sp. PCC 6803
pVZ322-pgm1	Complementation of *pgm1* deletion
pVZ322-pgm1S47A	Complementation of *pgm1* deletion and WT with PGM1 S47A mutant variant

HCl pH 7.5, 150 mM KCl, and 5 mM $MgCl_2$) and a 3 kDa cutoff dialysis tube. All purifications were checked via SDS-PAGE.

Measurement of PGM1 activity in cell extracts

To determine the PGM1 activity in *Synechocystis* cell extracts, an assay was adapted from Osanai et al. [42]. The PGM1 reaction was coupled to the G6PDH reaction and the glucose 6-phosphate-dependent conversion of $NADP^+$ to NADPH was monitored by measuring the absorbance at 340 nm. Cells were harvested by centrifugation at 4000 g for 10 min at 4 °C, resuspended in lysis buffer (100 mM Tris-HCl pH 7.5, 10 mM $MgCl_2$) and disrupted by using a "FastPrep®-24"(MP Biomedicals, Irvine, CA, USA). The lysate was centrifuged for 10 min at 4 °C before the protein content was determined. Approximately 50 μg of protein were used for each reaction. The reaction buffer was composed of 100 mM Tris-HCl pH 7.5, 10 mM $MgCl_2$, 1 mM $NADP^+$, 1 mM DTT and 1 $U{\cdot}mL^{-1}$ G6PDH from *Saccharomyces cerevisiae* (G6378, Sigma-Aldrich, St. Louis, MO, USA). The reaction was started by the addition of 10 mM glucose-1P. Absorption change at 340 nm was continuously measured for 15 min at 30 °C. As a blank, the change in absorption in the absence of glucose-1P was also measured and subtracted from the experimental values. The enzymatic activity was then calculated. At least three biological replicates were measured.

Measurement of PGM1 activity *in vitro*

The reaction buffer was composed of 100 mM Tris-HCl pH 7.5, 150 mM KCl, 10 mM $MgCl_2$, 1 mM DTT, 1 mM $NADP^+$, 40 μM glucose-1,6-bisphosphate, and 1 $U{\cdot}mL^{-1}$ G6PDH from *Saccharomyces cerevisiae* (G6378, Sigma-Aldrich). 100 ng of C-terminus Strep-tagged PGM1 were added to each reaction. The reaction was started by the addition of glucose-1P. Absorption change at 340 nm was continuously measured for 15 min at 30 °C. The enzymatic activity was then calculated. At least three replicates were measured.

Glucose-phosphate quantification

A total of 4 mL of chlorotic and resuscitating (24 h after $NaNO_3$ addition) cultures were collected (OD_{750} ~ 0.8).

Cells were harvested by centrifugation at 18 000 g for 1 min at 4 °C. Pellets were immediately frozen in liquid nitrogen. Cells were lysed by addition of 0.2 M HCl and incubation at 95 °C for 15 min. Lysates were centrifuged at 18 000 g for 10 min at room temperature, then the supernatants were transferred to clean 2 mL tubes. Samples were neutralized with 1 mL of 1 M Tris-HCl pH 8. A glucose-1P and glucose-6P calibration curve were prepared. $NADP^+$, KCl, and $MgCl_2$ were added to samples and standard solutions to a final concentration of 1, 150 and 10 mM, respectively. The absorbance of samples and standards were measured at 340 nm (blank measurement). 3 U of G6PDH from *Saccharomyces cerevisiae* (G6378, Sigma-Aldrich) were added to all samples and standards and their absorbance at 340 nm was measured after incubation for 5 min at room temperature (glucose-6P measurement). 3 U of Pgm from rabbit muscle (P3397, Sigma-Aldrich) were added to all samples and glucose-1P standards and their absorbance at 340 nm was measured after incubation for 5 min at room temperature (glucose-1P measurement). The blank measurements were subtracted from the glucose-6P measurements, and the glucose-6P standard curve was used to determine the concentration of glucose-6P in the samples. The glucose-6P measurements were subtracted from the glucose-1P measurements, and the glucose-1P standard curve was used to determine the concentration of glucose-1P in the samples. Data were normalized to the OD_{750} of the sampled cultures. Three biological replicates were measured.

Clear native PAGE – immunoblot analysis

Proteins from 20 mL cell culture aliquots were lysed in extraction buffer with or without phosphatase inhibitors (50 mM Tris/HCl, 5 mM EDTA, 5 mM sodium fluoride, 5 mM sodium orthovanadate, pH 7.4) with a RiboLyser, conducting five cycles with a speed of 6.5 $m{\cdot}s^{-1}$ for 15 s at 4 °C. When indicated, cell extracts were treated with 1 $U{\cdot}mL^{-1}$ alkaline phosphatase for 10 min at room temperature. Protein concentration was measured by Bradford assay and 10 µg total protein content was separated by non-denaturing clear native polyacrylamide gel electrophoresis (PAGE). Samples were mixed with loading buffer, loaded onto tris-glycine 8% separating native polyacrylamide gels, and run at 30 mA until the die reached the bottom of the gel. Protein transfer was performed on a semi-dry blotting system (PEQLAB, Wilmington, NC, USA) onto polyvinylidene fluoride (BioTrace™ PVDF, Pall Corporation, New York, NY, USA) membranes at 20 V for 30 min. Membranes were blocked overnight in TBS-T buffer (50 mM Tris, 150 mM NaCl, 0.1% Tween-20, pH7.5) and 5% milk powder at 4 °C. Membranes were washed with TBS-T buffer and incubated with polyclonal primary antibodies against PGM1 (serum, produced in rabbit) for 1 h at RT in a 1 : 5000 dilution in TBS-T buffer. Membranes were washed again and incubated with peroxidase coupled secondary antibodies (A6154, Sigma-Aldrich) for 1 h at RT in a 1 : 5000 dilution in TBS-T buffer. Proteins were visualized by Lumi-Light Plus detection reagent (Roche).

Phylogenetic analysis

Sequences of diverse members of the α-D-PHM superfamily were obtained from NCBI RefSeq_protein database. Alignment and phylogenetic tree data were obtained using NCBI Constraint-based Multiple Alignment Tool (COBALT) [43]. Phylogenetic tree was generated with the Interactive Tree Of Life (ITOL) v5 online tool [44].

Recovery assay

Serial dilutions of chlorotic cultures were prepared (10^0, 10^{-1}, 10^{-2}, 10^{-3}, 10^{-4} and 10^{-5}) starting with an OD_{750} of 1. 5 µL of these dilutions were dropped on solid BG_{11} agar plates and cultivated at 50 µmol photons$\cdot m^{-2}\cdot s^{-1}$ and 27 °C for 5 days.

Glycogen determination

Glycogen content was determined as described by Gründel et al. [29] with modifications established by Klotz et al. [7]. Two-milliliter samples were collected, span down and washed with distilled water. Cells were lysed by incubation in 30% KOH at 95 °C for 2 h. Glycogen was precipitated by addition of cold ethanol to a final concentration of 70% followed by an overnight incubation at −20 °C. The precipitated glycogen was pelleted by centrifugation at 15 000 g for 10 min and washed with 70% ethanol and 98% absolute ethanol, consecutively. The precipitated glycogen was dried and digested with 35 U of amyloglucosidase (10115, Sigma-Aldrich) in 1 mL of 100 sodium acetate pH 4.5 for 2 h. 200 µL of the samples were mixed with 1 mL of 6% O-toluidine in acetic acid and incubated at 100 °C for 10 min. Absorbance was then read at 635 nm. A glucose calibration curve was used to determine the amount of glycogen in the samples. For every condition, at least three biological replicates were measured.

Size exclusion chromatography

Experiments were carried out using an ÄKTA purifier system connected to a Superose 6 Increase 10/300 GL column (GE healthcare, Chicago, IL, USA) at a flow rate of 0.4 $mL{\cdot}min^{-1}$ in running buffer (100 mM Tris-HCl pH 7.5, 150 mM KCl, and 10 mM $MgCl_2$). The column was calibrated using the gel filtration calibration kit LMW and HMW (GE Healthcare) according to the manufacturer's instructions. Data analysis was performed using the software ASTRA 7 (Wyatt Technology, Santa Barbara, CA, USA) and UNICORN 5.20 (Build 500) (General Electric Company, Boston, MA, USA).

Statistical analysis

Statistical details for each experiment can be found in the figure legends. Samples taken from cultures that were inoculated with the same pre-cultures, but propagated, nitrogen-starved and resuscitated independently in different flasks under identical conditions were considered different biological replicates. GraphPad PRISM was used to perform one-way ANOVA to determine the statistical significance. Asterisks in the figures were used to symbolize the *P*-value: One asterisk represents $P \leq 0.05$, two asterisks $P \leq 0.01$, three asterisks $P \leq 0.001$, and four asterisks $P \leq 0.0001$.

Acknowledgements

We thank Dr. Libera Lo Presti for her assistance writing this manuscript. This work was supported by the German Research Council (DFG) FOR 2816 "The Autotrophy-Heterotrophy Switch in Cyanobacteria: Coherent Decision-Making at Multiple Regulatory Layers". Additionally, we acknowledge the infrastructural support from EXC 2124 "Controlling Microbes to Fight Infections" (ID 390838134). Open Access funding enabled and organized by Projekt DEAL.

Author contributions

SD performed cultivation experiments, cloning, protein purification, enzymatic assays, phylogenetic analysis, glycogen and glucose-phosphate determinations, immunoblot analysis, size exclusion chromatography, constructed mutants, analyzed data, and wrote manuscript with input from all authors. NN contributed cloning and sequence analysis. KF conceived study, interpreted data and edited manuscript.

Conflict of interest

The authors declare no conflict of interest.

Data availability statement

Enzymatic data generated during this study have been deposited on the data and model management platform FAIRDOMHub [45] under the SEEK ID: https://fairdomhub.org/studies/854

References

1 Prats C, Graham TE, Shearer J. The dynamic life of the glycogen granule. *J Biol Chem*. 2018;**293**:7089–98.
2 Klotz A, Forchhammer K. Glycogen, a major player for bacterial survival and awakening from dormancy. *Future Microbiol*. 2017;**12**:101–4.
3 Welkie DG, Rubin BE, Diamond S, Hood RD, Savage DF, Golden SS. A hard day's night: cyanobacteria in diel cycles. *Trends Microbiol*. 2019;**27**:231–42.
4 Preiss J. Bacterial glycogen synthesis and its regulation. *Annu Rev Microbiol*. 1984;**38**:419–58.
5 Forchhammer K, Schwarz R. Nitrogen chlorosis in unicellular cyanobacteria – a developmental program for surviving nitrogen deprivation. *Environ Microbiol*. 2019;**21**:1173–84.
6 Neumann N, Doello S, Forchhammer K. Recovery of unicellular cyanobacteria from nitrogen chlorosis : a model for resuscitation of dormant bacteria. *Microb Physiol*. 2021;**31**:78–87.
7 Klotz A, Georg J, Bučinská L, Watanabe S, Reimann V, Januszewski W, et al. Awakening of a dormant cyanobacterium from nitrogen chlorosis reveals a genetically determined program. *Curr Biol*. 2016;**26**:2862–72.
8 Doello S, Klotz A, Makowka A, Gutekunst K, Forchhammer K. A specific glycogen mobilization strategy enables rapid awakening of dormant cyanobacteria from chlorosis. *Plant Physiol*. 2018;**177**:594–603.
9 Spät P, Klotz A, Rexroth S, Maček B, Forchhammer K. Chlorosis as a developmental program in cyanobacteria: the proteomic fundament for survival and awakening. *Mol Cell Proteomics*. 2018;**17**:1650–69.
10 Liu L, Hu HH, Gao H, Xu XD. Role of two phosphohexomutase genes in glycogen synthesis in *Synechocystis* sp. PCC6803. *Chinese Sci Bull*. 2013;**58**:4616–21.
11 Neumann N, Friz S, Forchhammer K. Glucose-1,6-bisphosphate, a key metabolic regulator, is synthesized by a distinct family of α-phosphohexomutases widely distributed in prokaryotes. *bioRxiv*. 2021;2021.12.02.470922. [PREPRINT] https://doi.org/10.1101/2021.12.02.470922
12 Liu Y, Ray WJ, Baranidharan S. Structure of rabbit muscle phosphoglucomutase refined at 2.4 Å resolution. *Acta Crystallogr D Biol Crystallogr*. 1997;**53**:392–405.
13 Backe PH, Laerdahl JK, Kittelsen LS, Dalhus B, Mørkrid L, Bjørås M. Structural basis for substrate and product recognition in human phosphoglucomutase-1 (PGM1) isoform 2, a member of the α-d-phosphohexomutase superfamily. *Sci Rep*. 2020;**10**:1–14.
14 Osanai T, Oikawa A, Numata K, Kuwahara A, Iijima H, Doi Y, et al. Pathway-level acceleration of glycogen catabolism by a response regulator in the cyanobacterium *Synechocystis* species PCC 6803. *Plant Physiol*. 2014;**164**:1831–41.
15 Nakao M, Okamoto S, Kohara M, Fujishiro T, Fujisawa T, Sato S, et al. CyanoBase: the cyanobacteria genome database update 2010. *Nucleic Acids Res*. 2009;**38**:2009–11.

16 Stiers KM, Muenks AG, Beamer LJ. Biology, mechanism, and structure of enzymes in the α-D-phosphohexomutase superfamily. *Adv Protein Chem Struct Biol*. 2017;**109**:265–304.
17 Lu S, Wang J, Chitsaz F, Derbyshire MK, Geer RC, Gonzales NR, et al. CDD/SPARCLE: the conserved domain database in 2020. *Nucleic Acids Res*. 2020;**48**: D265–8.
18 Regni C, Naught L, Tipton PA, Beamer LJ. Structural basis of diverse substrate recognition by the enzyme PMM/PGM from *P. aeruginosa*. *Structure*. 2004;**12**:55–63.
19 Shackelford GS, Regni CA, Beamer LJ. Evolutionary trace analysis of the α-D-phosphohexomutase superfamily. *Protein Sci*. 2004;**13**:2130–8.
20 Goto LS, Vessoni Alexandrino A, Malvessi Pereira C, Silva Martins C, D'Muniz Pereira H, Brandão-Neto J, et al. Structural and functional characterization of the phosphoglucomutase from *Xanthomonas citri* subsp. citri. *Biochim Biophys Acta Proteins Proteomics*. 2016;**1864**:1658–66.
21 Mehra-Chaudhary R, Mick J, Tanner JJ, Henzl MT, Beamer LJ. Crystal structure of a bacterial phosphoglucomutase, an enzyme involved in the virulence of multiple human pathogens. *Proteins*. 2011;**79**:1215–29.
22 Li L, Kim SA, Fang R, Han NS. Expression of manB gene from *Escherichia coli* in *Lactococcus lactis* and characterization of its bifunctional enzyme, phosphomannomutase. *J Microbiol Biotechnol*. 2018;**28**:1293–8.
23 Accorsi A, Piatti E, Piacentini MP, Faz A, Gini S. Isoenzymes of phosphoglucomutase from hunan red blood cells: isolation and kinetic properties. *Prep Biochem*. 1989;**19**:251–71.
24 Naught LE, Regni C, Beamer LJ, Tipton PA. Roles of active site residues in *Pseudomonas aeruginosa* phosphomannomutase/phosphoglucomutase. *Biochemistry*. 2003;**42**:9946–51.
25 Jolly L, Ferrari P, Blanot D, Van Heijenoort J, Fassy F, Mengin-Lecreulx D. Reaction mechanism of phosphoglucosamine mutase from *Escherichia coli*. *J Bacteriol*. 1999;**262**:202–10.
26 Walther T, Baylac A, Alkim C, Vax A, Cordier H, François JM. The PGM3 gene encodes the major phosphoribomutase in the yeast *Saccharomyces cerevisiae*. *FEBS Lett*. 2012;**586**:4114–8.
27 Carlson DM. Phosphoacetylglucosamine mutase from pig submaxillary gland. *Methods Enzymol*. 1966;**8**:179–82.
28 Mitschke J, Georg J, Scholz I, Sharma CM, Dienst D, Bantscheff J, et al. An experimentally anchored map of transcriptional start sites in the model cyanobacterium *Synechocystis* sp. PCC6803. *Proc Natl Acad Sci USA*. 2011;**108**:2124–9.
29 Gründel M, Scheunemann R, Lockau W, Zilliges Y. Impaired glycogen synthesis causes metabolic overflow reactions and affects stress responses in the cyanobacterium *Synechocystis* sp. PCC 6803. *Microbiology (Reading)*. 2012;**158**:3032–43.
30 Bian Y, Song C, Cheng K, Dong M, Wang F, Huang J, et al. An enzyme assisted RP-RPLC approach for in-depth analysis of human liver phosphoproteome. *J Proteomics*. 2014;**96**:253–62.
31 Huttlin EL, Jedrychowski MP, Elias JE, Goswami T, Rad R, Beausoleil SA, et al. A tissue-specific atlas of mouse protein phosphorylation and expression. *Cell*. 2010;**143**:1174–89.
32 Lee Y, Stiers KM, Kain BN, Beamer LJ. Compromised catalysis and potential folding defects in in vitro studies of missense mutants associated with hereditary phosphoglucomutase 1 deficiency. *J Biol Chem*. 2014;**289**:32010–9.
33 Gururaj A, Barnes CJ, Vadlamudi RK, Kumar R. Regulation of phosphoglucomutase 1 phosphorylation and activity by a signaling kinase. *Oncogene*. 2004;**23**:8118–27.
34 Bro C, Knudsen S, Regenberg B, Olsson L, Nielsen J. Improvement of galactose uptake in *Saccharomyces cerevisiae* through overexpression of phosphoglucomutase: example of transcript analysis as a tool in inverse metabolic engineering. *Appl Environ Microbiol*. 2005;**71**:6465–72.
35 Jin GZ, Zhang Y, Cong WM, Wu X, Wang X, Wu S, et al. Phosphoglucomutase 1 inhibits hepatocellular carcinoma progression by regulating glucose trafficking. *PLoS Biol*. 2018;**16**:1–27.
36 Malinova I, Kunz HH, Alseekh S, Herbst K, Fernie AR, Gierth M, et al. Reduction of the cytosolic phosphoglucomutase in Arabidopsis reveals impact on plant growth, seed and root development, and carbohydrate partitioning. *PLoS One*. 2014;**9**:1–11.
37 Seibold GM, Eikmanns BJ. Inactivation of the phosphoglucomutase gene pgm in *Corynebacterium glutamicum* affects cell shape and glycogen metabolism. *Biosci Rep*. 2013;**33**:645–54.
38 Müller S, Diederichs K, Breed J, Kissmehl R, Hauser K, Plattner H, et al. Crystal structure analysis of the exocytosis-sensitive phosphoprotein, pp63/parafusin (phosphoglucomutase), from paramecium reveals significant conformational variability. *J Mol Biol*. 2002;**315**:141–53.
39 Beamer LJ. Mutations in hereditary phosphoglucomutase 1 deficiency map to key regions of enzyme structure and function. *J Inherit Metab Dis*. 2015;**38**:243–56.
40 Rippka R, Deruelles J, Waterbury JB, Herdman M, Stanier RY. Generic assignments, strain histories and properties of pure cultures of cyanobacteria. *Microbiology*. 1979;**111**:1–61.

41 Schlebusch M, Forchhammer K. Requirement of the nitrogen starvation-induced protein s110783 for polyhydroxybutyrate accumulation in *Synechocystis* sp. strain PCC 6803. *Appl Environ Microbiol*. 2010;**76**:6101–7.
42 Osanai T, Oikawa A, Azuma M, Tanaka K, Saito K, Hirai MY, et al. Genetic engineering of group 2 σ factor SigE widely activates expressions of sugar catabolic genes in *Synechocystis* species PCC 6803. *J Biol Chem*. 2011;**286**:30962–71.
43 Papadopoulos JS, Agarwala R. COBALT: constraint-based alignment tool for multiple protein sequences. *Bioinformatics*. 2007;**23**:1073–9.
44 Letunic I, Bork P. Interactive Tree Of Life (iTOL) v5: an online tool for phylogenetic tree display and annotation. *Nucleic Acids Res*. 2021;**49**:W293–6.
45 Wolstencroft K, Krebs O, Snoep JL, Stanford NJ, Bacall F, Golebiewski M, et al. FAIRDOMHub: a repository and collaboration environment for sharing systems biology research. *Nucleic Acids Res*. 2017;**45**: D404–7.
46 Waterhouse AM, Procter JB, Martin DMA, Clamp M, Barton GJ. Jalview Version 2—a multiple sequence alignment editor and analysis workbench. *Bioinformatics*. 2009;**25**:1189–91.

Publication 5: Research article

Neumann N., Friz S., Forchhammer K.

Glucose-1,6-bisphosphate, a key metabolic regulator, is synthesized by a distinct family of α-phosphohexomutases widely distributed in prokaryotes

mBio • Vol. 13, No. 4

AMERICAN SOCIETY FOR MICROBIOLOGY | mBio®

RESEARCH ARTICLE

Glucose-1,6-Bisphosphate, a Key Metabolic Regulator, Is Synthesized by a Distinct Family of α-Phosphohexomutases Widely Distributed in Prokaryotes

Niels Neumann,[a,b] Simon Friz,[a,b] Karl Forchhammer[a,b]

[a]Interfaculty Institute of Microbiology and Infection Medicine, University of Tübingen, Tübingen, Germany
[b]Cluster of Excellence: EXC 2124: Controlling Microbes to Fight Infection, Tübingen, Germany

ABSTRACT The reactions of α-d-phosphohexomutases (αPHM) are ubiquitous, key to primary metabolism, and essential for several processes in all domains of life. The functionality of these enzymes relies on an initial phosphorylation step which requires the presence of α-d-glucose-1,6-bisphosphate (Glc-1,6-BP). While well investigated in vertebrates, the origin of this activator compound in bacteria is unknown. Here we show that the Slr1334 protein from the unicellular cyanobacterium *Synechocysitis* sp. PCC 6803 is a Glc-1,6-BP-synthase. Biochemical analysis revealed that Slr1334 efficiently converts fructose-1,6-bisphosphate (Frc-1,6-BP) and α-d-glucose-1-phosphate/α-d-glucose-6-phosphate into Glc-1,6-BP and also catalyzes the reverse reaction. As inferred from phylogenetic analysis, the *slr1334* product belongs to a primordial subfamily of αPHMs that is present especially in deeply branching bacteria and also includes human commensals and pathogens. Remarkably, the homologue of Slr1334 in the human gut bacterium *Bacteroides salyersiae* catalyzes the same reaction, suggesting a conserved and essential role for the members of this αPHM subfamily.

IMPORTANCE Glc-1,6-BP is known as an essential activator of phosphoglucomutase (PGM) and other members of the αPHM superfamily, making it a central regulator in glycogen metabolism, glycolysis, amino sugar formation as well as bacterial cell wall and capsule formation. Despite this essential role in carbon metabolism, its origin in prokaryotes has so far remained elusive. In this study we identify a member of a specific αPHM subfamily as the first bacterial Glc-1,6-BP synthase, forming free Glc-1,6-BP by using Frc-1,6-BP as phosphoryl-donor. PGMs of this subfamily are widely distributed among prokaryotes including human commensals and pathogens. By showing that a distinct subfamily member can also form Glc-1,6-BP, we provide evidence that Glc-1,6-BP synthase activity is a general feature of this group.

KEYWORDS carbon metabolism, glucose-1,6-bisphosphate, glycolysis, phosphoglucomutase

The α-d-phosphohexomutase (αPHM) superfamily is ubiquitous and found in all domains of life. All known members of this superfamily catalyze a reversible intramolecular phosphoryl transfer on their phosphosugar substrates. This reaction requires a bound metal ion (usually Mg^{2+}) together with a conserved phosphorylated seryl residue in the active site and proceeds via a bis-phosphorylated sugar intermediate (1). While showing similar properties in structure and reaction mechanism, these enzymes differ strongly in substrate specificity. Based on their preferred substrate, the αPHMs are traditionally divided into four main groups: (i) Phosphoglucomutases (PGM), (ii) phosphoglucosamine mutases (PNGM), (iii) phosphoacetylglucosamine mutases (PAGM), and (iv) the group of bifunctional phosphoglucomutases/phosphomannomutases (PGM/PMM) (1). The most recent expansion to this classification has been the discovery of the mammalian phosphopentomutase (PGM2) and

Editor Eleftherios T. Papoutsakis, University of Delaware

Address correspondence to Karl Forchhammer, karl.forchhammer@uni-tuebingen.de.

The authors declare no conflict of interest.

Received 2 June 2022
Accepted 5 July 2022
Published 20 July 2022

TABLE 1 Subfamilies in the αPHM superfamily with their identifier and proposed main function according to the NCBI conserved domain database (CDD)

CDD group name	CDD identifier	Proposed main function
PGM1	cd03085	Phosphoglucomutase
PGM2	cd05799	Phosphopentomutase (PGM2)/Glc-1,6-BP synthase (PGM2L1)
PGM3(PAGM)	cd03086	Phosphoacetylglucosamine mutase
PMM/PGM	cd03089	Bi-functional phosphomanno-/phosphoglucomutase
PGM like 1	cd03087	Unknown
PGM like 2	cd05800	Unknown
PGM like 3	cd05801	Phosphoglucomutase
PGM like 4	cd05803	Unknown
ManB	cd03088	Phosphomannomutase
GlmM	cd05802	Phosphoglucosamine mutase

glucose-1,6-bisphosphate-synthase (PGM2L1) (2, 3). This classification, however, lacks a more detailed subdivision in between the main groups and also does not take into account αPHMs preferably catalyzing other reactions (e.g., straight phosphomannomutases) (3). The NCBI conserved domain database (CDD), instead, classifies the αPHM superfamily in 11 different subfamilies on a phylogenetic basis (4). This phylogenetic model enables a more detailed classification and includes several groups of bacterial and archaeal enzymes showing typical αPHM properties but being only poorly characterized (Table 1).

The PGM (cd03085) from rabbit and human as well as the bacterial PGM (cd05801) from *Salmonella typhimurium* and the bacterial bifunctional PMM/PGM (cd03089) from *Pseudomonas aeruginosa* are among the best characterized αPHMs with available crystal structures and detailed description of reaction mechanisms (5–9). Catalyzing the interconversion of α-d-glucose-1P (Glc-1P) and α-d-glucose-6P (Glc-6P) makes PGM a key enzyme in glycogen metabolism, glycolysis, and gluconeogenesis. During this reaction, a phosphoserine at the active site of PGM donates the phosphoryl group to the substrate Glc-6P or Glc-1P resulting in the synthesis of the transient intermediate α-d-glucose-1,6-bisphosphate (Glc-1,6-BP). After a reorientation in the catalytic center, the intermediate product re-phosphorylates the active site serine yielding Glc-1P or Glc-6P, respectively. Glc-1,6-BP itself acts as an essential activator of PGM by providing an initial phosphorylation of the active site and was first discovered by Leloir, Trucco (10) in yeast extract (11). While Glc-1,6-BP is not a free metabolite in any metabolic pathway, it is known to be a potent regulator of several enzymes in central carbon metabolism in eukaryotes: in addition to PGMs and other αPHMs, it was shown to regulate hexokinases, 6-phosphogluconate dehydrogenase, phosphofructokinase and pyruvate kinase (12). In mammalian tissues the majority of Glc-1,6-BP is catalyzed by the PGM2L1 enzyme, a member of the cd05799 subfamily exclusive to eukaryotes, utilizing 1,3-bisphosphoglyceric acid (1,3-BPG) as phosphoryl donor for Glc-1P (3). In contrast, despite its essential role in the activity of prokaryotic PGM and other enzymes, the origin of Glc-1,6-BP in prokaryotes has been overlooked and no enzyme producing free Glc-1,6-BP has been identified so far (13, 14).

The unicellular cyanobacterium *Synechocystis* sp. PCC 6803 (hereafter *Synechocystis*) expresses two enzymes that are encoded by the genes *sll0726* and *slr1334* and annotated as PGM-like (4, 15). While Sll0726 exhibits typical properties of PGMs (16–18), little is known about Slr1334. The only study addressing this issue reported that purified *Synechocystis* Sll0726 has about a 10-fold higher activity *in vitro* than Slr1334 and that a *sll0726* knockout mutant only shows around 3% PGM activity compared to the wild-type (19). Despite its low contribution to overall PGM activity, the Slr1334 product appeared to be essential as it was not possible to acquire fully segregated knockout mutants of the *slr1334* gene, which raised the question of the role of Slr1334 in *Synechocystis*.

In this work, we show that Slr1334 has a phosphotransferase activity catalyzing the production of free Glc-1,6-BP from Glc-1P/Glc-6P and fructose-1,6-bisphosphate (Frc-1,6-BP). Thereby, Slr1334 is responsible for the formation of the key activator of PGM,

10.1128/mbio.01469-22

Glc-1,6-BP, making it a major regulator in glycolysis and other carbon pathways. Our finding makes Slr1334 the first bacterial enzyme specific for the production of free Glc-1,6-BP. Importantly, we show that the homologue of Slr1334 in the human gut bacterium *Bacteroides salyersiae* catalyzes the same reaction.

RESULTS

Classification of the two PGM isoenzymes from *Synechocystis*. *Synechocystis* possesses two genes annotated as PGMs, the genes *sll0726* and *slr1334*. To classify them within the αPHM superfamily, we performed a phylogenetic analysis by multi-level alignment of all αPHM subfamilies that are considered PGM or "PGM_like." For this, we collected the entry sequences from the NCBI Conserved Domains Database (CDD) (4) and retrieved further sequences by performing BLAST searches in the NCBI RefSeq_protein database. To focus on glucose-specific αPHMs, the groups of enzymes specific for other sugars like PMMs, PNGM and PAGMs (cd03086 cd03088, cd05802, cd05805) were omitted from the analysis (Fig. 1). In general, the αPHMs can be divided into four conserved regions which are from N- to C-terminus: (i) the active site domain, (ii) the metal binding domain, (iii) the sugar binding, and (iv) the phosphate binding domain. While the domains 1, 2, and 4 are usually highly conserved between the different subfamilies, the sugar binding domain shows a greater variance and can assist in the categorization of αPHMs (Table S1 in the supplemental material) (2).

Slr1334 is part of the cd05800 (PGM_like2) subfamily present in many bacterial groups. In agreement with the CDD, our phylogenetic analysis shows that this subfamily forms a distinct cluster of PGMs which clearly separates from other PGM and PGM like enzymes. The Sll0726 PGM, by contrast, is a member of the cd05801 subfamily, to which the well characterized PGM from *S. typhimurium* belongs. With the chosen parameters (see methods part) we detected a total of 2140 hits for Slr1334 homologues.

Slr1334 shows low PGM activity compared to Sll0726 but behaves differently in the presence of fructose-1,6-BP. To gain deeper insights into the role of the enigmatic Slr1334, we overexpressed Sll0726 along with Slr1334 in *Escherichia coli* and assessed the PGM enzymatic activity of the purified proteins by measuring the interconversion of Glc-1-P to Glc-6-P in an assay that couples Glc-6-P formation to its subsequent oxidation using glucose-6-phosphate-dehydrogenase (G6PDH) and $NADP^+$. We could show that Slr1334 only displays about 5% of catalytic efficiency compared to Sll0726 when both PGMs were tested with saturating amounts of the activator Glc-1,6-BP (60 μM) (Fig. 2, Table 2; see also Fig. 3). Interestingly, the PGM activity of both enzymes was also measurable without addition of Glc-1,6-BP, which is considered to be an essential activator. However, in the absence of Glc-1,6-BP, the catalytic efficiency was about 70 times lower due to a significantly increased Michaelis-Menten constant (K_m) for Sll0726 and Slr1334 alike.

Fructose-1,6- bisphosphate is an endogenous intermediate of the glycolytic pathway and is known to be an inhibitor of PGM most likely by competing with the reaction intermediate Glc-1,6-BP (20, 21). In a preliminary experiment we tested the effect of different concentrations of Frc-1,6-BP on Sll0726 and observed major inhibition already at concentrations of 100 μM (data not shown). When testing PGM activity by replacing 60 μM Glc-1,6-BP with 100 μM Frc-1,6-BP, we detected a decrease in catalytic efficiency to 19% as a consequence of a strongly increased K_m (Fig. 2, Table 2). Strikingly, however, for Slr1334 we detected a different effect: while the catalytic rate constant (k_{cat}) decreased by about 2-fold, we measured an approximately 100-fold reduced K_m resulting in 50 times increased catalytic efficiency. This raised the question of how Frc-1,6-BP affected the PGM-activity of Slr1334. We speculated that Frc-1,6-BP might either function as a direct activator similar to Glc-1,6-BP or be required for the synthesis of the activating compound Glc-1,6-BP during the reaction of Slr1334. As we will show below, the activating compound turned out to be Glc-1,6-BP and not Frc-1,6-BP.

Slr1334 forms a product out of Frc-1,6-BP and Glc-1P/Glc-6P that strongly activates PGM reaction of Sll0726. To determine the amount of Glc-1,6-BP needed to achieve activation of the Sll0726 PGM reaction at 1 mM Glc-1P we first tested PGM activity

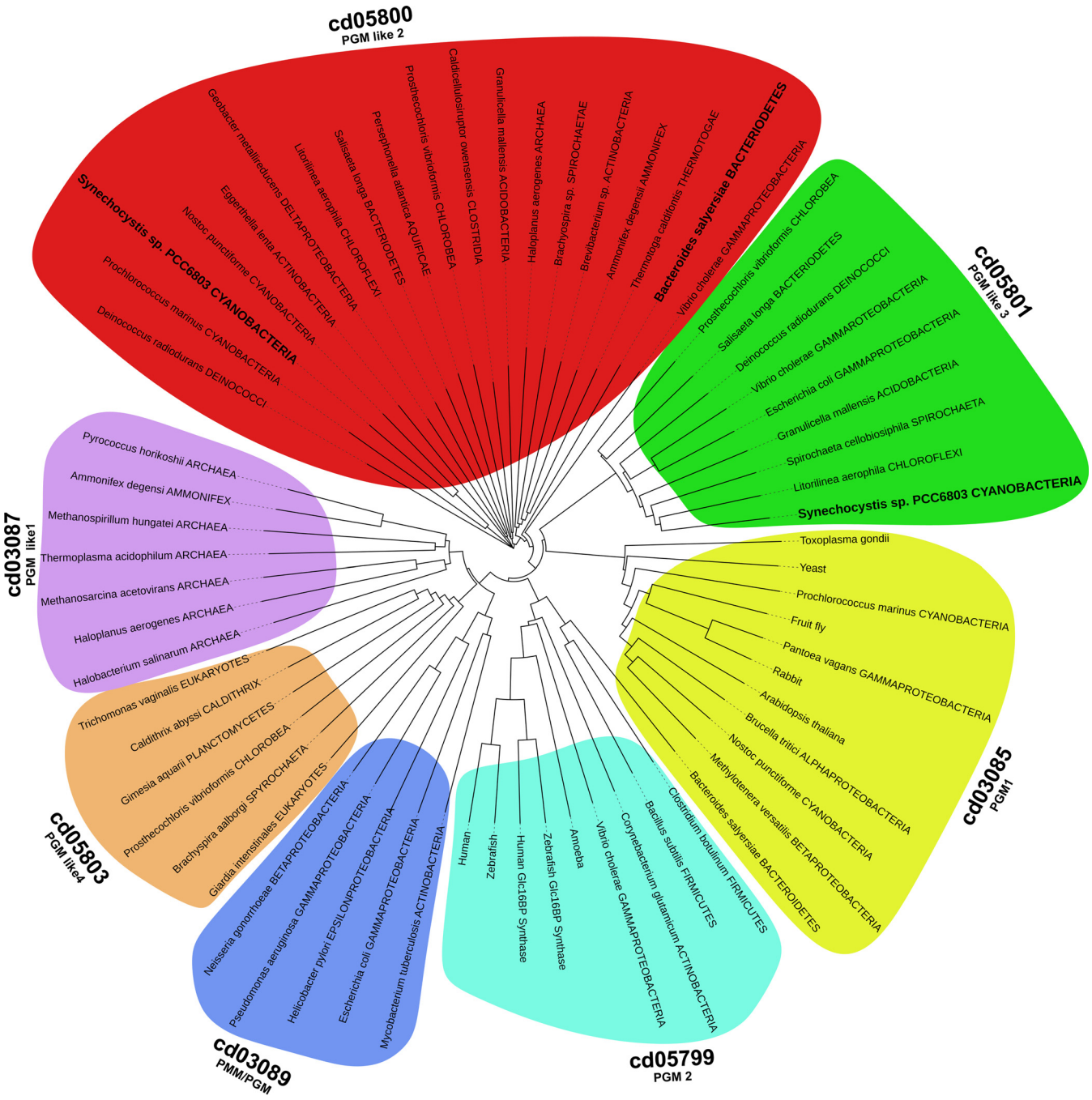

FIG 1 Phylogenetic tree of the αPHM subfamilies that are considered to be "PGM-like" according to CDD. The tree was built on the taxonomy based on the protein sequences present in the NCBI RefSeq_protein database. The CDD subfamilies cd03086, cd03088, cd05802 and cd05805, which are known to catalyze distinct reactions, were omitted from the analysis. The organisms investigated in this study are highlighted in bold letters.

of Sll0726 at different Glc-1,6-BP concentrations. Maximum activation was achieved at Glc-1,6-BP concentrations between 30 and 60 μM resulting in a 5-fold increased activity compared to a control reaction without any effectors (Fig. 3). Next, we incubated Slr1334 (0.5 μM) with the phosphorylated sugars Frc-1,6-BP, Glc-1P and Glc-6P (1 mM each) in different combinations and subsequently tested whether the Sll0726 PGM reaction could be activated by the corresponding reaction products (Fig. 3). As a control, we incubated the same phosphosugars with Sll0726 (0.5 μM) instead of Slr1334 before testing activation of the Sll0726 PGM reaction. After incubating Slr1334 and the control reaction with the phosphosugars for 1.5 h, the reaction was stopped by heat inactivation and the supernatant was added in a dilution of 1:10 to the reaction mixture of the Sll0726 PGM reaction assay,

10.1128/mbio.01469-22

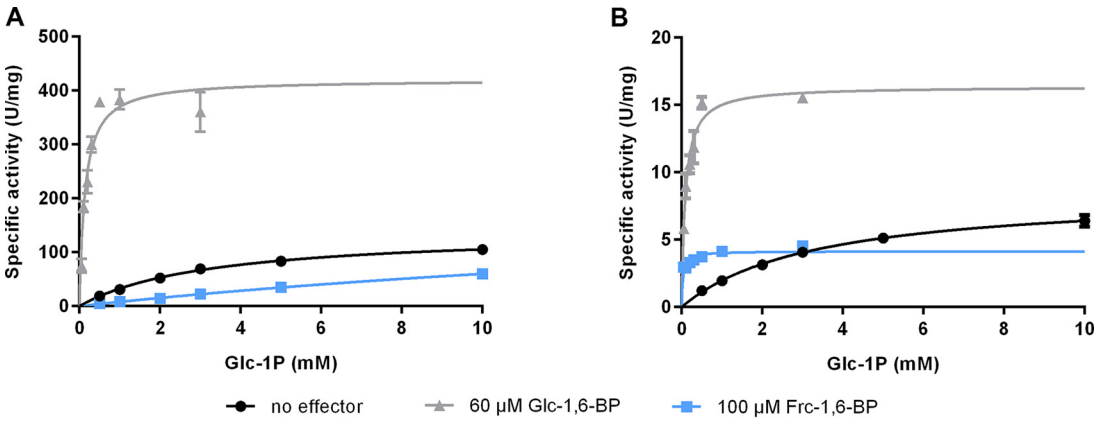

FIG 2 Slr1334 shows lower PGM activity then Sll0726 and behaves differently in the presence of Frc-1,6-BP. Shown are the Michaelis-Menten kinetics of Sll0726 (A) and Slr1334 (B): in black, without addition of effectors; in light gray in the presence of 60 μM Glc-1,6-BP; in blue, in the presence of 100 μM Frc-1,6-BP. Three replicates were measured for each data-point. Error bars represent the SD.

which was then started by adding 1 mM Glc-1P. Only after adding the supernatant of the Slr1334 reaction containing Frc-1,6-BP and Glc-1P (or Glc-6P) as substrates, the velocity of the Sll0726 PGM reaction was increased by 5-fold in comparison to the control reaction without any effector (Fig. 3). When the Sll0726 PGM reaction was performed with the supernatant of the Sll0726 control reaction or the reaction products of Slr1334 using Frc-1,6-BP as sole substrate, the enzyme velocity was lower than the control without effectors. This reduction can be explained by the inhibitory effect of Frc-1,6-BP on Sll0726 as shown in Fig. 2.

In addition to Frc-1,6-BP, we also tested whether Slr1334 can utilize 1,3-BPG instead of Frc-1,6-BP for Glc-1,6-BP formation as described for the mammalian PGM2L1. Since 1,3-BPG is not commercially available, we established an assay whereby we continuously produced 1,3-BPG by a phosphoglycerate kinase (PGK) reaction using a His-tagged purified PGK in combination with 1 mM 3PG and 1 mM ATP (see methods part). This reaction was directly coupled to the reaction of Slr1334 with Glc-1P or Glc-6P or no substrate. As a control the same reaction was performed with Sll0726 instead of Slr1334. To test the possible formation of Glc-1,6-BP, the supernatants of these reactions were added to the Sll0726 PGM reaction before performing the enzymatic assay as described above.

We detected an increase in the Sll0726 PGM activity by approximately 2.5-fold compared to the control without effectors when the supernatant of the Slr1334 reaction contained 1,3-BPG and either Glc-1P or Glc-6P. No increase in activity was detected when the supernatant solely contained 1,3-BPG. The supernatant of the control reaction with Sll0726 instead of Slr1334 resulted in no marked change in activity.

By comparing the activation of the Sll0726 PGM reaction by the Slr1334 reaction products to the activation at different concentration of Glc-1,6-BP we attempted to estimate the efficiency of Glc-1,6-BP formation from either Frc-1,6-BP or 1,3-BPG. In this experiment, the Slr1334-catalyzed reaction using 1,3-BPG and G1P as substrates produced an estimated 1–5 μM the activating compound, while the F-1,6-BP + G1P

TABLE 2 Kinetic parameters for the conversion of Glc-1P to Glc-6P by Sll0726 and Slr1334 in the presence of different effector molecules as indicated[a]

	Sll0726			Slr1334			Catalytic efficiency ratio (%)
Effector	K_m (mM)	K_{cat} (s^{-1})	K_{cat}/K_m ($M^{-1}s^{-1}$)	K_m (mM)	K_{cat} (s^{-1})	K_{cat}/K_m ($M^{-1}s^{-1}$)	(Slr1334/Sll0726)
No effector	3.27 ± 0.21	138 ± 3.7	42.2 × 10^3	3.31 ± 0.14	7.5 ± 0.1	2.3 × 10^3	5.5
Glc-1,6-BP	0.19 ± 0.04	415 ± 30.6	3038.9 × 10^3	0.09 ± 0.02	14.4 ± 0.7	158.1 × 10^3	5.2
Frc-1,6-BP	26.86 ± 3.35	218 ± 21.3	8.1 × 10^3	0.03 ± 0.01	3.6 ± 0.2	117.5 × 10^3	1,450

[a] K_m and K_{cat} values are means of triplicates with ± SD. Catalytic efficiency ratio is given in percentage and was calculated by the ratio of K_{cat}/K_m of Slr1334 and Sll0726.

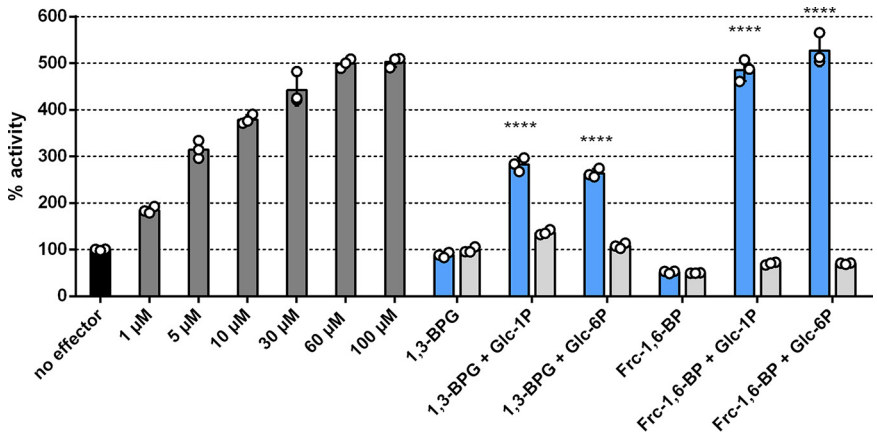

FIG 3 Activation of Sll0726 PGM reaction by Glc-1,6-BP or by the reaction products of Slr1334. Shown is the Sll0726 PGM activity in the presence of different effectors relative to the activity in the absence of effector molecules (set as 100%, black bar). The different bars represent the following reactions: Dark gray bars: Relative PGM activity in the presence of different concentrations of activator molecule Glc-1,6-BP, as indicated. Blue bars: Relative PGM activity in the presence of the supernatant of the Slr1334 reaction carried out with different combinations of substrates, as indicated. Light gray bars: Same conditions as adjacent blue bars, except that Slr1334 was replaced by Sll0726, as a control. Three biological replicates were measured for each datapoint. Error bars represent the SD; asterisks represent the statistical significance in comparison to the reaction without effectors.

reaction produced an estimated 30–60 μM the activating compound Glc-1,6-BP (Fig. 3). This implies that Frc-1,6-BP as phosphorylating sugar is about 10-fold more effective than 1,3-BPG for the Slr1334 reaction.

The product of the Slr1334 reaction is not degradable by the Frc-1,6-BP-aldolase. To confirm that the activating compound formed from Glc-1P/Glc-6P and Frc-1,6-BP through the Slr1334 reaction is in fact Glc-1,6-BP, we analyzed the reaction product via liquid chromatography-mass spectrometry (LC/MS). Therefore, we incubated Slr1334 together with 500 μM Frc-1,6-BP and 1 mM Glc-1P for 1.5 h. As a control, the same substrates were incubated without enzyme. Since LC/MS analysis does not allow discriminating Glc-1,6-BP from Frc-1,6-BP, we performed an additional reaction step to specifically degrade Frc-1,6-BP. Therefore, after heat inactivation, the reaction mixture was incubated with Frc-1,6-BP-aldolase (Fba) and glycerol-3-phosphate-dehydrogenase (GPDH) as well as 1 mM NADH:Fba specifically cleaves Frc-1,6-BP into dihydroxyacetone phosphate (DHAP) and glyceraldehyde-3P while Glc-1,6-BP is unaffected. GPDH subsequently forms glycerol-3-phosphate (glycerol-3P) and NAD^+ out of DHAP and NADH. This is necessary to enable full degradation of Frc-1,6-BP.

After this treatment, LC/MS analysis revealed that a compound with a mass corresponding to either Glc-1,6-BP or Frc-1,6-BP was present in the Slr1334 reaction while this mass was not detectable in the control reaction where no Slr1334 was present (Fig. 4). This indicates that Frc-1,6-BP in the control reaction was completely degraded in the subsequent reaction by Fba as expected, while Frc-1,6-BP in the Slr1334 reaction was metabolized into a molecule of the same mass that was not degraded by Fba. This is precisely what is expected when Glc-1,6-BP is produced from Frc-1,6-BP turn-over. Furthermore, the reaction products from the coupled GPDH reaction, NAD^+ and glycerol-3P were more abundant in the control reaction without Slr1334 compared to the reaction with Slr1334. This indicated that more Frc-1,6-BP was degraded out of the control reaction than out of the reaction containing Slr1334 due to partial conversion of Frc-1,6-BP into Glc-1,6-BP by Slr1334 (Fig. 4). Altogether, this experiment strongly indicated that in the presence of Slr1334, Frc-1,6-BP was partially utilized to form Glc-1,6-BP. The fact that only a part of Frc-1,6-BP was consumed could be either due to a too short reaction time or because the reaction reached an equilibrium state.

Slr1334 keeps Frc-1,6-BP and Glc-1,6-BP in an equilibrium. For investigating whether the formation of Glc-1,6-BP out of Glc-1P/Glc-6P and Frc-1,6-BP is an equilibrium reaction, we performed an enzymatic assay to determine the amount of the

10.1128/mbio.01469-22

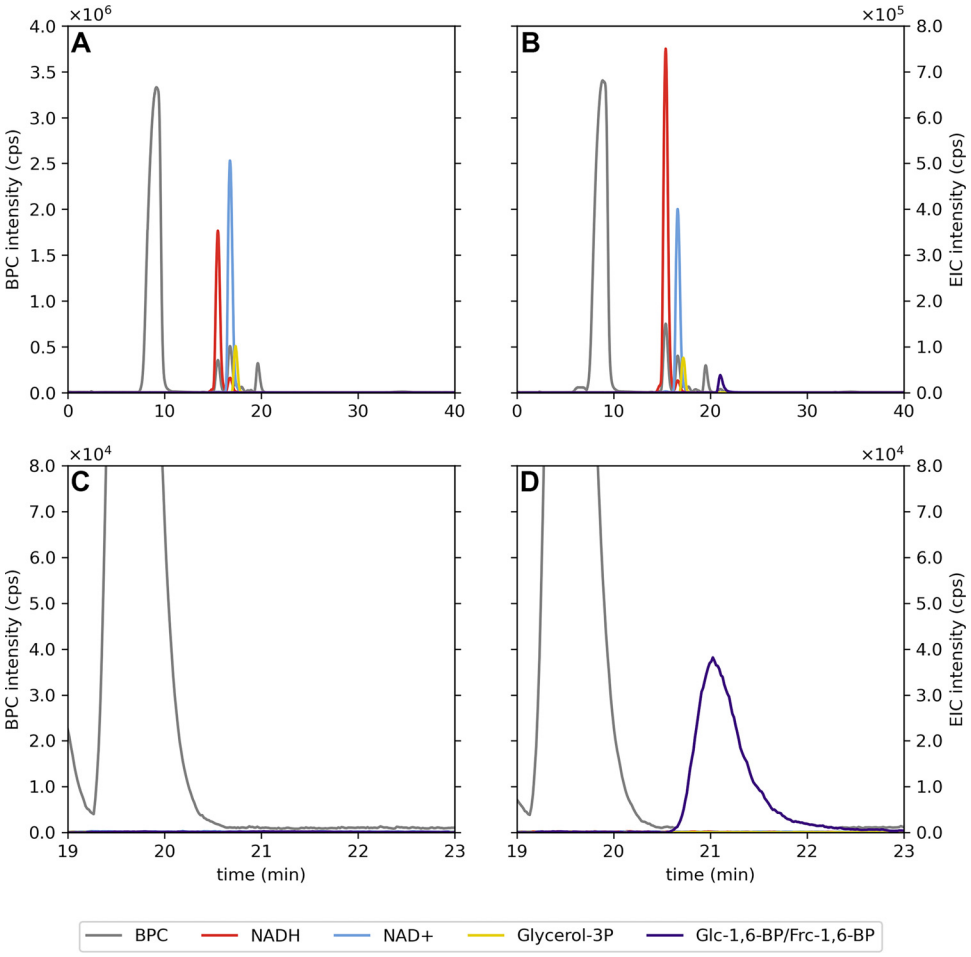

FIG 4 LC-MS analysis reveals that Slr1334 metabolizes Frc-1,6-BP into a molecule of identical mass that is not degraded by Frc-1,6-BP-aldolase. Analysis of the products of the reaction without (A) and with Slr1334 (B) via LC/MS. Shown are the base peak chromatograms (BPC) in the mass range (M-H)- *m/z* = 79–1,601 (gray) and the extracted ion chromatograms (EIC) based on the exact masses of NAD^+ $(M\text{-}H)^-$ = 662.101 *m/z* (light blue), NADH $(M\text{-}H)^-$ = 664.117 *m/z* (red), Glycerol 3-P $(M\text{-}H)^-$ = 171.006 *m/z* (yellow), Glc-1,6-BP/Frc-1,6-BP $(M\text{-}H)^-$ = 338.988 *m/z* (purple). The presence of the NAD^+ (blue) and Glycerol-3P (yellow) peaks in (B) shows that Frc-1,6-BP was not fully metabolized into Glc-1,6-BP. Magnification and adjustment of the graphs in (A) and (B) is clear evidence of the absence (C) or formation (D) of Glc-1,6-BP.

remaining Frc-1,6-BP. Therefore, Slr1334 was incubated with 500 μM Frc-1,6-BP and 1 mM Glc-1P for 1.5 h. As controls, the same assays were performed with Sll0726 or without any enzyme. After the reaction was stopped by heat inactivation, the supernatant was used to run the coupled Fba/GPDH assay in a dilution of 1:10, which would correspond to a final concentration of 50 μM Frc-1,6-BP if no Frc-1,6-BP was consumed. As further controls, standards of 50 μM and 25 μM Frc-1,6-BP were used in the Fba/GPDH assay. This experiment showed that the concentration of Frc-1,6-BP decreased by about 50% when in the first reaction Slr1334 was present, while apparently no Frc-1,6-BP was utilized in the control reactions (Fig. 5). This result agreed with the assumption that the reaction reaches an equilibrium at 50% product formation, either because of the reversibility of the reaction or product inhibition.

The Slr1334 reaction is reversible. To reveal whether Slr1334 can catalyze the proposed reverse reaction and synthesize Frc-1,6-BP from Glc-1,6-BP and fructose-1P (Frc-1P)/fructose-6P (Frc-6P), formation of Frc-1,6-BP was coupled to the Fba and GPDH reaction. For the assay, 50 μM Glc-1,6-BP was used and the reaction was started by the addition of 5 mM Frc-6-P. As control reaction, *Synechocystis* Sll0726 was used. In addition, we also tested PGM1 from rabbit since this type of PGM was stated to possibly catalyze this reaction albeit at a very low efficiency (22, 23). The results clearly showed

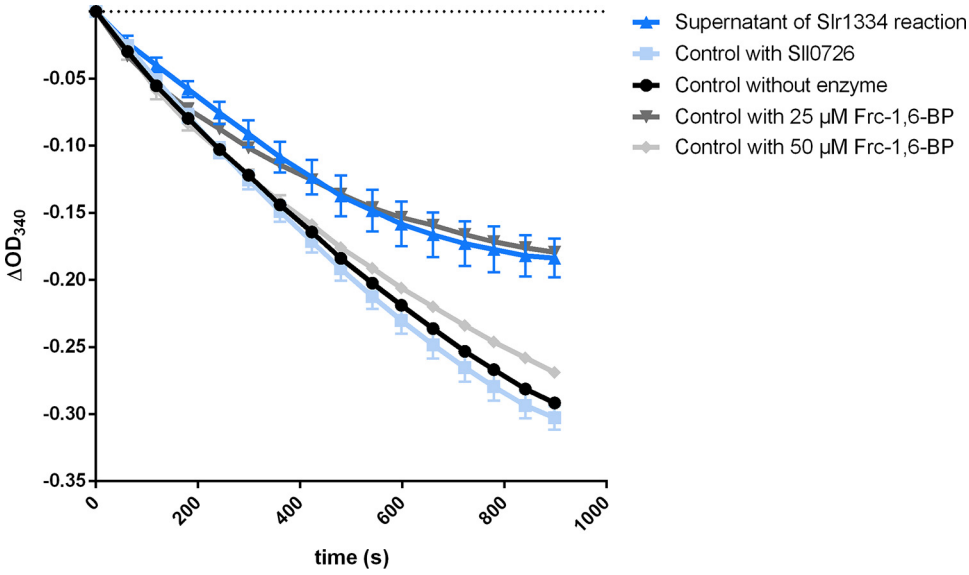

FIG 5 Slr1334 produces Glc-1,6-BP out of Frc-1,6-BP in an equilibrium reaction. Shown is the Frc-1,6-BP-aldolase activity: in dark blue, after addition of the supernatant of the Slr1334 reaction; in light blue, after addition of the supernatant of the Sll0726 reaction as a control; in black, after addition of the supernatant without any enzyme. In dark gray and light gray, the aldolase activity measured at Frc-1,6-BP concentrations of 25 μM and 50 μM, respectively, as further control. Frc-1,6-BP was used at concentrations of 500 μM in the Slr1334 reaction and respective control reactions. Therefore, its final concentration in the Sll0726 assay after 1:10 dilution was expected to be 50 μM assuming no consumption of Frc-1,6-BP in the Slr1334 reaction. Three replicates were measured for each datapoint. Error bars represent the SD.

that Slr1334 could produce Frc-1,6-BP, resulting in measurable aldolase activity while the Sll0726 and rabbit PGM controls showed no marked activity (Fig. 6a). Using this assay, we tried to determine the kinetic constants for the two substrates Frc-6-P and Glc-1,6-BP. For Frc-6P, a K_m of 1 mM and a K_{cat} of 1.2 s^{-1} could be determined (Fig. 6b, Table 3). By contrast, the affinity of Slr1334 for Glc-1,6-BP was so high that, even at the lowest measurable substrate concentrations (2 μM), the reaction proceeded with maximal velocity (Fig. 6c). Altogether these experiments unequivocally demonstrate that Slr1334 is the first characterized bacterial Glc-1,6-BP synthase. In contrast to the eukaryotic Glc-1,6-BP synthase, the prokaryotic enzyme uses Frc-1,6-BP as major phosphoryl donor for Glc-1,6-BP production.

The Glc-1,6-BP synthase reaction is also performed by other members of the cd05800 group. To determine whether the reaction catalyzed by Slr1334 is representative for αPHM enzymes of the cd05800 family, we decided to analyze the corresponding homologue from the human microbiome associated bacterium *Bacteroides salyersiae*. Therefore, we tested formation of Glc-1,6-BP under the same conditions as described above for Slr1334 by incubating the recombinant cd05800 enzyme from *B. salyersiae* with Frc-1,6-BP and Glc-1P or Glc-6P and subsequently adding the supernatant of this reaction to the Sll0726 assay. As a positive control we used the reaction of Slr1334.

The addition of the supernatant from the *B. salyersiae* cd05800 PGM increased the velocity of Sll0726 in a comparable manner as the supernatant of the Slr1334 reaction (Fig. 7). This indicates that similar amounts of Glc-1,6-BP have been formed in both reactions, hence revealing that *B. salyersiae* cd05800 PGM catalyzes the same reaction as Slr1334.

DISCUSSION

Among the key reactions in carbon metabolism are the phosphoryl transfer reactions on different phosphosugars, which are catalyzed by the members of the αPHM superfamily. These reactions are essential for glycogen metabolism, amino sugar metabolism as well as cell wall synthesis and are conserved throughout all domains of life. The interconversion of Glc-1P to Glc-6P and vice versa by PGM is by far the best

10.1128/mbio.01469-22

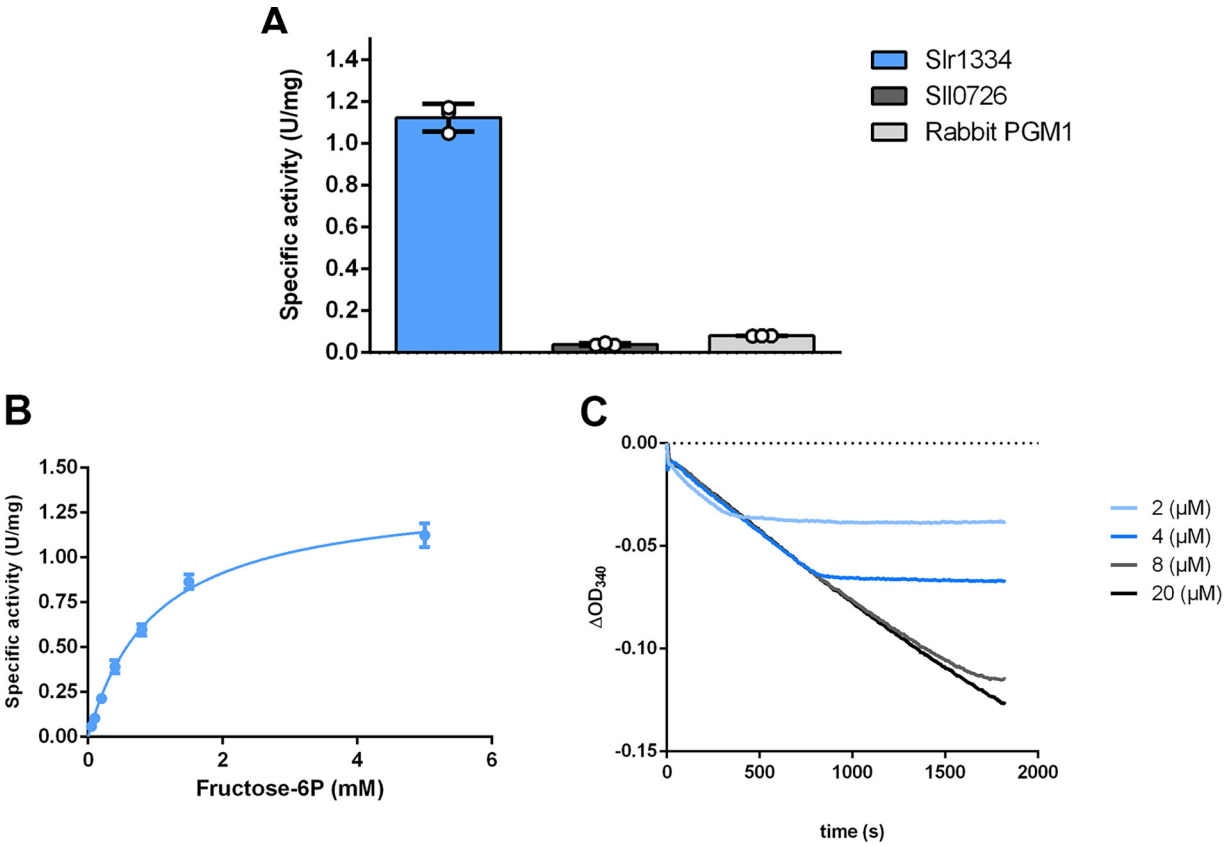

FIG 6 Slr1334 catalyzes the reverse reaction to form Frc-1,6-BP out of Glc-1,6-BP and Frc-6P. (A) Activity of Slr1334 (blue), Sll0726 (gray), and rabbit PGM1 (black) using 50 μM Glc-1,6-BP and 5 mM Frc-6P. (B) Michaelis-Menten kinetics of Slr1334 using different concentrations of Frc-6P and 50 μM Glc-1,6-BP. (C) Slr1334 reaction at different concentrations of Glc-1,6-BP and 0.5 mM Frc-6P. Three replicates were measured for each datapoint. Error bars represent the SD; asterisks represent the statistical significance.

studied of these reactions and investigation of PGM goes back to the 1940s. It has long been known that PGM requires Glc-1,6-BP as a activator (10). While in mammals free Glc-1,6-BP has been shown to derive from the reaction of the PGM2L1 enzyme utilizing Glc-1P and 1,3-BPG as substrates, its origin in prokaryotes has remained unknown (3).

In this study, we used the unicellular cyanobacterium *Synechocystis* sp. PCC6803 as a model organism to identify the first bacterial glucose-1,6-BP synthase. This reversible reaction is a novel function of a member of a distinct αPHM subfamily producing free α-d-Glc-1,6-BP and Frc-6P from Frc-1,6-BP and Glc-1P/Glc-6P.

Glc-1,6-BP is essential for PGM activity due to the requirement for phosphorylation of the serine residue at the active site for enzyme activation. The activating reaction converts Glc-1,6-BP into either Glc-1P or Glc-6P. After this initial activation, the interconversion of Glc-1P to Glc-6P is mediated by a transfer of the phosphate group from the serine residue at the active site to the 1′ or 6′ position of the substrate respectively, forming a Glc-1,6-BP intermediate. This intermediate has to reconfigure inside the enzyme and transfer the phosphate of its 6′ or 1′ position back to the active site serine leading to the release of Glc-6P or Glc-1P, respectively. As a result of this mechanism, the active site remains phosphorylated, and the enzyme is ready for a new cycle. However, it has been shown that the phosphorylation of PGM at the active site is lost after an aver-

TABLE 3 Kinetic parameters of Frc-1,6-BP synthesis by Slr1334[a]

Substrate	K_m (mM)	K_{cat} (s^{-1})	K_{cat}/K_m ($M^{-1}s^{-1}$)
Glc-1,6-BP	<0.002	1.2 ± 0.03	600,000
Frc-6P	1.0 ± 0.07		>1,200

[a] K_m and Kcat values are means of triplicates with ± SD.

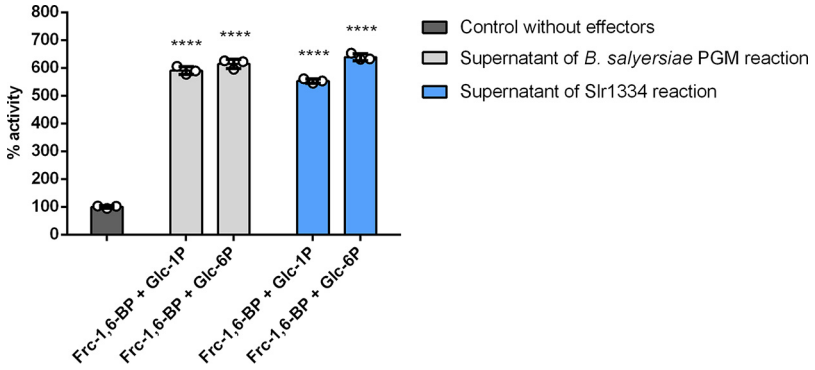

FIG 7 Slr1334 homologue from *B.salyersiae* also forms Glc-1,6-BP out of Frc-1,6-BP. Shown is the Sll0726 PGM activity in the presence of different effectors relative to the activity in the absence of effector molecules (set as 100%, dark gray bar): The different bars represent the following reactions: Light gray bars: Relative PGM activity in the presence of the supernatant of the *B. salyersiae* PGM reaction carried out with different combinations of substrates, as indicated. Blue bars: Same conditions as adjacent blue bars, except that *B. salyersiae* PGM was replaced by Slr1334, as a positive control. Error bars represent the SD; asterisks represent the statistical significance in comparison to the reaction without effectors.

age of 15–20 reaction cycles by a spontaneous dissociation of the intermediate Glc-1,6-BP leaving behind an inactive dephosphoenzyme. Therefore, a constant level of Glc-1,6-BP is necessary to ensure that PGM is kept in an active state (24, 25). While the loss of the intermediate might be regarded as an unfavorable event, it can also be considered as a regulatory mechanism that enables regulation of PGM activity based on Glc-1,6-BP levels. For other αPHMs like PMM and PNGM it is known that the corresponding intermediates (e.g., α-d-mannose-1,6-BP and α-d-glucosamine-1,6-BP) are formed during the reaction of the respective enzymes in the same way as for PGM but no source of those intermediates is known that would enable an initial activation of these αPHMs or would keep them in an active state overtime when phosphorylation is lost. However, because many members of the αPHM family show at least some residual PGM activity, Glc-1,6-BP was suggested to be the activating compound for these enzymes as well. This has in fact been shown for PNGM from *E. coli* which is considered to be an essential enzyme (26). This makes the role of Glc-1,6-BP in carbon metabolism even more relevant and would explain the failed attempts to delete the *slr1334* gene (19).

In mammals, it was shown that Glc-1,6-BP can also regulate central enzymes of carbon pathways by inhibiting hexokinases, 6-phosphogluconate dehydrogenase and fructose-1,6-bisphosphatase and by activating phosphofructokinase and pyruvate kinase (12). Further studies in mammals showed that Glc-1,6-BP is especially elevated in brain tissue to a level that highly exceeds the regulatory concentrations needed for PGM activity, and that reduced levels of Glc-1,6-BP cause severe neurological problems (27). This indicates that at least in mammals there are likely more functions of Glc-1,6-BP to be discovered. Given the important role of Glc-1,6-BP in eukaryotic metabolism, it is surprising that very little is known on the role of Glc-1,6-BP in bacterial physiology. The only study about the origin of α-d-Glc-1,6-BP production in bacteria proposed a phosphodismutase reaction with Glc-1P as the sole substrate in *E. coli* (28). Moreover, the levels of Glc-1,6-BP in eukaryotes are affected by a specific Glc-1,6-BP phosphatase, PMM1, which is a phosphomannomutase that is not part of the αPHM superfamily. Whether a homologue exists in bacteria is currently unknown (29).

In the absence of Glc-1,6-BP, both Slr1334 and Sll0726 showed low PGM activity. This residual activity can be explained by the fact that a phosphorylation of the active site serine can also be achieved at high concentrations of Glc-1P but at a much lower efficiency, leading to high K_m values and overall strongly reduced activity (11). In the presence of Frc-1,6-BP, Sll0726 was strongly inhibited, which agrees with the inhibitory effect of Frc-1,6-BP on other PGMs (20, 21). By contrast, Frc-1,6-BP enhanced the overall

10.1128/mbio.01469-22

catalytic activity of Slr1334, primarily because of a strongly decreased K_m. This effect can now be attributed to the formation of the activator Glc-1,6-BP.

Like mammalian PGM2L1, Slr1334 can utilize 1,3-BPG as a phosphorylating compound for Glc-1,6-BP formation, however with a much lower efficiency than Frc-1,6-BP. Although it cannot be excluded that 1,3-BPG could play a role under certain conditions, Frc-1,6-BP seems to be more important as it can accumulate to high levels in bacteria (30).

For the mammalian PGM2L1 a reverse reaction (formation of 1,3-BPG and Glc-1P from Glc-1,6-BP and 3-PG) has not been shown. For Slr1334, we could clearly show reversibility of the reaction, producing Frc-1,6-BP from Glc-1,6-BP and Frc-6P. Provided that both directions of the reaction have similar kinetic properties, Slr1334 appears to be a *bona-fide* Glc-1,6-BP synthase, which is prone to activate the main PGM Sll0726.

In contrast to Glc-1,6-BP, Frc-1,6-BP is an obligatory intermediate in glycolysis, gluconeogenesis and Calvin-Benson-Bassham cycle. In contrast to mammalian PGM2L1, *Synechocystis* Slr1334 uses this sugar as the major substrate for Glc-1,6-BP synthesis. This links the synthesis of Glc-1,6-BP to the levels of Frc-1,6-BP. Its steady state level depends on the activity of the opposing reactions of phosphofructokinase (Pfk) and fructose-1,6-bisphosphatase (FBPase), both of which are regulated in an opposite manner: While PFK is usually activated by the low energy state metabolites ADP and AMP and downregulated by the high energy state metabolites ATP and citrate, FBPase is downregulated by AMP while unaffected by high energy compounds. The level of Frc-1,6-BP is further determined by the Frc-1,6-BP-aldolase activity. Frc-1,6-BP is also known to be an allosteric activator of pyruvate kinase (PK), the final step in glycolysis (31).

Altogether, in the cyanobacterium *Synechocystis* PCC6803, Frc-1,6-BP appears to have two counteracting effects on PGM activity. On the one hand, it acts as a direct inhibitor of PGM; on the other hand, it gives rise to the synthesis of the PGM activator Glc-1,6-BP through the activity of Slr1334. Furthermore, since these double phosphorylated sugars may affect further enzyme reactions, by connecting these two metabolites, Slr1334 might represent a crucial regulatory point in glycolysis (Fig. 8). This conclusion would further underline the essential role of *slr1334* (19).

Interestingly, our phylogenetic analysis revealed the cd05800 subfamily as the most primordial group of phosphoglucomutases. This group appears to be especially present in bacterial classes that are considered deeply branching bacteria meaning they are relatively close to the last common universal ancestor. Examples for this are the classes of Deinococci, Aquificae, Thermotogae, Bacteroidetes, and Cyanobacteria, where this PGM subfamily is widely distributed. This finding is supported by the fact that cd05800 members can also be found in archaea. In agreement with this, the first characterized representative of this group, Slr1334 shows both PGM and Glc-1,6-BP activity. This suggests that in primordial systems these PGMs with broad functionality could have performed PGM reactions without the requirement for specific Glc-1,6-BP synthase enzymes. During subsequent functional diversification, the PGMs may have adopted unique functions, with specialization toward efficient conversion of Glc-6-P into Glc-1P on the one hand. On the other hand, they may have lost the ability to sufficiently catalyze other reactions like Glc-1,6-BP synthesis. This assumption agrees with our observation that in some bacteria the primordial, more universal cd05800 PGM is the only subfamily found. In contrast, the more specialized and highly efficient cd03085 and cd05801 PGMs are always accompanied by other subfamily members (mainly cd05800). Conversely, the cd03089 PGM/PMM, often associated with pathogenic bacteria, is never accompanied with a cd05800 representative which raises the question how those strains produce Glc-1,6-BP (Table S2). To clarify these issues, further investigations on αPHM members from various bacterial groups are required.

We were able to show that the cd05800 PGM from the human gut commensal bacterium *B. salyersiae* also catalyzes the synthesis of Glc-1,6-BP out of Frc-1,6-BP like Slr1334 (Fig. 7). In the case of *B. salyersiae*, the enzyme appears to have an even higher catalytic efficiency for the Glc-1,6-BP synthase reaction than for the standard PGM reaction (Fig. S1 in the supplemental material). Therefore, we conclude that the formation

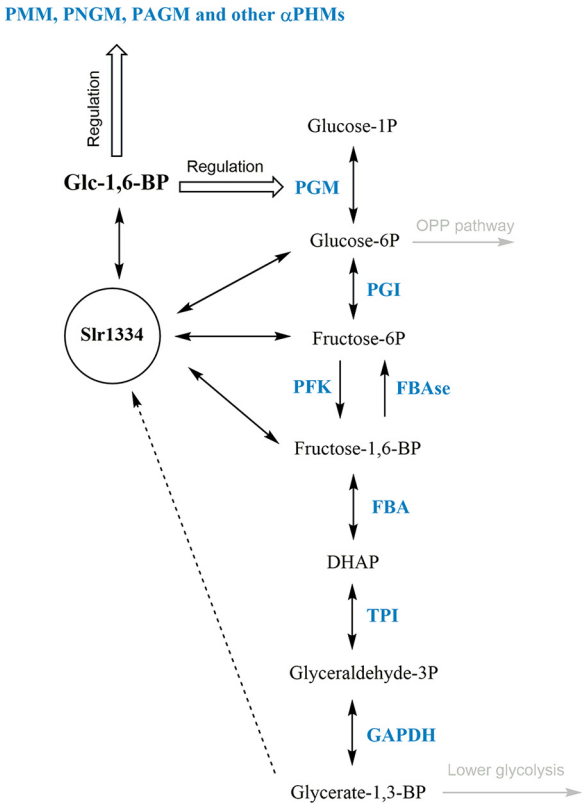

FIG 8 Potential role of Slr1334 in glycolysis. Shown is the potential role of Slr1334 in regulating activity of αPHMs and the concentration of key metabolites in glycolysis. PGM: Phosphoglucomutase; PGI: Glc-6P-Isomerase; PFK: Phosphofruktokinase; FBAse: fructose-6P phosphatase; FBA: Frc-1,6-BP-aldolase; TPI: Triosephosphate isomerase; GAPDH: Glyceraldehyde-3P dehydrogenase; DHAP: Dihydroxyacetone phosphate.

of Glc-1,6-BP might be a general feature of this PHM subfamily. However, further studies on members of this group are required to support this hypothesis.

Interestingly, members of the cd05800 group are also present in emerging human pathogenic species like *Vibrio*, *Eggerthella*, and *Brachyospyra* (Fig. 1) and are likely to play a key role in the metabolism of these pathogens. In fact, due to their crucial role in capsule and cell wall synthesis PGMs have been suggested as novel targets for the development of anti-infectives in prophylactic and therapeutic interventions (5, 32). It is tempting to speculate that Glc-1,6-BP synthases of the cd05800 family, in virtue of their absence in eukaryotes, may also be interesting candidates for the development of novel drugs modulating the microbiota with little collateral damage to the host.

MATERIALS AND METHODS

Isothermal, single-reaction DNA assembly (Gibson cloning). Cloning was performed as described by Gibson, Young (33) using *E. coli* NEB10β cells (details in Table S5). All primers and plasmids used are shown in Table S3 and Table S4 in the supplemental material, respectively.

Cultivation of *Escherichia coli*. If not otherwise stated *E. coli* was grown in Luria-Bertani medium at 37°C (34). For growth on plates, 1.5% (wt/vol) agar-agar was added. For cells containing plasmids, the appropriate concentration of antibiotics was used. All *E. coli* strains used in this study are listed in Table S5 in the supplemental material.

Protein overexpression and purification. The plasmids used for protein overexpression are shown in Table S4 in the supplemental material. *Escherichia coli* Rosetta-gami (DE3) (details Table S5) was used for the overexpression of all proteins. For this, cells were cultivated in 2xYT (3.5% tryptone, 2% yeast extract, 0.5% NaCl; 1L of culture in 5L flasks) at 37°C until reaching exponential growth (OD_{600} 0.6–0.8). Protein overexpression was induced by adding 75 μg/L anhydrotetracycline, followed by incubation at 20°C for 16 h. Cells were harvested by centrifugation at 4000 g for 10 min at 4°C. Cell disruption was performed by sonication in 40 mL of lysis buffer (100 mM Tris-HCl pH 7.5, 500 mM NaCl, 10 mM $MgCl_2$, 20 mM Imidazole for His-tagged proteins and 100 mM Tris-HCl pH 8, 150 mM NaCl, 10 mM $MgCl_2$ for Strep-tagged proteins); lysis buffers were supplemented with DNase I and cOmplete^{TM} protease inhibitor cocktail (Roche, Basel).

10.1128/mbio.01469-22

The cell lysate was centrifuged at 40,000 g for 45 min at 4°C and the supernatant was filtered with a 0.22 μM filter.

For the purification of His-tagged proteins, 5 mL Ni-NTA HisTrap columns (GE Healthcare, IL, USA) were used. The cell extracts were loaded onto the columns, washed with wash buffer (50 mM Tris-HCl pH 7.4, 500 mM NaCl, and 50 mM Imidazole) and eluted with elution buffer (50 mM Tris-HCl pH 7.4, 500 mm NaCl, and 500 mM Imidazole).

Measurement of PGM activity of Sll0726 and Slr1334 *in vitro*. Buffer for enzymatic reactions was composed of 50 mM HEPES-KOH pH 7.5, 150 mM KCl, 10 mM $MgCl_2$, 1 mM $NADP^+$, 1 mM DTT, and 1 U/mL G6PDH from *Saccharomyces cerevisiae* (G6378, Sigma-Aldrich). For Sll0726 activity, 60 ng of Strep-tagged purified protein was added to each reaction. For slr1334 activity, 650 ng of purified protein was added. For tests with saturating Glc-1,6-BP concentrations, 60 μM Glc-1,6-BP have been used. Reaction was started by the addition of glucose-1P. Reactions were carried out in a total of 300 μL in a 96-well microplate. Absorption change at 340 nm was continuously measured for 15 min at 30°C in a TECAN Spark Multiplate reader (Tecan Group AG, Männedorf, Switzerland). At least three replicates were measured.

Measurement of Glc-1,6-BP formation. The reaction buffer was composed of 50 mM HEPES-KOH pH 7.5, 150 mM KCl and 10 mM $MgCl_2$. To test the formation of Glc-1,6-BP out of Frc-1,6-BP 1 mM Frc-1,6-BP, 1 mM Glc1P or 1 mM Glc-6P were added in different combinations. To test the formation of Glc-1,6-BP out of 1,3-BPG instead of Frc-1,6-BP, 1 mM ATP, 1 mM 3-PG and 60 μg PGK have been used. Sll0726 and Slr1334 concentration were 30 μg/mL. The reactions were performed for 1.5 h at 30°C followed by heat inactivation at 90°C for 10 min with subsequent centrifugation at 25000 g for 10 min at 4° C. The supernatants of the various reactions were used at 1:10 dilution in the Sll0726 activity assay.

Measurement of Frc16BP formation by coupling to Frc-1,6-BP aldolase assay. To measure the formation of Frc-1,6-BP by Slr1334, the reaction buffer was composed of 50 mM HEPES-KOH pH 7.5, 150 mM KCl, 10 mM $MgCl_2$, 0.2 mM NAD, 7 μg Slr1334, 1U/mL FBP-aldolase from rabbit muscle and 1U/mL GDH from rabbit muscle. Concentrations of Glc-1,6-BP and Frc-6P were varying depending on the experiment. Reaction was started by the addition of Glc-1,6-BP or Frc-6P depending on the experiment.

To measure residual Frc-1,6-BP after running the Slr1334 reaction, the buffer was composed of 50 mM HEPES-KOH pH 7.5, 150 mM KCl, 10 mM $MgCl_2$, 0.2 mM NAD, 0.02U/mL aldolase from rabbit muscle and 1U/mL GDH from rabbit muscle.

All reactions were carried out in a total of 300 μL in a 96-well microplate. Absorption change at 340 nm was continuously measured for 15 min at 30°C in a TECAN Spark Multiplate reader (Tecan Group AG, Männedorf, Switzerland). The enzymatic activity was then calculated. At least three replicates were measured.

LC-MS measurement. *Sample preparation*. Reaction buffer was composed of 50 mM HEPES-KOH pH 7.5, 150 mM KCl and 10 mM $MgCl_2$. For the reaction without enzyme 500 μM Frc-1,6-BP and 1 mM Glc1-P were added. For the Slr1334 reaction, 30 μg of Slr1334 have been used additionally. Reaction was carried out in a total volume of 1 mL at 30°C for 1h. Afterwards, reaction was stopped by heat inactivation at 90° C followed by centrifugation at 25000 g for 10 min at 4°C.

For degradation of Frc-1,6-BP, 1 mM NADH, 2U/mL of aldolase from rabbit muscle and 2U/mL of GDH from rabbit muscle were added. Reaction was carried out followed by inactivation at the same conditions as before.

***LC/MS analysis*.** LC/MS analysis was performed using an electrospray ionization time of flight (ESI-TOF) mass spectrometer (MicrOTOF II; Bruker Daltonics), operated in negative ion-mode connected to an UltiMate 3000 high-performance liquid chromatography (HPLC) system (Dionex). The separation in the HPLC was carried out using a SeQuant ZIC-pHILIC column (PEEK 150 $\times$ 2.1 mm, 5 μm, 110 Å, Merck) at 30°C with an CH_3CN (buffer A) and 100 mM $(NH_4)_2CO_3$, pH 9 (buffer B) buffer system. A single run (injection volume of 5 μL) was performed with a flow rate of 0.2 mL/min and a linear gradient of 25 min, reducing the concentration of buffer A from 82% to 42%. Before (5 min) and after (10 min) the gradient, the column was equilibrated with 82% buffer A.

Phylogenetic analysis of αPHM subfamilies. The occurrence of members of the αPHM subfamilies was investigated in organisms included in the NCBI RefSeq_protein database using the default settings of blastp. The search returned 2140 hits for Slr1334 homologues and >5000 hits for Sll0726 homologues by using the following threshold:

E-value $\leq 10^{-40}$; sequence identity $\geq$ 30%; Query coverage $\geq$ 95%

Phylogenetic tree data were created using the ClustalW implementation from the European Bioinformatics Institute and the phylogenetic tree was created using the Interactive Tree of Life (iTOL) v5 online tool (35, 36).

Statistical analysis. Statistical details for each experiment can be found in the figure legends. GraphPad PRISM was used to perform one-sided ANOVA to determine the statistical significance. Asterisks (*) in the figures symbolize the *P*-value: one asterisk represents $P \leq 0.05$, two asterisks $P \leq 0.01$, three asterisks $P \leq 0.001$, and four asterisks $P \leq 0.0001$.

SUPPLEMENTAL MATERIAL

Supplemental material is available online only.

FIG S1, TIF file, 0.1 MB.

TABLE S1, DOCX file, 0.02 MB.

TABLE S2, DOCX file, 0.02 MB.

TABLE S3, DOCX file, 0.01 MB.

TABLE S4, DOCX file, 0.01 MB.
TABLE S5, DOCX file, 0.02 MB.

ACKNOWLEDGMENTS

We thank Libera Lo Presti for her assistance in writing this manuscript and Gaia Bianchi for support in performing enzymatic assays.

This work was supported by FOR2816 "The Autotrophy-Heterotrophy Switch in Cyanobacteria: Coherent Decision-Making at Multiple Regulatory Layers" and EXC2121 "Controlling Microbes to Fight Infections" (CMFI).

N.N. performed cloning, protein purification, enzymatic assays phylogenetic analysis and wrote manuscript. S.F. performed LC/MS analysis. K.F. conceived study, interpreted data, and edited manuscript.

We declare no competing interest.

REFERENCES

1. Shackelford GS, Regni CA, Beamer LJ. 2004. Evolutionary trace analysis of the α-D-phosphohexomutase superfamily. Protein Sci 13:2130–2138. https://doi.org/10.1110/ps.04801104.
2. Stiers KM, Muenks AG, Beamer LJ. 2017. Biology, mechanism, and structure of enzymes in the α-d-phosphohexomutase superfamily. Adv Protein Chem Struct Biol 109:265–304. https://doi.org/10.1016/bs.apcsb.2017.04.005.
3. Maliekal P, Sokolova T, Vertommen D, Veiga-da-Cunha M, Van Schaftingen E. 2007. Molecular identification of mammalian phosphopentomutase and glucose-1,6-bisphosphate synthase, two members of the alpha-D-phosphohexomutase family. J Biol Chem 282:31844–31851. https://doi.org/10.1074/jbc.M706818200.
4. Lu S, Wang J, Chitsaz F, Derbyshire MK, Geer RC, Gonzales NR, Gwadz M, Hurwitz DI, Marchler GH, Song JS, Thanki N, Yamashita RA, Yang M, Zhang D, Zheng C, Lanczycki CJ, Marchler-Bauer A. 2020. CDD/SPARCLE: the conserved domain database in 2020. Nucleic Acids Res 48:D265–D268. https://doi.org/10.1093/nar/gkz991.
5. Regni C, Tipton PA, Beamer LJ. 2002. Crystal structure of PMM/PGM: an enzyme in the biosynthetic pathway of P aeruginosa virulence factors. Structure 10:269–279. https://doi.org/10.1016/S0969-2126(02)00705-0.
6. Regni C, Naught L, Tipton PA, Beamer LJ. 2004. Structural basis of diverse substrate recognition by the enzyme PMM/PGM from P aeruginosa. Structure 12:55–63. https://doi.org/10.1016/j.str.2003.11.015.
7. Akutsu J-I, Zhang Z, Tsujimura M, Sasaki M, Yohda M, Kawarabayasi Y. 2005. Characterization of a thermostable enzyme with phosphomannomutase/phosphoglucomutase activities from the hyperthermophilic archaeon pyrococcus horikoshii OT3. J Biochem 138:159–166. https://doi.org/10.1093/jb/mvi115.
8. Liu Y, Ray WJ, Jr, Baranidharan S. 1997. Structure of rabbit muscle phosphoglucomutase refined at 2.4 A resolution. Acta Crystallogr D Biol Crystallogr 53:392–405. https://doi.org/10.1107/S0907444997000875.
9. Backe PH, Laerdahl JK, Kittelsen LS, Dalhus B, Mørkrid L, Bjørås M. 2020. Structural basis for substrate and product recognition in human phosphoglucomutase-1 (PGM1) isoform 2, a member of the α-d-phosphohexomutase superfamily. Sci Rep 10:5656. https://doi.org/10.1038/s41598-020-62548-0.
10. Leloir LF, Trucco RE, Cardini CE, Paladini AC, Caputto R. 1948. The co-enzyme of phosphoglucomutase. Arch Biochem 19:339.
11. Naught LE, Tipton PA. 2001. Kinetic mechanism and pH dependence of the kinetic parameters of Pseudomonas aeruginosa phosphomannomutase/phosphoglucomutase. Arch Biochem Biophys 396:111–118. https://doi.org/10.1006/abbi.2001.2618.
12. Carreras J, Bartrons R, Climent F, Cusso R. 1986. Bisphosphorylated metabolites of glycerate, glucose, and fructose: functions, metabolism and molecular pathology. Clinical Biochemistry 19:348–358. https://doi.org/10.1016/S0009-9120(86)80008-X.
13. Joshi JG, Handler P. 1964. Phosphoglucomutase: I. Purification and properties of phosphoglucomutase from *escherichia coli*. J Biol Chem 239:2741–2751. https://doi.org/10.1016/S0021-9258(18)93809-3.
14. Morán-Zorzano MT, Viale AM, Muñoz FJ, Alonso-Casajús N, Eydallín GG, Zugasti B, Baroja-Fernández E, Pozueta-Romero J. 2007. *Escherichia coli* AspP activity is enhanced by macromolecular crowding and by both glucose-1,6-bisphosphate and nucleotide-sugars. FEBS Lett 581:1035–1040. https://doi.org/10.1016/j.febslet.2007.02.004.
15. Spat P, Klotz A, Rexroth S, Macek B, Forchhammer K. 2018. Chlorosis as a developmental program in cyanobacteria: the proteomic fundament for survival and awakening. Molecular & Cellular Proteomics 17(9):1650–1669. https://doi.org/10.1074/mcp.RA118.000699.
16. Lindahl M, Florencio FJ. 2003. Thioredoxin-linked processes in cyanobacteria are as numerous as in chloroplasts, but targets are different. Proc Natl Acad Sci U S A 100:16107–16112. https://doi.org/10.1073/pnas.2534397100.
17. Mehra-Chaudhary R, Mick J, Tanner JJ, Henzl MT, Beamer LJ. 2011. Crystal structure of a bacterial phosphoglucomutase, an enzyme involved in the virulence of multiple human pathogens. Proteins 79:1215–1229. https://doi.org/10.1002/prot.22957.
18. Doello S, Neumann N, Forchhammer K. 2022. Regulatory phosphorylation event of phosphoglucomutase 1 tunes its activity to regulate glycogen metabolism. FEBS J. https://doi.org/10.1111/febs.16471.
19. Liu L, Hu HHua, Gao H, Xu X. 2013. Role of two phosphohexomutase genes in glycogen synthesis in *Synechocystis sp.* PCC6803. Chin Sci Bull 58:4616–4621. https://doi.org/10.1007/s11434-013-5958-0.
20. Maino VC, Young FE. 1974. Regulation of glucosylation of teichoic acid: II. Partial characterization of phosphoglucomutase in bacillus subtilis 168. J Biol Chem 249:5176–5181. https://doi.org/10.1016/S0021-9258(19)42344-2.
21. Fazi A, Piacentini MP, Piatti E, Accorsi A. 1990. Purification and partial characterization of the phosphoglucomutase isozymes from human placenta. Prep Biochem 20:219–240. https://doi.org/10.1080/00327489008050198.
22. Passonneau JV, Lowry OH, Schulz DW, Brown JG. 1969. Glucose 1,6-diphosphate formation by phosphoglucomutase in mammalian tissues. J Biol Chem 244:902–909. https://doi.org/10.1016/S0021-9258(18)91871-5.
23. Hirose M, Ueda M, Chiba H. 1976. Multifunctional properties of beef liver phosphoglucomutase. Agricultural and Biological Chemistry 40:2433–2439. https://doi.org/10.1080/00021369.1976.10862415.
24. Naught LE, Tipton PA. 2005. Formation and reorientation of glucose 1,6-bisphosphate in the PMM/PGM reaction: transient-state kinetic studies. Biochemistry 44:6831–6836. https://doi.org/10.1021/bi0501380.
25. Ray WJ, Jr, Roscelli GA. 1964. A kinetic study of the phosphoglucomutase pathway. J Biol Chem 239:1228–1236. https://doi.org/10.1016/S0021-9258(18)91416-X.
26. Jolly L, Pompeo F, van Heijenoort J, Fassy F, Mengin-Lecreulx D. 2000. Autophosphorylation of phosphoglucosamine mutase from *Escherichia coli*. J Bacteriol 182:1280–1285. https://doi.org/10.1128/JB.182.5.1280-1285.2000.
27. Morava E, Schatz UA, Torring PM, Abbott M-A, Baumann M, Brasch-Andersen C, Chevalier N, Dunkhase-Heinl U, Fleger M, Haack TB, Nelson S, Potelle S, Radenkovic S, Bommer GT, Van Schaftingen E, Veiga-da-Cunha M. 2021. Impaired glucose-1,6-biphosphate production due to bi-allelic PGM2L1 mutations is associated with a neurodevelopmental disorder. Am J Hum Genet 108:1151–1160. https://doi.org/10.1016/j.ajhg.2021.04.017.
28. Leloir LF, Trucco RE. and., 1949. The formation of glucose diphosphate by Escherichia coli. Arch Biochem 24:65–74.
29. Veiga-da-Cunha M, Vleugels W, Maliekal P, Matthijs G, Van Schaftingen E. 2008. Mammalian phosphomannomutase PMM1 is the brain IMP-sensitive glucose-1,6-bisphosphatase. J Biol Chem 283:33988–33993. https://doi.org/10.1074/jbc.M805224200.

30. Bennett BD, Kimball EH, Gao M, Osterhout R, Van Dien SJ, Rabinowitz JD. 2009. Absolute metabolite concentrations and implied enzyme active site occupancy in *Escherichia coli*. Nat Chem Biol 5:593–599. https://doi.org/10.1038/nchembio.186.
31. Waygood EB, Mort JS, Sanwal BD. 1976. The control of pyruvate kinase of *Escherichia coli.* Binding of substrate and allosteric effectors to the enzyme activated by fructose 1,6-bisphosphate. Biochemistry 15:277–282. https://doi.org/10.1021/bi00647a006.
32. Zhang Y, Li T, Zhang J, Li Z, Zhang Y, Wang Z, Feng H, Wang Y, Chen C, Zhang H. 2016. The Brucella melitensis M5–90 phosphoglucomutase (PGM) mutant is attenuated and confers protection against wild-type challenge in BALB/c mice. World J Microbiol Biotechnol 32:58. https://doi.org/10.1007/s11274-016-2015-6.
33. Gibson DG, Young L, Chuang R-Y, Venter JC, Hutchison CA, Smith HO. 2009. Enzymatic assembly of DNA molecules up to several hundred kilobases. Nat Methods 6:343–345. https://doi.org/10.1038/nmeth.1318.
34. Bertani G. 1951. Studies on lysogenesis: I. The mode of phage liberation by lysogenic *Escherichia coli*. J Bacteriol 62:293–300. https://doi.org/10.1128/jb.62.3.293-300.1951.
35. Letunic I, Bork P. 2021. Interactive Tree of Life (iTOL) v5: an online tool for phylogenetic tree display and annotation. Nucleic Acids Res 49:W293–W296. https://doi.org/10.1093/nar/gkab301.
36. Madeira F, Park YM, Lee J, Buso N, Gur T, Madhusoodanan N, Basutkar P, Tivey ARN, Potter SC, Finn RD, Lopez R. 2019. The EMBL-EBI search and sequence analysis tools APIs in 2019. Nucleic Acids Res 47:W636–W641. https://doi.org/10.1093/nar/gkz268.

Supplementary Material

Name	Typical length (aa)	Sugar-binding domain sequence motif
cd03085 (PGM1)	~550	**CGEESFG**
cd05799 (PGM2)	550 – 650	AF**EE**AIG
cd03089 (PMM/PGM)	~450	A**GEMS**G**H**
cd03087 (PGM_like1)	~450	G**GE**G**NG**G
cd05800 (PGM_like2)	~450	G**GEESGG**
cd05801 (PGM_like3)	~550	G**GEESAG**
cd05803 (PGM_like4)	~450	**GGEGNGG**

Table S1: **PGM and "PGM like" subfamilies according to CDD:**

Given is the typical length and characteristic sugar-binding sequence motif of each PGM subfamily. Highly conserved amino acids are highlighted in bold

	cd03085	cd05799	cd03089	cd03087	cd05800	cd05801	cd05803
Mycobacterium tuberculosis		+	+			+	
Escherichia coli			+			+	
Helicobacter pylori			+				
Bordetella pertussis			+				
Neisseria gonorrhoeae			+				
Eggerthella lenta					+		
Bacteroides salyersisae		+			+		+
Synechocystis sp. PCC6803					+	+	
Prochlorococcus marinus	+				+		
Nostoc punctiforme	+				+		
Deinococcus radiodurans					+	+	
Geobacter metallireducens					+		
Litorilinea aerophilia					+	+	
Prosthecochloris vibrioformis					+	+	+
Granulicella mallensis					+	+	
Ammonifex degensii				+	+		+
Vibrio cholerae		+			+	+	
Caldicellulosiruptor owensis					+		
Thermotoga caldifontis					+		
Haloplanus aerogenes				+	+		
Persephonella atlantica					+		
Bacillus subtilis		+					
Staphylococcus aureus	+	+					

Table S2: Distribution of PHM subfamilies considered to be PGM or "PGM_like" in different bacterial strains

Blue color with (+) shows the presence of the respective αPHM subfamily in the listed strains

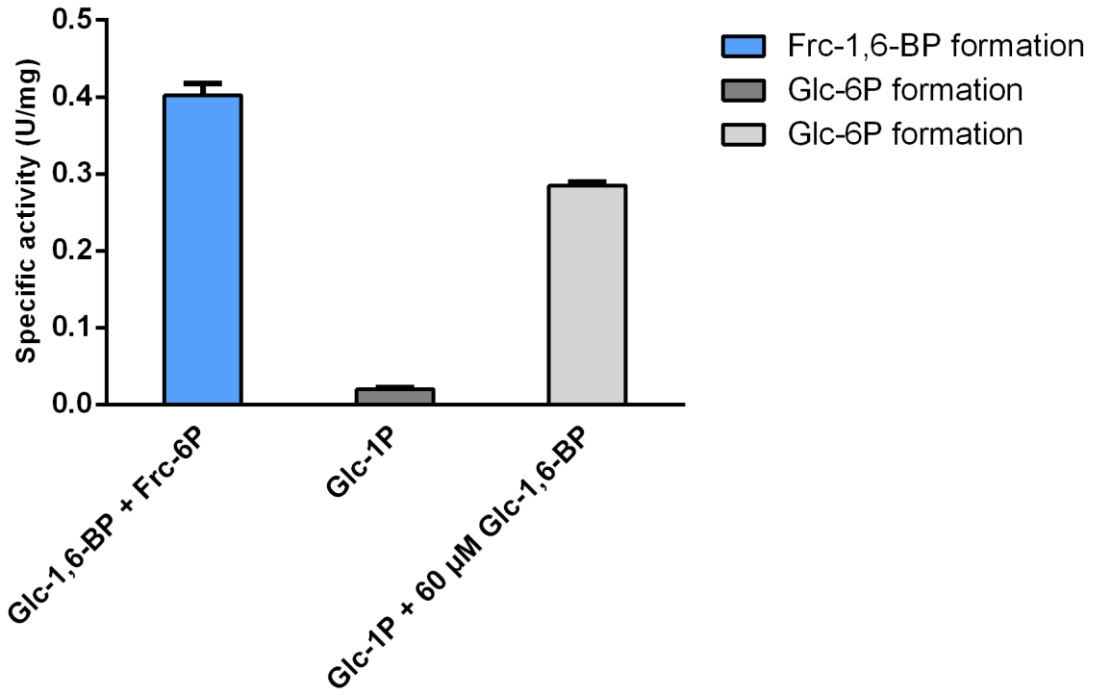

Figure S1: Specific activity of the Slr1334 orthologue from Bacteroides salyersiae:

Shown is: in blue, the reversible Glc-1,6-BP synthase activity of the *B. salyersiae* Slr1334 orthologue in the presence of 50 µM Glc-1,6-BP and 5 mM Frc-6P yielding Frc-1,6-BP; in dark gray and light gray, the PGM activity of the *B. salyersiae* Slr1334 orthologue in the sole presence of 1 mM Glc-1P, or in the simultaneous presence of 60 µM Glc-1,6-BP and 1 mM Glc-1P, respectively.

Primer	**Sequence (5' - 3')**
pASK-C(slr1334)_fw	TAGAAATAATTTTGTTTAACTTTAAGAAGGAGATATACAAATGGTTTACACTC CTGCTCC
pASK-C(slr1334)_rev	GGTCTTATTTTTCGAACTGCGGGTGGCTCCAGCTAGCCATGTGAGATGATT GTGCAGGCTTG
pASK-C(sll0726)_fw	TAGAAATAATTTTGTTTAACTTTAAGAAGGAGATATACAAATGACAAGCAGA ATTAATCC
pASK-C(sll0726)_rev	GGTCTTATTTTTCGAACTGCGGGTGGCTCCAGCTAGCCATGCCCAAAGCCGA GGTAACAATG
pASK-IBA5_Cterm_fw	GGCTAGCTGGAGCCACCCGCAGTTCGAAAAATAAGACCATGGTCTCTGATAT CTAACTAAG
pASK-IBA5_Cterm_rev	TTGTATATCTCCTTCTTAAAGTTAAAC

Table S3: List of the primers used in this study

Plasmid	Purpose
pASK-C(sll0726)	Expression of Strep-tagged Sll0726 in *E.coli*
pASK-C(slr1334)	Expression of Strep-tagged Slr1334 in *E.coli*
pET15b(PGK)	Expression of His-tagged Phosphoglycerate-kinase in *E.coli*

Table S4. List of the plasmids used in this study

Strain	Genotype	Purpose	Manufacturer
E. coli NEB10β	Δ(ara-leu) 7697 araD139 fhuAΔlacX74 galK16 galE15 e14-Φ80dlacZΔM15 recA1 relA1 endA1 nupGrpsL(StrR) rphspoT1 Δ(mrr-hsdRMS-mcrBC)	Molecular cloning	New England Biolabs (Ipswich (Massachusetts), USA)
E. coli Rosetta gami (DE3)	Δ(ara-leu)7697 ΔlacX74 ΔphoA PvuII phoR araD139 ahpC galE galK rpsL (DE3) F'[lac$^+$ lacI^q pro] gor522::Tn10 trxB pLysSRARE (Cam^R, Str^R, Tet^R)	Protein overexpression	Merck Millipore (Billerica (Massachusetts), USA)

Table S5. List of the bacterial strains used in this study

Publication 6: Research article

Neumann N., Lee K., Forchhammer K.

On the role of glycogen degrading enzymes in *Synechocystis* PCC6803

doi: https://doi.org/10.1101/2022.11.21.517384

On the role and regulation of glycogen catabolic isoenzymes in *Synechocystis* sp. PCC6803

Niels Neumann, Kenric Lee, Karl Forchhammer

Interfaculty Institute of Microbiology and Infection Medicine, University of Tübingen, Auf der Morgenstelle 28, 72076 Tübingen, Germany

Abstract

Glycogen is the main carbon storage polymer in many organisms and widespread throughout all domains of life. In cyanobacteria glycogen degradation plays an essential role when metabolism changes to a heterotrophic mode during dark phases or the resuscitation from nitrogen starvation. Like many other cyanobacteria the genome of *Synechocystis* sp. PCC 6803 encodes for several homologues of glycogen catabolic enzymes. The role and regulation of this isoenzymes has so far been only partly understood. Here we show via biochemical analysis that the glycogen phosphorylase GlgP1 is regulated by a C-terminal redox switch unique to certain cyanobacteria. This is the first time a redox regulation of a glycogen degrading enzyme has been shown in prokaryotes. Remarkably, GlgP1 is inactivated in its reduced state and gets activated via oxidation by ROS. We conclude that GlgP1 is especially important for rapid glycogen degradation in certain stress conditions during photoautotrophic growth. We suggest that thereby carbon is channeled through the OPP pathway, to stabilize photosynthesis during situations of high ribulose-1,5-BP demands. Furthermore, we suggest that the concomitant formation of NADPH within this pathway is essential to regenerate ROS scavenging compounds like GSH to reduce potential oxidative damage and to improve survivability under prolonged phases of oxidative stress. In addition, we show for the first time the role of the two glycogen debranching isoenzymes where GlgX1 turned out to be the essential glycogen debranching enzyme during resuscitation from chlorosis, while the role of GlgX2 remains elusive.

Introduction

Glycogen is the major carbon storage compound in animals, fungi and most bacteria. It's a glucose polymer linked at position α-1,4 with branches at position α-1,6. In bacteria, particularly in free living strains, glycogen is usually built up under conditions of carbon surplus and degraded when energy or carbon supplies are limited [1-3]. In cyanobacteria glycogen plays a key role in carbon metabolism and is tightly coupled to a photoautotrophic lifestyle where excess fixed CO_2 is stored as glycogen during the day which thereon gets catabolized during the night when metabolism switches to a heterotrophic mode. This essential role is further underlined by the fact that glycogen metabolic enzymes are conserved in all known cyanobacterial strains [4]. Next to providing energy during dark phases, glycogen degradation is also known to play a crucial role during acclimation to environmental stress conditions, such as the lack of available combined nitrogen sources, frequently occurring in marine and terrestrial ecosystems [5]. Adaptation to nitrogen starvation in non-diazotrophic cyanobacteria is characterized by the initiation of a genetically determined program, called chlorosis, where cells enter a state of dormancy, enabling them to outlive long periods of nitrogen deprivation. From this state the cells can resuscitate within 48 hours once combined nitrogen sources are available again [6]. This resuscitation process is supported by a rapid degradation of the previously accumulated high amounts of glycogen, which provides the building blocks for re-establishing the metabolic processes [7, 8]. Glycogen breakdown requires the coordinated action of glycogen phosphorylase (GlgP) and glycogen debranching enzyme (GlgX): The GlgP reaction releases Glc-1P by transferring orthophosphate to the non-reducing end of glucose residues which is considered the rate limiting step in glycogen catabolism [9]. This processive reaction stops once GlgP reaches the last four glucose residues left on a branch. In prokaryotes those remaining glucose units are hydrolyzed by "direct" debranching enzymes, releasing maltotetraose which can be further metabolized by maltodextrin phosphorylase (MalP) and by a-1,4-glucanotransferase (MalQ) [10]. The released Glc-1P is then turned to Glc-6P by phosphoglucomutase (PGM) and can fuel different metabolic pathways including the Embden–Meyerhof–Parnas (EMP), the Entner-Doudoroff (ED) and the oxidative-pentose-phosphate (OPP) pathway.

Like many other cyanobacteria, the genome of the unicellular model organism *Synechocystis* sp. PCC6803 encodes for several isoenzymes involved in glycogen catabolism, including the glycogen phosphorylases *sll1356* (*glgP1*) and *slr1367* (*glgp2*) and the glycogen debranching enzymes *slr0237* (*glgX1*) and *slr1857* (*glgX2*). Of the two phosphorylases it has been shown that only GlgP2 is responsible for glycogen degradation during the dark and during resuscitation from chlorosis. GlgP1 on the other hand does not contribute to glycogen degradation under those conditions but has been shown to be relevant for growth at high temperatures [8, 11]. The roles of GlgX1 and GlgX2 have so far not been investigated at all and it is unclear if these enzymes also diverge in their activity and role in *Synechocystis*. The need to switch between autotrophic and heterotrophic modes in cyanobacteria implies that glycogen catabolism must undergo a strict regulation to prevent a premature degradation of

glycogen. While our previous work showed that PGM plays an essential role in the regulation of glycogen metabolism during chlorosis and resuscitation, the diverging roles of GlgP1 and GlgP2 also imply a direct regulation of these enzymes [12].

In this study we show that the activity of GlgP1 but not GlgP2 is strongly regulated by a C-terminal isoenzyme specific redox switch, unique in certain cyanobacterial strains. We assume that GlgP1 activity is closely linked to stress conditions during photosynthetic growth. Thereby, carbon flow through the OPP can provide a way for fast ribulose-1,5-BP regeneration and the formation of reduction equivalents, which are highly demanded during certain stress conditions. Furthermore, we show that GlgX1 is the major glycogen debranching enzyme essential for resuscitation from chlorosis and significantly enhances GlgP activity. This enhancement is particularly evident with glycogen originating from *Synechocystis*.

Results

GlgP1 activity is inhibited under reducing conditions

Synechocystis expresses two isoforms of glycogen phosphorylases, the product of sll1356 (*glgP1*) and slr1367 (*glgP2*). Previous studies showed that GlgP2 is essential for glycogen degradation during the night and resuscitation from chlorosis while GlgP1 does not contribute to glycogen degradation under those conditions. However, the enzymatic activity and regulation of GlgP1 and GlgP2 has so far not been investigated.

To determine the enzymatic activity of GlgP1 and GlgP2 we purified the respective recombinant proteins overexpressed in *Escherichia coli.* Since GlgP requires pyridoxal phosphate (PLP) as an essential co-factor, we measured UV/Vis absorbance to ensure that both enzymes show equal loading with PLP (**Figure S1**). We assessed the GlgP enzymatic activity by measuring the release of Glc-1P in an assay that couples Glc-1P interconversion to Glc-6P by phosphoglucomutase (PGM) followed by oxidation using glucose-6-phosphate-dehydrogenase (G6PDH) and $NADP^+$. As substrates we used a fixed concentration of 10 mM KH_2PO_4 (saturating conditions, data not shown) and glycogen derived from oyster at final concentrations between 0.1 and 1 % to start the reaction. We could show that both purified GlgPs were active and were able to degrade glycogen *in vitro*. Interestingly, GlgP1 and GlgP2 have similar K_M values for glycogen, but GlgP1 shows a higher overall catalytic efficiency (**Figure 1**, **Table 1**).

Inspired by the findings of Florencio, Pérez-Pérez [13] who identified GlgP2 as a possible target of TrxA, we tested if performing the GlgP assay under reducing conditions modulates the activity of GlgP1 and GlgP2. Therefore, we incubated the GlgP1 and GlgP2 master mix with 5 mM of the reducing agent dithiothreitol (DTT) for 30 minutes before starting the enzymatic assay by addition of glycogen. Strikingly, we observed that under reducing conditions GlgP1 did not follow standard Michaelis-Menten kinetics anymore but showed an allosteric/sigmoidal kinetic curve. Catalytic efficiency of GlgP1 dropped to 7.5 % of the original activity as a result of a strongly increased $K_{0.5}$ and a reduced K_{cat}. GlgP2 activity was not markedly changed under reducing conditions (**Figure 1**, **Table 1**).

Next, to find out which concentrations of DTT are needed for GlgP1 to show maximum inhibition we performed a redox titration where we treated GlgP1 with different concentrations of DTT, ranging from 1 to 10 mM for 30 min. As shown in **Figure 1C**, treatment with 5 mM DTT for 30 min is sufficient for maximum inhibition of GlgP1 and higher DTT concentrations do not further reduce enzymatic activity. GlgP1 treated with 5 mM DTT was therefore used as a reference for a fully reduced enzyme in all upcoming experiments. Treatment of the purified GlgP1 with H_2O_2 on the other hand did not increase enzymatic activity, suggesting that our purified, untreated GlgP1 is already fully oxidized.

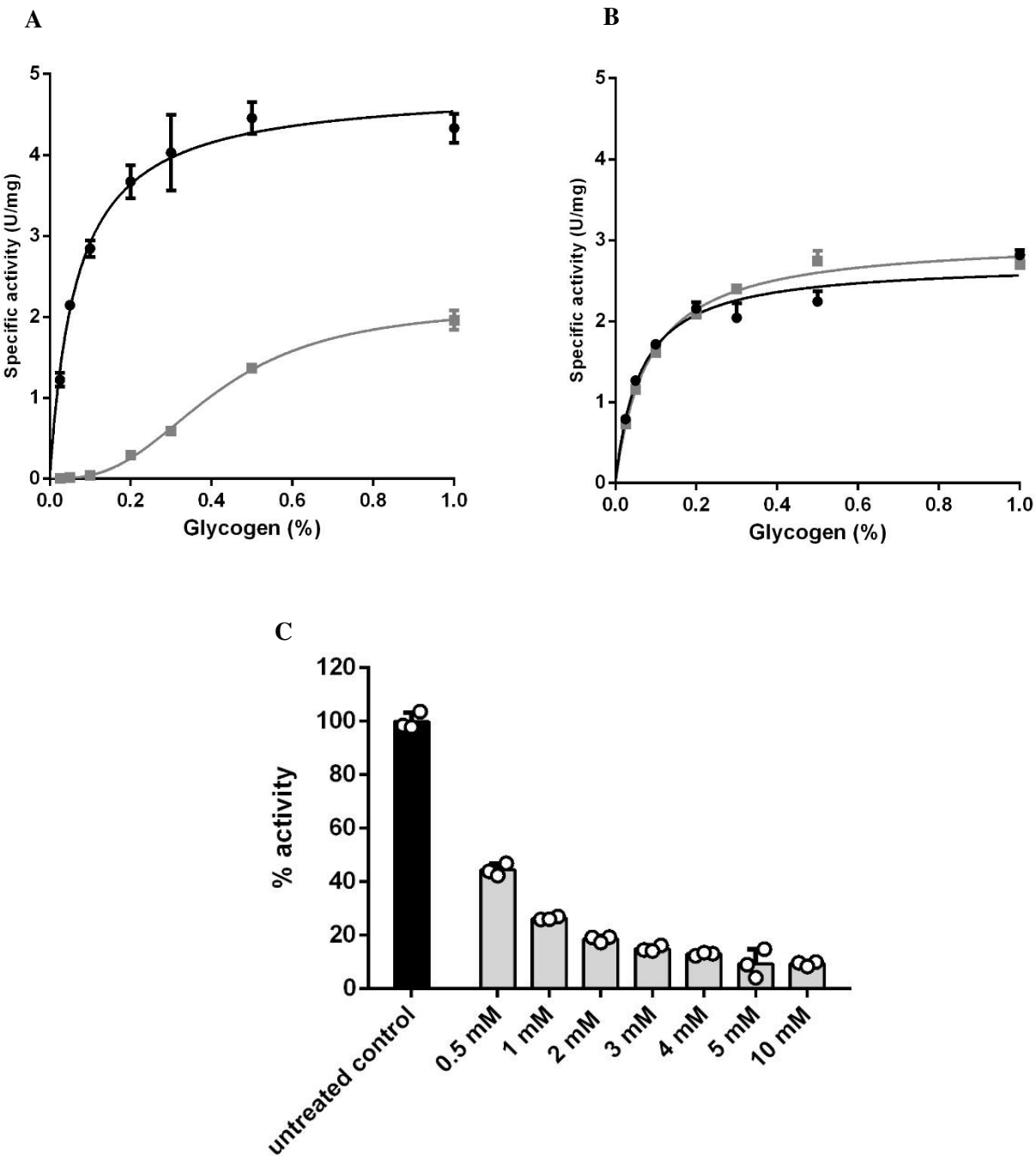

Figure 1: GlgP1 is strongly inhibited in presence of DTT

Shown is the Michaelis-Menten kinetics of GlgP1 (A) and GlgP2 (B): In black, without addition of effectors; in light grey, after 30 min incubation with 5 mM DTT. At least three replicates were measured for each data-point. Error bars represent the SD. (C): Shown is the activity of GlgP1 at 0.1% glycogen: In black, an untreated control which was considered 100%; in light grey bars, activity at different concentrations of DTT as indicated on the x-axis.

	GlgP1			GlgP2		
Treatment	**Kcat**	**K_M or $K_{0.5}$**	**Catalytic efficiency Kcat/K_m or $K_{0.5}$**	**Kcat**	**KM**	**Catalytic efficiency Kcat/Km**
Untreated	6.56 ± 0.16	0.07 ± 0.01	**93.71**	4.44 ± 0.14	0.06 ± 0.01	**74.00**
5 mM DTT	2.90 ± 0.08	0.41 ± 0.09	**7.07**	4.94 ± 0.09	0.08 ± 0.01	**61.75**

Table 1: Kinetic parameters of GlgP1 and GlgP2 with and without 5 mM DTT

K_M/$K_{0.5}$ and Kcat values are means of triplicates with ± SD.

GlgP1 activity is modulated by TrXA and gets activated by oxidation

To gain deeper insights in the apparent redox regulation of GlgP1, we tested the enzymatic activity of GlgP1 in comparison to GlgP2 under the influence of different reducing agents to see if we observe a similar effect as with DTT before. Therefore, we compared the treatment of GlgP1 and GlgP2 (25 nM each) with 5 mM DTT with the treatment of the thiol independent reducing agent TECEP. Furthermore, we tested the intracellular present redox active molecules glutathione (GSH) and cysteine (all in concentrations of 5 mM). In addition, we also purified the product of *slr0623* encoding thioredoxin A (TrxA) and tested treatment of GlgP1 and GlgP2 with previously reduced TrxA (TrxA_red) and oxidized TrxA (TrxA_ox) at concentrations of 2.5 µM respectively. As substrates we used 10 mM KH_2PO_4 and 0.1% of oyster glycogen. The activity of untreated GlgP1 and GlgP2 served as a reference. The results showed that in addition to 5 mM DTT, TrxA_red showed the strongest effect on GlgP1 by decreasing its activity to about 20% of the original activity. With about 40 % remaining activity, treatment with TECEP showed a weaker inhibition than DTT and TrxA even though TECEP and DTT have comparable reduction potentials (-0.29 V vs. -0,33 V). GSH, cysteine and TrxA_ox showed no marked effect on GlgP1 (**Figure 2A**). Furthermore, GlgP2 activity was not markedly affected by any of these treatments (**Figure 2B**).

These results clearly demonstrate inhibition of GlgP1 activity by the presence of certain reducing agents. The fact that TrXA_red is highly efficient in reducing GlgP1 at low concentrations, whereas other intracellular reducing compounds like GSH and cysteine show no effect even at high concentrations, indicates a specific modulation of GlgP1 activity by TrXA.

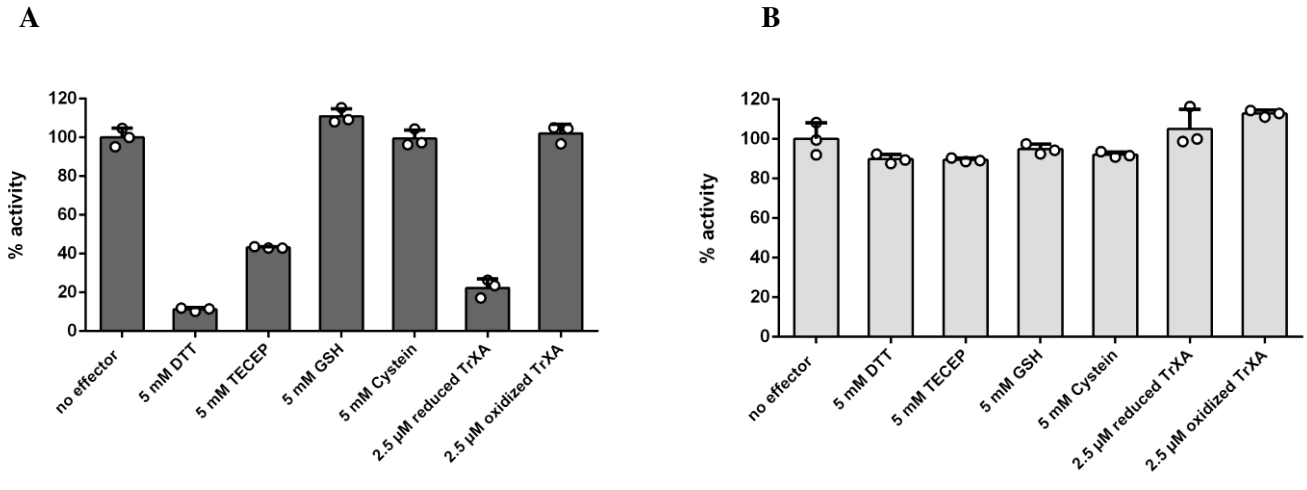

Figure 2: GlgP1 activity is specifically modulated by TrXA:

(A) shows the activity of GlgP1 after 30 min incubation with different reducing agents. Values represent relative activity and are compared to the reaction with no effectors which was considered 100%. (B) shows the same experiment as a for GlgP2. At least three replicates were measured for each datapoint. Error bars represent the SD.

Activity of reduced GlgP1 can be restored by H_2O_2 and glutathione disulfide (GSSG)

Do determine if reduced GlgP1 can be re-activated by oxidation, we incubated the previously DTT-reduced GlgP1 with the following oxidizing agents for 30 minutes: oxidized DTT (DTTox) glutathione disulfide (GSSG) (5 mM each) and TrXA_ox (10 µM). For the stronger and potentially protein damaging oxidizing agents $CuCl_2$ and H_2O_2 we determined the ideal concentration in a previous titration experiment (data not shown). This turned out to be 5 µM of $CuCl_2$ and 0.08% of H_2O_2. We considered the activity of untreated GlgP1 as 100% while the reduced GlgP1 showed about 10% remaining activity. The strongest re-activation of GlgP1 could be achieved by treatment with H_2O_2 and GSSG leading to an increase in activity to 65% and 50% of the original activity, respectively. Treatment with $CuCl_2$ lead to an increase in activity to about 30% of original activity. Treatment with DTT_ox only led to an increase to about 20 % of original activity while the treatment with TrX_ox showed no marked increase in activity at all (**Figure 3**). Altogether, activity of reduced GlgP1 could be restored by certain oxidizing conditions, indicating the presence of a specific redox switch that is lacking in GlgP2.

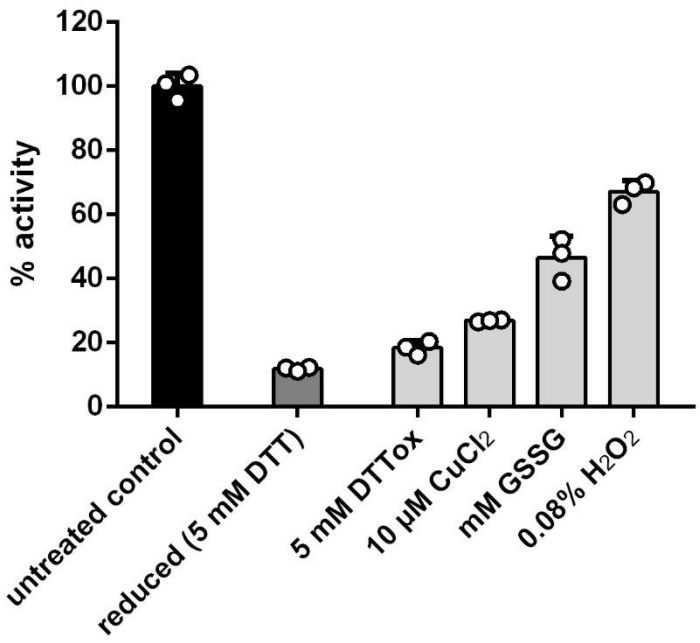

Figure 3: Activity of reduced GlgP1 can be restored by oxidation.

Shown is the activity of GlgP1: in black the untreated control which was considered 100%; in dark grey, fully reduced with 5 mM DTT; in light grey fully reduced with subsequent treatment with different oxidizing agents. At least three replicates were measured. Error bars represent the SD.

GlgP1 activity is regulated by a C-terminal redox switch.

To determine the regulatory site involved in redox regulation of GlgP1 we aligned the aa sequence of GlgP1 and GlgP2, revealing a high overall sequence identity of 62 %. By searching for prominent cysteine residues which might form disulfide bonds, we identified a characteristic motif at the C-terminal domain of GlgP1 containing two cysteine residues at position 837 and 842. By searching for this domain in other organisms we also identified that this domain is unique to certain strains of cyanobacteria. (**Figure 4A**). Prediction of the respective protein structure by AlphaFold suggests a surface exposed hairpin structure with a potential disulfide formation between the cysteines C837 and C842 (**Figure 4B**). To analyze whether this domain is in fact responsible for redox regulation, we created a point mutation by exchanging the cysteine at position 837 with a serine residue to mimic a permanently reduced state of the enzyme. The activity of the GlgP1 C837S variant corresponded precisely to the activity of the fully reduced GlgP1 WT, but in contrast to the WT enzyme this variant did not respond to treatment with oxidizing agents **(Figure 4C, Figure S1)**. This result clearly demonstrates that the C-terminal segment of GlgP1 acts as a redox sensitive element to tune the activity of this enzyme.

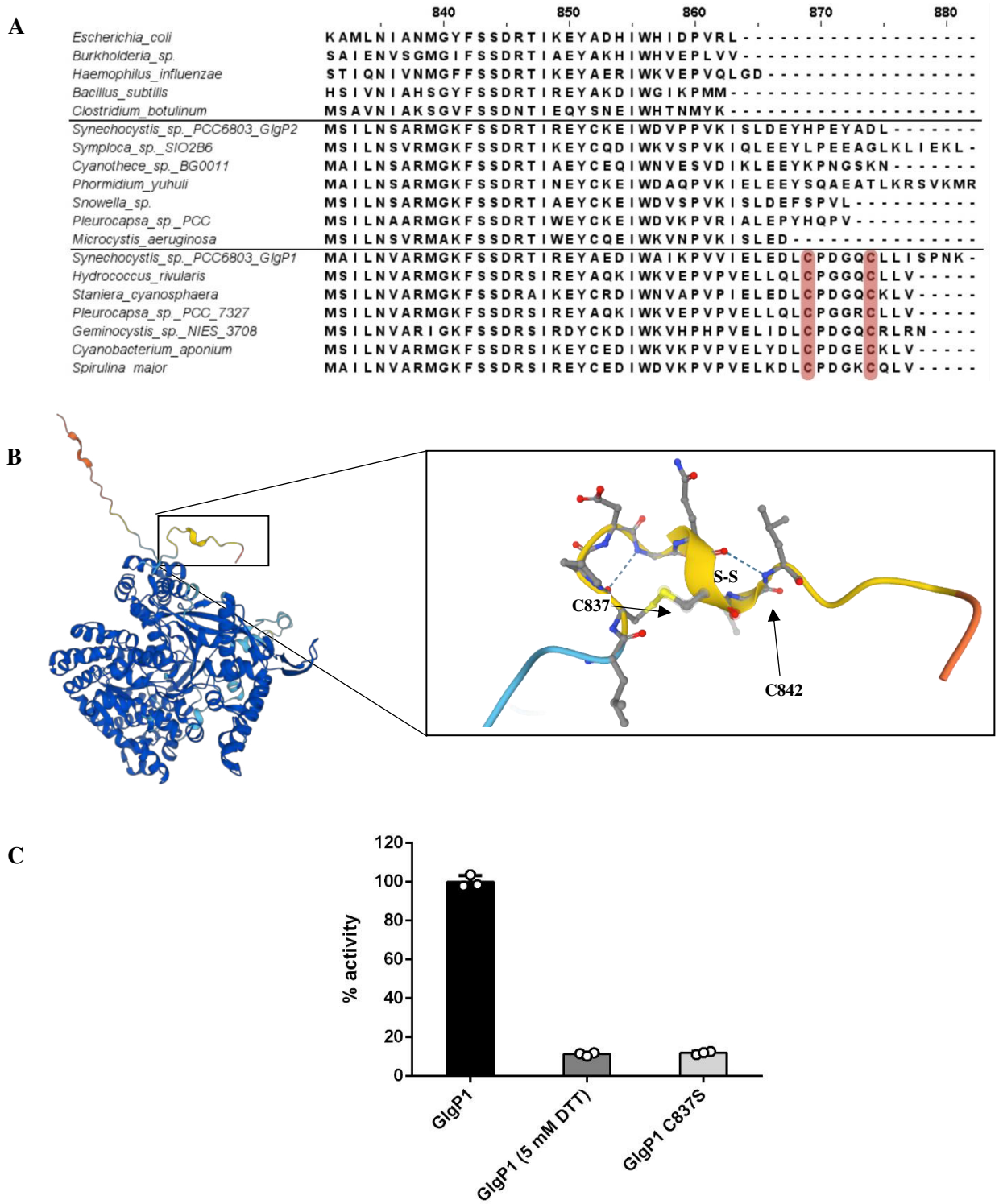

Figure 4: GlgP1 is regulated by a C-terminal redox switch exclusive to cyanobacteria.

(A): Alignment of the C-terminal domain of different bacterial GlgP homologues. Marked in red is the characteristic cysteine motif in GlgP1 homologues.
(B): Structure of *Synechocystis* GlgP1 predicted by AlphaFold. Shown in detail is the unique C-terminal domain with a predicted disulfide bond formation of Cys837 and Cys842.
(C): Shown is the GlgP1 activity: in black, without effector which was considered 100%; in dark grey, in the fully reduced state after treatment with 5 mM DTT; in light grey, activity of the GlgP1 C837S variant without any effectors. At least three replicates were measured. Error bars represent the SD.

A *glgp1* knockout mutant shows growth inhibition when light intensity is increased

Regulation of Glgp1 by TrXA and ROS implies a connection to photosynthetic activity. To determine if a *glgp1* deficient mutant shows growth impairment when light intensity is increased, we compared growth of a *glgp1* and a *glgp2* deficient mutant to the wildtype at elevated light intensities. For this experiment the cultures were first grown at 50 µE for 24 hours followed by an increase in light intensity to 120 µE. Strikingly, we observed an immediate growth impairment for *glgp1* which resulted in a fully restricted growth after 72h while WT and the *glgp2* mutant were unaffected (**Figure 5**). Since ROS formation should be increased after changing light intensity to 120 µE this finding supports our hypothesis in *glgp1* being important under situations of increased oxidative stress.

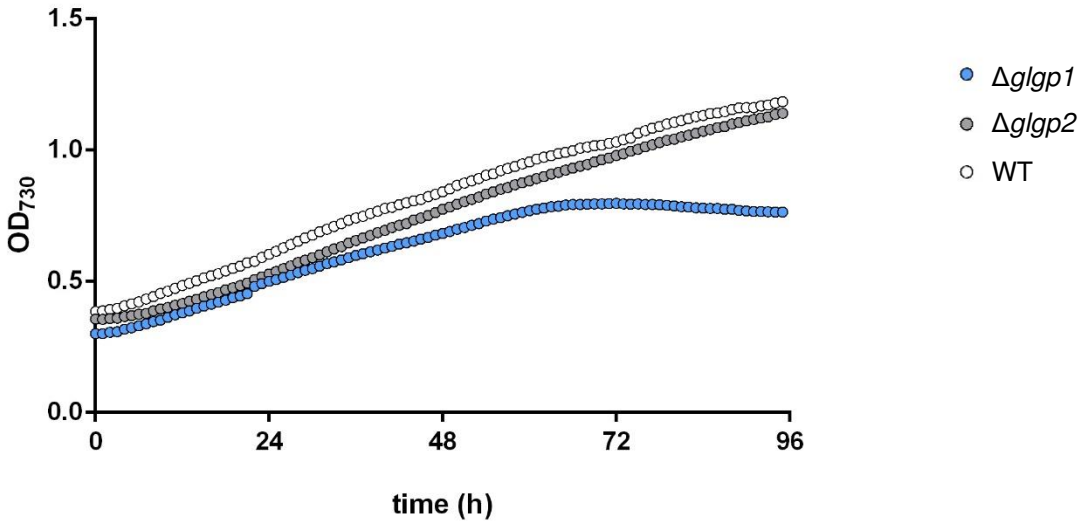

Figure 5: GlgP1 plays a role in growth at moderate light intensities

Shown are the growth curves of Δ*glgp1* (blue) and Δ*glgp2* (grey) deficient mutants compared to the WT (white). Strains grown with ambient air at 28°C with constant illumination at 50 µmol·m^{-2}·s^{-1} for 24 hours, before elevation to 120 µmol·m^{-2}·s^{-1}.

A *glgx1* knockout mutant is impaired in recovery from chlorosis

For a complete breakdown of glycogen, the activity of the glycogen phosphorylase GlgP needs to be accompanied by a glycogen debranching enzyme. Like with GlgP1 and GlgP2, *Synechocystis* possesses two annotated isoenzymes of glycogen debranching enzymes, Slr0237 (GlgX1) and Slr1857 (GlgX2), which have so far not been investigated regarding their role and activity. To gain deeper insights into the physiological role of GlgX1 and GlgX2 we created knockout mutants of *glgx1* and *glgx2* and investigated their viability during diurnal growth and during resuscitation from chlorosis by estimating viable cells counts using the drop-plate assay. When cells were grown at diurnal rhythm, none of the mutants showed growth impairment compared to the wildtype. However, during resuscitation from nitrogen chlorosis, a strong growth impairment of the *glgx1* knockout mutant became apparent while the *glgx2* knockout was unaffected. This phenotype got even more pronounced when resuscitation was done in day night rhythm or after a prolonged period of chlorosis (**Figure 6**). This experiment clearly shows that GlgX1 appears to be the crucial glycogen debranching enzyme in resuscitating chlorotic cells, while GlgX2 does not seem to be important under this condition.

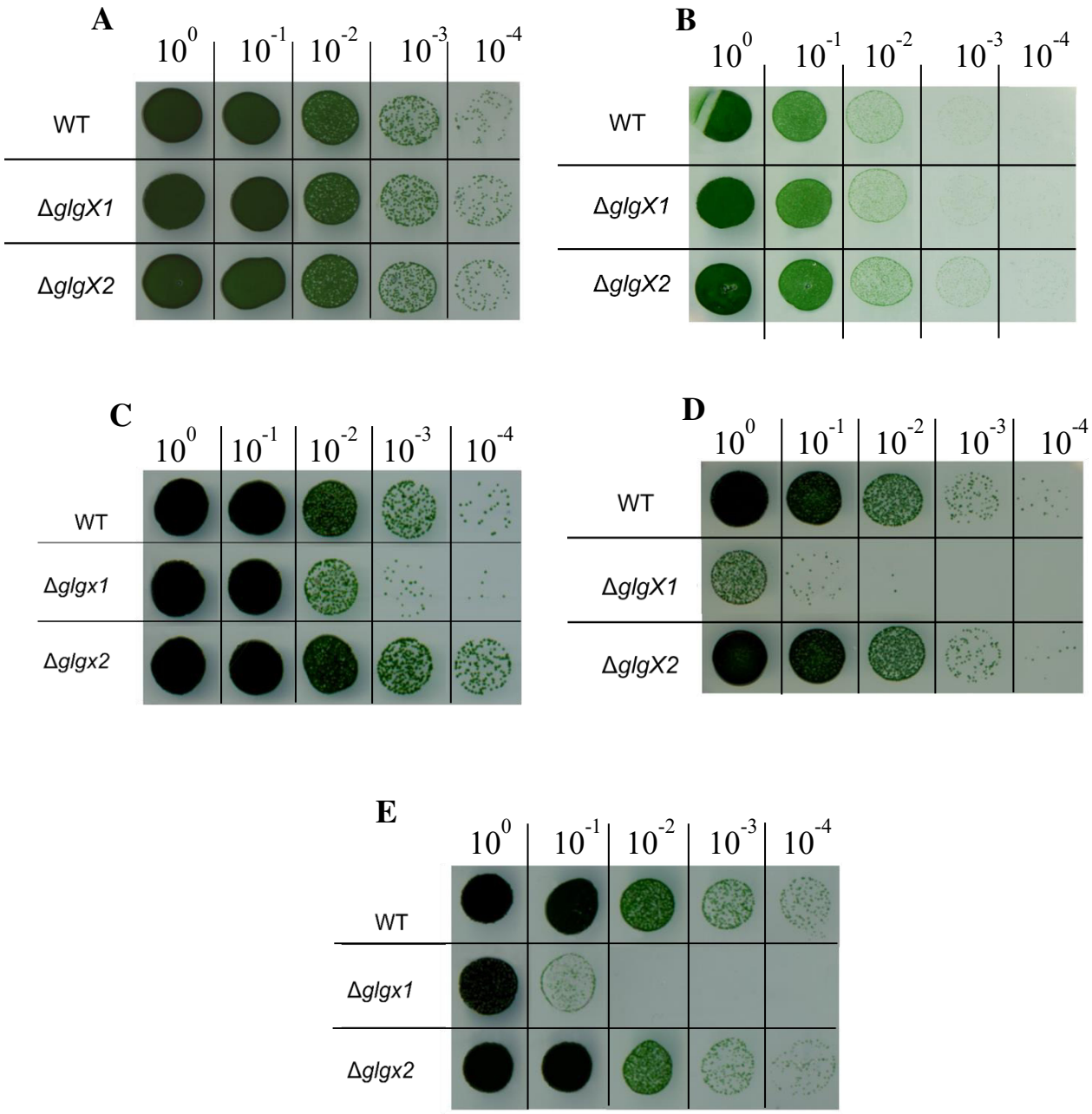

Figure 6: GlgX1 is essential for recovery from long term chlorosis.

Shown are spot viability assays on solid BG11 agar of *glgx1* and *glgx2* deficient mutants compared against the wildtype (WT). Dilutions are indicated in the top row. The following conditions have been tested:

(A) Growth under constant light; (B) growth at light-dark cycle (12h – 12h); (C) Resuscitation after 14 days of chlorosis under constant light. (D) Resuscitation after 14 days of chlorosis at light-dark cycle (12h-12h); (E) Resuscitation after 21 days of chlorosis under constant light.

315

316

317

GlgX1 enhances GlgP1 and GlgP2 activity in degrading glycogen originating from *Synechocystis*

To further investigate GlgX1 and GlgX2 *in vitro*, we overexpressed strep-tagged versions of the enzymes in *E. coli* and assessed the activity of the purified enzymes by adding them to the GlgP assay. Next to glycogen from oyster we also included glycogen purified from nitrogen starved *Synechocystis* cultures (both at a final concentration of 0.1%) to see how the properties of the glycogen itself influences enzymatic activity. When oyster glycogen was used as a substrate, GlgX1 enhanced GlgP1 and GlgP2 activity both by around 25% whereas GlgX2 had no effect on GlgP activity. Repeating the experiment with glycogen purified from nitrogen starved *Synechcoystis* cells yielded two major findings:

First, compared to oyster glycogen, *Synechocystis* glycogen as substrate gives rise to generally lower GlgP activities, in particular 60% for GlgP1 and 40% for GlgP2 (without GlgX addition). Second, addition of GlgX1 enhanced the overall degradation of *Synechocystis* glycogen much stronger than degradation of oyster glycogen. In combination with GlgP1, GlgX1 increased the overall activity by around 65% while with GlgP2, the activity increased by 105%. However, since GlgP2 is less efficient with *Synechocystis* glycogen, the total activity of GlgP2 with GlgX1 was still lower than for oyster glycogen (**Figure 7**).

This result agrees well with the observed phenotype of the corresponding mutants in resuscitation from chlorosis, where GlgX1, similar to GlgP2, appeared to be essential, while GlgX2 and GlgP1 were redundant.

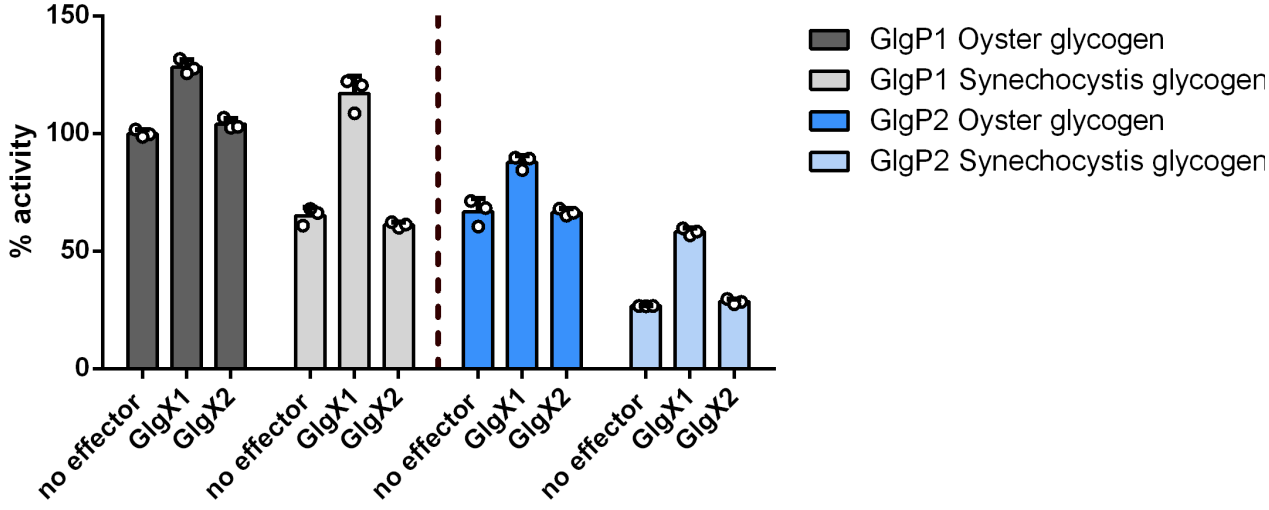

Figure 7: GlgX1 enhances GlgP1 and GlgP2 activity.

Shown is the GlgP1 and GlgP2 activity in presence of GlgX1 or GlgX2 or without any effector: In dark grey GlgP1 activity with oyster glycogen; in light grey GlgP1 activity with *Synechocystis* glycogen; in dark blue, GlgP2 activity with oyster glycogen; in light blue GlgP2 activity with *Synechocystis* glycogen. Values represent relative activity compared to the no effector oyster glycogen measurement which was considered 100%. At least three replicates were measured for each data point. Error bars represent the SD.

Discussion

Regulation of glycogen metabolism is essential for cyanobacteria to enable survivability in an ever-changing environment. Therefore, investigating the role and regulation of glycogen associated enzymes is essential to gain a deeper understanding of cyanobacteria in general. In this study we investigated the role and regulation of the glycogen catabolic enzymes in *Synechocystis*. We could show that GlgP1 is strongly regulated via a C-terminal redox switch, which is the first time this mode of regulation for glycogen phosphorylases was shown in bacteria. Activation of GlgP1 by oxidation connects glycogen degradation by GlgP1 to the formation of ROS from which we conclude that GlgP1 plays an essential role in adaptation to certain stress conditions. Furthermore, we show that GlgX1 is essential during recovery from chlorosis and enhances glycogen degradation by GlgP activity in dependence of the used glycogen source, while the role of GlgX2 remains elusive.

GlgP1 shows a novel mode of redox regulation for bacterial glycogen phosphorylases

It has been shown before that GlgP2 is the essential glycogen phosphorylase for glycogen degradation during the night and resuscitation from chlorosis, while GlgP1 was not contributing to glycogen degradation under those conditions [8]. This suggests a different mode of regulation for the two isoenzymes. We could show that both purified GlgP isoenzymes are active *in vitro* and follow standard Michaelis-Menten kinetics, with GlgP1 showing a higher overall catalytic efficiency compared to GlgP2. In the presence of reducing agents, GlgP1 activity strongly decreases and kinetics show an sigmoidal kinetic profile. Compared to GlgPs from other bacteria, cyanobacterial GlgPs have a C-terminal extension of up to 15 amino acids. We discovered that the redox regulation of GlgP1 was located at this C-terminal extension which carries two characteristic cysteine residues at position 837 and 842, not present in GlgP2, that are predicted to form a disulfide bond. Formation of a C837S variant of GlgP1 showed a strongly diminished activity on the level of a fully reduced GlgP1. From these results we conclude that the disruption of this disulfide bond leads to a conformational change of the C-terminal extension, inactivating the enzyme. The change of the kinetic profile in the reduced state implies a strongly reduced affinity for glycogen from which we conclude that the altered conformation of the C-terminal extension impairs binding of glycogen to the active site. Another explanation could be a hindered oligomerization since glycogen phosphorylases are known to be active as homodimers. While the C-terminal extension seems to be a general feature in cyanobacterial GlgPs, the double cysteine motif in this domain is only found certain strains including non-diazotrophic and diazotrophic strains alike. This raises the question on how this mechanism has developed over the course of evolution. To our knowledge the only indication of a redox dependent regulation of an enzyme involved in glycogen degradation in bacteria has been observed for a specific amylase of the cyanobacterium *Nostoc* sp. PCC7119 [14]. In humans an isoenzyme-specific redox regulation of the brain glycogen phosphorylase

was shown, affecting binding of its activator AMP, which is not known to be an activator for bacterial GlgPs [15]. However, conversely to this known redox regulations GlgP1 gets activated by oxidation making this a unique mode of GlgP regulation.

Activation of GlgP1 by ROS is connected to photosynthesis and high light stress

Being active only in the oxidized state, can explain why GlgP1 is inactive during resuscitation from chlorosis or during the night but also raises the question on the potential role of GlgP1 and under which situations it gets activated. By testing different intracellularly present reducing agents we could show that reduction and inactivation of GlgP1 was especially effective with TrXA, an m-type thioredoxin which has been shown to be essential in *Synechocystis* [16]. Thioredoxin has been assumed before to play a role in regulation of glycogen metabolism: A proteomic approach by Pérez-Pérez et al. revealed that TrxA potentially interacts with several glycogen associated enzymes in *Synechocystis*. However, GlgP1 was not identified in this study Florencio, Pérez-Pérez [13]. Inactivation of GlgP1 was reversible by oxidation which was most effective with H_2O_2 and GSSG. While H_2O_2 is a common ROS species, GSSG is formed as a product of ROS scavenging by GSH and therefore closely connected to ROS formation. Thereby, a low GSH/GSSG ratio is an indicator for high oxidative stress. Being exclusive to cyanobacteria and the fact that regulation was especially effective with TrXA and H_2O_2/GSSG strongly indicates a connection of GlgP1 activity to photosynthetic activity: TrxA as a part of the ferredoxin/thioredoxin system is known to provide the biochemical link between light reactions and the regulation of carbon metabolism in photoautotrophic organisms [17]. ROS on the other hand are a byproduct of the photosynthetic electron transport chain, whose formation increases with light intensity and are encountered by all photosynthetically active organisms.

Linking GlgP1 to photosynthetic activity is consistent with data on its expression levels, where it was shown that *glgp1* expression is upregulated during the day and downregulated during the night which is the reverse for *glgp2* [18]. The only study that directly addressed the potential role of GlgP1 by Fu and Xu discovered that GlgP1 is important for survivability at high temperatures but also that GlgP1 is only active during illumination. High temperature has been shown to cause strong ROS formation in bacteria and in nature high temperature and high light are often associated with one another [19]. We could show that independently from temperature an increase in light intensity also leads to growth impairment of a *glgp1* deficient mutant (**Figure 5**).

While the formation of ROS is unfavorable due to oxidative damage it is also known that they contribute to signaling during several stress conditions [20-22]. This suggests that glycogen degradation by GlgP1 signaled by ROS could be a measure to counter different environmental stress condition, including heat stress and higher light intensities.

It has been shown before that high temperatures have negative influence on photosynthetic rate by making RuBisCo more likely to incorporate O_2 instead of CO_2 and due to the fact that CO_2 shows a worse water solubility at higher temperatures then O_2 [23]. This increases the demand of ribulose-1,5-BP due to a higher rate of photorespiration. Several studies have shown that glycogen degradation can contribute to replenish the ribulose-1,5-BP pool by shuffling carbon through the OPP pathway to stabilize photosynthesis [24]. This mechanism appears to be especially important during the "restart" of photosynthesis after the night phase where it has been shown that glycogen degradation at the end of the dark phase can fill up the depleted ribulose-1,5-BP pools, leading to a faster start of photosynthesis while glycogen free mutants show a strong delay [25]. We assume that the same pathway contributes to ribulose-1,5-BP formation during heat stress. Furthermore, it was shown that the survivability under higher temperature and high ROS formation is dependent on the availability of GSH [26, 27]. Reduction of GSSG by glutathione reductase is dependent on NADPH which is mainly formed at the end of photosynthetic linear electron transport, but also in the OPP. The oxygen evolving complex of PSII has also been shown to be prone to heat damage which would inhibiting the NADPH formation by linear electron transport, making the OPP the only source of NADPH.

GlgX1 is the essential glycogen debranching enzyme during resuscitation from chlorosis

On average, one third of the glycogen granule is presumed to be accessible for GlgP without the need to cleave alpha-1,6 branches. [28]. Therefore, GlgX activity is especially important for a full and efficient breakdown of the glycogen granule. Data on the contribution of debranching enzymes to cyanobacterial glycogen degradation are scarce and the role of the two isoenzymes in *Synechocystis* has so far not been investigated. With our findings we show that GlgX1 is the main glycogen debranching enzyme. A knockout mutant of *glgx1* shows strong impairment in resuscitation from chlorosis while a *glgx2* knockout mutant appears to be unaffected. The phenotype of a *glgx1* deficient mutant gets more pronounced during prolonged periods of chlorosis and also when recovery is done in day/night rhythm. We assume that under those conditions the cells have to rely longer on respiration and therefore glycogen must get degraded more thoroughly. During day/night neither *glgx1* nor *glgx2* KO mutants showed a visible phenotype. From this we conclude that glycogen breakdown by GlgP alone is sufficient under these conditions or the two debranching enzymes can replace each other under those conditons. The time period of a heterotrophic type of metabolism is longer during resuscitation from chlorosis than during the night (24h vs 12h). Additionally, it can be considered that during resuscitation from chlorosis the rate of glycogen degradation must be higher compared to dark phases due to a much higher demand of carbon building blocks. Nevertheless, day/night experiments with longer dark phases might also reveal a phenotype for *glgx1* or *glgx2*. In our experiments we couldn't detect any phenotype for a *glgx2* deficient mutant under the tested conditions and in our *in vitro* enzymatic assays GlgX2 didn't show any enzymatic activity. Compared to glycogen phosphorylases debranching enzymes are difficult to classify

and many enzymes possess a similar hydrolase domain. Therefore, GlgX2 could in fact have a different role than annotated.

Enhancement of GlgP activity by GlgX strongly depends on the type of glycogen used

We could clearly show that GlgX1 increases GlgP activity. Thereby, the enhancement of GlgP by GlgX1 appears to be strongly dependent on the used glycogen source and is markedly higher for glycogen originating from *Synechocystis* than for the commercially available oyster glycogen. Interestingly, glycogen degradation by GlgP2 shows a stronger dependance on GlgX1 than degradation by GlgP1 but only for glycogen from *Synechocystis*. The reason for this difference could be due to a difference in branching pattern but also other forms of glycogen modification might play a role as it was shown for eukaryotic glycogen [29]. In case of *Synechocystis* two glycogen synthases equally contribute to glycogen synthesis [30]. A study showed that the branching pattern slightly differs for glycogen from single glycogen synthase knockout mutants, while the WT appears to be a mixture of the two [31]. Future experiments have to elucidate if degradation by GlgP differs between the glycogen produced by the two synthases. Unlike for GlgP1 we could not detect any regulatory effect of glycogen debranching enzymes by treatment with reducing and oxidizing agents, indicating that the main regulation of degradation is achieved via the GlgP enzymes **(Figure S3)**.

The fact that GlgX1 particularly enhances GlgP2 activity and that a knockout of each enzyme shows a similar phenotype in resuscitation from chlorosis indicates that GlgX1 and GlgP2 form a functional pair.

Methods

Isothermal, Single-Reaction DNA Assembly (Gibson Cloning)

Cultivation of *Escherichia coli*

If not otherwise stated *E. coli* was grown in Luria-Bertani medium at 37°C. For growth on plates, 1.5% (w/v) agar-agar was added. For cells containing plasmids, the appropriate concentration of antibiotics was used. All *E. coli* strains used in this study are listed in **Table S5**.

Cultivation of *Synechocystis*

All *Synechocystis* sp. PCC 6803 strains used in this study were grown in BG_{11} supplemented with 5 mm $NaHCO_3$, as described previously [32]. A list of the strains used is provided in **Table 2**. Two kinds of wild-type strains, Glc sensitive and Glc tolerant, were used; both strains responded equally during nitrogen starvation and resuscitation. Cultivation was performed with continuous illumination (40–50 µmol photons m^{-2} s^{-1}) and shaking (130–140 rpm) at 27°C if not stated otherwise. Induction of nitrogen starvation and resuscitation was induced as described previously [33, 34]. If mutants or strains containing antibiotic markers were used, the precultures were propagated with the appropriate concentration of antibiotics. Biological replicates were inoculated with the same precultures but propagated, nitrogen starved, and resuscitated independently in different flasks under identical conditions.

Cultivation of *Synechocystis* under moderate light

Growth curves of WT and *glgP1*- and *glgP2* deficient mutants were aquired via liquid cultures in a Multi-Cultivator MC 1000-OD (Photon Systems Instruments, Czech Republic). All *Synechocystis* sp. PCC 6803 strains were grown as described above, before being transferred to fresh standard BG11 with respective antibiotics in Multi-Cultivator flasks for growth measurements, where the starting optical density of all cultures was adjusted to OD750 ~0.3. Cultivation was carried out with constant aeration using ambient air 28°C under constant illumination for 24 hours at 50 µmol·m^{-2}·s^{-1} before being raised to 120 µmol·m^{-2}·s^{-1}. Optical density readings were taken every hour for 96 hours using the instruments' inbuilt function.

520 **Spot viability assay**

521 Serial dilutions of chlorotic cultures were prepared (10^0, 10^{-1}, 10^{-2}, 10^{-3}, 10^{-4}, and 10^{-5}), starting with
522 an OD_{750} of 1.5 µL of these dilutions, dropped on solid BG_{11} agar plates, and cultivated at 50 µmol
523 photons m^{-2} s^{-1} and 27°C for 5 to 7 d.

524

525 **Protein purification**

526 The plasmids used for protein overexpression are shown in **Table 4**. *Escherichia coli* Rosetta-gami
527 (DE3) (details **Table 2**) was used for the overexpression of all proteins. For this, cells were cultivated
528 in 2xYT (3.5% tryptone, 2% yeast extract, 0.5% NaCl; 1L of culture in 5L flasks) at 37 °C until reaching
529 exponential growth (OD_{600} 0.6-0.8). Protein overexpression was induced by adding 75 µg/L
530 anhydrotetracycline, followed by incubation at 20°C for 16 h. Cells were harvested by centrifugation at
531 4000 g for 10 min at 4 °C. Cell disruption was performed by sonication in 40 mL of lysis buffer (100
532 mM Tris-HCl pH 7.5, 500 mM NaCl, 10 mM $MgCl_2$, 20 mM Imidazole for His-tagged proteins and 100
533 mM Tris-HCl pH 8, 150 mM NaCl, 10 mM $MgCl_2$ for Strep-tagged proteins) Lysis buffers were
534 supplemented with DNAse I, and cOmplete™ protease inhibitor cocktail (Roche, Basel)). The cell lysate
535 was centrifuged at 40,000 g for 45 min at 4°C and the supernatant was filtered with a 0.22 µM filter.

536 For the purification of His-tagged proteins, 5 mL Ni-NTA HisTrap columns (GE Healthcare, Illinois,
537 USA) were used. The cell extracts were loaded onto the columns, washed with wash buffer (50 mM
538 Tris-HCl pH 7.4, 500 mM NaCl, and 50 mM Imidazole) and eluted with elution buffer (50 mM Tris-
539 HCl pH 7.4, 500 mm NaCl, and 500 mM Imidazole).

540

541 **GlgP and GlgX enzymatic assays**

542 Buffer for enzymatic reactions was composed of 50 mM HEPES-KOH pH 7.5, 10 mM $MgCl_2$, 1 mM
543 $NADP^+$, 5mM KH_2PO_4, 1U/µl phosphoglucomutase from rabbit muscle, 10 µM Glucose-1,6-
544 bisphosphate and 1 U/mL G6PDH from *Saccharomyces cerevisiae* (G6378, Sigma Aldrich). For
545 GlgP1/2 activity, 2,5 µg of Strep-tagged purified protein was added to each reaction. Reaction was
546 started by the addition of glycogen. Reactions were carried out in a total of 300 µl in a 96-well
547 microplate. Absorption change at 340 nm was continuously measured for 15 min at 30 °C in a TECAN
548 Spark® Multiplate reader (Tecan Group AG, Männedorf, Switzerland). At least three replicates were
549 measured. For enzymatic assays with reducing or oxidizing agents, GlgP1 and GlgP2 were incubated
550 with the given amount of effector for 30 minutes at RT.

551 For determining GlgX activity, 15 µg of GlgX1 and GlgX2 Strep-tagged purified protein were added to
552 the GlgP assay mastermix respectively.

553

554 **Table2: List of strains used in this study**

E. coli NEB10β	Δ(ara-leu) 7697 araD139 fhuAΔlacX74 galK16 galE15 e14-Φ80dlacZΔM15 recA1 relA1 endA1 nupGrpsL(StrR) rphspoT1 Δ(mrr-hsdRMS-mcrBC)
E. coli Rosetta gami (DE3)	Δ(ara-leu)7697 ΔlacX74 ΔphoA PvuII phoR araD139 ahpC galE galK rpsL (DE3) F'[lac$^+$ lacI^q pro] gor522::Tn10 trxB pLysSRARE (Cam^R, Str^R, Tet^R)
Synechocystis sp. PCC 6803	Wildtype
Δ*glgp1*	*Sll1356::Kan^R*
Δ*glgp2*	*Slr1367::Spec^R*
Δ*glgx1*	*Slr0237::Spec^R*
Δ*glgx2*	*Slr1857::Kan^R*

555

556 **Table3: List if used primers**

Primer	**Sequence (5'- 3')**
pASKC_glgp1_fw	CTAGAAATAATTTTGTTTAACTTTAAGAAGGAGATATACAAATGGAGCACCTTCCCATGGC
pASKC_glgp1_rev	GGTCTTATTTTTCGAACTGCGGGTGGCTCCAGCTAGCCATTTTATTAGGAGAAATTAACAAAC
pASKC_glgp2_short_fw	TAGAAATAATTTTGTTTAACTTTAAGAAGGAGATATACAAATGATTGATCAATCTACCCTAAAC
pASKC_glgp2_rev	GTCTTATTTTTCGAACTGCGGGTGGCTCCAGCTAGCCATTAAATCGGCGTATTCGGGATGG
pASKC_glgx1_fw	TAGAAATAATTTTGTTTAACTTTAAGAAGGAGATATACAAGTGCCACAGTTGATATCTGTTC
pASKC_glgx1_rev	GGTCTTATTTTTCGAACTGCGGGTGGCTCCAGCTAGCCATTTTTGCCATTAACACCACAG
pASKC_glgx2_fw	TAGAAATAATTTTGTTTAACTTTAAGAAGGAGATATACAAATGGAACGCATAGATATTCATC
pASKC_glgx2_rev	GGTCTTATTTTTCGAACTGCGGGTGGCTCCAGCTAGCCATTTTAGCCAGTAAAATAACAAC
pET15b_trxA_fw	CAGCAGCGGCCTGGTGCCGCGCGGCAGCCATATGCTCGAGATGAGTGCTACCCCTCAAGTTTC
pET15b_trxA_rev	CCCTCAAGACCCGTTTAGAGGCCCCAAGGGGTTATGCTAGTTATTGCTCAGCGGTGGCAGCAGCCAAC
Glgp1_C837S_fw	AGAAGACCTCtctCCCGATGGTC
Glgp1_C837S_rev	AATTCAATTACCACGGGTTTG
GlgX1_DS_fw	CAAGGTAGTCGGCAAATAATCTAATTTACTGAGTTTTTGCCC
GlgX1_DS_rev	CGGCCAGTGAATTCGAGCTCGGTACCCGGGGATCCTCTAGCAATGTTAGATAAACTACATTG
GlgX1_Spec_fw	GAATCTGAACAATTTTTGGAATTGCCTGAGCTCTTGACCGAACGCAGCGGTGGTAAC
GlgX1_Spec_rev	GTTACCACCGCTGCGTTCGGTCAAGAGCTCAGGCAATTCCAAAAATTGTTCAGATTC
GlgX1_US_fw	GACCATGATTACGCCAAGCTTGCATGCCTGCAGGTCGACTTGGGGCAGGCAAGGCCATTGAC
Glgx1_US_rev	CCACTGCGCCGTTACCACCGCTGCGTTCGGTCAAGAGCTCAGGCAATTCCAAAAATTGTTC

GlgX2_DS_fw	CATTTGATGCTCGATGAGTTTTTCTAAATTGTCTTAAATTTCCCTTTCCCTTC
GlgX2_DS_fw_redesigned	GTTATCTTGGCAAATCATCTATTGTCTTAAATTTCCCTTTC
GlgX2_DS_rev	ATACCGCACAGATGCGTAAGGAGAAAATACCGCATCAGGCGCCATTCGCCATTCAGGCTGC
GlgX2_Kan_fw	GAGGCATTTTAGCAGGACACCCGAACCGAACAGGCTTATGTC
GlgX2_Kan_rev	CATTACTTTCCAAGTTGTGCCTCAGAGTTTGTAGAAACGCAAAAAG
GlgX2_US_fw	GACCATGATTACGCCAAGCTTGCATGCCTGCAGGTCGACTATCCCCGGATATTCTTCCCC
GlgX2_US_rev	GACATAAGCCTGTTCGGTTCGGGTGTCCTGCTAAAATGCCTC
GlgX2_prom_fw	TGCGTTTCTACAAACTCTGAGGCACAACTTGGAAAGTAATG
GlgX2_prom_rev	GAAAGGGAAATTTAAGACAATAGATGATTTGCCAAGATAAC

557

558

559 **Table4: List of used plasmids**

560

Plasmid	**Purpose**
pASKC_glgp1	Expression of C-terminal Strep-tagged *Synechocystis* GlgP1 in *E.coli*
pASKC_glgp2	Expression of C-terminal Strep-tagged *Synechocystis* GlgP2 in *E.coli*
pASKC_glgp1_C837S	Expression of C-terminal Strep-tagged *Synechocystis* GlgP1 C837S in *E.coli*
pASKC_glgx1	Expression of C-terminal Strep-tagged *Synechocystis* GlgX1 in *E.coli*
pASKC_glgx2	Expression of C-terminal Strep-tagged *Synechocystis* GlgX2 in *E.coli*
pASKC_trXA	Expression of C-terminal Strep-tagged *Synechocystis* TrXA in *E.coli*
pUC19_glgx1_KO	Replacement of *slr0237* for $Spec^R$ in *Synechocystis* sp. PCC 6803
pUC19_glgx2_KO	Replacement of *slr1857* for Kan^R in *Synechocystis* sp. PCC 6803

561

562

563 **Statistical analysis**

564

565 Statistical details for each experiment can be found in the figure legends. GraphPad PRISM was used
566 to perform one-sided ANOVA to determine the statistical significance. Asterisks (*) in the figures
567 symbolize the p-value: One asterisk represents $p \leq 0.05$, two asterisks $p \leq 0.01$, three asterisks $p \leq$
568 0.001, and four asterisks $p \leq 0.0001$

569

Author contributions

NN performed experiments and wrote manuscript

KL performed growth curves measurements.

KF conceived study and edited manuscript

Acknowledgments

This work was supported by FOR2816 “The Autotrophy-Heterotrophy Switch in Cyanobacteria: Coherent Decision-Making at Multiple Regulatory Layers”

References

1. Henrissat, B., E. Deleury, and P.M. Coutinho, *Glycogen metabolism loss: a common marker of parasitic behaviour in bacteria?* Trends in Genetics, 2002. **18**(9): p. 437-440.
2. Wang, L. and M.J. Wise, *Glycogen with short average chain length enhances bacterial durability.* Naturwissenschaften, 2011. **98**(9): p. 719.
3. Preiss, J., *Bacterial Glycogen Synthesis and its Regulation.* Annual Review of Microbiology, 1984. **38**(1): p. 419-458.
4. Beck, C., et al., *The diversity of cyanobacterial metabolism: genome analysis of multiple phototrophic microorganisms.* BMC Genomics, 2012. **13**(1): p. 56.
5. Vitousek, P.M. and R.W. Howarth, *Nitrogen limitation on land and in the sea: How can it occur?* Biogeochemistry, 1991. **13**(2): p. 87-115.
6. Sawers, R.G., *Dormancy: Illuminating How a Microbial Sleeping Beauty Awakens.* Current Biology, 2016. **26**(21): p. R1139-R1141.
7. Neumann, N., S. Doello, and K. Forchhammer, *Recovery of Unicellular Cyanobacteria from Nitrogen Chlorosis: A Model for Resuscitation of Dormant Bacteria.* Microb Physiol, 2021: p. 1-10.
8. Doello, S., et al., *A Specific Glycogen Mobilization Strategy Enables Rapid Awakening of Dormant Cyanobacteria from Chlorosis.* Plant Physiol, 2018. **177**(2): p. 594-603.
9. Alonso-Casajús, N., et al., *Glycogen Phosphorylase, the Product of the glgP Gene, Catalyzes Glycogen Breakdown by Removing Glucose Units from the Nonreducing Ends in Escherichia coli.* Journal of Bacteriology, 2006. **188**(14): p. 5266-5272.
10. Ball, S., et al., *The evolution of glycogen and starch metabolism in eukaryotes gives molecular clues to understand the establishment of plastid endosymbiosis.* Journal of Experimental Botany, 2011. **62**(6): p. 1775-1801.
11. Fu, J. and X. Xu, *The functional divergence of two glgP homologues in Synechocystis sp. PCC 6803.* FEMS Microbiology Letters, 2006. **260**(2): p. 201-209.
12. Doello, S., N. Neumann, and K. Forchhammer, *Regulatory phosphorylation event of phosphoglucomutase 1 tunes its activity to regulate glycogen metabolism.* The FEBS Journal. **n/a**(n/a).
13. Florencio, F.J., et al., *The diversity and complexity of the cyanobacterial thioredoxin systems.* Photosynthesis Research, 2006. **89**(2): p. 157-171.
14. Reyes-Sosa, F.M., F.P. Molina-Heredia, and M.A. De la Rosa, *A novel α-amylase from the cyanobacterium Nostoc sp. PCC 7119.* Applied Microbiology and Biotechnology, 2010. **86**(1): p. 131-141.
15. Mathieu, C., et al., *An Isozyme-specific Redox Switch in Human Brain Glycogen Phosphorylase Modulates Its Allosteric Activation by AMP.* J Biol Chem, 2016. **291**(46): p. 23842-23853.
16. Navarro, F. and F.J. Florencio, *The cyanobacterial thioredoxin gene is required for both photoautotrophic and heterotrophic growth.* Plant Physiol, 1996. **111**(4): p. 1067-75.
17. Schürmann, P. and B.B. Buchanan, *The ferredoxin/thioredoxin system of oxygenic photosynthesis.* Antioxid Redox Signal, 2008. **10**(7): p. 1235-74.
18. Saha, R., et al., *Diurnal Regulation of Cellular Processes in the Cyanobacterium Synechocystis sp. Strain PCC 6803: Insights from Transcriptomic, Fluxomic, and Physiological Analyses.* mBio, 2016. **7**(3): p. e00464-16.
19. Marcén, M., et al., *Oxidative stress in E. coli cells upon exposure to heat treatments.* Int J Food Microbiol, 2017. **241**: p. 198-205.
20. Galvez-Valdivieso, G. and P.M. Mullineaux, *The role of reactive oxygen species in signalling from chloroplasts to the nucleus.* Physiologia Plantarum, 2010. **138**(4): p. 430-439.
21. Desikan, R., et al., *Regulation of the Arabidopsis Transcriptome by Oxidative Stress.* Plant Physiology, 2001. **127**(1): p. 159-172.
22. Foyer, C.H. and S. Shigeoka, *Understanding Oxidative Stress and Antioxidant Functions to Enhance Photosynthesis.* Plant Physiology, 2010. **155**(1): p. 93-100.

23. Brooks, A. and G.D. Farquhar, *Effect of temperature on the CO2/O2 specificity of ribulose-1,5-bisphosphate carboxylase/oxygenase and the rate of respiration in the light.* Planta, 1985. **165**(3): p. 397-406.
24. Makowka, A., et al., *Glycolytic Shunts Replenish the Calvin-Benson-Bassham Cycle as Anaplerotic Reactions in Cyanobacteria.* Mol Plant, 2020. **13**(3): p. 471-482.
25. Shinde, S., et al., *Glycogen Metabolism Supports Photosynthesis Start through the Oxidative Pentose Phosphate Pathway in Cyanobacteria.* Plant Physiol, 2020. **182**(1): p. 507-517.
26. Suginaka, K., et al., *Effect of Intracellular Glutathione on Heat-induced Cell Death in the Cyanobacterium, Synechocystis PCC 6803.* Biosci Biotechnol Biochem, 1999. **63**(6): p. 1112-5.
27. Cameron, J.C. and H.B. Pakrasi, *Essential role of glutathione in acclimation to environmental and redox perturbations in the cyanobacterium Synechocystis sp. PCC 6803.* Plant Physiol, 2010. **154**(4): p. 1672-85.
28. Meléndez-Hevia, E., T.G. Waddell, and E.D. Shelton, *Optimization of molecular design in the evolution of metabolism: the glycogen molecule.* The Biochemical journal, 1993. **295 (Pt 2)**(Pt 2): p. 477-483.
29. Prats, C., T.E. Graham, and J. Shearer, *The dynamic life of the glycogen granule.* Journal of Biological Chemistry, 2018. **293**(19): p. 7089-7098.
30. Koch, M., et al., *PHB is Produced from Glycogen Turn-over during Nitrogen Starvation in Synechocystis sp. PCC 6803.* Int J Mol Sci, 2019. **20**(8).
31. Yoo, S.-H., et al., *Glycogen Synthase Isoforms in Synechocystis sp. PCC6803: Identification of Different Roles to Produce Glycogen by Targeted Mutagenesis.* PLOS ONE, 2014. **9**(3): p. e91524.
32. Rippka, R., et al., *Generic Assignments, Strain Histories and Properties of Pure Cultures of Cyanobacteria.* Journal of General Microbiology, 1979. **111**(1): p. 1-61.
33. Schlebusch, M. and K. Forchhammer, *Requirement of the Nitrogen Starvation-Induced Protein Sll0783 for Polyhydroxybutyrate Accumulation in Synechocystis sp. Strain PCC 6803.* Applied and Environmental Microbiology, 2010. **76**(18): p. 6101-6107.
34. Klotz, A., et al., *Awakening of a Dormant Cyanobacterium from Nitrogen Chlorosis Reveals a Genetically Determined Program.* Curr Biol, 2016. **26**(21): p. 2862-2872.

Danksagung

Eine Promotion ist ein langer Prozess mit vielen Höhen und Tiefen, aber stets hoher Intensität. Auch wenn ich sicherlich nicht allen gerecht werden kann, möchte ich nachfolgend versuchen den Personen zu danken, die mich auf diesem Weg in besonderer Weise begleitet haben:

Zuallererst meinem Doktorvater Karl Forchhammer, der mir die Arbeit an diesem Projekt überhaupt erst ermöglichte. Er hatte stets ein offenes Ohr, großartige Ideen, konstruktive Kritik und eine Begeisterung für die Mikrobiologie, die ansteckend ist. Ich habe in dieser Zeit unglaublich viel gelernt und hätte mir keine besseren Bedingungen für meine Promotion wünschen können. Vielen Dank!

Ein herzlicher Dank geht auch an meine Zweitbetreuerin Iris Maldener, die für Hilfe und Anregungen stets zur Verfügung stand!

Ich möchte außerdem Hannes Link für die Erstellung des Zweitgutachtens dieser Arbeit danken.

Von meinen Kolleginnen und Kollegen möchte ich besonders Moritz, Sofía und Phil hervorheben, die zu wertvollen Freunden geworden sind. Danke für eine tolle Zeit sowohl in- als auch außerhalb des Labors! Außerdem möchte ich mich gerne bei meinem ehemaligen Betreuer Alex bedanken, der mir Vieles beigebracht und für große Teile dieser Arbeit die Grundlagen gelegt hat. Generell geht ein großes Dankeschön an die gesamte Arbeitsgruppe für die Unterstützung und Hilfe, wann immer diese nötig war.

Ich danke Libera Lo Presti für ihre großartige Unterstützung, ihren unermüdlichen Fleiß und ihre Geduld (mit mir) beim Schreiben und Überarbeiten der Manuskripte.

Außerhalb der Arbeit möchte ich zunächst meinen FreundInnen und MitbewohnerInnen Andreas, Meike, Karo, Sebastian, Anna, Timo, Johanna, Flo und Nadine danken. Es ist schön, mit so tollen Menschen wie euch zusammen zu leben! :)

Von meinen Freunden möchte ich gerne Johanna besonders hervorheben, die stets für mich da war und immer an mich geglaubt hat!

Der Föhrberg darf natürlich nicht unerwähnt bleiben! Ich bin sehr froh, ein Teil dieser wunderbaren Gemeinschaft zu sein, die mich nachhaltig geprägt hat. Ich danke allen meinen dortigen Freundinnen und Freunden! Sie alle zu nennen, würde den Rahmen sprengen.

Ich möchte außerdem Familie Ridder - Jörn, Cathrin, Nora und Falk - für ihre Unterstützung und Herzlichkeit danken.

Ein riesiges Dankeschön geht auch an meine Eltern, die mich immer bestmöglich unterstützt haben. Ohne sie wäre mein Studium und diese Arbeit nicht möglich gewesen.

Und als Wichtigstes zum Schluss natürlich Linda, der ich für die durchgehende Unterstützung, Liebe, Trost und Halt in allen Lebenslagen wahrscheinlich niemals genug werde danken können!